

**Electropolymer based sensors for DNA bases and xanthenes
and their electrokinetic studies**

Thesis submitted to
Cochin University of Science and Technology
in partial fulfilment of the requirements
for the award of the degree of
Doctor of Philosophy
in
Chemistry

by
Jesny S.
(Reg. No: 3893)



Department of Applied Chemistry
Cochin University of Science and Technology
Kochi - 22

November 2017

Electropolymer based sensors for DNA bases and xanthenes and their electrokinetic studies

Ph.D. Thesis under the Faculty of Sciences

Author

Jesny S.

Assistant Professor
Department of Chemistry
Sree Narayana College, Cherthala
Alappuzha, India 688582
Email: jesnysmail@gmail.com

Supervising Guide

Dr. K. Girish Kumar

Professor and Head
Department of Applied Chemistry
Cochin University of Science and Technology
Kochi, India 682022
Email: giri@cusat.ac.in

Department of Applied Chemistry
Cochin University of Science and Technology
Kochi, India 682022

November 2017

DEPARTMENT OF APPLIED CHEMISTRY
COCHIN UNIVERSITY OF SCIENCE AND TECHNOLOGY
KOCHI - 682022, INDIA



Dr. K. Girish Kumar
Professor and Head

Tel: 0484 - 2575804
E-mail: chem@cusat.ac.in

Date: 16th November 2017

Certificate

Certified that the work entitled “**Electropolymer based sensors for DNA bases and xanthenes and their electrokinetic studies**”, submitted by Smt. Jesny S., in partial fulfilment of the requirements for the degree of Doctor of Philosophy in Chemistry to Cochin University of Science and Technology, is an authentic and bonafide record of the original research work carried out by her under my supervision at the Department of Applied Chemistry. Further, the results embodied in this thesis, in full or in part, have not been submitted previously for the award of any other degree. All the relevant corrections and modifications suggested by the audience during the pre-synopsis seminar and recommended by the Doctoral committee have been incorporated in the thesis.

K. Girish Kumar
(Supervising Guide)

DECLARATION

I hereby declare that the work presented in this thesis entitled **“Electropolymer based sensors for DNA bases and xanthenes and their electrokinetic studies”** is based on the original work carried out by me under the guidance of Dr. K. Girish Kumar, Professor and Head, Department of Applied Chemistry, Cochin University of Science and Technology and has not been included in any other thesis submitted previously for the award of any degree.

Jesny S.

Kochi-22
16/11/2017

Acknowledgements

A thesis is a treatise advancing a new point of view resulting from personal research. Certainly, the culmination of this thesis is the result of arduous personal hard work. But it would not have been possible without the active help and assistance from many persons. Therefore, this thesis would not be complete unless I acknowledge the help and assistance of all those who made this thesis possible in its present form and express my sincere gratitude for the same.

My supervising guide, Prof. K. Girish Kumar, Professor and Head, Department of Applied Chemistry, CUSAT is the first and foremost person I am indebted to. Without his patient guidance, relentless persuasion, subtle inspiration and his unwavering confidence in me, I would not have been able to complete this journey. He never gave me answers directly but coaxed them out of me. He questioned me but gave me the resources to answer them. The work culture that he demands from his group of students, though hard to keep up; is the reason we are able to sort out our research problems effectively. I am grateful for the 'conspiracy of the universe' that gave me an opportunity to work under the guidance of G. K. Sir. I owe my deepest gratitude to him for all the professional and personal lessons he taught us all. Above all, I am deeply indebted to him for not giving up on me. I remember with gratitude, the encouraging and supporting presence of the better half of my sir, Dr. Anitha I., Principal, Govt. College, Pathirippala.

Prof. K. Sreekumar, my doctoral committee member, has always supported me with suggestions and advices, as and when they were due. I sincerely thank him for all his assistance as the doctoral committee member and also for those during his tenure as the Head of the Department.

Thanks, are also due to Prof. S. Sugunan, with whom I initially joined as research scholar, but could not continue due to my personal circumstances. I am deeply indebted to him for his kindness and understanding throughout my association with the department. Along with Prof. S. Sugunan, I remember with gratitude my other MPhil teachers, Prof. K K. Mohammad Yusuff and Prof. S. Prathapan, who taught me the philosophy of research.

From the time I joined the Department of Applied Chemistry as a part-time research scholar, the various heads of the department Prof. K. Sreekumar, Dr. N. Manoj and Prof. M. R. Prathapachandra Kurup, had been kind to me and provided

me access to all the facilities of the department. I would like to extend my gratitude to each of them. I also remember with gratitude all the assistance I received from the other teaching and non-teaching staff of the department. I thank the Cochin University of Science and Technology for providing me all the necessary resources to conduct and complete my research programme.

I hereby place on record my sincere thanks to the University Grants Commission for the Teacher Fellowship under Faculty Development Programme of XII Plan. I would like to thank the Manager and the various principals of Sree Narayana College, Cherthala, (Prof. D. Murali, Dr. P.K. Sudarsanan and Dr. K. Anirudhan) for all their aid, in obtaining Teacher Fellowship. I remember with gratitude the support extended to me by my colleagues at the Department of Chemistry, S. N. College, Cherthala along with the non-teaching staff of the college during this period. I am indebted to Mrs. Praveena V. P. and Mr. Shamjith S., the respective substitute teachers who worked sincerely and efficiently in my place. Their presence in my absence at the college was instrumental in helping me complete my research work without having to worry about my duties as a teacher.

I learned the basics of research from my seniors at the Physical Chemistry Lab, DAC, CUSAT, Dr. Maya S., Dr. Radhika R, Dr. Kochurani George and Dr. Ramanathan and I am grateful to them for the strong foundation that they set in me. I also thank Dr. Reshmi M. for all her support.

The laboratory work culture that I possess today is the one that I learned from my seniors at the Analytical Chemistry lab. I cherish the fond memories of my time in the lab with Dr. Sindhu Issac, Dr. Renjini Joseph, Dr. Leena R., Dr. Sobhana Mathew, Dr. Laina A.L., Dr. Theresa C. J. and Dr. Divya Thomas. Later they were joined by Soumya, Dr. Ajith, Zafna, Dr. Anuja, Sreejith and Meera. We were not only friends and labmates, but siblings of heart. The support and help that I received from these friends are beyond any words of gratitude. The last two years of my research was completed in the company of Sheela teacher, Ammu, Unni, Shalini, Ambily, Sanu and Manna. I thank them for their scintillating company and the thought-provoking discussions. I am greatly thankful for the presence of Dr. Jinta Thomas and Dr. Monica Raina, who joined the lab during the last leg of my time in the lab, sharing their experience and expertise.

I remember with gratitude, the suggestions and advices of Dr. Theresa C. J. that helped me kick-start my work as well as her personal help during the initial stages of this work. I would like to thank Dr. Divya and Dr. Anuja for their support

especially during my part-time research days. I benefitted immensely from my conversations with Dr. Anuja, wherein she shared her experiences and expertise that she gained as a research student. The efforts taken by Ambily, Ammu, Unni and Dr. Monica in correcting the first draft of the thesis is responsible for bringing it to the present state and I sincerely thank them for the constructive criticism and creative suggestions. The suggestions from Ambily regarding the structure of the thesis, during my preparations for the pre-synopsis presentation proved invaluable and I am grateful to her for her timely advices. I would like to thank Ammu and Dr. Leena for their efforts in proof reading the thesis. I thank Shalini for all the support and the companionship that she extended during our time together in the lab. The friendship forged with Dr. Jinta during the gruesome period of thesis documentation immensely helped me to tide over the period.

Many others of the department extended their helping hand. I would like to acknowledge the technical help of Ashraf, Kiran, Shan, Lincy and Binitha. I remember with gratitude Shanty for her ever inspiring and ever helping presence. The good times I had while working with Noufia, Shinu, Rejitha, Sruthi and Gopika will always remain with me. Sometimes breakthrough aid came from unexpected avenues. Sreelakshmy, the MSc project student present in the lab during the crucial days of my work, as well as Akhila, the MSc project student who came during the final stages of my work were of immense help to me and I sincerely thank them. Ms. Soumini C., a fellow FDP teacher fellow shared with me the trials and tribulations of FDP and I thank her for all the help.

I remember with gratitude my friends Dr. Pramod Padmanabhan, IISER Pune and Mrs. Sreelakshmi Pramod who were just a call away, ready to help me in whatever I needed, whenever I asked.

With a deep sense of gratitude, I remember all my teachers who guided me throughout my academic journey and taught me everything that I know. I thank my high school chemistry teacher Mrs. Mildred Cabral, teachers at the undergraduate level Prof. Leni, Prof. Celine, Prof. Radha and the professors at the post graduate level, Prof. Babu Jose, Prof. P. J. Kuruvachan, Prof. (Sr.) Aliamma Zakariah. Prof. (Fr.) T. K. Jose, Prof. P.J. Joseph, Prof. P. M. Joseph who instilled in me, keen interest in Chemistry and encouraged me for further studies.

My research benefitted from the financial assistance received by our lab from the Directorate of Extramural Research and Property Rights, DRDO, New Delhi, UGC (One-time Grant) and KSCSTE, and I would like to extend my sincere

gratitude to these agencies. I would like to thank the Sophisticated Test and Instrumentation Centre (STIC), CUSAT for analysis.

I could satisfactorily complete my research only because of the unconditional support I received from my family. The blessings of my parents helped me focus on my aim and their emotional, financial and physical assistance helped me immensely in making this thesis a reality. Like a bow, they stretched back so that like an arrow, I could fly higher. The emotional brunt of my research largely fell upon my mother and her words had always helped me to propel forward despite the hurdles. My father never said 'no' to me and was ever ready to provide me with all the amenities needed for completing the thesis. Words are not sufficient to thank them. The support from my sister Roshny also meant a lot to me. My in-laws had been understanding regarding the hours I had to put in for my work and I am thankful to them for it. However, the person responsible for not only this thesis, but also for me to pursue Ph.D. is my husband, Mr. Uday Ananthan. He had been my friend, philosopher, navigator, caretaker, compass, bouncing board, punching bag, safety blanket and more throughout this journey. He kept me sane and focused. It is to him, my partner in life, that I dedicate the thesis.

Finally, I bow my head in reverence before the God Almighty, who made better plans for me, than any I could have ever imagined for myself.

If any names are left out, it is not intentional, for 'to err is human', and I thank them for forgiving, for 'to forgive is divine'.

Jesny S.

*Dedicated to my husband, Uday Ananthan
My friend, philosopher and navigator
Without whose encouragement, patience and support, this day
would have been but a dream*

PREFACE

Electrochemical sensors represent a rapidly growing class of chemical sensors. In comparison with optical, mass sensitive and heat sensitive sensors, electrochemical sensors offer advantages such as experimental simplicity, selective response and lower cost. Combined with the prospect of simultaneous determination of two or more analytes, thereby eliminating complex separation steps involving large quantities of solvents, voltammetric sensors constitute the most promising candidate in green chemical analysis. The key element in voltammetric sensing is the working electrode which can be tailored for specific use by chemical modification with species having functional groups to its surface. Electrogeneration of polymer films on to the surface of electrodes are much useful in this regard.

The thesis presents the development of electropolymer modified glassy carbon electrodes for the simultaneous determination of DNA bases guanine, adenine, thymine and cytosine along with uric acid, a DNA metabolite. Polymers with acidic functionalities were electrogenerated and deposited on to the electrode surface and used for the determination of DNA bases. Five different sensors were developed of which three were suitable for simultaneous determination. The success encountered with simultaneous determination of DNA bases was extended to develop a sensor for the simultaneous determination of xanthine and its derivatives, theophylline and caffeine. Investigation of the electrochemical behaviour of biological molecules are reported to be significant in understanding their biological redox behaviour. The kinetics of the electro-oxidation of these biological molecules has also been studied using two different voltammetric models.

These results have been expounded through the nine chapters in the thesis entitled 'Electropolymer based sensors for DNA bases and xanthines and their electrokinetic studies'.

Chapter 1 outlines the background of the present investigation with reference to voltammetric sensors, electropolymers and electropolymer modified electrodes. The various techniques employed in this work is described in detail. A review of the literature found on the voltammetric determination of DNA bases is given in this chapter.

Chapter 2 describes the fabrication procedure and characterisation of various electrodes used for the development of sensors. The experimental details involved in the development of the sensors is also described in this chapter.

Chapter 3 deals with the development of poly(aspartic acid) modified glassy carbon electrode as a sensor for adenine. Optimisation of experimental parameters such as supporting electrolyte and number of cycles of polymerisation is explained. Interferences produced by possibly co-existing species is explained and application of the sensor for the determination of adenine in acid denatured DNA sample is accounted. Study of variation of peak parameters with scan rate is described and use of the information extracted from this study for the determination of kinetic parameters and mechanism of the reaction is demonstrated. Study of kinetics of electro-oxidation of DNA bases on the developed sensor is described.

Chapter 4 illustrates progression of a poly(glutamic acid) modified glassy carbon electrode as a sensor for thymine. A description of optimisation of experimental parameters and influence of possibly co-existing species on the sensor performance is given. The determination of thymine in spiked synthetic serum and urine is illustrated. From the study of influence of pH and scan rate on the oxidation potential of thymine on poly(glutamic acid) modified glassy carbon electrode, the possible mechanism of the electro-oxidation is proposed. The kinetics of electro-oxidation of DNA bases on the poly(glutamic acid) modified glassy carbon electrode was studied and the results are discussed.

Chapter 5 gives a description of poly(para toluene sulfonic acid) modified glassy carbon electrode being used for the simultaneous determination of the

purine bases guanine and adenine along with its metabolite uric acid. The simultaneous determination of guanine, thymine and uric acid on the same sensor is also explored. Optimisation of experimental parameters, study of interferences produced by other species, variation of peak parameters with scan rate and chronoamperometric determination of diffusion coefficient are illustrated. Simultaneous determination of guanine and adenine in acid denatured DNA samples has been explained. Determination of rate constants for the electro-oxidation of DNA bases on the poly(para toluene sulfonic acid) modified glassy carbon electrode is also explained.

Chapter 6 details the simultaneous determination of guanine and adenine together with their metabolite uric acid on a poly(para amino benzene sulfonic acid) modified glassy carbon electrode. Calibration of the sensor for individual as well as simultaneous determination under the optimised experimental conditions has been explained. Successful application of the sensor for simultaneous determination of guanine and adenine in acid denatured DNA as well as simultaneous determination of guanine, adenine and uric acid in acid denatured DNA spiked with uric acid has been illustrated. From the information obtained from chronoamperometric measurements and linear sweep voltammetry at different scan rates, rate constant for electro-oxidation of each of the electro-oxidation process on poly(para amino benzene sulfonic acid) modified glassy carbon electrode has been calculated and presented in this chapter.

In **Chapter 7**, the electrocatalytic resolution of guanine, adenine, cytosine and uric acid on a poly(4- amino-3-hydroxy-naphthalene-1-sulfonic acid) modified glassy carbon electrode is presented. Optimisation of sensor performance, calibration, interferences and application of the sensor has been elaborated along with the kinetic studies of all the DNA bases.

The success encountered with simultaneous determination of DNA bases was extended to develop a sensor for the simultaneous determination of xanthine and its derivatives, theophylline and caffeine.

Chapter 8 is on the use of poly(para amino benzene sulfonic acid) modified glassy carbon electrode as a sensor for the simultaneous determination of xanthine, its methyl derivatives theophylline and caffeine. A brief review of the different sensors for the determination of xanthine, theophylline and caffeine based on modified carbon electrodes is presented. The calibration of the sensor for individual and simultaneous determination of these analytes under the optimised experimental conditions is explained. Study of interferences produced by possibly co-existing species has been explained in detail and the possibility of interference free simultaneous determination of xanthine, theophylline and caffeine along with uric acid, the oxidation product of xanthine is expounded. The utility of the sensor for determination of these analytes in real samples, tea bag, blended coffee powder and commercially available pharmaceutical formulation has been elaborated. The rate constants for electro-oxidation of xanthine, theophylline and caffeine on the developed sensor calculated from chronoamperometric and linear sweep voltammetric measurements have been listed in this chapter.

In **Chapter 9**, the work presented in the thesis has been summarised and the general conclusions regarding the sensor performance and kinetics of electro-oxidation of DNA bases on the developed sensors has been presented. The performance of the developed sensors for simultaneous determination is compared with other electropolymer modified electrodes reported in literature.

The list of references cited in the thesis is compiled at the end of the thesis as a separate section.

CONTENTS

Chapter 1 Introduction ----- 1-48

1.1	Electroanalytical Chemistry-----	1
1.2	Voltammetry -----	3
1.2.1	Voltammetric Cell -----	4
1.2.2	Reference electrode-----	5
1.2.3	Counter or Auxiliary electrode-----	5
1.2.4	Working electrode or Indicator electrode -----	5
1.2.4.1	Glassy Carbon Electrode (GCE) -----	6
1.2.4.2	Chemically Modified Electrodes (CME)-----	7
1.2.5	Solvent and supporting electrolyte -----	8
1.3	Electrode Processes -----	9
1.4	Voltammetric Techniques -----	11
1.4.1	Polarography -----	12
1.4.2	Cyclic Voltammetry (CV)-----	13
1.4.3	Pulse Voltammetry -----	15
1.4.3.1	Normal Pulse Voltammetry (NPV)-----	16
1.4.3.2	Differential Pulse Voltammetry (DPV)-----	16
1.4.3.3	Square Wave Voltammetry (SWV) -----	16
1.4.4	Stripping Voltammetry-----	17
1.4.5	Chronoamperometry-----	18
1.5	Electrochemical Impedance Spectroscopy (EIS)-----	19
1.6	Kinetics of electrochemical reactions-----	20
1.6.1	Reversible kinetics-----	21
1.6.2	Irreversible kinetics-----	22
1.7	Chemical Sensors-----	22
1.8	Electrochemical Sensors-----	24
1.9	Back ground features of the present investigation -----	25
1.9.1	Electropolymers-----	25
1.9.2	Simultaneous determinations-----	27
1.9.3	DNA bases-----	27
1.9.4	Literature review on chemically modified carbon electrodes for determination of DNA bases and Uric acid -----	31
1.9.5	Objectives of the present investigation -----	45

Chapter 2 Fabrication and Characterisation of Various Electropolymer Modified Electrodes ----- 49-71

2.1	Poly(aspartic acid) modified glassy carbon electrode	
2.1.1	Fabrication-----	50
2.1.2	Characterisation of <i>p</i> (AspA)/GCE -----	52

2.2	Poly(glutamic acid) modified glassy carbon electrode	
2.2.1	Fabrication	53
2.2.2	Characterisation of <i>p</i> (GA)/GCE	55
2.3	Poly(para toluene sulfonic acid) modified glassy carbon electrode	
2.3.1	Fabrication	57
2.3.2	Characterisation of the electrode	58
2.4	Poly(para amino benzene sulfonic acid) modified glassy carbon electrode	
2.4.1	Fabrication	60
2.4.2	Characterisation of the electrode	61
2.5	Poly(4-amino-3-hydroxy naphthalene-1-sulfonic acid) modified glassy carbon electrode	
2.5.1	Fabrication	63
2.5.2	Characterisation of the electrode	64
2.6	Comparison of charge transfer resistance of the fabricated electropolymer modified electrodes	66
2.7	Experimental	
2.7.1	Chemicals	67
2.7.2	Instrumentation	68
2.7.3	Preparation of stock solutions	68
2.7.4	Preparation of DNA sample	69
2.7.5	Preparation of Tea and Coffee samples	69
2.7.6	Preparation of pharmaceutical samples	69
2.7.7	Preparation of artificial urine	69
2.7.8	Preparation of artificial blood serum	70
2.7.9	Preparation of buffer solutions	70
2.7.10	Pre-treatment of glassy carbon electrode	70
2.7.11	Analytical Procedure	70
2.8	Summary	71

Chapter 3 Poly(Aspartic Acid) modified Glassy Carbon Electrode as Sensor for Adenine ----- 73-95

3.1	Introduction	73
3.2	Results and discussion	76
3.2.1	Optimisation of experimental parameters	76
3.2.1.1	Supporting electrolyte	76
3.2.1.2	Number of cycles of polymerization	76
3.2.2	Voltammetric behaviour of the DNA bases on the <i>p</i> (AspA)/GCE	77
3.2.3	Electrochemical Impedance Spectroscopy (EIS)	78
3.2.4	Electroactive surface area	79
3.2.5	Calibration curve	80

3.2.6	Mechanistic Studies -----	81
3.2.6.1	Effect of pH-----	81
3.2.6.2	Effect of scan rate -----	82
3.2.7	Effect of co-existing molecules -----	83
3.2.8	Application: Determination of Ad in acid denatured Herring Sperm DNA-----	85
3.2.9	Kinetics of electro-oxidation of DNA bases on <i>p</i> (AspA)/GCE	
3.2.9.1	Diffusion coefficient-----	85
3.2.9.2	Heterogeneous rate constant -----	90
3.3	Conclusions -----	95

**Chapter 4 Poly(Glutamic acid) modified Glassy Carbon
Electrode as Sensor for Thymine ----- 97-116**

4.1	Introduction -----	97
4.2	Results and discussion -----	100
4.2.1	Optimisation of experimental parameters	
4.2.1.1	Supporting electrolyte-----	100
4.2.1.2	Number of cycles of polymerization -----	101
4.2.2	Electrochemical behaviour of DNA bases on the <i>p</i> (GA)/GCE-----	101
4.2.3	Electro active surface area-----	103
4.2.4	Calibration -----	104
4.2.5	Mechanistic Studies	
4.2.5.1	Effect of scan rate-----	105
4.2.5.2	Effect of pH-----	106
4.2.6	Effect of co-existing molecules -----	107
4.2.7	Application: Determination of Thy in spiked artificial body fluids-----	108
4.2.8	Kinetics of electro-oxidation of DNA bases on <i>p</i> (GA)/GCE-----	109
4.2.8.1	Chronoamperometry-----	109
4.2.9.2	Heterogeneous rate constant -----	114
4.3	Conclusions -----	116

**Chapter 5 Poly(para Toluene Sulfonic Acid) modified Glassy
Carbon Electrode as Sensor for Simultaneous
Determination of Guanine, Adenine and Uric acid
as well as Guanine, Thymine and Uric Acid----- 117-146**

5.1	Introduction -----	118
5.2	Results and discussion -----	119
5.2.1	Optimisation of experimental parameters -----	119

5.2.2	Electrochemical behaviour of DNA bases on the <i>p</i> (TSA)/GCE	120
5.2.3	Electro active surface area	123
5.2.4	Calibration	124
5.2.4.1	Guanine	124
5.2.4.2	Adenine	126
5.2.4.3	Thymine	127
5.2.4.4	Uric acid	127
5.2.5	Simultaneous determination	128
5.2.5.1	Uric acid, Guanine and Adenine	128
5.2.5.2	Uric acid, Guanine and Thymine	129
5.2.6	Mechanistic Studies	131
5.2.7	Selectivity and Interferences	133
5.2.8	Application Studies	133
5.2.8.1	HS DNA	137
5.2.8.2	Synthetic Urine and Serum	139
5.2.9	Repeatability and reproducibility	140
5.2.10	Kinetics of electro-oxidation on <i>p</i> (TSA)/GCE	
5.2.10.1	Chronoamperometry	140
5.2.10.2	Heterogeneous rate constant	143
5.3	Conclusions	145

Chapter 6 Poly(para Amino Benzene Sulfonic Acid) modified Glassy Carbon Electrode as Sensor for Simultaneous Determination of Guanine, Adenine and Uric acid 147-169

6.1	Introduction	147
6.2	Results and discussion	150
6.2.1	Optimisation of experimental parameters	150
6.2.2	Electrochemical behaviour of DNA bases on <i>p</i> (ABSA)/GCE	151
6.2.3	Electro active surface area	154
6.2.4	Calibration	155
6.2.4.1	Guanine	155
6.2.4.2	Adenine	156
6.2.4.3	Uric Acid	157
6.2.4.4	Simultaneous determination	157
6.2.5	Mechanistic Studies	158
6.2.6	Selectivity and Interferences	161
6.2.7	Application Studies	163
6.2.7.1	HS DNA	163
6.2.8	Kinetics of electro-oxidation on <i>p</i> (ABSA)/GCE	165
6.2.8.1	Chronoamperometry	165
6.2.8.2	Heterogeneous rate constant	167
6.3	Conclusions	168

Chapter 7 Poly(4-amino-3-hydroxy naphthalene -1-sulfonic acid) modified Glassy Carbon Electrode as Sensor for Simultaneous determination of Guanine, Adenine, Cytosine and Uric acid as well as individual determination of Thymine ----- 171-194

7.1	Introduction -----	171
7.2	Results and discussion-----	173
7.2.1	Optimisation of experimental parameters -----	173
7.2.2	Electrochemical behaviour of DNA bases on the <i>p</i> (AHNSA)/GCE-----	174
7.2.3	Electro active surface area -----	176
7.2.4	Calibration -----	177
7.2.4.1	Guanine-----	177
7.2.4.2	Adenine-----	178
7.2.4.3	Thymine -----	178
7.2.4.4	Cytosine -----	179
7.2.4.5	Uric Acid -----	180
7.2.4.6	Simultaneous determination-----	180
7.2.5	Selectivity and Interferences -----	182
7.2.6	Application Studies -----	185
7.2.6.1	HS DNA-----	185
7.2.6.2	Synthetic Urine and Serum-----	185
7.2.7	Repeatability, reproducibility and stability-----	186
7.2.8	Mechanistic Studies-----	187
7.2.9	Kinetics of electro-oxidation on <i>p</i> (AHNSA)/GCE	
7.2.9.1	Chronoamperometry -----	190
7.2.9.2	Heterogeneous rate constant -----	192
7.3	Conclusions-----	193

Chapter 8 Poly(para Amino Benzene Sulfonic Acid) modified Glassy Carbon Electrode as Sensor for Simultaneous Determination of Xanthine, Theophylline and Caffeine along with Uric Acid 195-219

8.1	Introduction-----	196
8.2	Results and discussion-----	199
8.2.1	Optimisation of experimental parameters -----	199
8.2.1.1	Supporting electrolyte-----	199
8.2.1.2	pH of the supporting electrolyte -----	200
8.2.1.3	Number of cycles of polymerization-----	200
8.2.2	Electrochemical response for XT, TP and CF on <i>p</i> (ABSA)/GCE-----	201
8.2.3	Electro active surface area -----	203

8.2.4	Calibration -----	203
	8.2.4.1 Xanthine-----	204
	8.2.4.2 Theophylline-----	205
	8.2.4.3 Caffeine-----	205
	8.2.4.4 Simultaneous determination of XT, TP and CF -----	206
8.2.5	Selectivity and interferences -----	207
8.2.6	Determination of the purines in real samples -----	212
8.2.7	Mechanistic Studies-----	214
8.2.8	Kinetic Studies	
	8.2.8.1 Chronoamperometry -----	216
	8.2.8.2 Heterogeneous rate constant -----	218
8.3	Conclusions-----	219
Chapter 9 Summary and Conclusions-----		221-227
Supplementary Information-----		228
References -----		229-243
Publications based on the present work-----		245-246
Other publications -----		247-248
Resume of the author		

LIST OF TABLES

Table 2.1:	Change in R_{ct} -----	66
Table 3.1:	Variation of peak parameters with scan rate-----	82
Table 3.2:	Interference study -----	84
Table 3.3:	Diffusion coefficient of DNA bases -----	90
Table 3.4:	Kinetic parameters measured on $p(\text{AspA})/\text{GCE}$ -----	92
Table 3.5:	Kinetic parameters measured on bare GCE-----	94
Table 3.6:	Rate constants for electro-oxidation -----	94
Table 4.1:	Variation of peak parameters with scan rate-----	105
Table 4.2:	Effect of possibly co-existing species -----	108
Table 4.3:	Determination of Thy in spiked samples-----	109
Table 4.4:	Diffusion coefficient of DNA bases -----	113
Table 4.5:	Kinetic studies -----	114
Table 4.6:	Rate constants for electro-oxidation -----	115
Table 5.1:	R_{ct} values fitted from Nyquist plots-----	122
Table 5.2:	Variation of peak parameters with scan rate-----	131
Table 5.3:	Kinetic parameters for electro-oxidation-----	132
Table 5.4:	Influence of chemical species on the analytical signal -----	137
Table 5.5:	Determination of Ua in spiked DNA -----	139
Table 5.6:	Determination of Ua, Gu and Ad using $p(\text{TSA})/\text{GCE}$ in spiked samples-----	139
Table 5.7:	Calculated values of diffusion coefficients -----	143
Table 5.8:	Kinetic studies -----	144
Table 5.9:	Rate constants for electro-oxidation -----	144
Table 6.1:	R_{ct} values fitted from Nyquist plots-----	154
Table 6.2:	Variation of peak parameters with scan rate-----	160
Table 6.3:	Kinetic parameters for electro-oxidation-----	160
Table 6.4:	Interference Study-----	163
Table 6.5:	Determination of Ua in spiked HS DNA-----	164
Table 6.6:	Diffusion Coefficient -----	166

Table 6.7:	Kinetic studies -----	167
Table 6.8:	Rate constants for electro-oxidation -----	167
Table 7.1:	R_{ct} values fitted from Nyquist plots-----	175
Table 7.2:	Analytical Parameters -----	183
Table 7.3:	Interference study -----	184
Table 7.4:	Application studies -----	186
Table 7.5:	Variation of peak parameters with scan rate-----	188
Table 7.6:	Kinetic parameters for electro-oxidation-----	189
Table 7.7:	Calculated values of diffusion coefficients -----	191
Table 7.8:	Rate constants for electro-oxidation -----	192
Table 8.1:	R_{ct} values fitted from Nyquist plots-----	203
Table 8.2:	Interference Study-----	212
Table 8.3:	Determination of XT, TP and CF in commercially available samples-----	213
Table 8.4:	Determination of TP and CF in pharmaceutical formulations-----	213
Table 8.5:	Determination of XT, TP, CF and Ua in spiked synthetic urine and serum-----	214
Table 8.6:	Variation of peak parameters with scan rate-----	214
Table 8.7:	Mechanistic parameters -----	217
Table 8.8:	Kinetics of electro-oxidation-----	218
Table 9.1:	Various sensors developed by the present work -----	222
Table 9.2:	Oxidation potential of DNA bases on the developed electrodes-----	223
Table 9.3:	Limit of detection for individual analytes obtained on various electrodes -----	223
Table 9.4:	Rate constant for electro-oxidation on various electrodes -----	224
Table 9.5:	Comparison of performance characteristics of the developed sensors with previously reported sensors for simultaneous determination-----	226

LIST OF FIGURES

Figure 1.1:	Classification of electrochemical methods-----	03
Figure 1.2:	Representation of a three electrode voltammetric cell -----	04
Figure 1.3:	Electrical double layer and the variation of potential across it -----	11
Figure 1.4:	Cyclic voltammogram of a perfectly reversible reaction -----	14
Figure 1.5:	Excitation signal form of various pulse voltammetric techniques -----	17
Figure 1.6:	Equivalent electronic circuits that fit experimental impedance spectra-----	19
Figure 1.7:	Chemical Sensing Strategies-----	23
Figure 2.1:	Electropolymerisation of AspA on GCE-----	51
Figure 2.2:	SEM images of bare GCE (a) and <i>p</i> (AspA)/GCE (b and c) -----	52
Figure 2.3:	Nyquist plots of bare GCE and <i>p</i> (AspA)/GCE in 5.0×10^{-3} M $[\text{Fe}(\text{CN})_6]^{3-/4-}$ in 0.1 M KCl. Inset shows the overlay of cyclic voltammogram obtained on bare GCE and <i>p</i> (AspA)/GCE in the same solution-----	53
Figure 2.4:	Electropolymerisation of GA onto GCE -----	54
Figure 2.5:	SEM images of bare GCE (a) and <i>p</i> (GA)/GCE (b and c)-----	55
Figure 2.6:	Overlay of Nyquist plots of bare GCE and <i>p</i> (GA)/GCE in 5.0×10^{-3} M $[\text{Fe}(\text{CN})_6]^{3-/4-}$ in 0.1 M KCl. Inset shows the overlay of cyclic voltammogram obtained on bare GCE and <i>p</i> (GA)/GCE in the same solution -----	56
Figure 2.7:	Electropolymerisation of TSA on GCE -----	57
Figure 2.8:	SEM images of bare GCE (a) and <i>p</i> (TSA)/GCE-----	58
Figure 2.9:	Nyquist plots of bare GCE and <i>p</i> (TSA)/GCE recorded in 5.0×10^{-3} M $[\text{Fe}(\text{CN})_6]^{3-/4-}$ in 0.1 M KCl. Inset shows the overlay of cyclic voltammogram obtained on bare GCE and <i>p</i> (TSA)/GCE in the same solution -----	59
Figure 2.10:	Electropolymerisation of ABSA on GCE. Inset shows the schematic representation of the modified electrode -----	60
Figure 2.11:	SEM images of bare GCE (a) and <i>p</i> (ABSA)/GCE (b) -----	62

Figure 2.12:	Nyquist plots of bare GCE and $p(\text{ABSA})/\text{GCE}$ recorded in $5.0 \times 10^{-3} \text{ M } [\text{Fe}(\text{CN})_6]^{3-/4-}$ in 0.1 M KCl over a frequency range $1.0 \times 10^{-1} - 1.0 \times 10^4 \text{ Hz}$ and amplitude of 0.005 V. Inset shows the overlay of cyclic voltammogram obtained on bare GCE and $p(\text{ABSA})/\text{GCE}$ in the same solution -----	63
Figure 2.13:	Electropolymerisation of AHNSA on GCE-----	64
Figure 2.14:	SEM images of bare GCE (a) and $p(\text{AHNSA})/\text{GCE}$ (b)-----	65
Figure 2.15:	Nyquist plots of bare GCE and $p(\text{AHNSA})/\text{GCE}$ recorded in $5.0 \times 10^{-3} \text{ M } [\text{Fe}(\text{CN})_6]^{3-/4-}$ in 0.1 M KCl. Inset shows the overlay of cyclic voltammogram obtained on bare GCE and $p(\text{AHNSA})/\text{GCE}$ in the same solution -----	66
Figure 3.1:	Variation of peak parameters with number of cycles of polymerization-----	77
Figure 3.2:	DPV response for the oxidation of $5.0 \times 10^{-5} \text{ M Ad}$ on the bare GCE and $p(\text{AspA})/\text{GCE}$ -----	78
Figure 3.3:	Overlay of Nyquist plots of bare GCE and $p(\text{AspA})/\text{GCE}$ in $5.0 \times 10^{-5} \text{ M Ad}$ in 0.1 M NaOH in the frequency range $1.0 - 1.0 \times 10^5 \text{ Hz}$ at the corresponding oxidation potential ----	79
Figure 3.4:	Cyclic voltammograms of $2.0 \times 10^{-3} \text{ M } \text{K}_3[\text{Fe}(\text{CN})_6]$ on $p(\text{AspA})/\text{GCE}$ at scan rates 0.02 Vs^{-1} to 0.20 Vs^{-1} -----	80
Figure 3.5:	Cyclic voltammograms of $2.0 \times 10^{-3} \text{ M } \text{K}_3[\text{Fe}(\text{CN})_6]$ on GCE at scan rates 0.02 Vs^{-1} to 0.20 Vs^{-1} -----	80
Figure 3.6:	Overlay of DP voltammograms for the oxidation of $2.0 \times 10^{-5} \text{ M}$ to $1.2 \times 10^{-4} \text{ M Ad}$ on $p(\text{AspA})/\text{GCE}$ -----	81
Figure 3.7:	Calibration curve of Ad -----	81
Figure 3.8:	Overlay of LSV curves for the oxidation of $5.0 \times 10^{-4} \text{ M Ad}$ on $p(\text{AspA})/\text{GCE}$ at different scan rates ranging from 0.1 Vs^{-1} to 1.0 Vs^{-1} -----	82
Figure 3.9:	Overlay of DP voltammograms obtained in 1.5 mg mL^{-1} solution of HS DNA sample with those obtained on the addition of various concentrations of standard Ad solution ----	85
Figure 3.10:	a) Chronoamperograms obtained for the oxidation of various concentrations of Ad on $p(\text{AspA})/\text{GCE}$ with 0.1 M NaOH as supporting electrolyte. b) Plot of $I \text{ vs } t^{-1/2}$ at various concentrations of Ad -----	86
Figure 3.11:	Plot of slope ($I \text{ vs } t^{-1/2}$) against concentration of Ad -----	87

Figure 3.12:	Chronoamperograms obtained for the oxidation of various concentrations of Gu on <i>p</i> (AspA)/GCE with 0.1 M NaOH as supporting electrolyte. Inset shows corresponding I vs $t^{-1/2}$ plots -----	87
Figure 3.13:	Plot of slope of (I vs $t^{-1/2}$) against concentration of Gu -----	87
Figure 3.14:	Chronoamperograms obtained for the oxidation of various concentrations of Thy on <i>p</i> (AspA)/GCE with 0.1 M NaOH as supporting electrolyte. Inset shows corresponding I vs $t^{-1/2}$ plots -----	88
Figure 3.15:	Plot of slope (I vs $t^{-1/2}$) against concentration of Thy -----	88
Figure 3.16:	Chronoamperograms obtained for the oxidation of various concentrations of Cyt on <i>p</i> (AspA)/GCE with 0.1 M NaOH as supporting electrolyte. Inset shows corresponding I vs $t^{-1/2}$ plots -----	89
Figure 3.17:	Plot of slope (I vs $t^{-1/2}$) against concentration of Cyt -----	89
Figure 3.18:	Overlay of LSV curves for the oxidation of 5.0×10^{-5} M Gu, 1.0×10^{-3} M Thy and 5.0×10^{-3} M Cyt on <i>p</i> (AspA)/GCE at different scan rates -----	93
Figure 4.1:	Variation of peak parameters (1.0×10^{-4} M Thy in 0.1 M NaOH) with number of cycles of polymerization -----	101
Figure 4.2:	Overlay of SW voltammograms of 1.0×10^{-3} M Thy in 0.1 M NaOH on bare GCE and <i>p</i> (GA)/GCE -----	102
Figure 4.3:	Overlay of Nyquist Plots for bare GCE and <i>p</i> (GA)/GCE in 5.0×10^{-4} M Thy in the frequency range $1.0 - 1.0 \times 10^5$ Hz at the corresponding oxidation potential with 0.1 M NaOH as supporting electrolyte -----	103
Figure 4.4:	Overlay of cyclic voltammograms at different scan rates (0.02 Vs $^{-1}$ to 0.20 Vs $^{-1}$) for the oxidation of 2.0×10^{-3} M $K_3[Fe(CN)_6]$ on a) <i>p</i> (GA)/GCE b) bare GCE -----	103
Figure 4.5:	Overlay of SW voltammograms for the oxidation of 2.0×10^{-5} M to 2.0×10^{-4} M Thy (with incremental addition of 2.0×10^{-5} M Thy) and 3.0×10^{-4} M to 1.0×10^{-3} M Thy (in increments of 1.0×10^{-4} M Thy) on <i>p</i> (GA)/GCE -----	104
Figure 4.6:	Calibration plot for Thy -----	105
Figure 4.7:	Overlay of LSV curves for the oxidation of 1.0×10^{-3} M Thy in 0.1 M NaOH on <i>p</i> (GA)/GCE at different scan rates ranging from 0.1 Vs $^{-1}$ to 1.0 Vs $^{-1}$ -----	106

Figure 4.8:	Overlay of chronoamperograms obtained for the oxidation of 1.2×10^{-3} M to 2.4×10^{-3} M Thy in 0.1 M NaOH (incremental addition of 4.0×10^{-4} M Thy) on <i>p</i> (GA)/GCE ----	110
Figure 4.9:	Plot I vs $t^{-1/2}$ for 1.2×10^{-3} M to 2.4×10^{-3} M Thy in 0.1 M NaOH (with incremental addition of 2.0×10^{-4} M Thy) -----	110
Figure 4.10:	Plot of slope (I vs $t^{-1/2}$) against concentration of Thy-----	110
Figure 4.11:	Overlay of chronoamperograms obtained for various concentrations of Gu in 0.1 M NaOH on <i>p</i> (GA)/GCE. Inset shows the corresponding I vs $t^{-1/2}$ plots -----	111
Figure 4.12:	Plot of slope (I vs $t^{-1/2}$) against concentration of Gu -----	111
Figure 4.13:	Overlay of chronoamperograms obtained for various concentrations of Ad in 0.1 M NaOH on <i>p</i> (GA)/GCE. Inset shows the corresponding I vs $t^{-1/2}$ plots -----	112
Figure 4.14:	Plot of slope (I vs $t^{-1/2}$) against concentration of Ad -----	112
Figure 4.15:	Overlay of chronoamperograms obtained for various concentrations of Cyt in 0.1 M NaOH on <i>p</i> (GA)/GCE. Inset shows the corresponding I vs $t^{-1/2}$ plots-----	112
Figure 4.16:	Plot of slope (I vs $t^{-1/2}$) against concentration of Cyt-----	112
Figure 5.1:	Variation of peak parameters of 1.0×10^{-4} M Gu with number of cycles of polymerisation -----	120
Figure 5.2:	SW voltammograms of 3.0×10^{-4} M Ua, Gu and Ad on <i>p</i> (TSA)/GCE and GCE -----	121
Figure 5.3:	SW voltammograms of 3.0×10^{-4} M Ua, Gu and Thy on <i>p</i> (TSA)/GCE and GCE -----	121
Figure 5.4:	EIS Nyquist plots obtained on bare GCE and <i>p</i> (TSA)/GCE for 5.0×10^{-4} M concentrations of Gu, Ad, Thy and Ua in 0.1 M NaOH in the frequency range $1.0 - 1.0 \times 10^5$ Hz at the corresponding oxidation potential -----	122
Figure 5.5:	Cyclic voltammograms at different scan rates (0.02 Vs ⁻¹ to 0.20 Vs ⁻¹) for the oxidation of 2.0×10^{-3} M K ₃ [Fe(CN) ₆] on <i>p</i> (TSA)/GCE and bare GCE -----	123
Figure 5.6:	Plot of I vs $v^{1/2}$ for 2.0×10^{-3} M K ₃ [Fe(CN) ₆] at different scan rates -----	124
Figure 5.7:	SW voltammograms for the oxidation of various concentrations of Gu in 0.1 M NaOH on <i>p</i> (TSA)/GCE-----	125
Figure 5.8:	Variation of anodic peak current with concentration of Gu -----	125

Figure 5.9:	Calibration curve for Gu in the lower linear range -----	125
Figure 5.10:	SW voltammograms for the oxidation of various concentrations of Ad in 0.1 M NaOH on <i>p</i> (TSA)/GCE-----	126
Figure 5.11.	Variation of anodic peak current with concentration of Ad ----	126
Figure 5.12.	Calibration curve for Ad -----	126
Figure 5.13:	SW voltammograms of various concentrations of Thy in 0.1 M NaOH on <i>p</i> (TSA)/GCE-----	127
Figure 5.14:	Calibration curve for Thy -----	127
Figure 5.15:	Overlay of SW voltammograms for the oxidation of various concentrations of Ua on <i>p</i> (TSA)/GCE in 0.1 M NaOH -----	128
Figure 5.16:	Variation of anodic peak current with concentration of Ua ----	128
Figure 5.17:	Calibration curve for Ua-----	128
Figure 5.18:	Overlay of SW voltammograms of various equimolar solutions of Ua, Gu and Ad on <i>p</i> (TSA)/GCE in 0.1 M NaOH -----	129
Figure 5.19:	Calibration plot for simultaneous determination of Ua, Gu and Ad on <i>p</i> (TSA)/GCE -----	129
Figure 5.20:	SW voltammograms recorded in various equimolar solutions of Ua, Gu and Thy on <i>p</i> (TSA)/ GCE in 0.1 M NaOH -----	130
Figure 5.21:	Calibration plot for simultaneous determination of Ua, Gu and Thy on <i>p</i> (TSA)/ GCE -----	130
Figure 5.22:	Linear sweep voltammograms for the oxidation of 1.0×10^{-3} M Ua, Gu, Ad and Thy in 0.1 M NaOH on the <i>p</i> (TSA)/GCE at different scan rates-----	131
Figure 5.23:	Variation of oxidation current with concentration for Gu in presence of 1.0×10^{-4} M Ua and Ad. Inset shows the corresponding calibration curve-----	134
Figure 5.24:	Variation of oxidation current with concentration for Gu in presence of 1.0×10^{-4} M Ua and Thy. Inset shows the corresponding calibration curve-----	134
Figure 5.25:	Variation of oxidation current with concentration for Ua in presence of 1.0×10^{-5} M Gu and Ad. Inset shows the corresponding calibration curve -----	135
Figure 5.26:	Variation of oxidation current with concentration for Ua in presence of 1.0×10^{-5} M Gu and Thy. Inset shows the corresponding calibration curve -----	135

Figure 5.27:	Variation of oxidation current with concentration for Ad in presence of 5.0×10^{-5} M Gu and Ua. Inset shows the corresponding calibration curve-----	136
Figure 5.28:	Variation of oxidation current with concentration for Thy in presence of 1.0×10^{-4} M Gu and Ua. Inset shows the corresponding calibration curve-----	136
Figure 5.29:	SW voltammograms for various concentrations of DNA sample recorded on <i>p</i> (TSA)/GCE using 0.1 M NaOH as supporting electrolyte. Inset shows the variation of peak current with concentration of DNA solution -----	138
Figure 5.30:	Overlay of Chronoamperograms obtained on the <i>p</i> (TSA)/GCE for various concentrations of Gu, Ad, Thy and Cyt. The inset of each chronoamperogram shows the corresponding plot of <i>I</i> against $t^{-1/2}$ -----	141
Figure 5.31:	Plot of slope (<i>I</i> vs $t^{-1/2}$) against concentration for Gu, Ad, Thy and Cyt-----	141
Figure 5.32:	Overlay of chronoamperograms obtained for various concentrations of Ua in 0.1 M NaOH on <i>p</i> (GA)/GCE. Inset shows the corresponding <i>I</i> vs $t^{-1/2}$ plots -----	142
Figure 5.33:	Plot of slope (<i>I</i> vs $t^{-1/2}$) against concentration of Ua-----	142
Figure 6.1:	Effect of number of cycles of polymerisation on the anodic peak current of 5.0×10^{-5} M Ua, Gu and Ad in 0.1 M NaOH -----	151
Figure 6.2:	SW voltammograms for simultaneous oxidation of 5.0×10^{-5} M Ua, Gu and Ad in 0.1 M NaOH on <i>p</i> (ABSA)/GCE and GCE-----	152
Figure 6.3:	EIS Nyquist plots obtained on GCE and <i>p</i> (ABSA)/GCE for 5.0×10^{-4} M concentrations of Gu, Ad and Ua in 0.1 M NaOH in the frequency range 1.0 - 1.0×10^5 Hz at the corresponding oxidation potential-----	153
Figure 6.4:	Cyclic voltammograms obtained for the oxidation of 2.0×10^{-3} M $K_3[Fe(CN)_6]$ on bare GCE and <i>p</i> (ABSA)/GCE at different scan rates (0.02 Vs^{-1} to 0.20 Vs^{-1})-----	155
Figure 6.5:	SW voltammograms for the oxidation of different concentrations of Gu in 0.1 M NaOH on <i>p</i> (ABSA)/GCE. Inset shows variation of anodic peak current with concentration-----	156
Figure 6.6:	Calibration Curve for Gu-----	156

Figure 6.7:	Overlay of SW voltammograms for the oxidation of Ad on <i>p</i> (ABSA)/GCE-----	156
Figure 6.8:	Calibration Curve for Ad-----	156
Figure 6.9:	Overlay of SW voltammograms for the oxidation of Ua on <i>p</i> (ABSA)/GCE. Inset shows variation of anodic peak current with concentration -----	157
Figure 6.10:	Calibration Curve for Ua -----	157
Figure 6.11:	Overlay of SW voltammogram recorded in equimolar solutions of Ua, Gu and Ad on <i>p</i> (ABSA)/GCE in 0.1 M NaOH -----	158
Figure 6.12:	Variation of peak current with concentration of Ua, Gu and Ad on <i>p</i> (ABSA)/ GCE -----	158
Figure 6.13:	Linear sweep voltammograms for the oxidation of 1.0×10^{-3} M Gu, Ad and Ua in 0.1 M NaOH on the <i>p</i> (ABSA)/GCE at different scan rates -----	159
Figure 6.14:	Variation of oxidation current with concentration for an analyte in presence of a specific concentration of the other two-----	162
Figure 6.15:	Overlay of SW voltammograms for various concentrations of DNA sample recorded on <i>p</i> (ABSA)/GCE using 0.1 M NaOH as supporting electrolyte-----	164
Figure 6.16:	Chronoamperograms obtained for the oxidation of various concentrations of Gu and Ua on <i>p</i> (ABSA)/GCE with 0.1 M NaOH as supporting electrolyte. Inset of each chronoamperogram shows the corresponding plot of I vs $t^{-1/2}$ -----	165
Figure 7.1:	Variation of peak currents of 5.0×10^{-4} M Ua, Gu, Ad and Cyt in 0.1 M NaOH with number of cycles of polymerisation----	173
Figure 7.2:	SW voltammogram for simultaneous oxidation of 5.0×10^{-5} M Ua, Gu, Ad and Cyt on <i>p</i> (AHNSA)/GCE and GCE -----	174
Figure 7.3:	EIS Nyquist plots obtained for bare GCE and <i>p</i> (AHNSA)/GCE in 5.0×10^{-4} M Ua, Gu, Ad and Cyt in 0.1 M NaOH-----	175
Figure 7.4:	Overlay of cyclic voltammograms obtained for the oxidation of 2.0×10^{-3} M $K_3[Fe(CN)_6]$ on <i>p</i> (AHNSA)/GCE and bare GCE at different scan rates -----	176

Figure 7.5:	Overlay of SW voltammograms of different concentrations of Gu on <i>p</i> (AHNSA)/GCE. Inset shows the variation of peak current with concentration -----	177
Figure 7.6:	Calibration plot for Gu on <i>p</i> (AHNSA)/GCE -----	177
Figure 7.7:	Overlay of SW voltammograms of different concentrations of Ad on <i>p</i> (AHNSA)/GCE. Inset shows the variation of peak current with concentration -----	178
Figure 7.8:	Calibration plot for Ad on <i>p</i> (AHNSA)/GCE -----	178
Figure 7.9:	Overlay of SW voltammograms of different concentrations of Thy on <i>p</i> (AHNSA)/GCE. Inset shows the variation of peak current with concentration -----	179
Figure 7.10:	Calibration plot for Thy on <i>p</i> (AHNSA)/GCE -----	179
Figure 7.11:	Overlay of SW voltammograms for the oxidation of Cyt on <i>p</i> (AHNSA)/GCE. Inset shows the variation of peak current with concentration -----	179
Figure 7.12:	Calibration plot for Cyt on <i>p</i> (AHNSA)/GCE-----	179
Figure 7.13:	Overlay of SW voltammograms of different concentrations of Ua on <i>p</i> (AHNSA)/GCE. Inset shows the variation of peak current with concentration -----	180
Figure 7.14:	Calibration plot for Ua on <i>p</i> (AHNSA)/GCE-----	180
Figure 7.15:	Overlay of SW voltammograms recorded in equimolar solutions of Ua, Gu, Ad and Cyt using <i>p</i> (AHNSA)/GCE -----	181
Figure 7.16:	Calibration plot for the simultaneous determination of Ua, Gu, Ad and Cyt on <i>p</i> (AHNSA)/GCE -----	181
Figure 7.17:	Variation of oxidation current with concentration for an analyte in presence of a specific concentration of the other three recorded on <i>p</i> (AHNSA)/GCE-----	182
Figure 7.18:	Linear sweep voltammograms of 1.0×10^{-3} M concentrations of Gu, Ad, Thy and Cyt on <i>p</i> (AHNSA)/GCE at different scan rates -----	187
Figure 7.19:	Overlay of linear sweep voltammograms of 1.0×10^{-3} M Ua on <i>p</i> (AHNSA)/GCE at different scan rates -----	187
Figure 7.20:	Overlay of chronoamperograms obtained for various concentrations of Gu, Ad, Thy and Cyt. Inset I) of each overlay shows the corresponding I vs $t^{-1/2}$ plots and Inset II) shows the plot of $\frac{dI}{dt^{-1/2}}$ vs C -----	190

Figure 7.21:	Overlay of chronoamperograms obtained for various concentrations of Ua. Inset I) shows the corresponding I vs $t^{-1/2}$ plot and Inset II) shows the plot of $\frac{dI}{dt^{-1/2}}$ vs C -----	191
Figure 8.1:	SW voltammograms for the oxidation of 5.0×10^{-5} M XT, TP and CF on(a) bare GCE and (b) $p(\text{ABSA})/\text{GCE}$ (0.1 M PBS pH 7)-----	201
Figure 8.2:	Nyquist plots obtained on bare and modified GCE for 5.0×10^{-4} M concentrations of XT, TP and CF (0.1 M PBS pH 7)---	202
Figure 8.3:	SW voltammograms for the oxidation of different concentrations of XT on $p(\text{ABSA})/\text{GCE}$ (0.1 M PBS pH 7). Inset shows variation of anodic peak current with concentration-----	204
Figure 8.4:	Calibration plot for XT in the lower linear range -----	204
Figure 8.5:	SW voltammograms for the oxidation of different concentrations of TP on $p(\text{ABSA})/\text{GCE}$ (0.1 M PBS pH 7). Inset shows variation of anodic peak current with concentration-----	205
Figure 8.6:	Calibration plot for TP -----	205
Figure 8.7:	SW voltammograms for the oxidation of different concentrations of CF on $p(\text{ABSA})/\text{GCE}$ (0.1 M PBS pH 7). Inset shows variation of anodic peak current with concentration-----	206
Figure 8.8:	Calibration plot for CF -----	206
Figure 8.9:	Overlay of SW voltammograms for the simultaneous electro-oxidation of XT, TP and CF in 0.1 M PBS pH 7 on the $p(\text{ABSA})/\text{GCE}$ at various concentrations. Inset shows the magnification of the overlay of SWV for the electro-oxidation of XT-----	206
Figure 8.10:	Calibration plot for XT when determined simultaneously with TP and CF -----	207
Figure 8.11:	Calibration plot for TP and CF when determined simultaneously with XT -----	207
Figure 8.12:	Overlay of SW voltammograms for the oxidation of various concentrations of XT(I), TP (II) and CF (III) in presence of 5.0×10^{-5} M concentrations of the other two. Inset of each graph shows the corresponding calibration plot -----	208

- Figure 8.13: Overlay of SW voltammograms obtained on the $p(\text{ABSA})/\text{GCE}$, for the oxidation of various equimolar solutions of Ua, XT, TP and CF in 0.1 M PBS pH 7 -----210
- Figure 8.14: Calibration plot for the simultaneous determination of Ua, XT, TP and CF -----210
- Figure 8.15: SW voltammograms for the oxidation of different concentrations of Ua in 0.1 M PBS pH 7, on $p(\text{ABSA})/\text{GCE}$. Inset shows variation of anodic peak current with concentration -----210
- Figure 8.16: Calibration plot for Ua-----210
- Figure 8.17: Chronoamperograms obtained for the oxidation of various concentrations of XT, TP and CF on $p(\text{ABSA})/\text{GCE}$ with 0.1 M PBS pH 7 as supporting electrolyte. Inset of each chronoamperogram shows the corresponding plot of I vs $t^{-1/2}$ -----217

LIST OF SCHEMES

Scheme 2.1:	Formation of <i>p</i> (AspA) on GCE -----	51
Scheme 2.2:	<i>p</i> (GA)/GCE -----	55
Scheme 2.3:	<i>p</i> (TSA)/GCE -----	58
Scheme 2.4:	Electropolymerisation of ABSA on GCE -----	61
Scheme 3.1:	Possible mechanism of electro-oxidation of Ad on <i>p</i> (AspA)/GCE-----	83
Scheme 4.1:	Possible electrochemical reaction at the <i>p</i> (GA)/GCE -----	107
Scheme 5.1:	Electro-oxidation of Gu, Ad, Thy and Ua on <i>p</i> (TSA)/GCE -----	133
Scheme 6.1:	Electro-oxidation of Gu, Ad and Ua on <i>p</i> (ABSA)/GCE-----	161
Scheme 7.1.	Electro-oxidation of Gu, Ad, Thy and Cyt on <i>p</i> (AHNSA)/GCE -----	189
Scheme 8.1:	Electro-oxidation of XT, TP and CF on <i>p</i> (ABSA)/GCE-----	215

Chemical analysis is a fundamental requirement for all scientific studies and is indispensable for doctors, farmers, pharmacists, geologists, technologists etc. to name a few. This makes analytical chemistry as important as any branch of chemistry, applied or theoretical. Analytical chemistry employs physical, chemical and mathematical principles to obtain results, thus making it almost an independent discipline in its own right. At present the field has evolved much, from the classical methods to instrumental methods. Among the instrumental methods, electroanalytical methods are particularly significant. Electroanalysis is capable of obtaining real-time information with minimum impact to the environment. It can be considered as an analytical method which keeps in tune with the principles of green chemistry. Electroanalysis can be carried out using electrodes made of non-toxic materials and green solvents. As the sample volume required is very small, the waste generation is greatly reduced. The versatile electroanalytical detection system, with its high sensitivity and possibility of miniaturisation, can be easily adapted into analytical microsystems.

1.1 Electroanalytical Chemistry

The use of electrochemical principles for the qualitative and quantitative analysis of chemical species can be termed as electroanalytical chemistry or electroanalysis and the experimental methods used for such analyses, electroanalytical methods. Electroanalysis makes use of the interplay between electrical quantities like current **I**, Potential **V** or charge **Q** and chemical reactions for making inferences [1]. Electrochemistry which converts chemical information into electrical signals which are detectable by simple and cost-effective instrumentation [2] provides an attractive tool for

the analytical chemist. In addition to quantitative and qualitative analysis, electroanalytical methods can be used to obtain time-dependent information on kinetics of reactions [3]. Electrochemical methods of analysis, in comparison to other instrumental methods provide rapid, comparatively less expensive, sensitive and selective characteristic information about molecules and chemical systems along with qualitative and quantitative as well as thermodynamic and kinetic data [4]. They also offer options for miniaturisation, thus enabling real time analysis. Further, electrochemical methods of analysis require the use of very small quantities of solvents and reagents.

Based on the type of electrical signal used for quantitation, electroanalytical methods can be either potentiostatic or controlled potential methods or potentiometric or controlled current methods [1]. Potentiostatic electroanalytic methods are *conductometry*, *voltammetry*, *amperometry* as well as *coulometry*; whereas *potentiometry* and *coulometric titrations* are controlled current methods. Electroanalytical methods require at least two electrodes made of electrically conducting materials immersed in an electrolytic solution forming an electrochemical cell. The electrode which responds to the analyte is called the *working* or *indicator* electrode and the other which maintains a constant potential is called the *reference electrode*. Such a cell may be either *electrolytic*, consuming electrical energy to cause an electrochemical reaction or *galvanic*, producing electrical energy from electrochemical reaction.

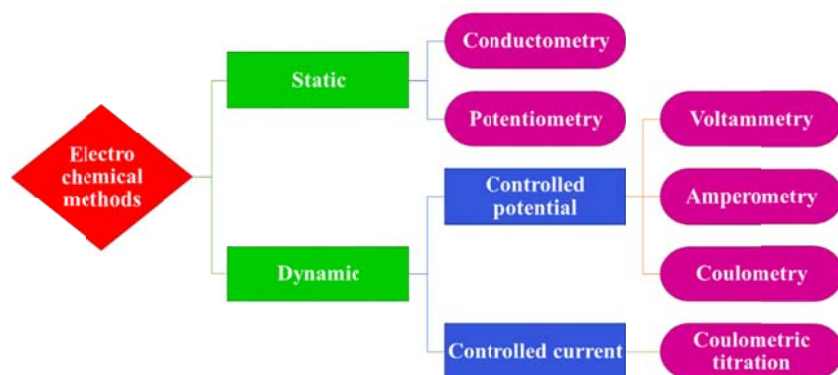


Figure 1.1: Classification of electrochemical methods

In *conductometry*, an AC voltage is applied between two electrodes immersed in a solution and the current developed is a measure of the electrolytic conductivity of the solution. In *voltammetry*, current flowing through a cell is measured as a function of the applied potential whereas in *amperometry*, current is measured at a fixed potential. *Coulometry* involves measuring the charge required for controlled potential electrolysis of the analyte, quantitatively to another oxidation state. The measurement of equilibrium potential of an indicator electrode against a reference electrode at zero current conditions is carried out in *potentiometry*. *Coulometric titration* also known as *amperostatic coulometry* involves maintaining a constant current through the cell by means of an amperostat, until the signal indicates completion of the reaction with the analyte [5].

1.2 Voltammetry

The term voltammetry was first used by Kolthoff in 1940, combining the units of the electrical parameters measured, **volt-ampere-metry** [6]. The term is used for all the methods in which the current flowing through an electrochemical cell is measured as a function of the applied potential. In voltammetry, current is measured under the condition of complete

concentration polarisation, i.e., the rate of the electrochemical reaction of the analyte is limited by the rate of mass transfer from the bulk solution to the electrode surface.

1.2.1 Voltammetric Cell

A typical voltammetric cell consists of three electrodes; working electrode, reference electrode and the counter electrode; dipping into an electrolyte solution, completing a circuit. A potentiostat controls the applied potential with minimum interference from ohmic drop and the current flowing through the cell is monitored. The electrochemical reaction of interest takes place at the working electrode, the potential of which is measured against the reference electrode. To minimize the current flowing through the reference electrode (thereby minimizing the polarisation of the reference electrode) and to keep the distribution of applied potential between the working and reference electrodes, the current is measured between the working electrode and a counter electrode.

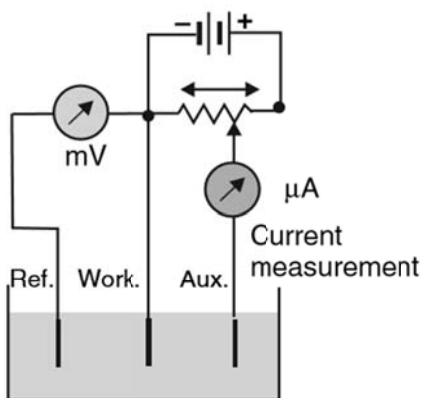


Figure 1.2: Representation of a three electrode voltammetric cell [5]

1.2.2 Reference electrode

Reference electrode has a well-known and stable electrode potential which does not vary with the composition of the analyte solution or on application of an external potential. The standard hydrogen electrode is the reference electrode whose potential is assumed to be zero. The potentials of other reference electrodes like silver-silver chloride (Ag/AgCl) electrode, calomel electrode and quinhydrone electrode are measured with respect to the standard hydrogen electrode [7].

1.2.3 Counter or Auxiliary electrode

An electrochemical cell employing a three-electrode system makes use of a counter or auxiliary electrode to measure the current flowing through the cell. This is to avoid current passage through the reference electrode which will alter its electrode potential. For an electrode to be used as a counter electrode it should not dissolve in the medium of the cell and its area should be larger than that of the working electrode to ensure that the area of the electrode will not control the limiting current [7]. Platinum wire/coil/thin foil or Titanium wire are most commonly used as counter electrodes. Carbon rods are also used in molten salt media.

1.2.4 Working electrode or Indicator electrode

The electrode at which the electrochemical reaction of analyte takes place is the working electrode. Ideally the working electrode should possess the following characteristics [7],

- Electrochemical inertness over a broad potential window
- High overvoltage towards hydrogen and oxygen evolution

- Low ohmic resistance
- Easy regeneration of the electrode surface
- Stable and non-toxic

The geometry of the working electrode is very important in determining its utility in voltammetric analysis. Working electrodes may be microelectrodes or ultramicroelectrodes, stationary or rotating, planar disk or planar ring, screen printed strip or thin film chips. Depending on the specific purpose any of these electrodes may be chosen as working electrode for electrochemical measurements.

Generally working electrodes are of four major types [8],

1. Inert metal electrodes: Mercury, Gold, Platinum etc.
2. Inert carbon electrodes: Pyrolytic graphite, Carbon paste, Glassy carbon, Diamond etc.
3. Reactive electrodes: Iron, Nickel, Copper etc.
4. Photo-excitabile electrodes: Silicon, Titanium dioxide, Zinc oxide etc.

In the work presented in this thesis glassy carbon electrode is used as the working electrode.

1.2.4.1 Glassy Carbon Electrode (GCE)

Glassy carbon, because of its exceptional mechanical and electrical properties, chemical inertness to solvents, broad working potential window and reproducible performance, is an attractive option as working electrode material [1]. It is prepared from a pre-modelled phenol-formaldehyde resin by subjecting it to a carefully controlled heating program. The structure of glassy carbon involves thin, tangled ribbons of cross-linked graphite-like

sheets. Before use, the glassy carbon electrode is subjected to surface pre-treatment to create active sites and improve its analytical performance. The pre-treatment involves polishing the surface to a mirror like finish using alumina particles of 0.05 microns size followed by rinsing in de-ionised water [1].

1.2.4.2 Chemically Modified Electrodes (CME)

The working electrodes described so far, in their native or bare form were not always suitable to meet many electrochemical requirements [9]. Their performance was limited by high overpotentials, persistent surface fouling, low sensitivity and selectivity. These factors drove the electrochemists to modify the surface of conventional electrodes with species which allowed them to tailor specific structural and electronic properties on to the surface to suit their needs. The resulting electrodes are called Chemically Modified Electrodes (CME). The IUPAC has defined CME as “an electrode made of a conducting or semiconducting material that is coated with a selected monomolecular, multimolecular, ionic, or polymeric film of a chemical modifier and that by means of faradaic (charge-transfer) reactions or interfacial potential differences (no net charge transfer) exhibits chemical, electrochemical, and/or optical properties of the film” [10]. The functionalization of electrode surface with molecular reagents find applications in energy conversion, electrochemical synthesis, microelectronic devices etc.

Surface modification of an electrode can be achieved by adsorption, chemical reaction or formation of a polymer layer [11]. Adsorption happens when certain species discover the electrode surface more hospitable than the bulk solution and hence gets attached to the surface spontaneously. For

example, organic species, that have double bonds, are often hydrophobic and chemically adsorb from aqueous solutions on to the surface of carbon or platinum electrodes [12]. Certain organometallic complexes as well as materials like carbon nanotubes (CNT), activated charcoal, carbon black, chitosan etc. can be physisorbed on to solid electrode surfaces by coating a non-aqueous solution of the material followed by solvent evaporation.

Chemical reaction can be carried out on the surface of the electrode resulting in covalent attachment of the modifier on to the electrode surface. Monolayers of alkanethiols can be attached on gold surfaces due to the strong interaction between gold and sulfur [1]. Such monolayers are commonly formed by immersing the gold electrode overnight in millimolar ethanolic solutions of alkanethiol. Nanoparticles can be electrodeposited onto the electrode surface thereby, altering the electrode properties significantly.

A common approach for incorporating a modifier onto the electrode surface has been coverage with an appropriate polymer film. Polymer modified electrodes can be prepared either by casting a solution droplet containing the dissolved polymer onto the surface and allowing the solvent to evaporate or by dip or spin coatings. Electropolymerisation in the presence of the dissolved monomer is another approach for fabricating polymer modified electrode. Electropolymerisation allows control of the film thickness and morphology, and is particularly useful to fabricate miniaturized sensor surfaces [1].

1.2.5 Solvent and supporting electrolyte

Electrochemical measurements are carried out in a medium which consists of a supporting electrolyte dissolved in a solvent. The solvent

should not react chemically with the analyte or products and should be electrochemically inactive over a broad potential window. Double distilled water is the most widely used solvent in electrochemical cells. For electrochemical measurements in non-aqueous medium, organic solvents such as methanol, acetonitrile, dimethyl formamide or dimethyl sulfoxide are also used. Such solvents should be purified and dried before use [1].

In potentiostatic experiments, a supporting electrolyte must be used to eliminate electro-migration effects. The supporting electrolyte should also be electrochemically inert in the potential window under investigation. It should be in large excess concentration in comparison to the electroactive species. Typically supporting electrolyte concentrations are in the range 0.1 M to 1.0 M. When water is used as the solvent, inorganic salts, mineral acids or buffers are used as supporting electrolyte. Tetra alkyl ammonium salts are used in organic medium [1].

1.3 Electrode Processes

The term ‘electrode processes’ encompasses all changes and processes taking place at the surface of electrode or its vicinity while current is flowing through the electrochemical cell. Electrode processes consist of the electrode reaction and the mass transport processes [11]. The electrode reaction involves the transfer of electron between an electrode and the species in solution. It occurs via quantum mechanical tunnelling between the electrode and analyte close to the electrode [13]; i.e., the electrode reaction is a heterogeneous process. For the electrode reaction to take place, the species should be transported to the electrode surface. The transport can take place by any of the following processes.

- Diffusion of electroactive species in response to the concentration gradient.
- Convection of species in response to mechanical stirring of the solution.
- Migration of electroactive species in response to the electrostatic attraction with the electrode.

In voltammetric methods of analysis, conditions are so created in solution that, mass transport by the migration and convection of species in solution is prevented. This is achieved by the addition of a large excess of an inert electrolyte called supporting electrolyte and keeping the solution unstirred respectively. In such a case, the current developed is termed diffusion controlled limiting current. That is, current flowing through the cell is a function of concentration of the bulk solution, making possible quantitative determination by measurement of current.

When a potential is initially applied between the electrodes, there is an accumulation of oppositely charged species at the vicinity of the electrode surface. The charged solution consists of two parts.

1. A compact inner layer where the potential decreases linearly with distance from the electrode surface.
2. A diffuse or loosely bound outer layer where the potential decrease is exponential.

This entire array of charged species and oriented dipoles at the electrode-electrolyte interface is called electrical double layer [14].

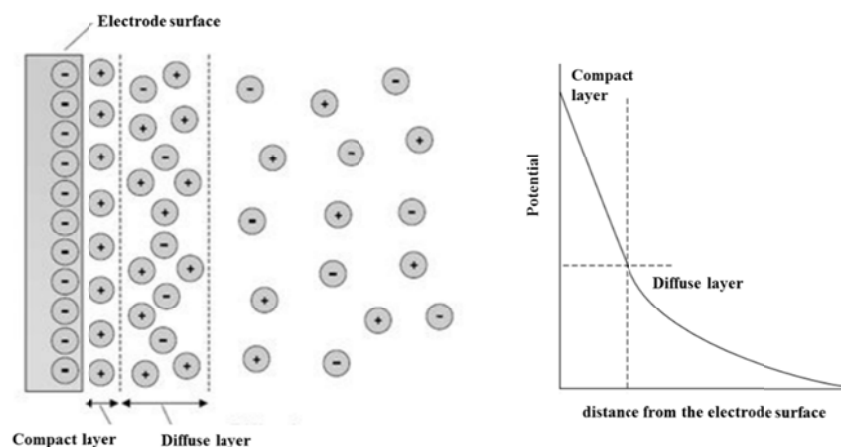


Figure 1.3: Electrical double layer and the variation of potential across it[14]

The current which is developed due to the charging of the electrical double layer is called charging current or residual current. This is a non-faradaic current. Faradaic current is that which arises from the redox reactions at the working and counter electrodes and is proportional to the concentration of the electroactive species in solution.

1.4 Voltammetric Techniques

Voltammetry finds application in a variety of fields such as inorganic chemistry, physical chemistry, and biological studies for quantitative or qualitative application as well as, for study of reaction mechanism, properties of systems, kinetic studies, redox activity, thermodynamic properties etc. Voltammetry offers a large number of techniques which can be used for specific purposes. The most common voltammetric techniques are described here.

- Polarography
- Cyclic Voltammetry (CV) and Linear Sweep Voltammetry (LSV)

- Pulse Voltammetry – Normal Pulse Voltammetry (NPV), Differential Pulse Voltammetry (DPV) and Square Wave Voltammetry (SWV)
- Stripping Voltammetry – Cathodic Stripping Voltammetry (CSV) and Anodic Stripping Voltammetry (ASV), Adsorptive stripping Voltammetry (AdSV)
- Chronoamperometry

These techniques are detailed in the following section.

1.4.1 Polarography

Polarography is the technique where the current is monitored when a potential is applied to a cell consisting of a large quiescent mercury anode, a small dropping mercury electrode (DME) as cathode and a dilute solution of the electroactive material under consideration. Polarography is widely used for the determination of reducible species due to its special properties such as wide cathodic potential range and constantly renewable surface. Polarography which was developed in 1922 by the Czech chemist Jaroslav Heyrovsky, is the fore-runner of voltammetry. Heyrovsky received the Noble Prize in Chemistry in the year 1959 for his discovery of polarography. In conventional polarography, the working electrode is subjected to a linearly increasing potential ramp. At a sufficiently negative potential, reduction of the analyte starts, thereby creating a concentration gradient and the current rises rapidly to its limiting value [1]. The current against potential response of a polarographic experiment known as the polarogram, is a sigmoid curve. The plateau of the sigmoid curve represents the diffusion controlled limiting current, **I** measured in Amperes (A) and is related to the concentration, **C** in molcm^{-3} , by the Ilkovic equation [1],

$$I = 708nD^{1/2} m^{2/3} t^{1/6} C$$

where **D** is the diffusion coefficient in cm^2s^{-1} , **m** is the rate of flow of mercury through the capillary in gs^{-1} , **t** is the drop time in **s** and **C** is the bulk analyte concentration.

Even though polarography is very useful for the determination of analytes which undergo reduction at potentials in the negative regime, it is not useful for analytes undergoing electrochemical reaction at higher positive potentials.

1.4.2 Cyclic Voltammetry (CV)

CV is the most widely used voltammetric technique to obtain rapid qualitative information regarding thermodynamics of redox processes, along with the kinetics of heterogeneous electron transfer reactions and coupled chemical reactions or adsorption processes. In CV, the potential at the working electrode is scanned linearly using a triangular waveform in both forward and reverse directions, while monitoring the current. If initial scan is in positive direction, at switching potential the scan will be reversed and run in the negative direction. If the scan is not reversed, then the technique is called linear sweep voltammetry (LSV). During the potential sweep, the potentiostat measures the current resulting from the applied potential. The measured current versus applied potential plot is termed as cyclic voltammogram.

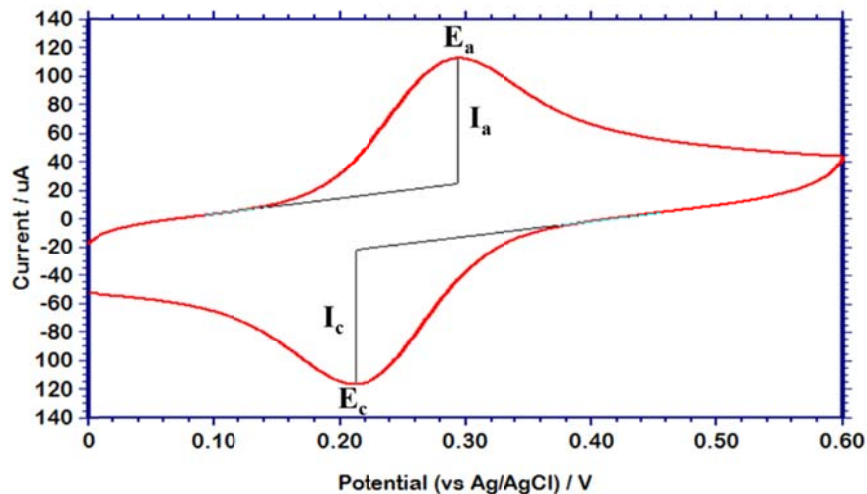


Figure 1.4: Cyclic voltammogram of a perfectly reversible reaction

The main features of a typical cyclic voltammogram are the parameters peak current I , (I_c cathodic peak current and I_a anodic peak current) and the peak potential E (E_c cathodic peak potential and E_a anodic peak potential). Data interpretation of a cyclic voltammogram is based on the electrochemical nature of the species under investigation.

For reversible systems, where electron transfer rate is very fast compared to diffusion and characterised by peaks in the forward and reverse scan, the separation between the redox peaks is given by [15],

$$\Delta E = E_a - E_c = \frac{0.059}{n}$$

where n is the number of electrons involved in the electrode reaction.

For such systems, the peak current I is related to the concentration C by the Randles - Sevcik expression [13],

$$I = 2.69 \times 10^5 a n^{3/2} D^{1/2} C v^{1/2}$$

where \mathbf{a} refers to the surface area of electrode (cm^2), \mathbf{D} refers to the diffusion coefficient (cm^2s^{-1}), \mathbf{C} refers to the concentration (molcm^{-3}) and \mathbf{v} refers to the scan rate (Vs^{-1}).

For irreversible systems, peak current \mathbf{I} , is related to the concentration \mathbf{C} by the Randles - Sevcik expression [13],

$$\mathbf{I} = 2.99 \times 10^5 \mathbf{a} \mathbf{n}(\alpha \mathbf{n}_\alpha)^{1/2} \mathbf{D}^{1/2} \mathbf{C} \mathbf{v}^{1/2}$$

where \mathbf{n}_α refers to the number of electrons taking part in the rate determining step and α denotes the charge transfer coefficient which is equal to

$$\alpha = \frac{0.047}{(\mathbf{E} - \mathbf{E}_{1/2}) \mathbf{n}_\alpha}$$

$\mathbf{E}_{1/2}$ being the half peak potential i.e, the potential at half the peak maximum [16]. The value of \mathbf{n}_α is calculated from the Tafel slope [16] (slope of \mathbf{E} vs $\ln \mathbf{I}$ or half the slope of \mathbf{E} vs $\ln \mathbf{v}$)

$$\text{Tafel slope} = \frac{\mathbf{RT}}{2\alpha \mathbf{n}_\alpha \mathbf{F}}$$

1.4.3 Pulse Voltammetry

These techniques introduced by Barker and Jenkin, are particularly useful for the detection of very low concentrations by increasing the ratio between faradaic and non-faradaic currents [1]. The main principle of pulse techniques is to measure the currents at a time when the difference between the desired faradaic current and the non-faradaic charging current is high [14]. The charging current decays exponentially whereas the faradaic current decays as a function of $\mathbf{t}^{-1/2}$ [17]. The difference between various pulse techniques is in the excitation wave form and the current sampling regime.

1.4.3.1 Normal Pulse Voltammetry (NPV)

A series of potential pulses of increasing amplitude is applied to the electrode and resulting current is measured at the end of each pulse, thereby allowing charging current to decay [18].

1.4.3.2 Differential Pulse Voltammetry (DPV)

In DPV, the potential is scanned in a series of pulses of small, fixed amplitude and is superimposed on a slowly changing base potential. The current is measured twice during each pulse; just before the application of the pulse and at the end of the pulse and this difference is plotted against the base potential to obtain the voltammogram. The sampling points are selected to allow the charging current to decay [18]. The background contribution is ten times smaller than that in NPV and hence measurements at concentrations as low as 10^{-8} M is possible with DPV. The width of the differential pulse voltammetric peak ($W_{1/2}$) is related to the electron stoichiometry [1],

$$W_{1/2} = \frac{3.52 RT}{nF}$$

1.4.3.3 Square Wave Voltammetry (SWV)

SWV is an extremely versatile pulse technique invented by Ramaley and Krause and developed extensively by Osteryoung and co-workers. It combines the best aspects of various pulse techniques including the sensitivity and better background current suppression of DPV and the diagnostic value of NPV. This technique offers access to a wider range of time scales [16]. The excitation signal in SWV consists of symmetrical square-wave (SW) pulses superimposed on a staircase waveform, where in the forward pulse the signal matches with the staircase step. The current is

measured twice during each square-wave cycle, once at the end of the forward pulse and once at the end of the reverse pulse. The difference between the two measurements is plotted against the base staircase potential. High sensitivity of this technique is because the net current is larger than either the forward or reverse components, since it is the difference between them. The square-wave currents are almost four times higher than the analogous differential-pulse response [1].

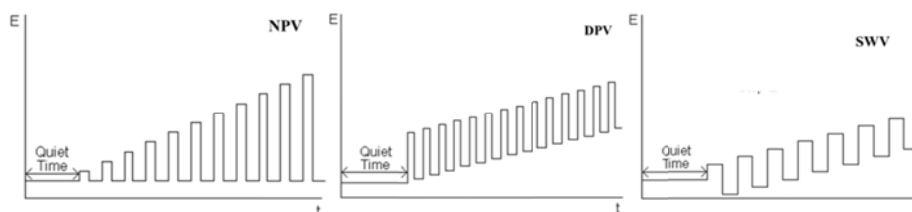


Figure 1.5: Excitation signal form of various pulse voltammetric techniques [14]

1.4.4 Stripping Voltammetry

In stripping voltammetric techniques, the analyte is first deposited on a working electrode from a stirred solution for a fixed time after which the deposited analyte is stripped from the electrode by any of the other voltammetric techniques [14]. Based on whether the working electrode acts as an anode or cathode during the stripping step, stripping voltammetry is either anodic stripping voltammetry (ASV) or cathodic stripping (CSV). ASV is used for the determination of metals even in trace amounts whereas CSV is used for the determination of substances that form insoluble salts with mercurous ion (DME as working electrode). A third type of stripping method is the adsorptive stripping voltammetry (AdSV) where deposition of analyte on the electrode is accomplished by adsorption on the electrode surface or by specific reactions at chemically modified electrodes rather than electrolysis. Nanomolar detections are achieved with stripping analysis

[12]. However, the capacity of electrodes for analyte accumulation is limited and the condition of linearity with concentration is satisfied only well below the electrode saturation [11].

1.4.5 Chronoamperometry

Chronoamperometry is a transient voltammetric technique where the current response is dependent on time [11]. In this technique, the potential at a stationary working electrode is stepped up suddenly from a potential at which no faradaic reaction occurs to one at which the surface concentration of the electro-active species is zero. The current–time dependence resulting from the step up is monitored. Under these conditions, the mass transport in the cell is exclusively by diffusion and hence the current–time plot reflects the change in concentration gradient near electrode surface. This involves a gradual expansion of the diffusion layer associated with the depletion of the reactant [1]. Consequently, the current decays with time following the Cottrell equation [19],

$$I = nFaD^{1/2}C\pi^{-1/2}t^{-1/2} = kt^{-1/2}$$

where **n** is the number of electrons involved in the electrode reaction, **a** is the surface area of electrode in cm^2 , **F** is the Faraday's constant (96500 coulombs), **D**, the diffusion coefficient of the electroactive species in cm^2s^{-1} and **C** is the concentration of electroactive species in mole cm^{-3} . Chronoamperometry is often used for measuring the diffusion coefficient of electroactive species or the surface area of the working electrode or the catalytic rate constant.

1.5 Electrochemical Impedance Spectroscopy (EIS)

EIS is a different type of electrochemical technique generally used for characterising electrode surfaces or to study the rates of electrochemical reactions. This technique is also used for the development of sensors. Impedance, Z is the frequency dependent resistance encountered when current flows through a circuit made of combinations of resistors, capacitors, or inductors. Electrochemical transformations occurring at the electrode–solution interface can be modelled using components of an electronic equivalent circuit. Generally, the electrode-electrolyte interface resembles Randles circuit or Randles-Ershler circuit, which includes the double-layer capacitance C_{dl} , the ohmic resistance of the electrolyte solution R_s , the charge transfer resistance R_{ct} , and the Warburg impedance W resulting from the diffusion of ions from the bulk solution to the electrode surface.

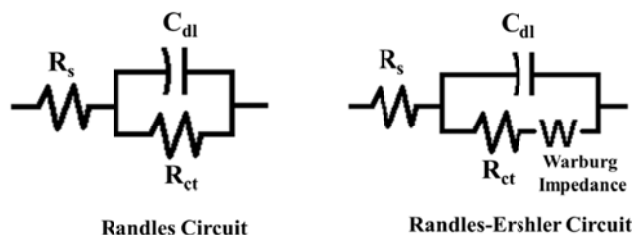


Figure 1.6: Equivalent electronic circuits that fit experimental impedance spectra

The impedance Z , encountered at an electrode electrolyte interface consists of a real part Z' and an imaginary part Z'' . During EIS measurement, small sinusoidal currents of definite frequencies are applied to the electrode and Z' and Z'' are measured at each frequency. The plot of Z' vs Z'' is known as Nyquist plot or Impedance spectra. Nyquist plots usually include a semicircle region followed by a straight line. The semicircle portion which is observed at higher frequencies corresponds to the electron-

transfer-limited process, while the straight line which is observed at low-frequencies represent the diffusion-limited process. Nyquist plots can be used for extracting the electron transfer kinetics and diffusional characteristics. In the case of very fast electron transfer processes the impedance spectrum includes only the linear part, while very slow electron transfer processes are characterized by a large semicircular region. The diameter of the semicircle equals the charge/electron transfer resistance R_{ct} . The value of R_{ct} can be used to calculate the value of the standard heterogeneous electron transfer rate constant k_h by the equation [16],

$$k_h = \frac{RT}{n^2 F^2 R_{ct} a C}$$

where n is the number of electrons involved in the electrode reaction, a is the surface area of electrode in cm^2 , F is the Faraday's constant (96500 coulombs), and C is the concentration of electroactive species in mole cm^{-3} . R and T have their usual meanings.

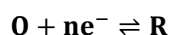
1.6 Kinetics of electrochemical reactions

The kinetics of electrochemical reaction are strongly dependent on the structure of the electrical double layer and in turn the double layer is influenced by the electrode material [20]. The kinetics of electrochemical reactions are described mainly in terms of k_h , the *standard heterogeneous electron transfer rate constant* and α , the *charge transfer coefficient*. k_h is a measure of the kinetic facility of a redox couple. A system with large k_h , will reach equilibrium rapidly and the one with small k_h , will be sluggish [16]. The value of k_h reflects the facility of reaction between a particular reactant and the electrode material used. α is a measure of the fraction of energy that is used to lower the activation energy [1].

1.6.1 Reversible kinetics

Electrochemical reversibility signifies compliance with Nernst equation and such systems are called Nernstian systems [18]. In such systems rate of electron transfer is much higher than rate of mass transport. Reversible reactions are characterised by peaks in both forward and backward scans in a cyclic voltammogram.

In Butler-Volmer model [16] of electrode kinetics for a general reversible reaction of the type,



the anodic and cathodic rate constants are given by,

$$\mathbf{k}_a = \mathbf{k}_h e^{\left[\frac{\alpha_a n F (E - E^0)}{RT} \right]}$$

$$\mathbf{k}_c = \mathbf{k}_h e^{\left[\frac{-\alpha_c n F (E - E^0)}{RT} \right]}$$

where \mathbf{k}_h is the standard heterogeneous rate constant of the reversible reaction and E^0 is the formal potential of the redox system. α_a and α_c represents the anodic and cathodic charge transfer coefficients respectively. The value of α_a and α_c can be determined from the equations [21],

$$E_a = a + \left[\frac{2.303RT}{\alpha_a n F} \right] \log v$$

$$E_c = b - \left[\frac{2.303RT}{\alpha_c n F} \right] \log v$$

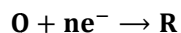
Where v is the scan rate, a and b are constants, in accordance with the Tafel equation [16],

$$\eta = A + B \log I$$

where A and B are called Tafel constants.

1.6.2 Irreversible kinetics

In electrochemistry, the kinetics is irreversible, when the charge transfer step is very slow [15]. In such cases, there is a single peak in the cyclic voltammogram, either oxidation peak or reduction peak. For a typical irreversible process,



the value of k_h for a diffusion limited system is calculated from the Nicholson-Shain equation [22],

$$E = E^0 - \frac{RT}{\alpha nF} \left[0.78 - \ln \frac{k_h}{D^{1/2}} + \ln \left[\frac{\alpha nFv}{RT} \right]^{1/2} \right]$$

When the electrochemical reaction at the electrode is slow when compared to diffusion, electron transfer kinetics controls the reaction and diffusion effects can be ignored. In such a case another rate constant k_s , the surface reaction rate constant can be calculated by making use of the Laviron equation [23],

$$E = E^0 + \frac{RT}{\alpha nF} \left(\ln \frac{RTk_s}{\alpha nF} - \ln v \right)$$

1.7 Chemical Sensors

A chemical sensor is a device that transforms chemical information, originating from a chemical reaction of the analyte or from a physical property of the system under investigation into an analytically useful signal. Every chemical sensor consists of two basic functional units: a receptor and a transducer. Receptor part of the sensor transforms the chemical information

into a form of energy which may be measured by the transducer. The selective chemistry takes place at the receptor. Transducer is a device capable of converting the energy carrying the chemical information concerning the analyte into a measurable analytical signal. Depending on the transducer type chemical sensors may be classified into optical, electrical, magnetic, mass sensitive, thermometric and electrochemical sensors [24].

In *optical* sensors, the transducer converts the optical changes due to receptor-analyte interaction to an analytical signal. The change in electrical properties caused by the interaction of the analyte is made use of in *electrical* sensors. *Magnetic* sensors make use of change in paramagnetic properties of the analyte to produce the analytical signal. *Mass sensitive* sensors have transducers which transform the mass change caused by accumulation of the analyte at a specially modified surface into a change of a property of the support material. In the case of *thermometric* sensors, the transducer is based on the measurement of the heat effects due to a specific chemical reaction involving the analyte or due to adsorption of the analyte. Electrochemical sensors have the transducer converting the electrochemical reaction taking place at the receptor-analyte region into an electrical signal.

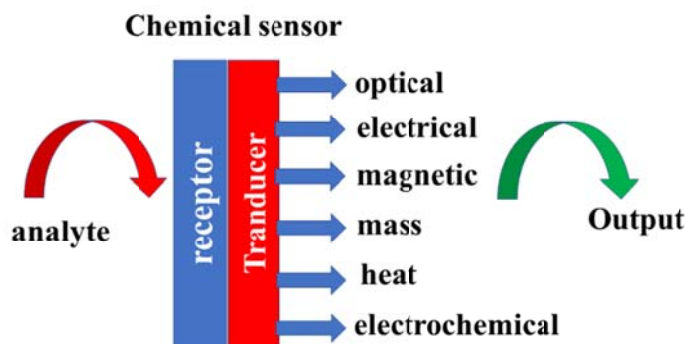


Figure 1.7: Chemical Sensing Strategies

Of the different types of chemical sensors, electrochemical sensors offer the advantage that, the receptor can sense the materials which are present within the host without doing any damage to the host system [25].

1.8 Electrochemical Sensors

Electrochemical sensors represent the rapidly growing class of chemical sensors which find important applications in clinical, industrial, agricultural and environmental fields [1]. In electrochemical sensors, the transducer converts the analyte information from an electrochemical reaction involving the analyte into an electrical signal. Electrochemical sensors can be classified into different types.

1. **Potentiometric Sensors:** Such sensors are based on the development of an electrical potential at the surface of a solid material when it is placed in a solution containing ions which can exchange with the surface [26]. The potential developed is a function of the number of ions in solution under zero current condition. The glass electrode used for pH measurements is the typical example of a potentiometric sensor. There are three main types of potentiometric sensors: ion-selective electrodes (IES), coated wire electrodes (CWES) and field effect transistors (FETS) [27].
2. **Conductometric Sensors:** The change in electrical conductivity of a film or bulk material on interaction with an analyte is monitored in conductometric sensors. Even though such sensors lack selectivity, the inherent simplicity and low-cost nature of such devices make them attractive [28].

3. Impedimetric Sensors: These sensors monitor the changes in the electrical properties such as resistance or capacitance, on the surface of a recognition element on interaction with the analyte [6].
4. Amperometric Sensors: Such type of devices continuously monitors the current resulting from an electrochemical reaction taking place at a constant potential. The Clark oxygen electrode is a typical example of an amperometric sensor [28].
5. Voltammetric Sensors: Such devices measure the current flowing through the cell containing a solution of an electroactive element as a function of the applied potential.

Voltammetric sensors have emerged as the most widely studied and in demand type of sensors in the last few decades. Chemically modified electrodes can be tailored to be used as voltammetric sensors for desired purposes. Such sensors can be fabricated by modifying conventional electrodes with suitable species like nanomaterials, metal complexes, dyes, polymers etc. Among these polymers, particularly those formed by electropolymerisation are especially attractive for sensor applications.

1.9 Back ground features of the present investigation

1.9.1 Electropolymers

Electropolymers or electrochemically synthesised polymers have received widespread applications in the development of biomimetic, enzyme and DNA sensors. Electropolymerisation results in formation of simple and reproducible polymer films with precise special resolution over the surface. Control over the thickness and morphology of the polymer coatings is possible with electropolymerisation. Electrogeneration of polymer films is

reported to be compatible with bulk manufacturing methods [29]. Additionally, electrogeneration of polymers can be performed under mild conditions, as the initiator of polymerisation is generated by an electrochemical reaction, thereby rendering the polymer free of chemical impurities [30]. These polymers protect the electrode surface from the impurities that adsorb onto the electrode surface during voltammetric scans causing a decrease in the electrode response [31]. Electro-polymers are used as electrode modifiers, immobilisation matrix for biomolecules, molecular imprinting substrates etc.

The first electro-polymer was prepared by Letheby in 1862 by subjecting aniline to anodic oxidation in sulfuric acid [32]. Electro-active polymers can be classified into redox polymers, or electronically conducting polymers [33].

- Redox polymers have localised conducting sites containing redox-active groups which is covalently bonded to an electrochemically inactive polymeric backbone. In these materials electron transfer occurs by ‘electron hopping’ i.e., sequential electron self-exchange between neighbouring redox-active sites. A typical example is poly(vinyl ferrocene).
- Electronically conducting polymers have extensively conjugated polymer backbone. Charge transfer takes place through polarons and bipolarons and is very rapid. A large number of aromatic and heteroaromatic compounds form electronically conducting polymers by oxidative electropolymerisation. Poly(aniline), poly(pyrrole) etc. are typical examples.

1.9.2 Simultaneous determinations

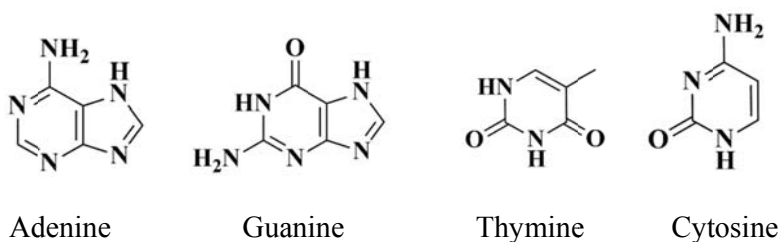
Simultaneous determination involves detection and/or estimation of more than one species from a multicomponent solution, using the same probe at the same time without the need for any prior separation step. Voltammetry, which is based on the electro-oxidation/reduction of chemical species at its characteristic potential has the prospects to achieve this. The resolution of voltammetric signals of chemically similar species which undergo electrochemical reaction at very close electrode potentials is the challenge in this regard. Chemical modification of electrodes provides an answer to this problem. Electrodes can be tailored with specific functionalities that can resolve the voltammetric signals providing ideal peak separations thereby imparting selectivity.

Simultaneous determination using voltammetry eliminates the need of a separation step, which is time consuming and expensive. Use of large quantities of solvents can be avoided and analysis can be completed without contamination of the sample. Loss of analyte due to incomplete separation can be avoided. Simultaneous voltammetric determination prevents wastage of chemicals and thereby reduces chemical pollution of the environment.

1.9.3 DNA bases

The genetic material in all living organisms, deoxy ribo nucleic acid or DNA is composed of four nitrogenous bases Adenine (Ad), Guanine (Gu), Thymine (Thy) and Cytosine (Cyt) covalently linked to each other and to a deoxy ribose sugar-phosphate backbone forming a polynucleotide strand. Adjacent polynucleotide strands are held together by hydrogen bonding between the base pairs Ad-Thy and Gu-Cyt forming a double

helical structure [34]. It is the sequencing of the four nucleic acid bases that determine the information stored in the DNA, regarding cell metabolism and protein biosynthesis [35]. The nitrogenous nucleic acid bases are either purines or pyrimidines. Purines are organic heterocyclic compounds in which a pyrimidine ring is fused with an imidazole ring. Ad and Gu are purines whereas Thy and Cyt are pyrimidines.



Ad or 9H-purin-6-amine, is a purine derivative with molecular mass of 135.13. It was named by Albrecht Kossel in 1885, when he extracted it from the pancreas of an ox, in reference to the Greek synonym for gland-‘aden’[36]. In DNA, Ad pairs with Thy to form the double helical structure. Ad is also a component of the energy rich adenosine triphosphate (ATP) and the co-factors nicotinamide adenine dinucleotide (NAD) and flavin adenine dinucleotide (FAD) thereby playing key roles in cellular respiration and protein biosynthesis. In addition to its role in DNA, Ad is reported to have several other biological functions. It inhibits growth of human lymphoblasts, cytoplasmic immunoglobulin production, as well as mononuclear leukocytes and IgE mediated mast cell activation. Ad has a protective role in whole blood storage also where by added Ad increases the post transfusion viability [37]. Elevated levels of Ad in urine is observed in patients with hepatocellular carcinoma [38].

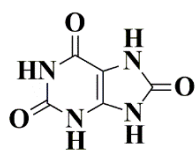
The other purine base found in DNA is Gu or 2-amino-9H-purin-6(1H)-one, having a molecular mass of 151.13. It was named after 'guano' the bird droppings which contain guanine in abundance. It is a main component of guanosine tri-phosphate which is very similar to ATP. Gu, being a DNA repair product, is an indicator of oxidative damage of DNA, by its levels in urine [39].

The pyrimidine nucleobase Thy was discovered by Albrecht Kossel in the early 1890s in calf thymus DNA after the removal of the purines [36]. Thy or 5-methylpyrimidine-2,4(1H,3H)-dione, has a molecular mass of 126.12. In combination with deoxy ribose sugar, Thy forms thymidine which is the major component of thymidine tri phosphate (TTP) which is involved in cellular respiration. Photodimerisation of adjacent thymine molecules is the major reason for mutations in DNA [34]. Thy levels are elevated in body fluids like urine, serum and cerebrospinal fluid in case of dihydrothymine dehydrogenase deficiency [40].

The fourth nucleobase is Cyt or 4-aminopyrimidin-2(1H)-one. It had a molecular mass of 111.1 and was discovered along with Thy. Being an unstable molecule, it is the most common site for mutations in DNA and RNA. On deamination, it gets converted to uracil and on methylation followed by deamination gets converted to Thy [34]. The nucleotide of Cyt with deoxyribose sugar known as cytidine is a component of the cofactor cytidine tri phosphate CTP, which plays an important role in carbohydrate and lipid metabolism [41]. Cyt, in combination with arabinose sugar forms cytosine arabinoside which is a chemotherapy medication [42].

Initially it was believed that DNA was made up of equal quantities of the four nucleobases, the tetranucleotide hypothesis. Chargaff after careful study of the composition of bases in the DNA of various species, put forward that although the relative amount of the nucleobases varied with species, there

was a 1:1 correspondence between purines and pyrimidines. i.e., in all the species, the amount of Ad was equal to Thy and the amount of Gu was equal to Cyt within the margin of error [43]. The ratio $\frac{[Ad+Thy]}{[Gu+Cyt]}$ is known as dissymmetry ratio and is a characteristic of a particular species [44].



Uric acid

Uric acid (Ua) or 7,9-dihydro-1H-purine-2,6,8(3H)-trione, is the primary product of purine metabolism [45]. It is a purine derivative with molecular mass 168.1. Ua formed by the metabolism of purines is typically excreted through urine in the range 250 -750 mg dL⁻¹[46]. In the range 4.1-8.8 mg dL⁻¹, Ua is one of the natural anti-oxidants present in blood [47]. Anomalous concentrations of Ua in body fluids occur in conditions of gout, hyperuricemia, cardiovascular abnormalities etc. [45].

The determination of DNA bases is very important for diagnosis of genetic diseases as well as for understanding the fundamental mechanisms involved in genetic coding [48]. In physiological fluids, Ua is generally found together with the purine nucleobases [49]. Among the various analytical methods available, voltammetry seems to be the most practical technique. DNA bases being electro-active, their sensitive, selective and rapid determination can be achieved with voltammetry. Voltammetry which requires only small volume of samples, offer the possibility of developing miniature sensors. The pioneering work on the electrochemical detection of nucleic acids by polarography had been carried out by E. Paleček [49a-49d] which inspired the development of numerous electrochemical nucleic acid sensors which have been reviewed by Paleček himself [49e-49i].

1.9.4 Literature review on chemically modified carbon electrodes for determination of DNA bases and Uric acid

There are several reports of electrochemical determination of purines on conventional electrodes [50-56], but those of pyrimidines are very few [57, 58]. This is because the oxidation of pyrimidines occur at very high positive potentials and the working potential window of the conventional electrodes are very narrow [59]. In addition, the sensitivity of such determinations is affected by the slow electron transfer rates for pyrimidine oxidation, large background currents and irreversible adsorption of the oxidation products onto the electrode surface [49].

Literature reports for voltammetric sensing of Ad on chemically modified carbon electrodes are discussed first.

Fullerene-C₆₀-modified glassy carbon electrode was fabricated by Goyal et al., for the voltammetric determination of 2-deoxyadenosine and Ad in human blood and urine. In PBS pH 7.2, the anodic peak of Ad appeared at 0.994 V in SWV mode. A wide linear range of 1.0×10^{-4} to 1.0×10^{-8} M with a detection limit of 9.8×10^{-9} M has been reported [38].

Zhang, Jin and Hu has reported the sensitive determination of Ad on poly(amido sulfonic acid) modified GCE with PBS pH 4 as supporting electrolyte. With DPV the limit of detection (LOD) was found to be as low as 8.0×10^{-9} M and wide linear range 1.0×10^{-6} M to 3.0×10^{-8} M. The sensor gave satisfactory results for the determination of Ad in pharmaceutical formulation [60].

Xu et al. reported a cysteic acid tailored electrode for the determination of Ad in Vitamin B4 tablets. The adsorption controlled

oxidation of Ad took place at 1.0 V in PBS pH 6, on the tailored electrode. The DPV response was linear over the range 1.0×10^{-4} M to 2.0×10^{-7} M and the sensor could detect Ad as low as 5.9×10^{-8} M [61].

Adsorption controlled oxidation of Ad at 0.990 V on a GCE modified with 1-phenyl-3-methyl-4-(2-furoyl)-5-pyrazolone has been reported by Song and Li. The DPV current response was found to be linear over the range 1.0×10^{-4} M to 5.0×10^{-7} M in 0.10 M phosphate buffer solution of pH 7, giving LOD of 1.25×10^{-7} M. application of the sensor for the determination of Ad in pharmaceutical formulation had been demonstrated [62]

Arvand et al., made use of carbon paste modified with a composite of multiwalled carbon nanotube and ionic liquid to fabricate a sensor for Ad. The oxidation peak for Ad was obtained at 0.790 V with a 2.8 times enhancement in peak current with respect to carbon paste electrode using phosphate buffer saline (PBS) of pH 10.5. The adsorption controlled electrochemical process, in DPV mode gave a linear range from 7.5×10^{-5} M to 5.0×10^{-7} M with a detection limit of 1.08×10^{-9} M. The authors have demonstrated the application of the sensor for the determination of Ad in hydrolysed denatured DNA of calf thymus and fish fin as well as biological fluids and milk powder [63].

Reports of carbon electrode based sensors that determine Gu alone are few. The utility of carbon paste electrodes modified with cobalt(II) phthalocyanine for electrocatalytic oxidation of Gu and single strand DNA has been demonstrated by Abbaspour, Mehrgardi and Kia. The detection limit was obtained to be 1.3×10^{-10} M with 0.2 M acetate buffer solution

(ABS) of pH 5.1 as supporting electrolyte. The electro-oxidation was found to be adsorption controlled based on scan rate studies [64].

Electrocatalytic oxidation and nanomolar determination of Gu at the surface of a molybdenum (VI) complex–TiO₂ nanoparticle modified carbon paste electrode using 0.1 M PBS pH 5 as supporting electrolyte has been reported by Ardakani et al. [65].

The fabrication of a polydopamine redox-polymer film modified screen printed electrode for the electrocatalytic determination of Gu has been reported by Kanyong, Rawlinson and Davis. In Britton Robinson (BR) buffer of pH 7, the calibration of the sensor for the Gu peak observed at 0.4 V was performed with SWV and the detection limit was obtained to be 1.58×10^{-5} M [66].

Most of the published works report determination of Gu simultaneously with Ad and there are a lot of different types of chemically modified electrodes being used for the simultaneous determination of Gu and Ad.

An electrochemical sensor for Gu and Ad based on cyclodextrin-modified poly(N-acetylaniline) on a carbon paste electrode has been developed by Abbaspour and Noori. The adsorption controlled oxidation response for both Gu and Ad showed linearity in the range of 1.0×10^{-2} M to 1.0×10^{-4} M by using DPV, with an experimental limit of detection down to 5.0×10^{-5} M [67].

Yin et al., has investigated the electrochemical oxidation behaviour of Gu and Ad on graphene–Nafion composite film modified GCE using DPV. Under the optimised experimental conditions, separation of the two oxidation peaks was 0.364 V in 0.1 M pH 4.4 ABS. When simultaneously

determined by DPV, Gu and Ad gave detection limit of 5.8×10^{-7} M and 7.5×10^{-7} M respectively. The proposed method was applied to determine Gu and Ad in milk powder, urine and herring sperm DNA samples with satisfactory results [68].

Ferencova et al., has reported simultaneous determination of Gu and Ad on a GCE modified with a composite of pearl-like CdS microspheres and chitosan. The DPV peak currents obtained at the modified GCE were more than ten times higher than those observed at bare GCE and the peak potentials were shifted to less positive values (from 0.746 V to 0.682 V for Gu and from 1.038 V to 0.948 V for Ad) in 0.1 M PBS pH 7.4. The electro-oxidation processes on the modified electrode are reported to be adsorption controlled. Detection limits as low as 2.0×10^{-9} M for Gu and 4.0×10^{-8} M for Ad was obtained in this work [69].

The simultaneous determination of Ad and Gu utilizing PbO₂-carbon nanotubes-ionic liquid composite film modified GCE has been reported by Liu et al. Gu and Ad oxidation responses on the modified GCE, were monitored by DPV and the simultaneous detection of Gu and Ad with a peak separation of 0.29 V in 0.1 M pH 7.0 PBS was obtained. The detection limit for individual determination of Gu and Ad was 6.0×10^{-9} M and 3.0×10^{-8} M, respectively. The measurements of Gu and Ad in herring sperm DNA was successfully demonstrated [70].

The electrochemical behaviour of Gu and Ad at the TiO₂-graphene nanocomposite modified GCE was investigated by Fan et al. Well defined oxidation peaks for Gu and Ad were obtained at 0.88 V and 1.19 V respectively in ABS pH 4.5 in DPV mode. Scan rate studies indicate that the electron oxidation processes are surface controlled. A wide linear range for

both Gu and Ad (2.0×10^{-4} M - 5.0×10^{-7} M) with detection limit of 1.0×10^{-7} M and 1.5×10^{-7} M respectively has been obtained with this sensor. The TiO₂-graphene/GCE electrochemical sensor was applied to determine the Gu and Ad content of thermally denatured DNA with satisfactory results [71].

Deng et al., has reported the fabrication of poly (2,6-pyridinedicarboxylic acid)/multiwalled nano tubes modified GCE for simultaneous determination of Gu and Ad in DNA. DPV was used to determine the concentration of Gu and Ad. The detection limit for Gu and Ad was 4.5×10^{-5} M and 5.0×10^{-5} M, respectively. The electrochemical method for the measurement of Gu and Ad in calf thymus DNA was also developed with this modified electrode and the result was reported to be satisfactory [72].

Simultaneous determination of Gu and Ad on graphene–ionic liquid–chitosan composite film modified GCE has been reported by Niu et al. The modified electrode was reported to exhibit good analytical performance and was successfully applied for individual and simultaneous determination of Gu and Ad. Detection limits of 7.5×10^{-7} M for Gu and 4.5×10^{-7} M for Ad were obtained, with the linear calibration curves over the concentration range 1.5×10^{-4} M - 2.5×10^{-6} M and 3.5×10^{-4} M - 1.5×10^{-6} M, respectively. The article also reports successful application of the sensor or the determination of Gu and Ad in denatured DNA samples [73].

Liu and co-workers proposed a promising electrochemical device for the sensitive determination of Gu, Ad and epinephrine was fabricated by electro-polymerization of melamine on the surface of GCE. The oxidation currents of Gu and Ad at the modified GCE increased 9 and 7 times respectively compared with that of bare GCE using SWV in pH 4.5 PBS.

The surface controlled electro-oxidation process gave good linear ranges for determination of Gu and Ad with LOD 8.0×10^{-8} M for Gu and 7.0×10^{-8} M for Ad respectively [74].

An ultrasensitive biosensor for the DPV detection of dopamine, Ua, Gu and Ad was developed by immobilizing three-dimensionally distributed gold nano particles on a poly(safranin T)-modified electrode by Niu and co-workers. All four analytes showed well-defined catalytic oxidation peaks at the modified electrode. dopamine, Ua, Gu, and Ad yielded wide linear ranges with the modified electrode and detection limits for the analytes were 2.0×10^{-10} M, 8.0×10^{-9} M, 5.0×10^{-10} M, and 4.0×10^{-9} M, respectively. The feasibility of the proposed assay for use in human serum and urine was investigated and satisfying results were reported [75].

An electrochemical sensor was developed for Gu and Ad detection using multiwall carbon nanotubes decorated with NiFe_2O_4 magnetic nanoparticles on a GCE by Ensafi and co-workers. The modified electrode was employed for detecting purine bases using LSV and hydrodynamic amperometry. On modification, the oxidation peak currents of Gu and Ad was found to increase sixfold in PBS of pH 7. The limit of detection was found to be 6.0×10^{-9} M and 6.0×10^{-8} M for Gu and Ad respectively. With amperometric technique, only individual determination was possible, whereas Gu and Ad could be measured simultaneously using LSV. The sensor was demonstrated to be useful for the simultaneous detection of guanine and adenine in salmon sperm DNA using LSV [76].

A novel strategy based on overoxidized polyimidazole and graphene oxide copolymer modified GCE was proposed for the simultaneous determination of ascorbic acid, dopamine, Ua, Gu and Ad by Liu et al. The

modified GCE was able to resolve the voltammetric peaks of ascorbic acid, dopamine, Ua, Gu and Ad at approximate potentials of 0.18 V, 0.32 V, 0.52 V, 0.90 V, and 1.20 V respectively in 0.1 M PBS pH 3. The detection limits were found to be 5.9×10^{-6} M, 4.8×10^{-6} M and 1.2×10^{-6} M for Ua, Gu and Ad respectively [77].

Wang et al., had reported a GCE modified with graphene quantum dots and silver nanoparticles for simultaneous determination of Gu and Ad. The large peak separations obtained with this electrode allow it to simultaneously detect Gu and Ad with no mutual interference. Moreover, a remarkable improvement in the kinetics of the electron transfer for diffusion controlled oxidation of Gu and Ad was observed on the surface of the modified electrode, by shifting negatively in anodic peak potentials (0.059 V for Gu and 0.079 V for Ad) and increasing the anodic peak current by threefold. The practical application of the sensor has been demonstrated in thermally denatured DNA sample [78].

The electrocatalytic activity of molybdenum disulfide nanosheets enhanced by self-doped polyaniline for highly sensitive and synergistic determination of Gu and Ad was demonstrated by Yang et al. In BR buffer pH 7, the carbon paste electrode modified with molybdenum disulfide nanosheets enhanced by self-doped polyaniline, resolved the peaks of Gu and Ad over a wide linear concentration range. The LOD for Gu and Ad using the modified electrode was obtained to be 4.5×10^{-9} M and 6.3×10^{-9} M respectively in DPV mode [79].

An electrochemical sensor for individual and simultaneous determination of Gu and Ad in biological fluids and in DNA based on a indium doped ceria nanoparticle modified glassy carbon paste electrode has

been proposed by Ibrahim, Temerk and Farhan. The electrochemical sensor exhibits a potent and persistent surface controlled electro-oxidation behaviour followed by well-separated oxidation peaks toward Gu and Ad. Low detection limits of 1.19×10^{-8} M and 2.86×10^{-8} M has been obtained for Gu and Ad respectively in SWV mode at pH 3. The practical application of the modified electrode was demonstrated by simultaneous detection of Gu and Ad contents in thermally denatured DNA using SWV [80].

Another electrochemical sensor was developed for the determination of purine bases, based on gold nanoparticles incorporated in mesoporous MFI zeolite by Song and colleagues. The simultaneous detection of Gu and Ad can be achieved at the composites modified GCE. The electrochemical sensor exhibits wide linear range with detection limit of 2.5×10^{-5} M and 2.9×10^{-5} M for Gu and Ad, respectively in PBS pH 7 with DPV. The use of the electrochemical sensor for the evaluation of Gu and Ad content in herring sperm DNA is also demonstrated [81].

There have been some reports of chemically modified carbon electrodes being used for the solo determination of Thy but those for Cyt are few.

Electrochemical oxidation of Thy on a β -cyclodextrin modified GCE had been studied by Wu and co-workers. In sodium bicarbonate-sodium carbonate buffer solution of pH 11, the electro-oxidation of Thy was found to be reversible and diffusion controlled. The anodic peak was observed at 0.935 V and cathodic peak at 0.903 V. With SWV, the variation of oxidation peak current was found to be linear in the concentration range 1.0×10^{-3} M to 2.5×10^{-5} M with detection limit of 6.2×10^{-6} M [82].

Wang and co-workers studied the electro-oxidation of Thy on α -cyclodextrin incorporated carbon nanotube coated pyrolytic graphite

electrode. An irreversible, diffusion controlled one electron oxidation of Thy was observed on the modified electrode. In sodium bicarbonate-sodium carbonate buffer solution of pH 10.8, the variation of peak current in the DPV mode was found to be linear in the concentration range 1.8×10^{-3} M to 2.5×10^{-5} M with a detection limit of 5.0×10^{-6} M [83].

The electrochemical determination of Thy on ionic liquid modified carbon electrode (CILE) in a pH 5.0 BR buffer solution was proposed by Sun et al. They have reported the appearance of a single well-defined irreversible oxidation peak by adsorption-controlled electrochemical process and enhanced electrochemical response on the CILE. The sensor showed a wide linear range 3.0×10^{-3} M to 3.0×10^{-6} M with a detection limit of 5.4×10^{-7} M in the DPV mode [84].

A sensitive electrochemical method was developed by Han and co-workers, for the voltammetric determination of Thy at a composite film-modified electrode: 1-phenyl-3-methyl-4-(2-furoyl)-5pyrazolone / polypyrrole / GCE. At pH 7.4, the oxidation peak of Thy was observed at 0.968 V on the modified electrode. A linear range of 1.0×10^{-4} M to 2.0×10^{-6} M and LOD of 4.8×10^{-7} M was obtained with DPV. One electron irreversible oxidation was found to be diffusion controlled. The application of the sensor for the determination of Thy in medical pipefish samples has been substantiated [85].

Simultaneous determination of purines and pyrimidines on chemically modified electrodes has received immense attention in the past decade as evident from the large number of literature reports. A few reports are based on the simultaneous determination of three of the nucleobases on electropolymer modified electrodes.

Shen and Wang have proposed a strategy for the simultaneous determination of Gu, Ad and Thy based on a GCE modified with a novel nanocomposite of β -cyclodextrins and multiwalled carbon nanotubes. Well separated DPV peaks with peak separation of 0.33 V for Gu and Ad, 0.17 V for Ad and Thy was obtained for the analyte mixture in 0.1 M PBS of pH 7. Detection limits of 7.5×10^{-7} M, 6.7×10^{-6} M and 3.3×10^{-5} M were obtained for Gu, Ad and Thy on the newly developed sensor [86].

Simultaneous determination of Ad, Gu and Thy at multi-walled carbon nanotubes incorporated with poly(new fuchsin) composite film modified GCE was proposed by Tang, Yogeswaran and Chen. At pH 7.2, the peaks for Gu, Ad and Thy appear at 0.556 V, 0.950 V and 1.280 V respectively on the modified electrode. The detection limits for the determination of these analytes in single stranded DNA was found to be 9.5×10^{-5} M, 7.4×10^{-6} M, 1.6×10^{-5} M respectively for Gu, Ad and Thy [87].

Feng and co-workers have prepared poly(sulfosalicylic acid) and single-stranded DNA composite modified glassy carbon electrode (GCE) by electropolymerization and then successfully used to simultaneously determine Gu, Ad and Thy. Separation of the oxidation peak potentials were 0.289 V and 0.262 V between Gu-Ad and Ad-Thy in pH 7.0 PBS. The electro-oxidations were found to be adsorption controlled. Practical detection limits of 2.2×10^{-8} M for both Gu and Ad and 1.4×10^{-6} M for Thy were obtained on the proposed sensor [88].

Sensors based on chemically modified electrodes which simultaneously determine all the four nucleobases have also been reported.

Ambrosi and Pumera have demonstrated the superior electrochemical performance of stacked graphene nanofibers for oxidation of DNA bases.

The simultaneous oxidation of Gu, Ad, Thy and Cyt could be achieved on the GCE modified with stacked graphene nanofibers with enhanced peak currents using 0.05 M PBS pH 7 as supporting electrolyte [89].

Simultaneous detection of DNA bases Gu, Ad, Thy and Cyt on a GCE modified with silicon carbide nanoparticles has been reported by Ghavami, Salami and Navaee. DPV with 0.1 M PBS pH 7 as supporting electrolyte gave detection limits in micromolar concentrations for Gu, Ad, Thy and Cyt [90].

Organic-inorganic hybrid poly(aniline)/MnO₂ nanocomposite, synthesized by the reaction of polyaniline and KMnO₄ in aqueous medium was used to modify GCE and used for the simultaneous determination of Gu, Ad, Thy and Cyt at physiological pH by Anu Prathap, Srivastava and Satpati. The DPV obtained for the quaternary mixture containing Gu, Ad, Thy and Cyt are well separated from each other with a potential difference of 0.27 V for Gu-Ad, 0.21 V for Ad-Thy and 0.17 V for Thy-Cyt which are large enough to simultaneously determine the concentration of Gu, Ad, Thy and Cyt. The modified electrode exhibited sensing abilities for Gu, Ad, Thy and Cyt in the linear range of 1.0×10^{-4} M to 1.0×10^{-5} M with lower detection limits of 4.8×10^{-6} M, 2.9×10^{-6} M, 1.3×10^{-6} M and 1.3×10^{-6} M for Gu, Ad, Thy and Cyt, respectively. The proposed sensor was applied for the determination of actual concentration of Gu, Ad, Thy and Cyt in calf thymus DNA sample with high accuracy [91].

Simultaneous detection of DNA bases on GCE chemically modified with graphene-new Fuchsin has been proposed by Chen et al. The oxidation of Gu took place at 0.71 V, Ad at 0.95 V, Thy at 1.11 V and Cyt at approximately 1.37 V on the modified electrode with 0.1 M PBS pH 7 as supporting electrolyte [92].

Kaur and Srivastava proposed an organic-inorganic hybrid material as electrode modification for the simultaneous determination of DNA bases. Ionic liquids coated nanocrystalline zeolite ZSM-5 was used to modify GCE and used for the simultaneous determination of Gu, Ad, Thy and Cyt. In 0.1 M PBS of pH 7, well resolved peaks were obtained for surface controlled oxidation of Gu, Ad, Thy and Cyt. The detection limits for Gu, Ad, Thy and Cyt on the modified electrode was found to be 4.2×10^{-6} M, 7.0×10^{-6} M, 9.6×10^{-6} M and 5.0×10^{-6} M respectively. The utility of the sensor for the determination of DNA bases in thermally denatured Calf thymus DNA has been demonstrated [93].

Ren and co-workers has presented direct electrocatalytic and simultaneous determination of purine and pyrimidine DNA bases using mesoporous carbon fibers as a novel electrocatalyst. The anodic peak responses for quaternary mixture were reported to be well separated from each other with a potential difference of 0.280 V, 0.170 V and 0.210 V for Gu-Ad, Ad-Thy and Thy-Cyt, respectively. At physiological pH, simultaneous determination of DNA bases was possible over a wide linear range and with low detection limit. In addition, the proposed sensor could determine the bases in herring sperm DNA sample with satisfactory result [94].

Shervedani et al., have immobilized 5-amino-1,10-phenanthroline-Fe(II) complex onto GCE and used for determination of DNA bases. The DPV oxidation peaks of Gu, Ad, Thy and Cyt, appeared, respectively, at 0.72 V, 1.01 V, 1.20 V and 1.38 V on modified GCE. The detection limits for Gu, Ad, Thy and Cyt were 1.5×10^{-10} M, 4.4×10^{-9} M, 1.3×10^{-7} M and 2.3×10^{-7} M respectively. Finally, the validity of the method and applicability of the sensor were successfully demonstrated by determination of the ratio of (Gu+Cy)/(Ad+Thy) in calf-thymus DNA [95].

There are several reports of voltammetric determination of Ua on polymer modified carbon electrodes.

Zang and Lin has reported a glassy carbon electrode covalently modified with glutamic acid being applied to the catalytic oxidation of Ua and ascorbic acid, wherein the overpotentials have been decreased by about 0.20 V and 0.30 V, respectively. The modified electrode resolved the overlapping voltammetric response of Ua and ascorbic acid into two well-defined voltammetric peaks with both CV and DPV, which can be used for the simultaneous determination of these species in a mixture. The catalytic peak current obtained from DPV was linearly dependent on the Ua and ascorbic acid concentration in the range 4.3×10^{-4} M - 2.3×10^{-6} M and 4.3×10^{-4} M - 1.0×10^{-6} M respectively. The detection limits for Ua and ascorbic acid were 1.1×10^{-6} M and 9.2×10^{-6} M respectively. The modified electrode shows good sensitivity, selectivity and stability, and has been applied to the determination of Ua and ascorbic acid simultaneously in human urine samples with satisfactory results [96].

Voltammetric sensing of Ua and ascorbic acid with poly(para toluene sulfonic acid) modified GCE has been presented by Wang and co-workers. In DPV, the polymer modified electrode could separate the oxidation peak potentials of Ua and ascorbic acid present in the same solution by about 0.3 V, though the bare electrode gave a single broad response. Elimination of fouling effect by the oxidized product of ascorbic acid on the response of Ua has been achieved at the polymer modified electrode. The detection limit of Ua in the presence of ascorbic acid was 5.0×10^{-7} M [97].

Lin et al. has reported a DNA/poly(p-amino benzene sulfonic acid) composite bi-layer modified GCE for determination of dopamine and Ua

under coexistence of ascorbic acid. In comparison with single layer modified electrodes, the composite bi-layer modification provided superior electrocatalytic activity towards the oxidation of dopamine, Ua and ascorbic acid and separated the originally overlapped DPV signals of dopamine, Ua and ascorbic acid oxidation at the bare electrode into three well-defined peaks at pH 7. The peak separation between ascorbic acid and dopamine, ascorbic acid and Ua was 0.176 V and 0.312 V, respectively. The anodic peak current of Ua was a linear function of concentration in the range 2.3×10^{-5} M – 4.0×10^{-7} M with a detection limit of 1.9×10^{-7} M in the presence of 5.0×10^{-4} M ascorbic acid [98]

Selective determination of Ua in the presence of ascorbic acid at poly(para aminobenzene sulfonic acid) modified glassy carbon electrode has been reported by Tang et al. The peak-to-peak separation between Ua and ascorbic acid was 0.267 V in a 0.1 M PBS at pH 7. DPV was used for detecting Ua and the anodic peak current of Ua was proportional to its concentration in the range of 8.0×10^{-4} M – 1.2×10^{-7} M with a detection limit of 4.0×10^{-8} M. The proposed sensor has been applied to the determination of Ua in human urine without any pre-treatment [99].

Zhang and co-workers conducted the simultaneous electrochemical determination of dopamine, ascorbic acid and Ua using poly(acid chrome blue K) modified GCE. In 0.05 M PBS pH 4, the separations of anodic peak potentials of, ascorbic acid-dopamine, dopamine-Ua and ascorbic acid-Ua on this modified electrode are 0.193, 0.166 and 0.359 V respectively with DPV. LOD for the determination of Ua in presence of dopamine and ascorbic acid was found to be 5.0×10^{-7} M [100].

Highly selective determination of ascorbic acid, dopamine and Ua by DPV using poly(sulfonazo III) modified GCE has been reported by Ensafi et al. The modified electrode not only improved the electro-catalytic oxidation of ascorbic acid, dopamine and Ua, but also resolved the overlapping anodic peaks. The proposed sensor was successfully applied to the determination of these compounds in real samples [101].

Sivasankaran et al., has proposed a simple voltammetric sensor for direct determination of Ua based on poly(bromophenol blue) - gold nanoparticles composite modified GCE. The electrooxidation of Ua in 0.1 M NaOH was observed at a potential of -0.105 V by SWV. The oxidation peak current increased linearly on increasing the concentration of Ua in the range 1.0×10^{-3} to 2.0×10^{-5} M with a limit of detection 2.2×10^{-6} M. The proposed method was effectively applied to determine Ua in artificial blood serum and urine samples [102].

1.9.5 Objectives of the present investigation

Rapid, selective and sensitive determinations are the need of the hour in clinical diagnostics. In this regard voltammetry is being pursued by analytical chemists to develop sensors for point of care applications. Genetic disorders and associated disease conditions are generally correlated with change in the amounts of DNA bases Gu, Ad, Thy and Cyt. In addition, cellular energy level changes, therapeutic responses, deficiencies in the immune system as well as diseases like cancer, epilepsy and AIDS result in abnormal levels of DNA bases in physiological fluids [103]. Hence the determination of DNA bases is important in clinical diagnosis. Owing to the close resemblance of biological redox reactions with electrochemical reactions, a study of electrochemical reactions of biomolecules may provide

valuable insights on the redox behaviour of biomolecules [57]. Thus, the voltammetry of DNA bases is important in clinical chemistry, analytical chemistry and bio-physical chemistry. Glassy carbon as an electrode material offers an excellent platform for electrochemical reactions. Chemical modification of GCE with electropolymers, thereby tailoring required functional groups on the surface makes the modified GCE more versatile. Our group has developed many sensors by chemically modifying GCE with electropolymers [102, 104-107]

In accordance with these observations, the initial objectives of the research work undertaken were as follows:

- Fabrication of electropolymer modified GCE

The subject of the electrochemical investigation being DNA bases, electropolymers having acidic functionalities on the surface are preferred for chemical modification. From a thorough review of literature on such electropolymers, those which are non-toxic, easily electro-polymerised and form stable films are to be chosen for the purpose.

- Study the electrochemical behaviour of DNA bases on the chemically modified GCE

The electrochemical response of the DNA bases, Gu, Ad, Thy and Cyt, on the GCE chemically modified with electropolymers with acidic functionalities are to be studied. The lowering of overpotential on the modified GCE compared to the bare GCE will be used as a criterion for analysing the effectiveness of the modification.

- Development of sensors based on GCE chemically modified with electropolymers

For the development of the modified GCE as a sensor the following steps are to be carried out. Optimisation of parameters to obtain the lowest overpotential for electrochemical reaction, such as thickness of the polymer film on the GCE surface, supporting electrolyte and pH, is the first step.

Under the optimised experimental parameters, the electrochemical response on the modified GCE should be calibrated. The calibration curve is constructed by plotting the measured peak current for each standard against the corresponding concentration. The concentration range over which the plot obeys the equation $y = mx + C$ is called the *linear range* of the sensor. The *correlation coefficient* R can be calculated for a calibration curve to ascertain the degree of correlation between the measured current and the concentration. Most graph plotting programs such as excel and origin provide a more comprehensive measure called *coefficient of determination* R^2 . As a general rule, a curve with $R^2 = 0.99$ shows an excellent fit, $0.90 < R^2 < 0.99$ represents a good curve and $0.81 < R^2 < 0.89$ represent a fair curve [108]. The slope of the calibration curve, m is usually called the sensitivity or calibration sensitivity [14]. The minimum concentration of the analyte that can be detected at a known confidence level is termed as *limit of detection* (LOD). It can be calculated either by extrapolation of the calibration graph or by making use of the equation $3S/m$, where S is the standard deviation of the y intercept and m is the slope of the calibration curve [108].

The third step involves, study of effect of possibly co-existing species on the analytical signal produced by the sensor. Signal change up to

5% is considered acceptable and any change above this limit is considered to be interfering.

Finally, the validity of the sensor is to be ascertained by applying it to the determination of the analyte in real samples. Recovery tests are also conducted.

- Probing the possibility of simultaneous determination

Simultaneous determination of more than one analyte on the same probe from the same sample is useful for rapid and contamination free determination. The possibility of determination of the four co-existing DNA bases on the same probe will be explored.

- Study the kinetics of electrochemical reactions of these molecules on the electropolymer modified GCE

The kinetics of the electrochemical reactions taking place at the developed electrodes are to be explained in terms of diffusion coefficient, charge transfer coefficient and standard heterogeneous rate constant. The information needed for the calculation of these parameters will be extracted from the data obtained by chronoamperometric measurements and LSV.

Based on the response obtained for purine DNA bases, on the developed sensors; the investigation was extended to other purines like xanthine (XT), theophylline (TP) and caffeine (CF).

..... *✂*

Fabrication and Characterisation of Various Electropolymer Modified Electrodes

The procedures adopted for the fabrication of various electropolymer modified electrodes are described in this chapter. The characterisation of these electrodes using scanning electron microscopy and electrochemical impedance spectroscopy is explained. A brief description of the chemicals used and experimental procedures adopted throughout the thesis is also included in this chapter.

Introduction

The objective of the research work undertaken was to develop electropolymer based sensors for DNA bases. The analytes under study being ‘bases’, electropolymers having acidic functionalities, to facilitate an ‘acid-base’ affinity, were chosen for this purpose. Electropolymers of most of the amino acids are reported in literature. But the electropolymerisation involves the carboxylic group and hence free acidic groups may not be present on the surface after polymerisation. However amino acids such as aspartic acid (AspA), and glutamic acid (GA) have an extra -COOH group; cysteine has an extra -SH group and serine has an extra -OH group, in addition to the α -COOH and α -NH₂ groups. Hence modification with polymers of these amino acids will produce acidic functionalities on the surface [109,110].

Preliminary investigations showed that electropolymers of cysteine and serine on glassy carbon electrode (GCE) did not result in an enhancement of electrode response towards oxidation of purine bases even though electropolymers of AspA and GA showed better performance.

Literature review revealed that electropolymers of aromatic sulfonic acids are widely used for sensing applications. Three aromatic sulfonic acids, para toluene sulfonic acid (TSA), para amino benzene sulfonic acid (ABSA) and 4-amino-3-hydroxy naphthalene-1-sulfonic acid (AHNSA) which were reported to form stable and uniform polymer films on GCE surface were chosen for the study [97,99,111].

The procedure adopted for the fabrication of sensors based on electropolymerisation of AspA, GA, TSA, ABSA, and AHNSA on GCE is described in the following sections. The surface morphology of the resulting electropolymer modified GCE has been studied by scanning electron microscopy (SEM) and the interface properties were investigated using electrochemical impedance spectroscopy (EIS).

2.1 Poly(aspartic acid) modified glassy carbon electrode

2.1.1 Fabrication

Mechanical cleaning of the GCE surface was carried out prior to electropolymerisation. The surface of the GCE was polished with alumina slurry of particle size 0.05 microns, to a mirror-like finish on a flat polishing pad. It was then subjected to ultrasonic agitation in methanol, 50% nitric acid and acetone successively (alternating with sonication in double distilled water) for 3 min each to remove any adsorbed impurities. The cleaned GCE was subjected to cyclic potential scanning between -0.80 to +2.00 V at a scan rate of 0.1 Vs^{-1} in $2.0 \times 10^{-3} \text{ M}$ L-aspartic acid (AspA) dissolved in 0.1 M PBS pH 5 for 10 cycles [109]. The cyclic voltammogram obtained for the polymerisation is shown in Fig.2.1.

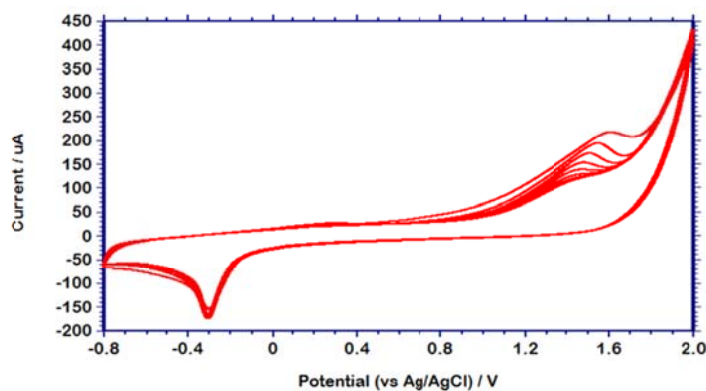
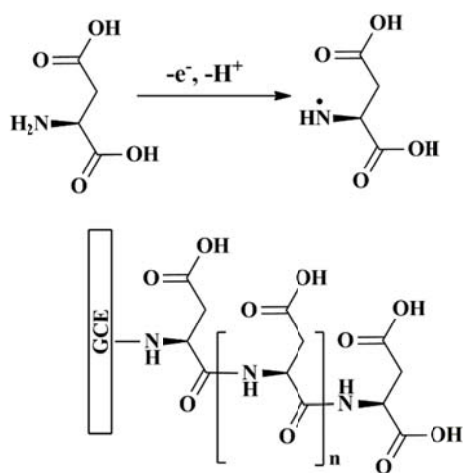


Figure 2.1: Electropolymerisation of AspA on GCE

Two peaks are evident in the CV, the anodic peak at the high positive potential of 1.54 V and the cathodic peak at -0.26 V. The peak at the high positive potential is attributed to the one electron oxidation of the amino group of AspA to its corresponding amino radical which links to the GCE surface [109]. The peak currents increased in subsequent cycles indicating the formation of a conducting polymer layer [112]. The formation of the polymer on the GCE as reported in literature is represented in Scheme 2.1.



Scheme 2.1: Formation of *p*(AspA) on GCE [108]

After the polymerisation, the GCE was taken out and washed with double distilled water to remove any monomers adsorbed on the surface. The electrode was dried in air before use. The fabricated electrode is denoted as $p(\text{AspA})/\text{GCE}$.

2.1.2 Characterisation of $p(\text{AspA})/\text{GCE}$

The scanning electron microscopy (SEM) images of the bare GCE and $p(\text{AspA})/\text{GCE}$ are shown in Fig. 2.2. It can be seen that there is a change in surface morphology upon formation of the polymer layer.

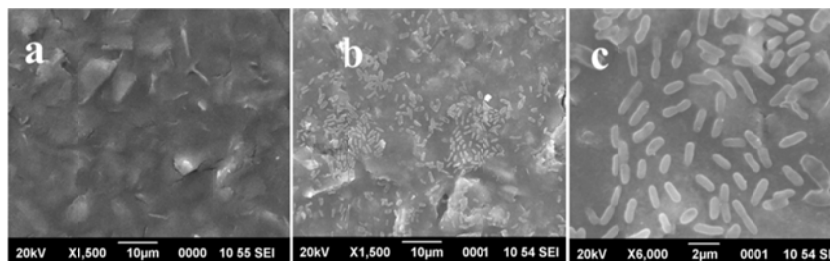


Figure 2.2: SEM images of bare GCE (a) and $p(\text{AspA})/\text{GCE}$ (b and c)

The change in interface properties of GCE upon modification with $p(\text{AspA})$ film was studied by EIS. The Nyquist plots obtained for bare GCE and $p(\text{AspA})/\text{GCE}$ in $5.0 \times 10^{-3} \text{ M } [\text{Fe}(\text{CN})_6]^{3-/4-}$ dissolved in 0.1 M KCl over a frequency range $1.0 \times 10^{-1} - 1.0 \times 10^5 \text{ Hz}$ and amplitude of 0.005 V is presented in Fig. 2.3.

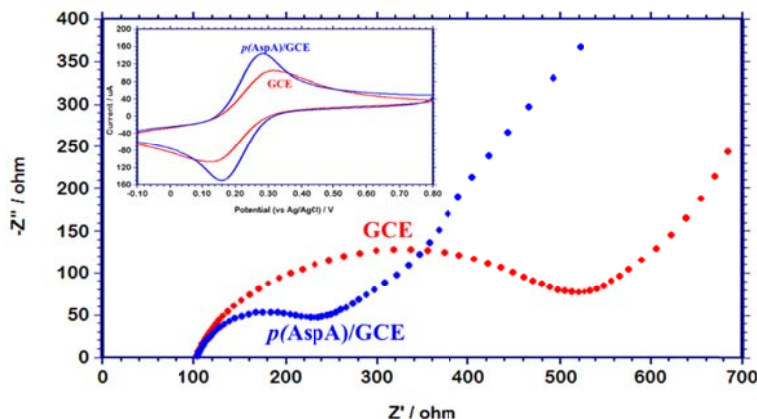


Figure 2.3: Nyquist plots of bare GCE and $p(\text{AspA})/\text{GCE}$ in $5.0 \times 10^{-3} \text{ M } [\text{Fe}(\text{CN})_6]^{3-/4-}$ in 0.1 M KCl. Inset shows the overlay of cyclic voltammogram obtained on bare GCE and $p(\text{AspA})/\text{GCE}$ in the same solution

The charge transfer resistance R_{ct} for the bare GCE was obtained to be 300.8Ω and that for $p(\text{AspA})/\text{GCE}$ was 98.5Ω when fitted to the Randles-Ershler circuit $\{R_s[C_{dl}(R_{ct}W)]\}$ using ZSimpWin software. There is a decrease in charge transfer resistance upon modification indicating that electron transfer has become easier across the $p(\text{AspA})$ film. This is again evident from the cyclic voltammograms obtained in the same solution (Inset of Fig. 2.3). The peak currents have increased on the $p(\text{AspA})/\text{GCE}$ compared to the bare GCE.

2.2 Poly(glutamic acid) modified glassy carbon electrode

2.2.1 Fabrication

GCE was polished with alumina slurry (0.05 microns) and ultrasonically cleaned in methanol, 50% nitric acid and acetone successively, alternating each step in double distilled water. The cleaned GCE was then activated by cycling the potential between -0.5 to $+1.0$ V in

0.5 M sulfuric acid until a stable voltammogram was obtained. Polymerisation of L-glutamic acid (GA) was carried out from 2.0×10^{-2} M solution of GA in 0.1 M PBS of pH 7 by cycling the potential between -0.8 to $+2.0$ V for 10 cycles [110].

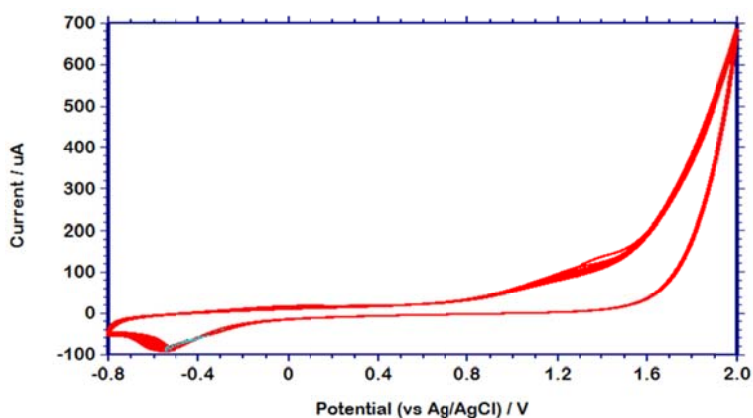
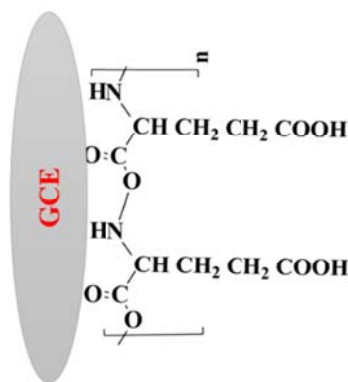


Figure 2.4: Electropolymerisation of GA onto GCE

The cyclic voltammogram obtained for the electropolymerisation process is shown in Fig. 2.4. In the first cycle, an irreversible oxidation peak was observed near 1.37 V. Primary amines are reported to undergo one electrode oxidation to the radical cation at high positive potentials [113]. During the electropolymerisation of GA, the radical cation is first formed which on reaction with the monomer (which exists in the anionic form at pH 7) results in propagation of polymer chain [114]. The polymer formed on the surface of GCE is represented in Scheme 2.2.



Scheme 2.2: $p(\text{GA})/\text{GCE}$ [8]

The electrode after the polymerisation was washed in double distilled water and dried in air before use. The fabricated electrode is denoted as $p(\text{GA})/\text{GCE}$.

2.2.2 Characterisation of $p(\text{GA})/\text{GCE}$

Surface morphology of $p(\text{GA})/\text{GCE}$ was explored by SEM. Fig. 2.5 shows the SEM images of the bare GCE and $p(\text{GA})/\text{GCE}$. The change in the surface on modification is evident in the image.

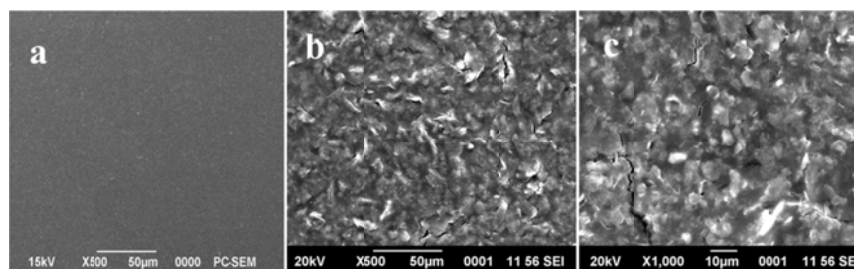


Figure 2.5: SEM images of bare GCE (a) and $p(\text{GA})/\text{GCE}$ (b and c)

Changes on the electrode surface on modification was further studied by electron impedance spectroscopy (EIS). A comparison of the Nyquist plots of the bare GCE and $p(\text{GA})/\text{GCE}$ in $5.0 \times 10^{-3} \text{ M } [\text{Fe}(\text{CN})_6]^{3-/4-}$ in

0.1 M KCl over a frequency range 1.0×10^{-1} – 1.0×10^5 Hz and amplitude of 0.005 V is shown in Fig. 2.6.

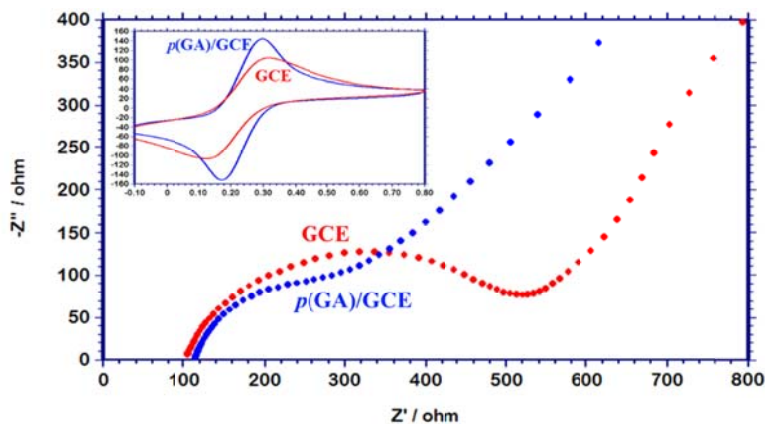


Figure 2.6: Overlay of Nyquist plots of bare GCE and $p(\text{GA})/\text{GCE}$ in 5.0×10^{-3} M $[\text{Fe}(\text{CN})_6]^{3-/4-}$ in 0.1 M KCl. Inset shows the overlay of cyclic voltammogram obtained on bare GCE and $p(\text{GA})/\text{GCE}$ in the same solution

The diameter of the semi-circular region of the Nyquist plot represent the charge transfer resistance R_{ct} , on the electrode surface for the electrochemical reaction. From the Nyquist plot it can be seen that, R_{ct} for the oxidation of Fe^{2+} to Fe^{3+} on $p(\text{GA})/\text{GCE}$ is smaller than that on the bare GCE. The R_{ct} values were obtained by fitting the obtained plot to the Randles-Ershler circuit using the ZSimpWin software. For $p(\text{GA})/\text{GCE}$ the value was 115.8Ω and that for bare GCE it was 300.8Ω . The cyclic voltammograms obtained on the bare and modified GCE validates this observation (Inset of Fig.2.6). The peak currents have increased on the modified electrode compared to the bare electrode.

2.3 Poly(para toluene sulfonic acid) modified glassy carbon electrode

2.3.1 Fabrication

The GCE was polished and cleaned as explained in previous sections before polymerisation. The polymer film was grown from a 1.0×10^{-3} M solution of para toluene sulfonic acid (TSA) in 0.1 M NaCl by cyclic potential sweeping from -2.0 to 2.5 V at the scan rate of 0.1 V s^{-1} for 20 cycles [97]. Fig. 2.7 shows the cyclic voltammogram of the electropolymerisation process.

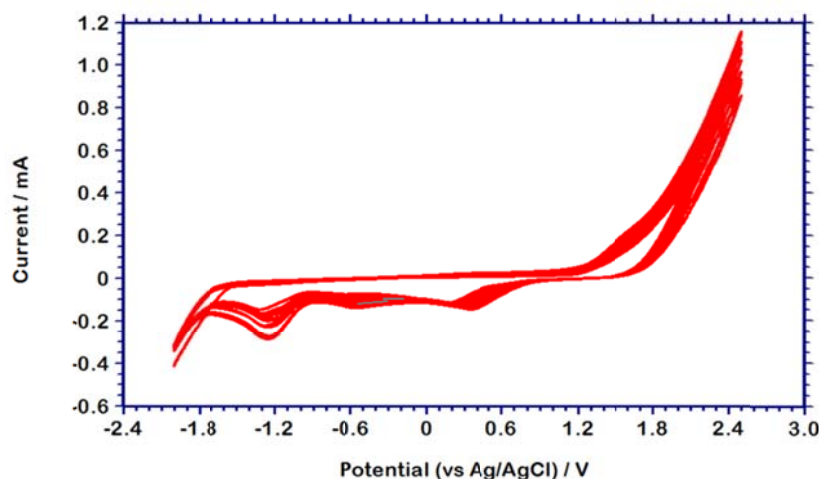
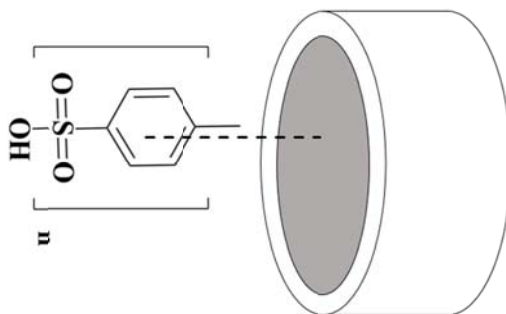


Figure 2.7: Electropolymerisation of TSA on GCE

On sweeping the potential from -2.0 V to +2.5 V, three reduction peaks are observed at 0.23 V, -0.59 V and -1.21V. These are attributed to the reduction of the monomer TSA [9]. The formation of the conducting polymer was indicated by the increase in peak current during the subsequent cycles.

The electrode after polymerisation was washed with double distilled water and dried in air. A uniform blue coloured film was seen adhering to the surface of the GCE. The modified electrode is denoted as $p(\text{TSA})/\text{GCE}$ and is represented in Scheme 2.3.



Scheme 2.3: $p(\text{TSA})/\text{GCE}$

2.3.2 Characterisation of the electrode

SEM images of the bare GCE and $p(\text{TSA})/\text{GCE}$ are shown in Fig. 2.8. From the images, it is evident that the surface morphology of GCE has changed on the formation of the polymer film.

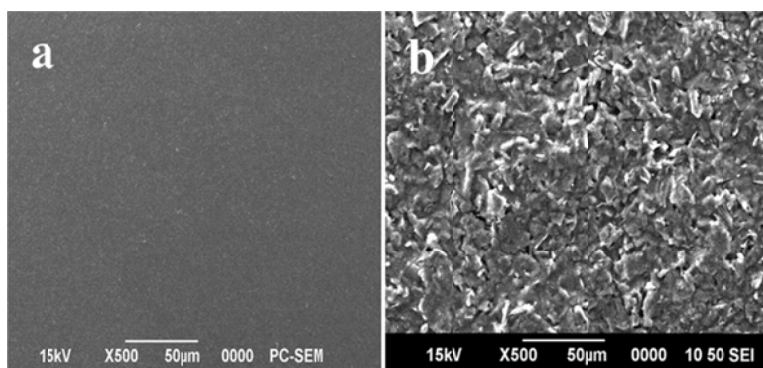


Figure 2.8: SEM images of bare GCE (a) and $p(\text{TSA})/\text{GCE}$

Nyquist plots of bare and $p(\text{TSA})/\text{GCE}$ recorded in $5.0 \times 10^{-3} \text{ M}$ $[\text{Fe}(\text{CN})_6]^{3-/4-}$ in 0.1 M KCl over a frequency range $1.0 \times 10^{-1} - 1.0 \times 10^4 \text{ Hz}$ and amplitude of 0.005 V is shown in Fig. 2.9.

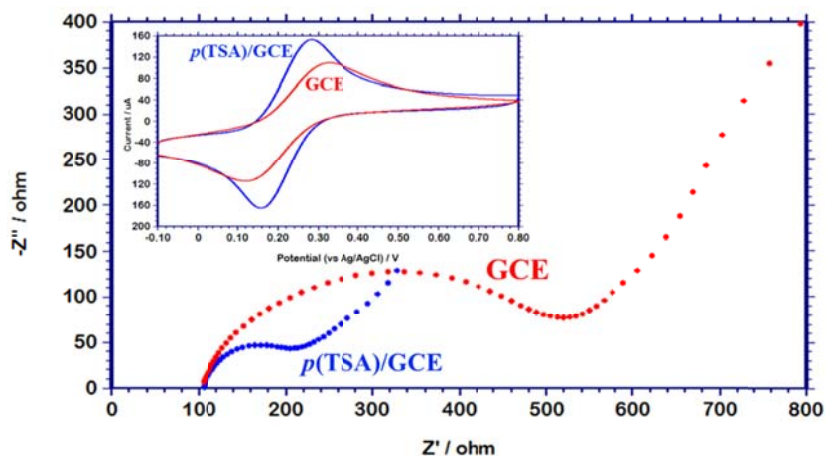


Figure 2.9: Nyquist plots of bare GCE and $p(\text{TSA})/\text{GCE}$ recorded in $5.0 \times 10^{-3} \text{ M}$ $[\text{Fe}(\text{CN})_6]^{3-/4-}$ in 0.1 M KCl. Inset shows the overlay of cyclic voltammogram obtained on bare GCE and $p(\text{TSA})/\text{GCE}$ in the same solution

There is a change in the Nyquist plots of bare GCE and $p(\text{TSA})/\text{GCE}$, indicating change in surface properties of GCE upon modification. The diameter of the semi-circular region or the charge transfer resistance of the GCE (300.8Ω when fitted to the equivalent circuit) is seen to be decreased on formation of $p(\text{TSA})$ layer (84.5Ω when fitted to the equivalent circuit). The cyclic voltammograms recorded in $5.0 \times 10^{-3} \text{ M}$ $[\text{Fe}(\text{CN})_6]^{3-/4-}$ in 0.1 M KCl on bare GCE and $p(\text{TSA})/\text{GCE}$ is shown in the inset of Fig. 2.9. There is a lowering of oxidation potential and an increase in peak currents on the $p(\text{TSA})/\text{GCE}$, compared to the GCE. These facts indicate that the electron transfer is facilitated across the polymer film.

2.4 Poly(para amino benzene sulfonic acid) modified glassy carbon electrode

2.4.1 Fabrication

Electropolymerisation of para amino benzene sulfonic acid (ABSA) on the GCE was carried out from a 2.0×10^{-3} M solution of the monomer in 0.1 M nitric acid by cyclic potential sweeping from -0.5 V to 2.0 V at a scan rate of 0.1 Vs^{-1} for 20 cycles [114]. The cyclic voltammogram of the electropolymerisation process is presented in Fig. 2.10. A schematic representation of the fabricated *p*(ABSA)/GCE is shown as the inset of Fig. 2.10.

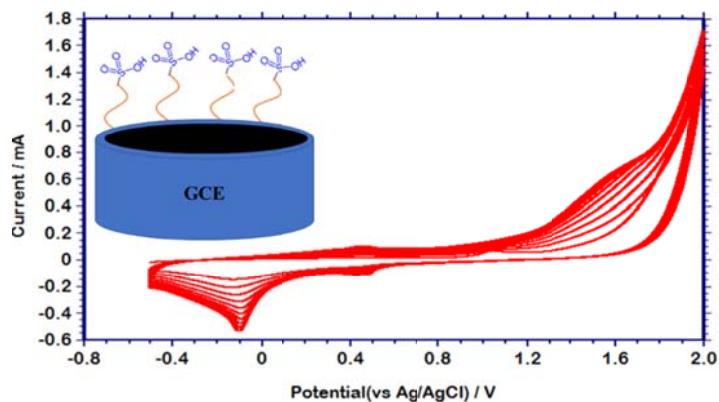
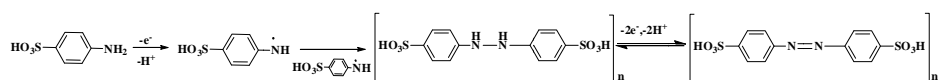


Figure 2.10: Electropolymerisation of ABSA on GCE. Inset shows the schematic representation of the modified electrode

The cyclic voltammogram obtained on the growth of poly(ABSA) on the GCE, is similar to the previously reported polymerisations [99,116]. In the first cycle, during the forward scan, a peak appears at 1.06 V corresponding to the one electron oxidation of the -NH₂ group of ABSA to a free radical. The generated ABSA radical auto-combine to give

hydrazobenzene sulfonic acid. During the second cycle, the forward scan produces a peak at 0.44 V in addition to first peak, whereas in the reverse scan peaks appear at 0.38 V and -0.15 V. The peaks at 0.44 V and 0.38 V are due to the reversible oxidation of azobenzene sulfonic acid to hydrazobenzene sulfonic acid [99]. The reduction peak at -0.15 V has been attributed to the insertion of anions such as NO_3^- to the polymer matrix together with hydrogenation [115]. As the number of scans increases, the current of each peak also increases, confirming the formation of a conducting polymer. Taking all these facts into consideration, the polymer film possibly formed on the surface of the GCE can be represented as shown in Scheme 2.4.



Scheme 2.4: Electropolymerisation of ABSA on GCE [16]

The GCE after polymerisation was washed with double distilled water and dried in air. The modified GCE is represented as $p(\text{ABSA})/\text{GCE}$. Prior to use, the $p(\text{ABSA})/\text{GCE}$ was electroactivated by potential cycling between -0.5 V to +1.5 V in 0.1 M PBS of pH 7 until a stable voltammogram was obtained.

2.4.2 Characterisation of the electrode

Surface morphology of $p(\text{ABSA})/\text{GCE}$ was studied by SEM. The SEM images of the bare and $p(\text{ABSA})/\text{GCE}$ (Fig. 2.11) indicate that the surface morphology of GCE has changed upon formation of the polymer on its surface.

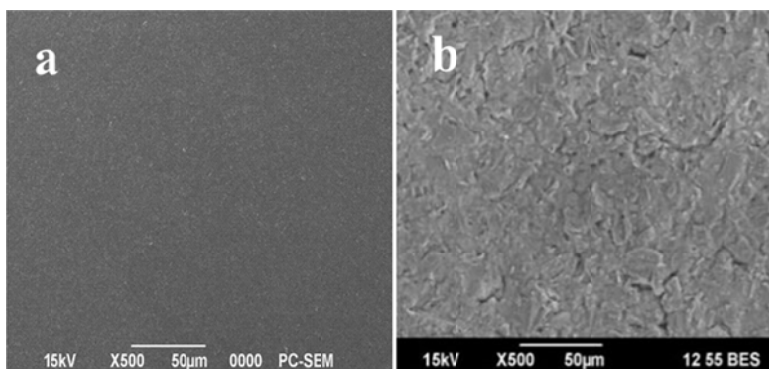


Figure 2.11: SEM images of bare GCE (a) and $p(\text{ABSA})/\text{GCE}$ (b)

The electrochemical impedance measurements, represented by the Nyquist plot, on the bare GCE and $p(\text{ABSA})/\text{GCE}$ is shown in Fig. 2.12. The value of charge transfer resistance obtained by fitting the Nyquist plot to the Randles-Ershler circuit is obtained to be 300.8Ω and 256.6Ω for the bare GCE and $p(\text{ABSA})/\text{GCE}$. This is evident from the decrease in the diameter of the semi-circular region of the Nyquist plot obtained for the polymer modified GCE compared to bare GCE. This indicates that the charge transfer resistance of the GCE has decreased upon modification. i.e., electron transfer is facilitated on $p(\text{ABSA})/\text{GCE}$. A large decrease in R_{ct} is not observed on the $p(\text{ABSA})/\text{GCE}$ possibly because of the repulsion between the negatively charged $[\text{Fe}(\text{CN})_6]^{3-/4-}$ and the ionised sulfonic acid groups present on the polymer surface. But still the negatively charged $[\text{Fe}(\text{CN})_6]^{3-/4-}$ can reach the surface of the electrode through the pin hole lacuna of the $p(\text{ABSA})$ film [99].

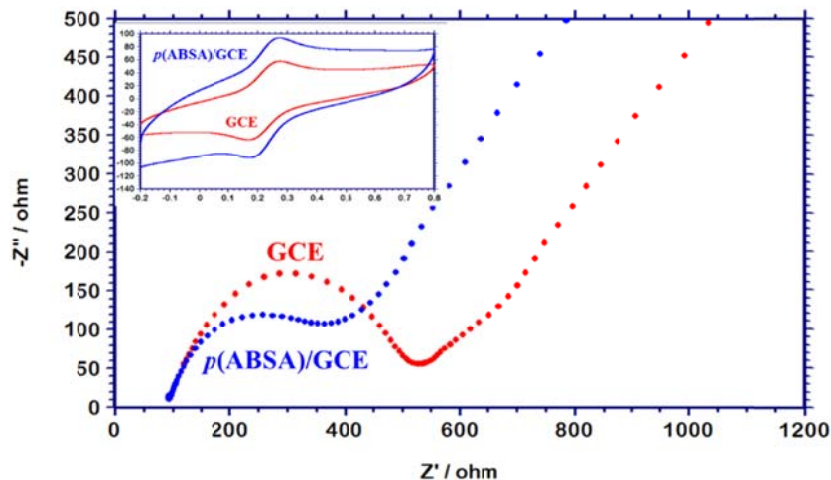


Figure 2.12: Nyquist plots of bare GCE and $p(\text{ABSA})/\text{GCE}$ recorded in 5.0×10^{-3} M $[\text{Fe}(\text{CN})_6]^{3-/4-}$ in 0.1 M KCl over a frequency range $1.0 \times 10^{-1} - 1.0 \times 10^4$ Hz and amplitude of 0.005 V. Inset shows the overlay of cyclic voltammogram obtained on bare GCE and $p(\text{ABSA})/\text{GCE}$ in the same solution

2.5 Poly(4-amino-3-hydroxy naphthalene-1-sulfonic acid) modified glassy carbon electrode

2.5.1 Fabrication

The polymer film was deposited on a polished and mechanically cleaned GCE by cycling the potential between -0.8 V to $+2.0$ V in 2.0×10^{-3} M solution of the monomer, 4-amino-3-hydroxy naphthalene-1-sulfonic acid (AHNSA) in 0.1 M HNO_3 for 25 cycles [111]. The cyclic voltammogram obtained for the polymerisation process is displayed as Fig. 2.13.

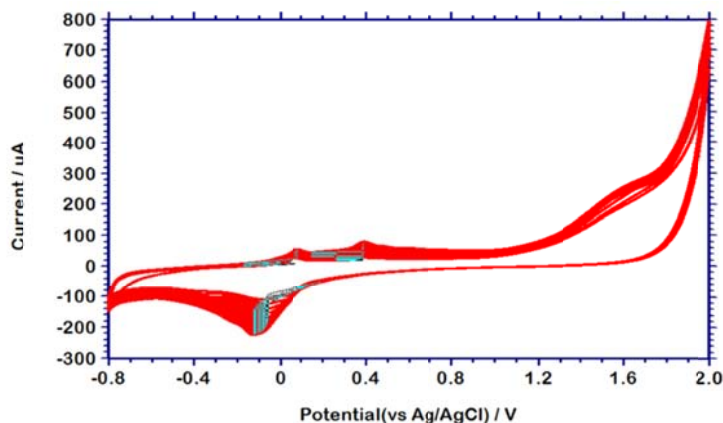


Figure 2.13: Electropolymerisation of AHNSA on GCE

During the polymerisation, anodic peaks appear at 0.032 V and 0.437 V, and the cathodic peak appears at -0.203 V. The peak current increases with subsequent cycles, indicating the growth of the polymer film on the GCE. After the polymerisation, the electrode was washed with double distilled water, dried in air and stored in 0.1M PBS of pH 7 till use. Prior to use, electro activation was carried out by sweeping the potential between -0.8 V to +1.0 V in 0.1 M PBS pH 7 until a stable voltammogram is obtained. The fabricated electrode is denoted as $p(\text{AHNSA})/\text{GCE}$.

2.5.2 Characterisation of the electrode

The SEM images of the $p(\text{AHNSA})/\text{GCE}$ obtained by electropolymerizing AHNSA onto GCE are shown in Fig.2.14. On formation of the polymer film the surface of GCE has become rough. This may lead to an increase in surface area of the GCE.

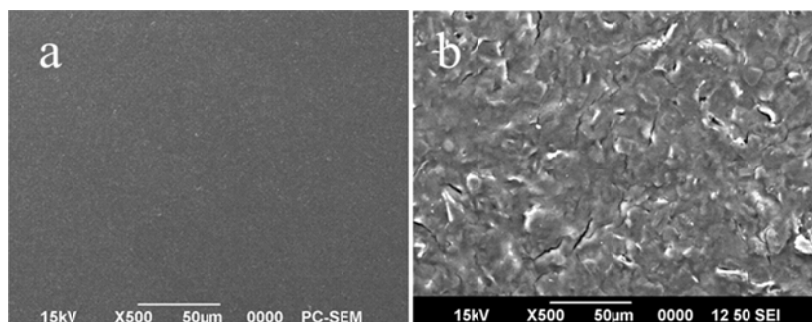


Figure 2.14: SEM images of bare GCE (a) and $p(\text{AHNSA})/\text{GCE}$ (b)

The electrochemical impedance spectra of the bare and modified electrodes can give an idea about the interface properties of the modified electrode. The Nyquist plots for bare GCE and $p(\text{AHNSA})/\text{GCE}$ was recorded in 5.0×10^{-3} M $[\text{Fe}(\text{CN})_6]^{3-/4-}$ dissolved in 0.1 M KCl over a frequency range $1.0 \times 10^{-1} - 1.0 \times 10^5$ Hz is presented in Fig 2.15. The charge transfer resistance, R_{ct} of the bare and $p(\text{AHNSA})/\text{GCE}$ are obtained to be 300.8Ω and 773.8Ω respectively when fitted to an equivalent circuit. There is an increase in charge transfer resistance upon modification. A possible explanation is the presence of phenolic and sulfonic acid groups which are ionised on the polymer backbone. The repulsion produced by the negative charges on the polymer modified surface hinder the approach of $[\text{Fe}(\text{CN})_6]^{3-/4-}$ thereby making the electron transfer at the interface difficult. This is evident from the cyclic voltammogram obtained in the same solution (Inset of Fig. 2.15). For the redox reaction, the peak currents were significantly lower on the $p(\text{AHNSA})/\text{GCE}$ although there was a decrease of overpotential.

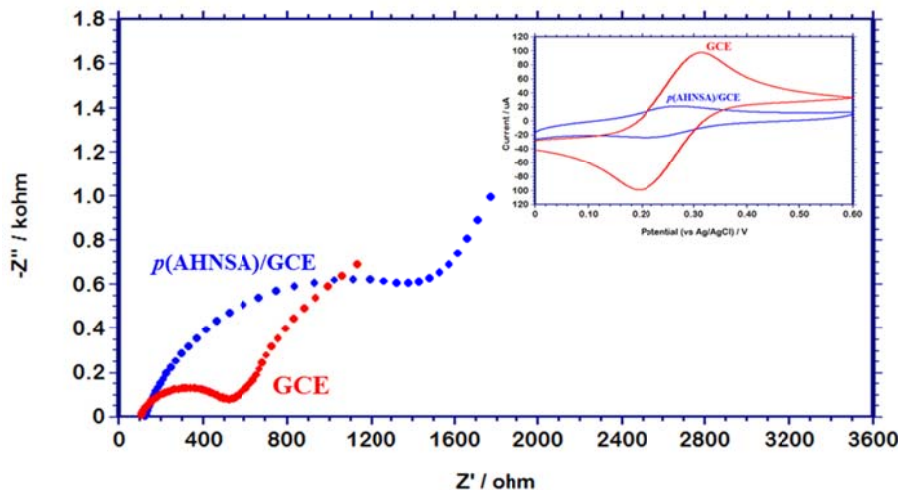


Figure 2.15: Nyquist plots of bare GCE and $p(\text{AHNSA})/\text{GCE}$ recorded in $5.0 \times 10^{-3} \text{ M } [\text{Fe}(\text{CN})_6]^{3-/4-}$ in 0.1 M KCl . Inset shows the overlay of cyclic voltammogram obtained on bare GCE and $p(\text{AHNSA})/\text{GCE}$ in the same solution

2.6 Comparison of charge transfer resistance of the fabricated electropolymer modified electrodes

The change in R_{ct} values of the GCE upon modification with various electropolymers is compiled in Table 2.1

Table 2.1: Change in R_{ct}

Electrode	Change in R_{ct} with respect to GCE
$p(\text{AspA})/\text{GCE}$	-202.3
$p(\text{GA})/\text{GCE}$	-185.0
$p(\text{TSA})/\text{GCE}$	-216.3
$p(\text{ABSA})/\text{GCE}$	-44.2
$p(\text{AHNSA})/\text{GCE}$	+472.2

GCEs modified with $p(\text{AspA})$, $p(\text{GA})$, $p(\text{TSA})$ and $p(\text{ABSA})$ showed a decrease in charge transfer resistance whereas $p(\text{AHNSA})$ modified GCEs showed an increase in charge transfer resistance. $p(\text{AHNSA})$ films with high electron density along with the ionisable sulfonic acid and phenolic groups would repel the negatively charged $[\text{Fe}(\text{CN})_6]^{3-/4-}$, thereby making the transfer of electron from the ion to the electrode difficult. But such effect was not observed with $p(\text{TSA})$ or $p(\text{ABSA})$ film, even though they also have ionisable sulfonic acid groups. This may be due to the morphology of the $p(\text{TSA})$ and $p(\text{ABSA})$ film. Even with the outwardly projecting sulfonic acid moieties, $[\text{Fe}(\text{CN})_6]^{3-/4-}$ can reach the surface of the electrode through the pinhole lacuna of the polymer structure [99]. This may be the reason for the decrease in R_{ct} .

2.7 Experimental

2.7.1 Chemicals

All reagents were used as received and aqueous solutions made with Millipore water. AspA and cytosine were sourced from Spectrochem Pvt. Ltd, India whereas GA, adenine, thymine and theophylline were from Himedia laboratories Pvt. Ltd, India. Central Drug House Pvt. Ltd., India supplied AHNSA. ABSA and guanine were purchased from s.. Fine Chemicals Pvt. Ltd., India. Sisco Research Laboratories provided uric acid, xanthine, and Herring Sperm DNA. Caffeine was purchased from Alfa Aesar, England. Merck Life Sciences Pvt. Ltd., India, furnished sodium acetate trihydrate, acetic acid, trisodium citrate, monosodium dihydrogen phosphate, disodium hydrogen phosphate, sodium hydroxide and sodium chloride. Boric acid, citric acid and phosphoric acid as well as ammonium

chloride, calcium chloride, potassium chloride, potassium phosphate and sodium sulphite were supplied by s. d. Fine chemicals Pvt. Ltd., India.

Pharmaceutical formulations of caffeine and theophylline as well as tea and coffee samples were obtained from local supermarket.

2.7.2 Instrumentation

The voltammetric measurements were performed using the CHI electrochemical analyser model no: CHI6023D (CH Instruments Inc. USA) and Impedance studies were carried out on CHI6017D electrochemical analyser which were integrated to a desk top computer. The three-electrode set up with Ag/AgCl electrode, Platinum wire counter electrode and glassy carbon as working electrode was employed for the electrochemical measurements. Unless otherwise stated, differential pulse voltammograms were recorded at with an amplitude of 0.05 V, pulse width of 0.06 s, sample width of 0.02 s and pulse period of 0.5 s and square wave voltammograms at an amplitude of 0.025 V, increment of 0.004 V and frequency of 15 Hz. CV and LSV were carried out at the scan rate of 0.1 Vs⁻¹ and sample interval of 0.001 V.

Metrohm pH meter was used to adjust the pH of buffer solutions.

Scanning Electron Microscopy images were recorded on JEOL 6390LV instrument.

2.7.3 Preparation of stock solutions

1.0×10^{-2} M stock solutions of Gu, Ad, Thy, Cyt, Ua and XT were prepared in 0.1 M NaOH and solutions of required concentration were prepared by serial dilution of the stock solution with Millipore water.

1.0×10^{-2} M solution of TP and CF were prepared in 0.01 M PBS pH 4 and diluted with Millipore water to prepare lower concentrations.

2.7.4 Preparation of DNA sample

The purchased DNA sample was subjected to acid denaturation using the procedure reported by Brett and Serrano [117]. 30.4 mg of the DNA was accurately weighed and ultrasonically dissolved in 0.5 mL HClO₄. It is then neutralised with 0.5 mL of 9 M NaOH and made up to 50 mL with 0.1 M NaOH.

2.7.5 Preparation of Tea and Coffee samples

2 g of the sample (tea or coffee powder) was accurately weighed and boiled with 50 mL water for 15 minutes. It is then cooled, filtered and made up to 100 mL with Millipore water.

2.7.6 Preparation of pharmaceutical samples

10 tablets were grinded to a homogeneous fine powder using a mortar and pestle. 100 mg of this powder was accurately weighed, dissolved in 0.1 M PBS of pH 4 and made up to 100 mL with Millipore water.

2.7.7 Preparation of artificial urine

Artificial urine was prepared according to the DIN EN 1616:1999 standard procedure. 2.5 g urea, 1.0 gm NaCl, 0.5 g creatinine, 0.2 g each of disodium hydrogen phosphate, potassium phosphate, sodium sulphite and ammonium chloride, 0.05 g each of calcium chloride, magnesium chloride, sodium citrate and uric acid and 0.01 g of bovine serum albumin was dissolved in 100 mL Millipore water. The pH of the resulting solution was adjusted with 0.01 M ammonium hydroxide to 6.6 [118].

2.7.8 Preparation of artificial blood serum

Ringer's solution is a solution which is isotonic with blood serum. It is prepared by dissolving 7.2 g of NaCl, 0.37 g of KCl and 0.17 g of calcium chloride in 1000 mL Millipore water [119].

2.7.9 Preparation of buffer solutions

0.1 M Acetate buffer solution (ABS) of a specific pH was prepared by mixing required amounts of sodium acetate trihydrate and acetic acid. Trisodium citrate and citric acid were mixed to prepare 0.1 M citrate buffer (CBS) of required pH. Monosodium dihydrogen phosphate and disodium hydrogen phosphate were weighed out and made up to a definite volume to prepare 0.1 M phosphate buffer solutions of required pH. 0.1 M Britton-Robinson (BR) buffer solution was prepared by mixing 0.1 M acetic acid, 0.1 M boric acid and 0.1 M phosphoric acid and adjusting to required pH with 1.0 M NaOH.

2.7.10 Pre-treatment of glassy carbon electrode

Prior to its use, the bare GCE was polished and cleaned every time. GCE was first fine polished with 0.05 microns alumina slurry on a microcloth polishing pad to a mirror like finish and rinsed with double distilled water. It was then washed ultrasonically in methanol, 50% HNO₃, acetone and double distilled water successively to remove any adsorbed particles.

2.7.11 Analytical Procedure

10 mL of the supporting electrolyte is taken in the voltammetric cell. The desired volume of the analyte is pipetted out into to cell followed by

deaeration with nitrogen gas. The programme for the required voltammetric technique is applied and the output given by the instrument is noted.

2.8 Summary

The procedure employed for the fabrication of five electropolymers modified electrodes, $p(\text{AspA})/\text{GCE}$, $p(\text{GA})/\text{GCE}$, $p(\text{TSA})/\text{GCE}$, $p(\text{ABSA})/\text{GCE}$ and $p(\text{AHNSA})/\text{GCE}$ has been elucidated. The surface morphology and the interfacial properties of the fabricated electrodes have been studied using SEM imaging and EIS. A brief description of the materials and experimental methods employed throughout is also given.

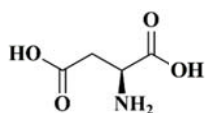
..... 

Poly(Aspartic Acid) modified Glassy Carbon Electrode as Sensor for Adenine

Adenine is one of the two purine nucleic acid bases, found in DNA and RNA. The present chapter describes the electro-oxidation of adenine on a glassy carbon electrode modified with poly(aspartic acid) when 0.1 M NaOH is used as supporting electrolyte. On the modified electrode, oxidation of 5.0×10^{-4} M adenine takes place irreversibly at a potential of 0.568 V and current of 1.6×10^{-5} A. The process was found to be diffusion controlled. The variation of peak current with concentration was found to be linear in the range from 1.3×10^{-4} M to 2.0×10^{-5} M with a detection limit of 6.7×10^{-6} M. The application of the modified electrode for the determination of adenine in herring sperm DNA is demonstrated. The kinetics of electro-oxidation of all the DNA bases on the poly(aspartic acid) modified electrode has been studied by linear sweep voltammetry and the results obtained are discussed.

3.1 Introduction

Aspartic acid (AspA) is an α -amino acid with molecular formula $C_4H_7NO_4$



Aspartic acid

This non-essential amino acid was first discovered by Auguste-Arthur Plisson and Étienne Ossian Henry from asparagus juice. AspA is an acidic amino acid (pK_a = 3.9) with a second carboxylic acid group in

addition to the α carboxylic acid group. The L-isomer of AspA is incorporated into proteins [120].

There are several reports of AspA being polymerised on to carbon based electrodes especially glassy carbon electrode (GCE).

Zang and Lin have reported covalent grafting of DL-AspA onto the GCE surface by electropolymerisation from a 1.0×10^{-3} M solution of AspA in absolute acetonitrile containing 0.1 M NBu_4BF_4 . The cyclic potential scanning was in range from 0.50–1.70 V, at a scan rate of 0.02 V s^{-1} for five cycles. The use of the $p(\text{AspA})/\text{GCE}$ for the simultaneous determination of dopamine and ascorbic acid was also demonstrated by them [121].

The same procedure was taken up by Wang et al., to produce covalently grafted $p(\text{AspA})/\text{GCE}$ and the electrode was used for the simultaneous determination of catechol and hydroquinone [122].

Electropolymerisation of AspA from aqueous media was reported by Wang and co-workers. They polymerised AspA from 1.0×10^{-3} M L-AspA solution in 0.025 M PBS (pH 6.8), by cyclic scanning of potential in the range -1.2 to 1.9 V for 15 cycles at the scan rate of 0.1 Vs^{-1} . They demonstrated the application of the modified electrode for fast detection of catechin in tea beverage [123].

Yu and co-workers adopted a similar procedure for preparing $p(\text{AspA})/\text{GCE}$. They made use of cycling scanning of potential between -0.80 to +2.40 V for eight cycles at a scan rate of 0.1 Vs^{-1} on GCE immersed in 2.0×10^{-3} M L-AspA in 0.1 M PBS pH 5. The fabricated electrode exhibited excellent electrocatalytic activity for the oxidation-reduction reactions of epinephrine, eliminating the interference of ascorbic

acid and uric acid (Ua) [124]. The same group has demonstrated the application of *p*(AspA)/GCE for the determination of dopamine and nor-epinephrine, eliminating interference from ascorbic acid and Ua [125].

Li and Zhang had electropolymerised AspA onto GCE from a 1.0×10^{-3} M L-AspA aqueous solution by cycling the potential between -1.5 V to 2.0 V at a scan rate of 0.1 Vs^{-1} . Nano gold was electrodeposited on the *p*(AspA)/GCE and the electrode was used for simultaneous determination of dopamine, ascorbic acid and Ua [126].

Liu et al., prepared *p*(AspA)/GCE by cyclic scanning between -1.1 and 2.3 V at 0.1 V s^{-1} in 0.1 M PBS pH 7.4 containing 2.5×10^{-3} M AspA and used it for the elucidation of electrochemical behaviour of brucine [127]. They repeated the same procedure using 0.1 M PBS pH 5.8 containing 2.5×10^{-3} M AspA and the fabricated electrode was further modified with multiwalled carbon nanotubes. The composite electrode was used for the determination of pesticide imidacloprid [128].

AspA was polymerised on to a carbon paste electrode modified with TiO_2 hollow spheres and multiwalled carbon nanotubes to develop a composite electrode for the simultaneous determination of levodopa and acetaminophen in presence of ascorbic acid by Babaei and Sohrabi [129].

We have adopted the method suggested by Yu et al. [124] and fabricated the *p*(AspA)/GCE by electropolymerizing AspA from 2.0×10^{-3} M L-AspA dissolved in 0.1 M PBS pH 5 by cyclic potential scanning between -0.80 to +2.0 V at a scan rate of 0.1 Vs^{-1} . The electrochemical behaviour of DNA bases on the fabricated electrode was studied. To the best of our knowledge, *p*(AspA)/GCE has not been developed as a sensor for any of the DNA bases.

3.2 Results and discussion

The performance of *p*(AspA)/GCE fabricated and characterised as described in chapter 2, towards electro-oxidation of adenine (Ad) was optimised.

3.2.1 Optimisation of experimental parameters

3.2.1.1 Supporting electrolyte

The DPV response of 5.0×10^{-5} M Ad on *p*(AspA)/GCE was studied in 0.1 M concentration of different electrolytes such as H₂SO₄, HNO₃, NaCl, KCl, KNO₃, NaOH, KOH and electrolytic buffer solutions such as PBS, acetate buffer (ABS) and citrate buffer (CBS). The lowest potential for electro-oxidation was observed in NaOH and hence 0.1 M NaOH was used as the supporting electrolyte in all further experiments.

3.2.1.2 Number of cycles of polymerisation

Variation of electrochemical response of 5.0×10^{-5} M Ad with increase in the number of cycles of polymerisation is represented in Fig. 3.1. It can be seen that as the number of cycles of polymerisation increases from 5 to 16, the lowest peak potential and highest peak current was observed when the number of polymerisation cycles was 14. Hence the number of cycles of polymerisation to produce the best sensor performance was deduced to be 14.

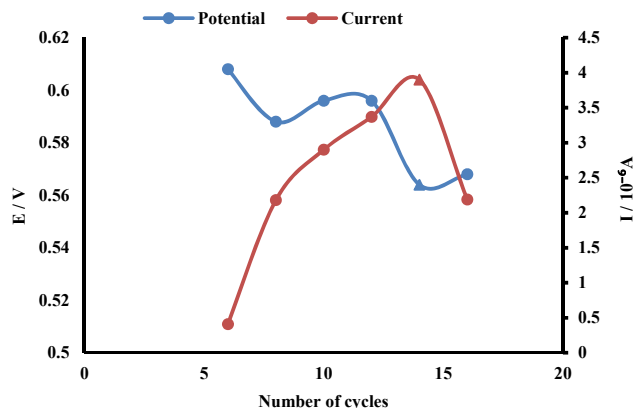


Figure 3.1: Variation of peak parameters with number of cycles of polymerisation

3.2.2 Voltammetric behaviour of the DNA bases on the *p*(AspA)/GCE

The differential pulse (DP) voltammetric response of 5.0×10^{-4} M concentrations of DNA bases; guanine (Gu), adenine (Ad), thymine (Thy) and cytosine (Cyt); was studied in 0.1 M NaOH. On the bare GCE, the peaks due to the oxidation of 5.0×10^{-5} M Gu, Ad, Thy and Cy appeared at 0.348 V, 0.600 V, 0.780 V and 1.002 V respectively, in the differential pulse mode. Oxidation of Gu took place at 0.332 V, Ad at 0.568 V, Thy at 0.765 V and Cy at 0.984 V on the *p*(AspA)/GCE under the same conditions. The maximum lowering of peak potential was observed for Ad and hence optimisation of the sensor for determination of Ad was attempted.

On the bare GCE, oxidation of 5.0×10^{-4} M Ad, took place at a potential of 0.600 V with a peak current of 7.8×10^{-6} A, whereas on the *p*(AspA)/GCE, the oxidation took place at a potential of 0.568 V with a peak current of 1.6×10^{-5} A in DPV mode. The peak potential was decreased by 0.032 V and there is a twofold enhancement of peak current on the modified electrode in comparison to the bare GCE (Fig 3.2).

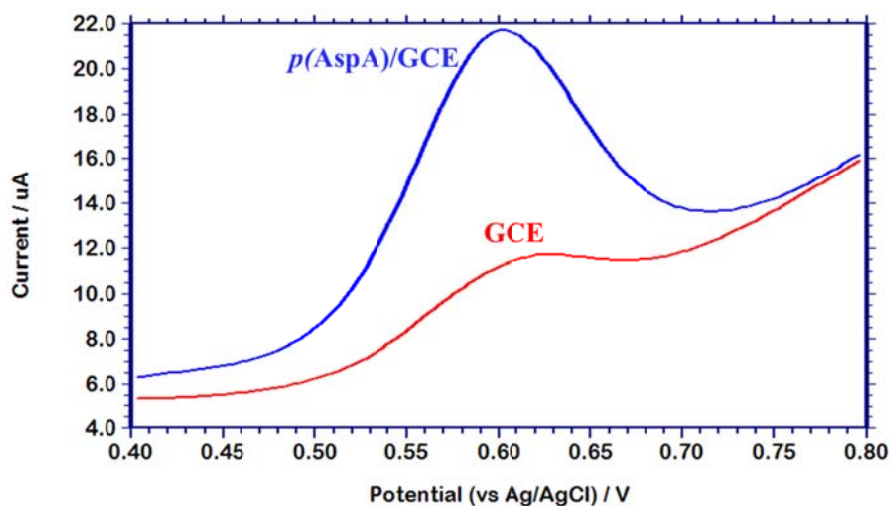


Figure 3.2: DPV response for the oxidation of 5.0×10^{-5} M Ad on the bare GCE and $p(\text{AspA})/\text{GCE}$

Cyclic voltammogram of Ad on the $p(\text{AspA})/\text{GCE}$ showed a single oxidation peak in the forward scan at 0.640 V and a peak was not obtained in the reverse scan (scan rate of 0.1 Vs^{-1}) indicating that the electro-oxidation of Ad is irreversible.

3.2.3 Electrochemical Impedance Spectroscopy (EIS)

EIS measurements for the oxidation of Ad on the bare and modified electrodes show that the charge transfer resistance (R_{ct}) has decreased on the modified electrode compared to the bare electrode. Overlay of EIS Nyquist plots of the bare GCE and $p(\text{AspA})/\text{GCE}$ in 5.0×10^{-5} M Ad in 0.1 M NaOH in the frequency range $1.0 - 1.0 \times 10^5$ Hz at the corresponding oxidation potential is shown in Fig 3.3. The R_{ct} value on GCE was found to be $2.62 \times 10^4 \Omega$ and that for $p(\text{AspA})/\text{GCE}$ was obtained to be $1.27 \times 10^4 \Omega$ when fitted to the circuit $\{R_s[C_{dl}(R_{ct}W)]\}$ using ZSimpWin software (R_s being solution resistance, C_{dl} , the double layer capacitance and W , the

Warburg Impedance). The presence of the polymer on the surface of the GCE, may be the reason for decrease in charge transfer resistance.

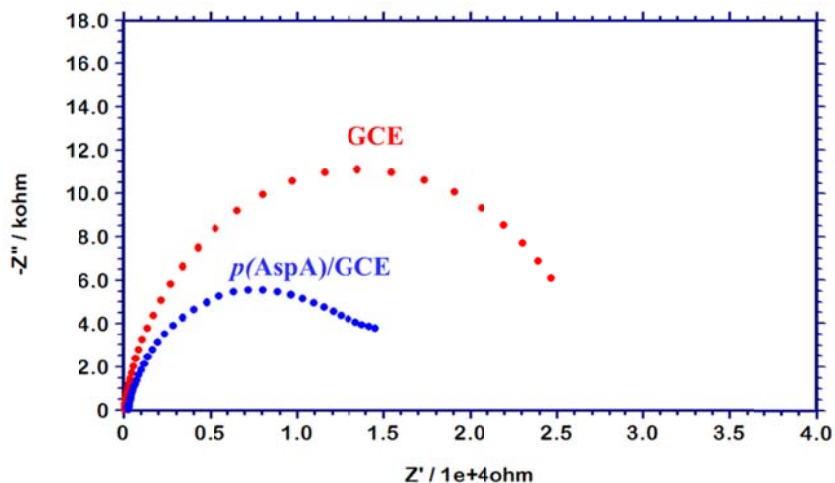


Figure 3.3: Overlay of Nyquist plots of bare GCE and $p(\text{AspA})/\text{GCE}$ in $5.0 \times 10^{-5} \text{ M Ad}$ in 0.1 M NaOH in the frequency range $1.0 - 1.0 \times 10^5 \text{ Hz}$ at the corresponding oxidation potential

3.2.4 Electroactive surface area

Cyclic voltammogram of $\text{K}_3[\text{Fe}(\text{CN})_6]$ shows redox peaks due to the reversible oxidation of Fe^{3+} to Fe^{2+} . Cyclic voltammogram for the electro-oxidation of $2.0 \times 10^{-3} \text{ M K}_3[\text{Fe}(\text{CN})_6]$ on the $p(\text{AspA})/\text{GCE}$ was recorded at different scan rates ranging from 0.02 Vs^{-1} to 0.20 Vs^{-1} (Fig 3.4). The plot of peak current I versus square root of scan rate $\nu^{1/2}$ gave a linear graph with regression equation,

$$I (\text{A}) = 1.245 \times 10^{-4} \nu^{1/2} (\text{Vs}^{-1}) - 5.781 \times 10^{-6} \quad [R^2 = 0.997]$$

Comparing with the Randles-Sevcik equation [130],

$$I = 2.69 \times 10^5 a n^{3/2} D^{1/2} C \nu^{1/2}$$

the slope of I vs $v^{1/2}$,

$$\text{slope} = 2.69 \times 10^5 a n^{3/2} D^{1/2} C$$

From this, a , the electroactive surface area of the electrode can be determined, since n , the number of electrons involved in the electrochemical reaction is 1; D , the diffusion coefficient is $7.6 \times 10^{-6} \text{ cm}^2\text{s}^{-1}$ and C , the concentration of the electroactive species is $2.0 \times 10^{-6} \text{ moles cm}^{-3}$. Electroactive surface area of the modified electrode was calculated to be 0.084 cm^2 . The surface area of bare GCE calculated using the same approach (Fig 3.5) was found to be 0.066 cm^2 .

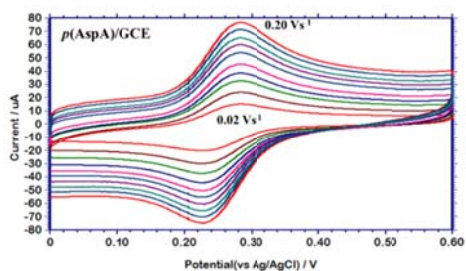


Figure 3.4: Cyclic voltammograms of $2.0 \times 10^{-3} \text{ M}$ $\text{K}_3[\text{Fe}(\text{CN})_6]$ on $p(\text{AspA})/\text{GCE}$ at scan rates 0.02 Vs^{-1} to 0.20 Vs^{-1}

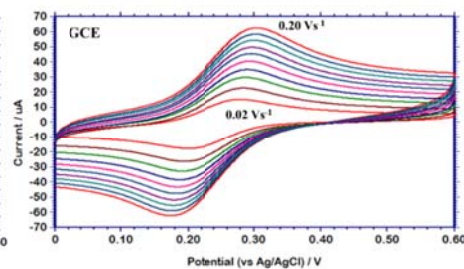


Figure 3.5: Cyclic voltammograms of $2.0 \times 10^{-3} \text{ M}$ $\text{K}_3[\text{Fe}(\text{CN})_6]$ on GCE at scan rates 0.02 Vs^{-1} to 0.20 Vs^{-1}

3.2.5 Calibration curve

The oxidation peak current of Ad showed an increase with increase in concentration (Fig 3.6). The variation of peak current with concentration was found to be linear from $1.3 \times 10^{-4} \text{ M}$ to $2.0 \times 10^{-5} \text{ M}$ (Fig. 3.7) with regression equation,

$$I (\text{A}) = 0.030C (\text{M}) + 0.731 \times 10^{-6} \quad [R^2 = 0.997]$$

The value of detection limit calculated using the formula $3S/m$ (where S is the standard deviation of the analytical signal and m is the slope of the calibration curve) was 6.7×10^{-6} M.

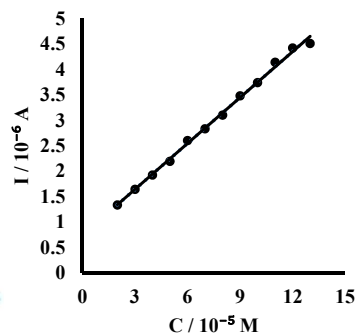
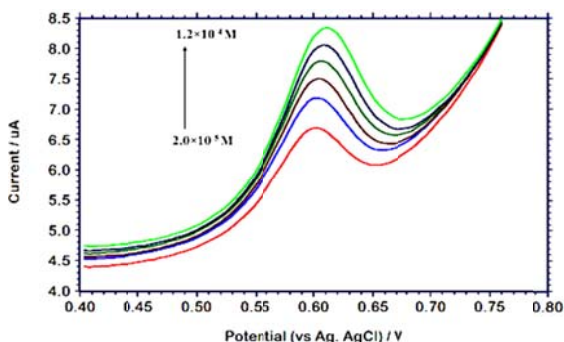


Figure 3.6: Overlay of DP voltammograms for the oxidation of 2.0×10^{-5} M to 1.2×10^{-4} M Ad on $p(\text{AspA})/\text{GCE}$

Figure 3.7: Calibration curve of Ad

3.2.6 Mechanistic Studies

To get an insight into the mechanism of the electro-oxidation process, effect of pH of the medium and that of scan rate on the peak parameters were studied.

3.2.6.1 Effect of pH

Effect of pH on the peak potential for electro-oxidation of Ad was inspected in 0.1 M PBS in the pH range 3-11. With increasing pH, the peak potential shifted negatively as per the equation,

$$E \text{ (V)} = -0.070\text{pH} + 1.549 \quad [R^2 = 0.958]$$

The slope of the plot of **E** vs **pH** was found to be 0.07 which is closer to the theoretical value of 0.06 expected for an electron transfer followed by transfer of equal number of protons [131].

3.2.6.2 Effect of scan rate

The variation of peak parameters for the electro-oxidation of 5.0×10^{-4} M Ad with scan rate in the LSV mode was studied in the range from 0.1 Vs^{-1} to 1.0 Vs^{-1} (Fig. 3.8 and Table 3.1). The peak current varied linearly with square root of scan rate [132], with the plot of $\log I$ vs $\log v$ giving a slope of 0.55. Since the value is close to the theoretical value of 0.5 for a diffusion controlled process [133], the electrochemical oxidation of Ad on *p*(AspA)/GCE is deduced to be a diffusion controlled process.

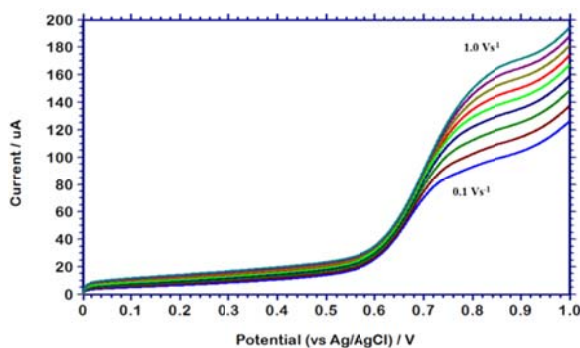


Figure 3.8: Overlay of LSV curves for the oxidation of 5.0×10^{-4} M Ad on *p*(AspA)/GCE at different scan rates ranging from 0.1 Vs^{-1} to 1.0 Vs^{-1}

Table 3.1: Variation of peak parameters with scan rate

Regression equation	R^2
$E \text{ (V)} = 0.0313 \ln v \text{ (Vs}^{-1}\text{)} + 0.689$	0.991
$I \text{ (A)} = 3.524 \times 10^{-4} v^{1/2} \text{ (Vs}^{-1}\text{)} + 6.215 \times 10^{-6}$	0.997
$\log I \text{ (A)} = 0.545 \log v \text{ (Vs}^{-1}\text{)} - 3.432$	0.988

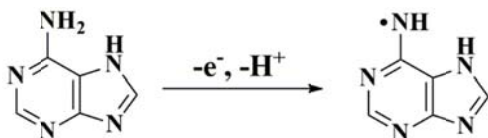
The value of Tafel slope can be obtained from the plot of E vs $\ln v$,

$$\text{Slope} = \frac{RT}{2(1 - \alpha)n_{\alpha}F}$$

where R is the universal gas constant, T is the temperature (298 K), n_{α} , the number of electrons involved in the rate determining step, F the faraday constant (96500) and α , the charge transfer coefficient given by,

$$E - E_{1/2} = \frac{0.047}{\alpha n_{\alpha}}$$

Solving the equations, the charge transfer coefficient α and the number of electrons involved in the rate determining step can be calculated [134]. For the electro-oxidation of Ad on $p(\text{AspA})/\text{GCE}$ the value of α , was found to be 0.623 and that of n_{α} was obtained as 1. The electro-oxidation of Ad on the $p(\text{AspA})/\text{GCE}$ is controlled by diffusion of Ad on to the electrode surface where it undergoes a one electron, one proton transfer reaction (Scheme 3.1). Such mechanism of electro-oxidation of Ad has been reported in literature [67,135].



Scheme 3.1: Possible mechanism of electro-oxidation of Ad [67]

3.2.7 Effect of co-existing molecules

DNA contains, in addition to Ad, other bases like Gu, Thy and Cyt as well as sugar residue, phosphoric acid moiety etc. To evaluate the effect of these molecules on the determination of Ad by $p(\text{AspA})/\text{GCE}$, the signal

change produced by these molecules on the peak current of Ad when present in hundred-fold excess concentrations was studied (Table 3.2). It was observed that Gu, Cyt, sucrose and phosphate ions did not interfere with the determination of Ad, when present at hundred-fold excess concentrations. Thy interfered with the determination when present at the same concentration as Ad. Uracil, the nucleic acid base which replaces Thy in RNA, and Ua, the product of Ad and Gu metabolism, produced signal change within the acceptable limit of 5% when present in 1:100 molar ratio. Molecules such as urea, glucose, fructose and NaCl, which are commonly found in biological fluids did not produce significant interference. Ca^{2+} showed interference in the determination of Ad by $p(\text{AspA})/\text{GCE}$, when present at hundred-fold excess concentration.

Table 3.2: Interference study

Species	Concentration Ratio	Signal change (%)
Gu	1:100	- 3.0
Thy	10:1	-4.1
	1:1	Peak distortion
Cyt, Uracil	1:100	-3.0
Ua	1:1	-4.2
Urea	1:100	-4.8
Glucose, Fructose	1:100	-0.1
NaCl	1:100	-1.9
Sodium phosphate	1:100	-0.4
K^+	1:100	-3.0
Ca^{2+}	1:100	+8.4

3.2.8 Application: Determination of Ad in acid denatured Herring Sperm DNA

Acid denatured HS DNA solution was prepared as explained in section 2.7.4 of chapter 2. DPV of acid denatured Herring Sperm (HS) DNA shows an oxidation peak at 0.560 V, corresponding to the oxidation of Ad, on the *p*(AspA)/GCE in 0.1 M NaOH (Fig. 3.9). Using the standard addition method, the percentage of Ad in the sample was determined to be 27.9%, which is very close to the expected value of 27.8% as reported in literature [136]. The relative standard deviation (RSD) for this measurement (for six replicate measurements) was found to be 0.89%.

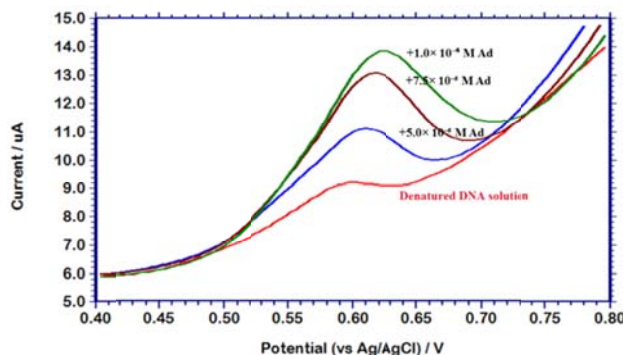


Figure 3.9: Overlay of DP voltammograms obtained in 1.5 mg mL^{-1} solution of HS DNA sample with those obtained on the addition of various concentrations of standard Ad solution.

3.2.9 Kinetics of electro-oxidation of DNA bases on *p*(AspA)/GCE

3.2.9.1 Diffusion coefficient

The diffusion coefficient, **D** is related to the limiting current **I**, by the Cottrell equation,

$$I = nFAD^{1/2}C\pi^{-1/2}t^{-1/2}$$

where n , is the number of electrons involved in the electrochemical reaction at the electrode surface of area a cm^2 , C is the bulk concentration of the electro active species in moles cm^{-3} and t , the time in seconds.

The faradaic decrease in oxidation current of Ad with time (t) was recorded by chronoamperometry in the concentration range 2.0×10^{-4} M to 2.0×10^{-3} M (Fig 3.10a). For each case, I vs $t^{-1/2}$ was plotted (Fig 3.10b) and the corresponding slopes were plotted against concentration, C (Fig 3.11). [In Cottrell equation I is measured in A and C in moles cm^{-3} . When I is measured in μA , concentration should be expressed in moles m^{-3} or mM]. The diffusion coefficient (D) of Ad under the sensor conditions was calculated from the slope of the resulting curve.

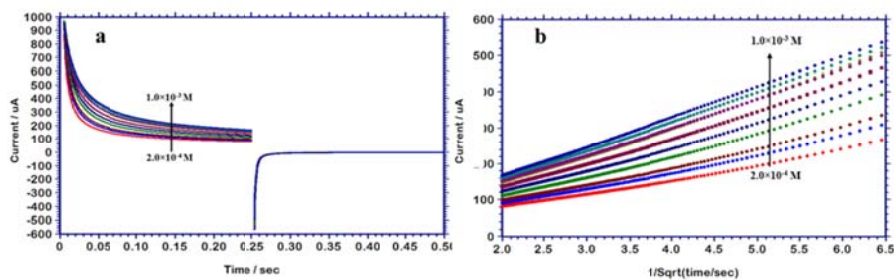


Figure 3.10: a) Chronoamperograms obtained for the oxidation of various concentrations of Ad on $p(\text{AspA})/\text{GCE}$ with 0.1 M NaOH as supporting electrolyte. b) Plot of I vs $t^{-1/2}$ at various concentrations of Ad

The value of diffusion coefficient for Ad under the experimental conditions was determined to be $6.8 \times 10^{-5} \text{ cm}^2\text{s}^{-1}$. Under the same conditions, the value of diffusion coefficient determined using the bare electrode was $1.8 \times 10^{-6} \text{ cm}^2\text{s}^{-1}$ which was an order of magnitude less than that obtained using the modified electrode.

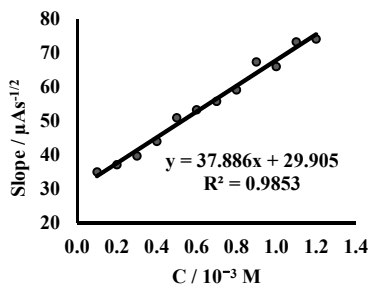


Figure 3.11: Plot of slope (I vs $t^{-1/2}$) against concentration of Ad

Similarly, the chronoamperograms of the other DNA bases Gu, Thy and Cyt were recorded at different concentrations using the bare GCE and $p(\text{AspA})/\text{GCE}$ and the diffusion coefficient of each analyte under the optimised experimental conditions was determined using the above-mentioned approach.

For Gu, the chronoamperograms were recorded in the range from 8.0×10^{-5} M to 2.0×10^{-4} M (Fig 3.12) by setting the working electrode potential at 0.350 V. The slopes of the corresponding I vs $t^{-1/2}$ plots (inset of Fig. 3.12) were plotted against concentration (Fig. 3.13).

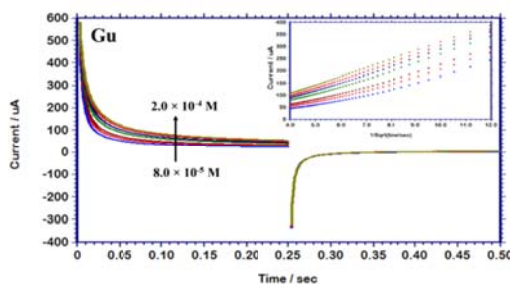


Figure 3.12: Chronoamperograms obtained for the oxidation of various concentrations of Gu on $p(\text{AspA})/\text{GCE}$ with 0.1 M NaOH as supporting electrolyte. Inset shows corresponding I vs $t^{-1/2}$ plots

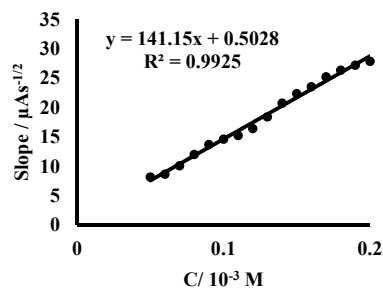


Figure 3.13: Plot of slope of (I vs $t^{-1/2}$) against concentration of Gu

The diffusion coefficient of Gu under the experimental conditions on the $p(\text{AspA})/\text{GCE}$ was found to be $2.4 \times 10^{-4} \text{ cm}^2 \text{ s}^{-1}$ whereas that on the bare GCE it was obtained to be $6.9 \times 10^{-6} \text{ cm}^2 \text{ s}^{-1}$. The diffusion coefficient of Gu was found to be increased by two orders of magnitude on the $p(\text{AspA})/\text{GCE}$ compared to the bare GCE. Using a molybdenum complex and TiO_2 nano particles modified carbon paste electrode, M. Mazloum Ardakani et al., had previously reported the diffusion coefficient of Gu in 0.1 M PBS of pH 5 to be $4.2 \times 10^{-5} \text{ cm}^2 \text{ s}^{-1}$ [65]. In ABS of pH 5.1, the diffusion coefficient of Gu has been reported to be $2.2 \times 10^{-6} \text{ cm}^2 \text{ s}^{-1}$ by A. Abbaspour et al., using cobalt phthalocyanine modified carbon paste electrode [64].

The chronoamperograms of Thy on the $p(\text{AspA})/\text{GCE}$ were recorded in the range from $9.0 \times 10^{-4} \text{ M}$ to $1.9 \times 10^{-3} \text{ M}$ (Fig.3.14) at the working electrode potential of 0.80 V. The corresponding I vs $t^{-1/2}$ plots are shown in the inset of Fig. 3.14. The slope of each plot was plotted against the corresponding concentration and the slope of the resulting graph (Fig. 3.15) was used to calculate the diffusion coefficient.

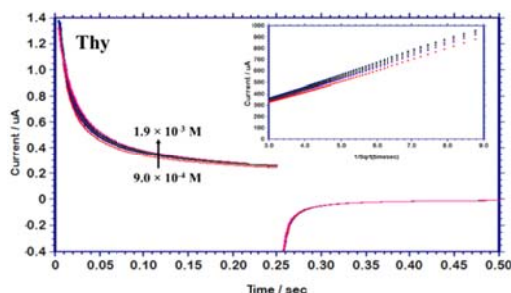


Figure 3.14: Chronoamperograms obtained for the oxidation of various concentrations of Thy on $p(\text{AspA})/\text{GCE}$ with 0.1 M NaOH as supporting electrolyte. Inset shows corresponding I vs $t^{-1/2}$ plots

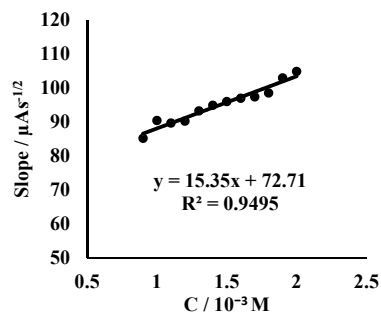


Figure 3.15: Plot of slope (I vs $t^{-1/2}$) against concentration of Thy

Using the Cottrell equation, the diffusion coefficient of Thy observed on the *p*(AspA)/GCE under the experimental conditions was obtained to be $1.1 \times 10^{-5} \text{ cm}^2 \text{ s}^{-1}$ and that on the bare GCE by the same approach was found to be $4.5 \times 10^{-6} \text{ cm}^2 \text{ s}^{-1}$. The diffusion coefficient has increased by a factor of 2.5 when measured using the *p*(AspA)/GCE compared to the bare GCE. To the best of our knowledge the chronoamperometric determination of diffusion coefficient of Thy or Cyt has not been reported before.

For Cyt, the chronoamperograms were recorded in the range $5.0 \times 10^{-5} \text{ M}$ to $5.0 \times 10^{-4} \text{ M}$ (Fig. 3.16) by setting the potential of *p*(AspA)/GCE at 1.4 V. The inset of Fig. 3.16 shows the corresponding *I* vs $t^{-1/2}$ plots. Using the slope of the $\frac{dI}{dt^{-1/2}}$ vs *C* plot (Fig. 3.17) in the Cottrell equation, the diffusion coefficient was calculated to be $1.9 \times 10^{-3} \text{ cm}^2 \text{ s}^{-1}$. Using the bare GCE, the diffusion coefficient was obtained to be $6.6 \times 10^{-5} \text{ cm}^2 \text{ s}^{-1}$.

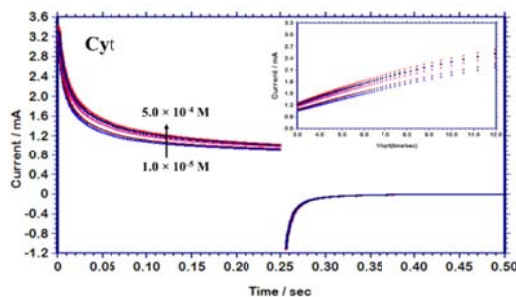


Figure 3.16: Chronoamperograms obtained for the oxidation of various concentrations of Cyt on *p*(AspA)/GCE with 0.1 M NaOH as supporting electrolyte. Inset shows corresponding *I* vs $t^{-1/2}$ plots

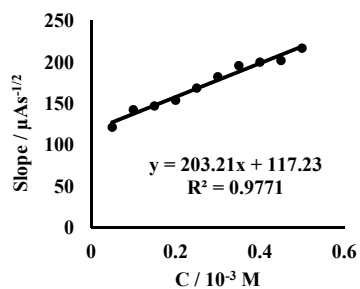


Figure 3.17: Plot of slope (*I* vs $t^{-1/2}$) against concentration of Cyt

The obtained results are consolidated in table 3.3.

Table 3.3: Diffusion coefficient of DNA bases

Analyte	Slope [$\frac{d(I \text{ vs } t^{-1/2})}{dc}$]		D (cm ² s ⁻¹)	
	GCE	<i>p</i> (AspA)/GCE	GCE	<i>p</i> (AspA)/GCE
Ad	9.8	37.9	1.8×10^{-6}	6.8×10^{-5}
Gu	18.9	141.2	6.9×10^{-6}	2.4×10^{-4}
Thy	7.7	15.1	4.5×10^{-6}	1.1×10^{-5}
Cyt	29.3	203.2	6.6×10^{-5}	1.9×10^{-3}

For all the DNA bases, the value of diffusion coefficient obtained is higher on the *p*(AspA)/GCE than the bare electrode. Diffusion coefficient depends on the electroactive surface area of the electrode. The modified electrode has greater surface area than the bare electrode. For Gu and Cyt the increase in diffusion coefficient is much higher than that observed for Ad and Thy. This cannot be accounted for by the increase in surface area on modification alone. Ad and Gu showed 38-fold and 35-fold increase in D respectively, whereas Cyt showed 29-fold increase. For Thy, the increase was just threefold. The presence of electrostatic interaction between the DNA bases and the *p*(AspA) layer on the GCE with outwardly projecting acidic functionalities may be a reason for this increase in diffusion coefficient.

3.2.9.2 Heterogeneous rate constant

The heterogeneous rate constant for the electro-oxidation was determined using two different approaches, one based on the Nicholson-Shain model and the second based on Laviron model. Both methods employ a study of variation of peak potential with scan rate in the LSV mode.

The Nicholson-Shain model is applied for diffusion limited systems. As the electrochemical reactions were found to be diffusion controlled, the Nicholson -Shain model for determining rate constant is studied.

According to Nicholson-Shain equation for an irreversible oxidation process,

$$E = E^0 + \frac{RT}{(1-\alpha)nF} \left[0.78 - \ln \frac{k_h}{D^{1/2}} + \frac{1}{2} \ln \frac{(1-\alpha)nFv}{RT} \right]$$

Here E is the anodic potential at scan rate v , E^0 , the formal electrode potential and other symbols have the usual meaning. A plot of E versus $\ln v$, will give

$$\text{Slope} = \frac{RT}{2(1-\alpha)nF}$$

$$\text{Intercept} = E^0 + \frac{RT}{(1-\alpha)nF} \left[0.78 - \ln \frac{k_h}{D^{1/2}} + \frac{1}{2} \ln \frac{\alpha nF}{RT} \right]$$

The value of E^0 is obtained from the intercept of E vs v plot. For the electro-oxidation of Ad on $p(\text{AspA})/\text{GCE}$, the value of slope and intercept from E versus $\ln v$ plot was obtained to be 0.0313 and 0.689 respectively, whereas the value of E^0 was found to be 0.614 V. Using the value of D determined from chronoamperometric measurements, the value of k_h for the electro-oxidation of Ad on the $p(\text{AspA})/\text{GCE}$ was calculated to be $1.94 \times 10^{-2} \text{ cm s}^{-1}$. On the bare GCE, the same was calculated to be $4.55 \times 10^{-4} \text{ cm s}^{-1}$.

The Laviron model assumes that the electrochemical reaction at the electrode is slow when compared to diffusion. In such a case the electron transfer kinetics controls the reaction and diffusion effects can be ignored. In order to confirm whether electron transfer kinetics or diffusion effects

control the electrochemical reaction, the Laviron rate constant k_s was also determined

According to Laviron equation for an irreversible oxidation reaction,

$$E = E^0 + \frac{RT}{(1-\alpha)nF} \left[\ln \frac{(1-\alpha)nF}{RTk_s} + \ln v \right]$$

By this approach a plot of E versus $\ln v$ should give a slope of $\frac{RT}{(1-\alpha)nF}$ and the intercept will be $E = E^0 + \frac{RT}{(1-\alpha)nF} \left[\ln \frac{(1-\alpha)nF}{RTk_s} \right]$. The value of E^0 is obtained from the intercept of E vs v plot, at lower scan rates. k_s for the electro-oxidation of Ad on $p(\text{AspA})/\text{GCE}$, calculated by the Laviron approach was 2.9 s^{-1} . The rate constant was also determined for the electro-oxidation of Ad on bare GCE and the value of Laviron rate constant for bare GCE was obtained to be 2.4 s^{-1} .

The variation of peak potential with scan rate was studied for other DNA bases using LSV and the kinetic parameters determined (Table 3.4).

Table 3.4: Kinetic parameters measured on $p(\text{AspA})/\text{GCE}$

	Regression equation		$(1-\alpha)n_\alpha$	αn_α	α	n_α^*
	E vs $\ln v$	E vs v				
Ad	$E = 0.031 \ln v + 0.689$	$E = 0.110 v + 0.614$	0.414	0.748	0.623	1 (1.2)
Gu	$E = 0.013 \ln v + 0.458$	$E = 0.142 v + 0.411$	0.987	1.060	0.517	2 (2.1)
Thy	$E = 0.017 \ln v + 0.772$	$E = 0.750 v + 0.678$	0.755	0.353	0.321	1(1.1)
Cyt	$E = 0.023 \ln v + 0.968$	$E = 0.386 v + 0.863$	0.443	1.084	0.710	1 (1.3)

*calculated value is shown in brackets

For Gu and Thy, the variation of peak potential with scan rate (Fig. 3.18) was studied in the range from 0.1 Vs^{-1} to 1.0 Vs^{-1} whereas for Cyt the variation was studied in the range from 0.05 Vs^{-1} to 0.50 Vs^{-1} .

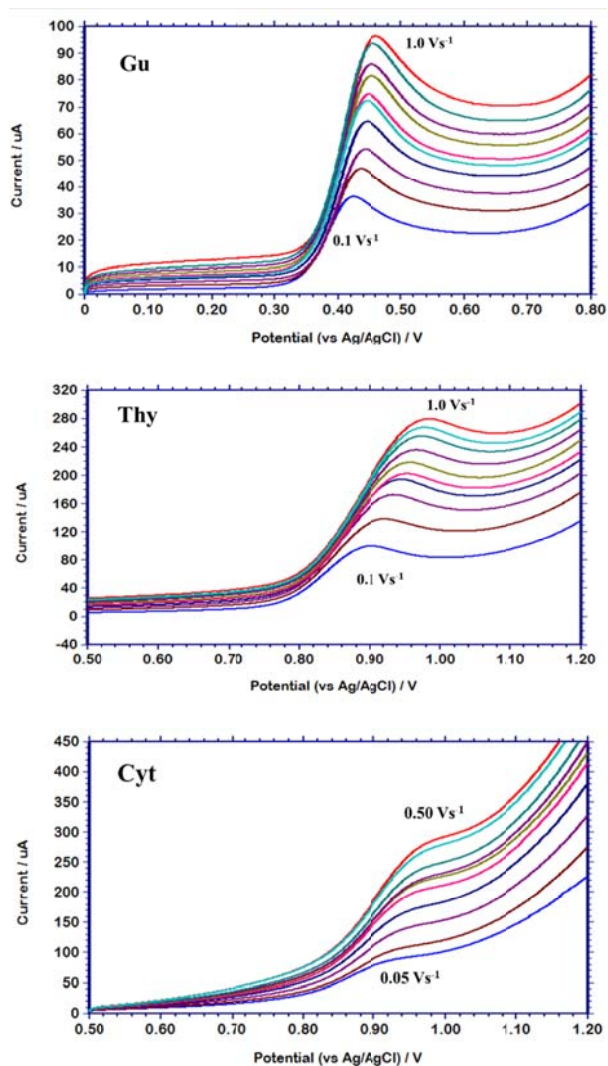


Figure 3.18: Overlay of LSV curves for the oxidation of 5.0×10^{-5} M Gu, 1.0×10^{-3} M Thy and 5.0×10^{-3} M Cyt on *p*(AspA)/GCE at different scan rates

For electro-oxidation on bare GCE, the variation of peak potential with scan rate and the corresponding kinetic parameters are represented in Table 3.5.

Table 3.5: Kinetic parameters measured on bare GCE

	Regression equation		$(1 - \alpha)n_\alpha$	αn_α	α	n_α^*
	E vs $\ln v$	E vs v				
Ad	$E = 0.030 \ln v + 0.622$	$E = 0.088 v + 0.568$	0.428	0.554	0.616	1 (0.9)
Gu	$E = 0.027 \ln v + 0.448$	$E = 0.138 v + 0.390$	0.460	1.109	0.693	2 (1.6)
Thy	$E = 0.022 \ln v + 0.970$	$E = 0.465 v + 0.876$	0.584	0.385	0.397	1(0.9)
Cyt	$E = 0.024 \ln v + 0.927$	$E = 0.886 v + 0.869$	0.442	0.535	0.548	1 (0.9)

*calculated value is shown in brackets

The value of rate constant for the electro-oxidation of DNA bases on $p(\text{AspA})/\text{GCE}$ and bare GCE, calculated by these two approaches are presented in Table 3.6.

Table 3.6: Rate constants for electro-oxidation

	k_h cm s^{-1}		k_s s^{-1}	
	GCE	$p(\text{AspA})/\text{GCE}$	GCE	$p(\text{AspA})/\text{GCE}$
Ad	4.55×10^{-4}	1.94×10^{-2}	2.43	2.90
Gu	1.18×10^{-3}	1.86×10^{-2}	2.07	2.06
Thy	1.65×10^{-3}	2.46×10^{-3}	0.45	0.29
Cyt	6.31×10^{-3}	4.60×10^{-2}	0.37	0.45

From the values obtained it is evident that in the case of Nicholson-Shain rate constant, there is a significant increase in the value of rate constant upon modification. In the case of Laviron rate constant the values obtained are comparable for both bare and modified electrodes. Hence it could be concluded that the increase in diffusion effects is the reason for the enhanced performance of the modified electrode rather than increase in electron transfer kinetics.

For electro-oxidation on $p(\text{AspA})/\text{GCE}$, the value of D as well as the Nicholson-Shain rate constant k_h is highest for Cyt. The lowest value of k_h as well as the diffusion coefficient D was obtained for Thy. The value of k_h

varied in the same order as the variation in **D**, i.e., Cyt > Ad > Gu > Thy. Laviron rate constant k_s followed the trend Ad > Gu > Cyt > Thy. Thy showed the lowest value for both Nicholson-Shain and Laviron constant.

3.3 Conclusions

The electrocatalytic oxidation of the DNA bases on *p*(AspA)/GCE was studied. The maximum lowering of overpotential was observed for Ad and hence the performance of *p*(AspA)/GCE as a sensor for Ad was optimised. The DPV current response was linear in the range from 1.3×10^{-4} M to 2.0×10^{-5} M with a limit of detection 6.7×10^{-6} M. Electro-oxidation of Ad on *p*(AspA)/GCE was found to be diffusion controlled and irreversible involving the transfer of one electron. The developed sensor was found to be suitable for the determination of Ad in acid denatured HS DNA. Diffusion coefficient of DNA bases under the sensor conditions has been determined using chronoamperometry. Highest value of diffusion coefficient was obtained for Cyt and the lowest value for Thy. LSV was used to study the kinetics of the electro-oxidation processes. The value of rate constant calculated using Nicholson-Shain approach followed the trend Cyt > Gu > Ad > Thy whereas when calculated using Laviron approach, the trend was Ad > Gu > Cyt > Thy. Thus, the kinetic studies indicate that the oxidation of Thy was the least facile on *p*(AspA)/GCE.

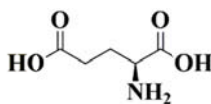
..... 

Poly(Glutamic acid) modified Glassy Carbon Electrode as Sensor for Thymine

Thymine is the pyrimidine base which pairs with adenine in DNA. In this chapter, the electro-oxidation of thymine is studied on a glassy carbon electrode modified with poly(L-glutamic acid), as the probe. On the probe, the overpotential for thymine oxidation in alkaline medium has been significantly decreased, attesting the electrocatalytic nature of the polymer film. The experimental parameters to obtain lowest oxidation potential have been optimised and the current response on the probe calibrated for determination of thymine. The determination of thymine in spiked synthetic blood serum and urine has been conducted to demonstrate the application of the sensor for thymine determination in real samples. Electrochemical kinetic parameters, namely charge transfer coefficient α and the rate constants for the electrooxidation of all the DNA bases on poly(L-glutamic acid) modified glassy carbon electrode have been determined and presented in this chapter.

4.1 Introduction

Glutamic acid (GA) is a non-essential amino acid with molecular formula $C_5H_9NO_4$. In addition to the characteristic $-COOH$ group of an α -amino acid, GA has an extra $-COOH$ group, making it an acidic amino acid.



Glutamic acid

GA (molecular mass 147.1), in the natural state exists in the L-form. It is the most common excitatory neurotransmitter in the central nervous system [137].

There are several reports of *p*(GA) based sensors for various analytes with the fabrication of *p*(GA) being performed at different conditions.

The electropolymerisation of GA on GCE from 2.0×10^{-2} M monomer solution (PBS pH 7.0) by cycling the potential between -0.8 and 2.0 V at a scan rate of 0.1 V s^{-1} was reported by Yu and Chen [2,3]. The *p*(GA)/GCE was applied for the determination of ascorbic acid along with dopamine [110] and for the amperometric determination of hydrazine [138]. The procedure reported by Yu and Chen for fabrication of *p*(GA)/GCE was used by Santos and co-workers and the sensor was used for selective determination of phenolic anti-oxidants caffeic acid and chlorogenic acid [138].

Zang and Lin had reported electropolymerisation of L-GA onto the GCE surface from 1.0×10^{-3} M GA solution in absolute acetonitrile containing 0.1 M NBu_4BF_4 . The fabricated sensor was used for the simultaneous determination of uric acid (Ua) and ascorbic acid [113].

p(GA)/GCE fabricated by cycling potential scanning from -1.5 V to 2.5 V at a scan rate of 0.1 Vs^{-1} in a 0.01 M L-GA solution in PBS pH 7 was used by Wang et al., for the electrochemical determination of hydroquinone and catechol [140].

L-GA was electropolymerised on to carbon paste electrode from a 0.01 M solution in PBS pH 7, by cycling the potential between -2.0 V to 2.0 V followed by electrodeposition of gold nanoparticles to fabricate a sensor for paracetamol by Zang and co-workers [141].

Liu and co-workers have reported the fabrication of a carbon nanotube doped carbon paste electrode modified with electropolymerised film of GA for the determination of tryptophan [142].

Bui et al., fabricated a sensor for dopamine by electropolymerizing L-GA on to single walled carbon nanotube film. They used cyclic potential scanning from -0.4 V to 1.5 V to deposit the polymer from 5.0×10^{-3} M aqueous solution of the monomer [143]. The same group have also reported the fabrication of a sensor for acetaminophen by electrochemically co-depositing L-GA and gold nano particles on a single walled carbon nanotube film by the same procedure [144].

The development of a non-enzymatic glucose sensor on a GCE modified with a composite of electropolymerised L-GA and electrodeposited platinum nanoparticles had been reported by Zhou and co-workers [145]. The electropolymerisation of L-GA was achieved from a 0.01 M aqueous solution of the monomer under a potential cycling from -0.5 V to 2.0 V. They have also developed an enzymatic glucose sensor on *p*(GA)/GCE prepared by the same method [146].

β -cyclodextrins were self-assembled on to, *p*(GA) electropolymerised on a GCE surface and a sensor was fabricated for the selective recognition of tryptophan enantiomers by Tao and co-workers [114]. They adopted the procedure reported by Santos et al. and Liu et al. for the electropolymerisation of L-GA.

The development of a sensor for the simultaneous determination of ascorbic acid, norepinephrine and Ua on a *p*(GA) modified carbon paste electrode has been described by Ganesh and Swamy [147]. They electropolymerised L-GA on GCE from a 2.0×10^{-3} M aqueous GA solution in PBS pH 7.4 by potential scanning from -1.0 V to 1.3 V at a scan rate of 0.1 Vs^{-1} .

The application of a pencil graphite electrode modified with electropolymerised *p*(GA) as a sensor for Hepatitis C virus has been demonstrated by Donmez, Arslan and Arslan [148]. They adopted the method proposed by Yu and Chen.

Recently there has been a report of a poly(melamine) and *p*(GA) copolymer based electrochemical sensor for the determination of 2-Thioxanthine [149].

Herein, fabrication of *p*(GA)/GCE was carried out by the procedure proposed by Yu and Chen [110, 138] and used to study the electrochemical response of DNA bases Guanine (Gu), Adenine (Ad), Thymine (Thy) and Cytosine (Cyt).

4.2 Results and discussion

p(GA)/GCE was fabricated as described in Chapter 2, Section 2.2.1 and its characterisation by SEM imaging and EIS measurements are described in Section 2.2.2. The performance of *p*(GA)/GCE was optimised for the electrochemical oxidation of Thy observed on the electrode.

4.2.1 Optimisation of experimental parameters

4.2.1.1 Supporting electrolyte

The effect of 0.1 M concentrations of various electrolytes such as H₂SO₄, HCl, NaCl, NaOH and KOH along with buffer solutions such as ABS and PBS, on the peak parameters for the electro-oxidation of Thy on the *p*(GA)/GCE was investigated. For 1.0×10^{-4} M Thy, the lowest peak potential was observed in 0.1 M NaOH and hence it was selected as the supporting electrolyte for further experiments.

4.2.1.2 Number of cycles of polymerisation

The electro-oxidation of 1.0×10^{-4} M Thy was studied on GCE modified with *p*(GA) deposited by various sweep cycles (Fig. 4.1). It was on the electrode modified by depositing *p*(GA) with 20 cycles of polymerisation, the oxidation of 1.0×10^{-4} M Thy took place at the lowest overpotential. Even though the oxidation current was maximum on the electrode with *p*(GA) deposited by 25 cycles, the optimum number of cycles was decided to be 20, considering the maximum lowering of overpotential.

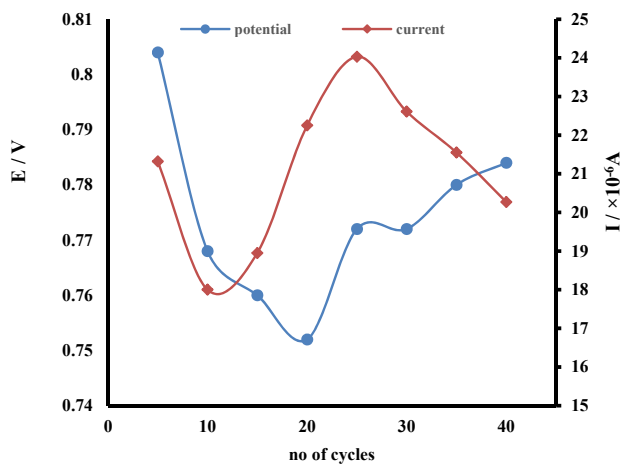


Figure 4.1: Variation of peak parameters (1.0×10^{-4} M Thy in 0.1 M NaOH) with number of cycles of polymerization

4.2.2 Electrochemical behaviour of DNA bases on the *p*(GA)/GCE

On the bare GCE, peaks due to the electro-oxidation of 3.0×10^{-4} M Gu, Ad, Thy and Cyt appeared at 0.343 V, 0.632 V, 0.780 V and 1.002 V respectively whereas on the optimised *p*(GA)/GCE, the corresponding peaks appeared at 0.330 V, 0.610 V, 0.752 V and 1.004 V respectively in the SWV mode. These results were obtained using 0.1 M NaOH as supporting

electrolyte. The overpotential has decreased by 0.007 V, 0.022 V and 0.028 V for Gu, Ad and Thy on the modified electrode. Since Thy showed the maximum lowering of oxidation potential on the modified electrode, the sensor performance has been optimised for Thy determination.

The SWV response of 1.0×10^{-3} M Thy on the bare as well as *p*(GA)/GCE is shown in Fig.4.2. The oxidation current on the modified electrode is increased more than twofold indicating an improvement in electrode kinetics on modification.

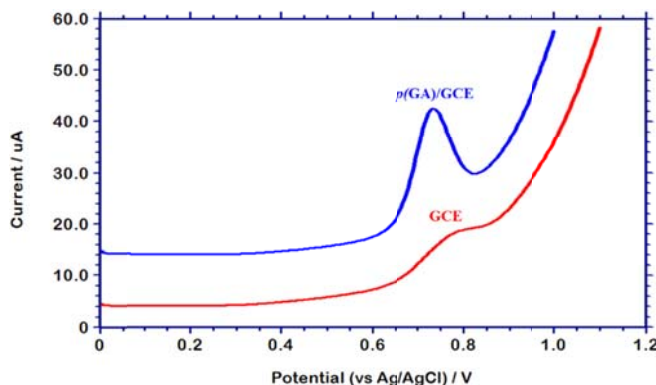


Figure 4.2: Overlay of SW voltammograms of 1.0×10^{-3} M Thy in 0.1 M NaOH on bare GCE and *p*(GA)/GCE

The Nyquist plots of bare GCE and *p*(GA)/GCE in 1.0×10^{-3} M Thy with 0.1 M NaOH as supporting electrolyte in the frequency range 1.0 - 1.0×10^5 Hz at the potential of 1.0 V is shown in Fig. 4.3. The diameter of the semi-circular region represents the charge transfer resistance R_{ct} on the electrode for Thy oxidation. For bare GCE, a large semi-circular region is obtained ($R_{ct} = 6.03 \times 10^3 \Omega$) which on modification ($R_{ct} = 9.65 \times 10^2 \Omega$) is decreased significantly. This is a clear indication that the electro-oxidation of Thy is facilitated on the modified GCE than the bare GCE.

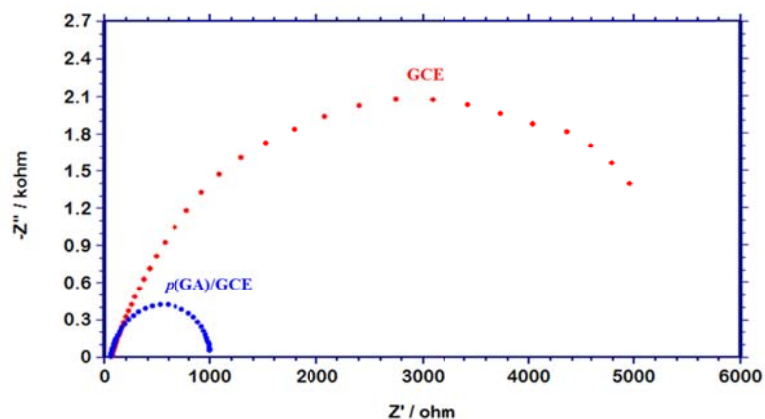


Figure 4.3: Overlay of Nyquist Plots for bare GCE and $p(\text{GA})/\text{GCE}$ in 5.0×10^{-4} M Thy in the frequency range $1.0 - 1.0 \times 10^5$ Hz at the corresponding oxidation potential with 0.1 M NaOH as supporting electrolyte

4.2.3 Electro active surface area

The variation of peak currents of the perfect redox couple in 2.0×10^{-3} M $\text{K}_3[\text{Fe}(\text{CN})_6]$, with scan rate ν was investigated in the range 0.01 Vs^{-1} to 0.20 Vs^{-1} on the $p(\text{GA})/\text{GCE}$ as well as bare GCE (Fig. 4.4).

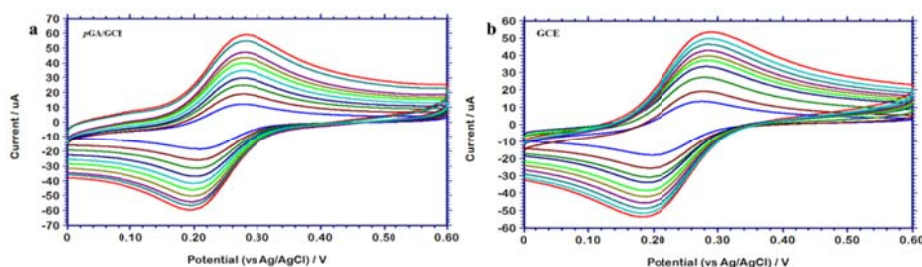


Figure 4.4: Overlay of cyclic voltammograms at different scan rates (0.02 Vs^{-1} to 0.20 Vs^{-1}) for the oxidation of 2.0×10^{-3} M $\text{K}_3[\text{Fe}(\text{CN})_6]$ on **a)** $p(\text{GA})/\text{GCE}$ **b)** bare GCE

For $p(\text{GA})/\text{GCE}$, $I(\text{A}) = 1.12 \times 10^{-4} \nu^{1/2} (\text{Vs}^{-1}) + 5.86 \times 10^{-7}$

And for bare GCE, $I(\text{A}) = 9.72 \times 10^{-5} \nu^{1/2} (\text{Vs}^{-1}) - 3.89 \times 10^{-7}$

By applying the Randles-Sevcik equation, as explained in section 3.2.4 of chapter 3, the electroactive surface area of the *p*(GA)/GCE was found to be 0.075 cm² and that of the bare GCE 0.066 cm². The electroactive surface area of the modified electrode has increased by 14% on the formation of *p*(GA) layer.

4.2.4 Calibration

Under the optimised sensor conditions, the oxidation of Thy gave a well-defined peak at 0.752 V whose peak current increased with increase in concentration of Thy. A linear relationship,

$$I \text{ (A)} = 0.027C \text{ (M)} + 2.165 \times 10^{-6} \quad [R^2 = 0.994]$$

was obtained in the range 1.0×10^{-5} M to 3.0×10^{-3} M Thy (Fig. 4.5 and 4.6). The LOD of Thy on the *p*(GA)/GCE was calculated to be 9.2×10^{-6} M.

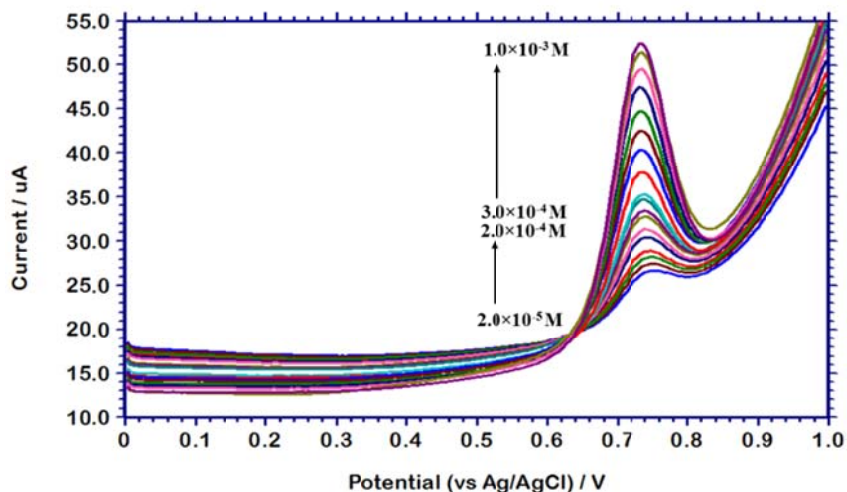


Figure 4.5: Overlay of SW voltammograms for the oxidation of 2.0×10^{-5} M to 2.0×10^{-4} M Thy (with incremental addition of 2.0×10^{-5} M Thy) and 3.0×10^{-4} M to 1.0×10^{-3} M Thy (in increments of 1.0×10^{-4} M Thy) on *p*(GA)/GCE

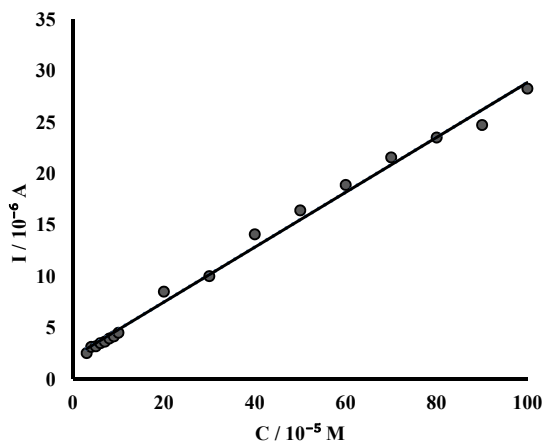


Figure 4.6: Calibration plot for Thy

4.2.5 Mechanistic Studies

4.2.5.1 Effect of scan rate

The LSV of 7.0×10^{-5} M Thy was recorded at different scan rates in the range from 0.1 Vs^{-1} to 1.0 Vs^{-1} (Fig. 4.7). The peak potential shifted to more positive values on increasing the scan rate as expected for an irreversible electrode reaction [13]. The observed variation of peak parameters with scan rate is consolidated in Table 4.1.

Table 4.1: Variation of peak parameters with scan rate

Regression equation	R ²
$E \text{ (V)} = 0.0189 \ln v \text{ (Vs}^{-1}\text{)} + 0.915$	0.987
$I \text{ (A)} = 2.712 \times 10^{-4} v^{1/2} \text{ (Vs}^{-1}\text{)} + 3.071 \times 10^{-6}$	0.992
$\log I \text{ (A)} = 0.475 \log v \text{ (Vs}^{-1}\text{)} - 3.576$	0.997

The linear variation of oxidation current with square root of scan rate and the slope of $\log I$ vs $\log v$ being 0.475 (the theoretical value being 0.5) points to the diffusion controlled nature of the electrochemical process [131].

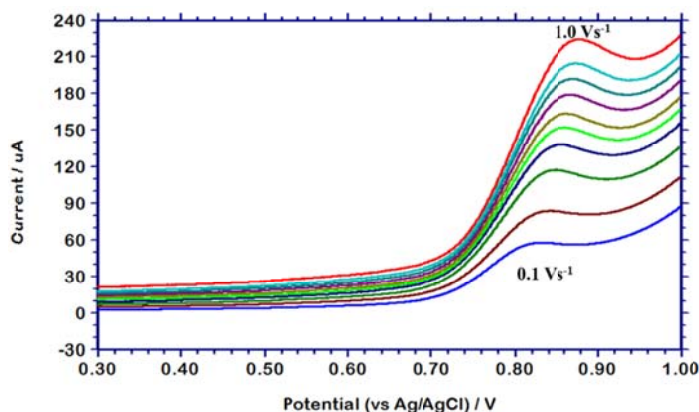


Figure 4.7: Overlay of LSV curves for the oxidation of 1.0×10^{-3} M Thy in 0.1 M NaOH on *p*(GA)/GCE at different scan rates ranging from 0.1 Vs^{-1} to 1.0 Vs^{-1}

From the Tafel slope $\frac{RT}{2(1-\alpha)n_{\alpha}F}$ (0.037), the value of $(1 - \alpha)n_{\alpha}$ was obtained to be 0.688 and from LS voltammogram of Thy, $\alpha n_{\alpha} = \frac{0.047}{E - E_{1/2}}$ was obtained to be 0.619. Hence the value of n_{α} , the number of electrons involved in the rate determining step was determined to be 1 (calculated value = 1.3).

4.2.5.2 Effect of pH

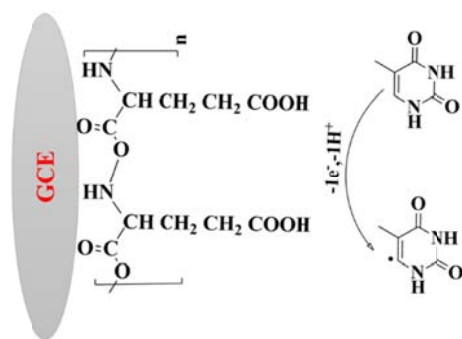
On the *p*(GA)/GCE, the variation of Thy oxidation peak potential with pH of the medium was studied in the range 3-9 using 0.1 M PBS as supporting electrolyte. The oxidation potential shifted negatively with pH of the medium as per the equation,

$$E \text{ (V)} = -0.068\text{pH} + 1.609 \quad [R^2 = 0.988]$$

For an electrochemical reaction involving 'm' protons and 'n' electrons,

$$E = -\frac{0.059m}{n}\text{pH}$$

Hence, for an electrochemical reaction involving equal number of protons and electrons, the slope of **E** vs **pH** would be expected to be -0.059. In this study, the obtained slope is comparable to this value. Since the number of electrons involved in the electrode reaction was already determined to be 1 (section 4.2.5.1), the number of protons was also deduced to be the same. i.e., equal number of protons and electrons were involved in the electrochemical process. In accordance with these observations, a mechanism involving one electron and one proton for electro-oxidation of Thy is proposed [150]. Scheme 4.1 represents the possible structure of the *p*(GA)/GCE and the electrochemical reaction taking place on it.



Scheme 4.1: Possible electrochemical reaction at the *p*(GA)/GCE

4.2.6 Effect of co-existing molecules

To determine the effectiveness of the sensor for the quantitative determination of Thy, the effect of possibly co-existing molecules on the analytical signal of Thy was investigated. The purine bases Ad and Gu, the pyrimidine base Cyt, sugar residues and phosphate ions are generally present along with Thy in DNA. Species such as ascorbic acid, uric acid, urea, creatinine, glucose, fructose and electrolytes such as NaCl, KCl etc. which are present in physiological fluids can be considered as possibly interfering

species. The signal change produced by tenfold excess of these species except Ad and Cyt was well within the tolerance limit (5% signal change). Cyt interfered when its concentration ratio exceeded 1:10⁻¹. Even tenfold lower concentrations of Ad interfered with the determination of Thy. Hence determination of Thy in DNA could be attempted only after removal of Ad and Cyt, whereas interference free determination of Thy is possible in physiological fluids using the *p*(GA)/GCE. The change in the analytical signal of Thy produced in the presence of various chemical species when present in various Thy: added species, concentration ratio is presented in Table 4.2.

Table 4.2: Effect of possibly co-existing species

Species	Concentration ratio	Signal change (%)
Cyt	10:1	4.8
Ad	10:1	Peak distortion
Gu	1:10	1.9
Uracil	1:10	2.2
Urea	1:100	1.6
Ua	1:100	2.1
Creatinine	1:100	3.3
Dextrose	1:10	2.1
Fructose	1:10	1.9
Sucrose	1:10	3.3
Sodium phosphate	1:10	1.7
Sodium chloride, Potassium chloride	1:100	< 1.0

4.2.7 Application: Determination of Thy in spiked artificial body fluids

In acid denatured HS DNA, the peak corresponding to electrochemical oxidation of Thy was absent when run in SWV mode. This is not surprising as it has been reported that the determination of pyrimidine

bases in presence of equal concentrations of purines is difficult [151]. Thy is secreted in elevated levels into urine, blood and cerebrospinal fluids in cases of dihydrothymine dehydrogenase deficiency [40]. Hence the determination of Thy in spiked artificial urine and blood was attempted. Artificial urine and serum samples were prepared as described in section 2.7.7 and section 2.7.8 of chapter 2. Recoveries obtained were good indicating the possible application of the sensor for real sample analysis.

Table 4.3: Determination of Thy in spiked samples

Urine				Serum			
Added (M)	Found (M)	Recovery	RSD* %	Added (M)	Found (M)	Recovery	RSD* %
5.00×10^{-4}	4.99×10^{-4}	100	1.4	5.00×10^{-4}	4.95×10^{-4}	98	1.7
5.00×10^{-5}	5.01×10^{-5}			5.00×10^{-5}	4.79×10^{-5}		

*for 6 replicate measurements

4.2.8 Kinetics of electro-oxidation of DNA bases on p(GA)/GCE

4.2.8.1 Chronoamperometry

Decay of transient current **I** with time **t** for the electro-oxidation of Thy on the p(GA)/GCE under the sensor conditions was studied using chronoamperometry. Consistent with the Cottrell equation,

$$I = nFaD^{1/2}C\pi^{-1/2}t^{-1/2}$$

chronoamperograms were obtained in the range 1.0×10^{-3} M to 2.5×10^{-3} M. The overlay of chronoamperograms recorded in 1.2×10^{-3} M to 2.4×10^{-3} M Thy in 0.1 M NaOH are shown in Fig. 4.8. For each concentration, the **I** vs $t^{-1/2}$ graph was plotted (Fig. 4.9) and the slope obtained in each case were plotted against corresponding concentration (Fig 4.10).

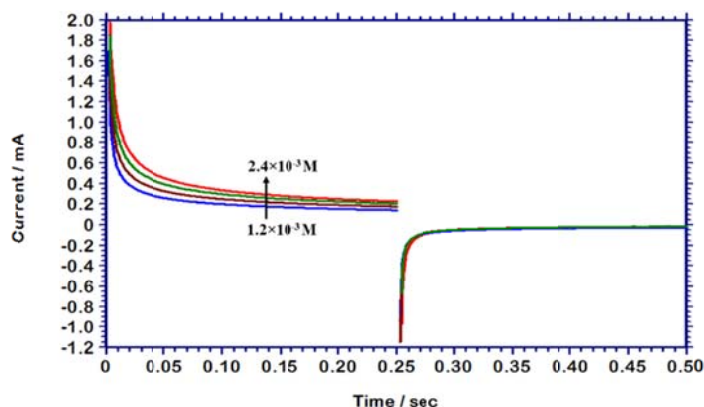


Figure 4.8: Overlay of chronoamperograms obtained for the oxidation of 1.2×10^{-3} M to 2.4×10^{-3} M Thy in 0.1 M NaOH (incremental addition of 4.0×10^{-4} M Thy) on *p*(GA)/GCE

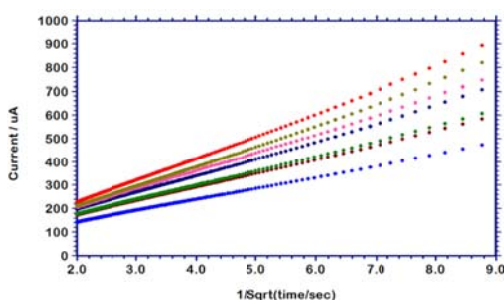


Figure 4.9: Plot I vs $t^{-1/2}$ for 1.2×10^{-3} M to 2.4×10^{-3} M Thy in 0.1 M NaOH (with incremental addition of 2.0×10^{-4} M Thy)

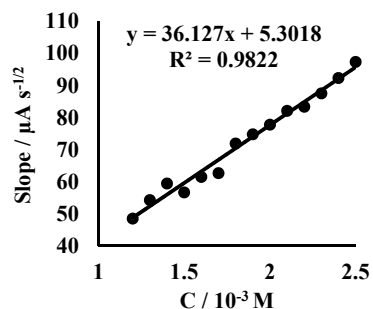


Figure 4.10: Plot of slope (I vs $t^{-1/2}$) against concentration of Thy

Using the value of the obtained slope in Cottrell equation, the diffusion coefficient of Thy under the conditions of present study was obtained as 7.8×10^{-5} $\text{cm}^2 \text{s}^{-1}$. In comparison to the diffusion coefficient obtained on bare GCE (Table 4.4) this is a 17fold increase in diffusion coefficient. Such an increase in diffusion coefficient could be attributed to electrostatic attraction between the electrode surface having acidic functionality and the nucleic acid base.

Chronoamperograms were recorded at different concentrations for the other DNA bases Gu, Ad and Cyt, and using the same method, the diffusion coefficients were calculated.

Chronoamperograms for Gu were recorded in the range 2.0×10^{-5} M to 2.2×10^{-4} M after stepping the potential of the working electrode *p*(GA)/GCE to 0.5 V in 0.1 M NaOH (Fig. 4.11). The slopes of the corresponding **I** vs $t^{-1/2}$ plots (Inset of Fig. 4.11) were plotted against concentration (Fig. 4.12) and the slope of the resulting plot was used in the Cottrell equation and the diffusion coefficient of Gu was obtained to be 7.1×10^{-5} cm² s⁻¹.

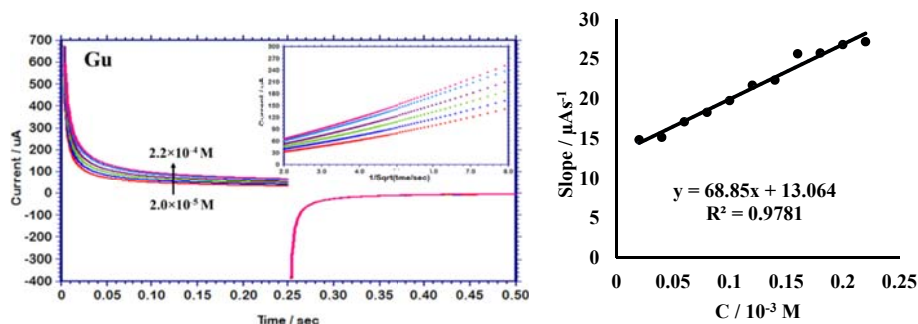


Figure 4.11: Overlay of chronoamperograms obtained for various concentrations of Gu in 0.1 M NaOH on *p*(GA)/GCE. Inset shows the corresponding **I** vs $t^{-1/2}$ plots

Figure 4.12: Plot of slope (**I** vs $t^{-1/2}$) against concentration of Gu

For Ad, the chronoamperograms recorded in the concentration range 1.0×10^{-4} M to 1.0×10^{-3} M on stepping up the *p*(GA)/GCE potential to 0.90 V and the corresponding **I** vs $t^{-1/2}$ plots are shown in Fig. 4.13. The plot of $\frac{dI}{dt^{-1/2}}$ against the concentration **C** is shown in Fig.4.14. The diffusion coefficient of Ad was calculated to be 2.7×10^{-4} cm² s⁻¹.

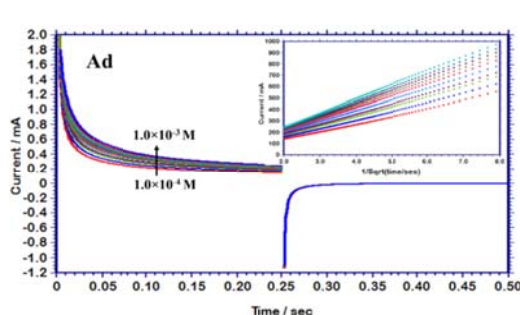


Figure 4.13: Overlay of chronoamperograms obtained for various concentrations of Ad in 0.1 M NaOH on *p*(GA)/GCE. Inset shows the corresponding I vs $t^{-1/2}$ plots

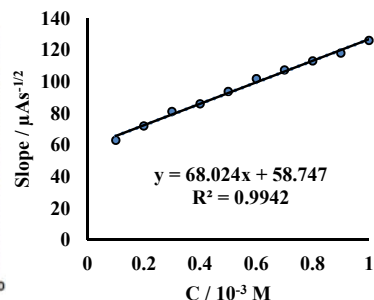


Figure 4.14: Plot of slope (I vs $t^{-1/2}$) against concentration of Ad

Fig. 4.15 shows the chronoamperograms for 1.0×10^{-4} M to 1.0×10^{-3} M Cyt in 0.1 M NaOH recorded by stepping the potential of the working electrode from 0.5 V to 1.2 V. Slopes of I vs $t^{-1/2}$ shown in the inset of Fig. 4.15 is plotted against the corresponding concentration in Fig. 4.16.

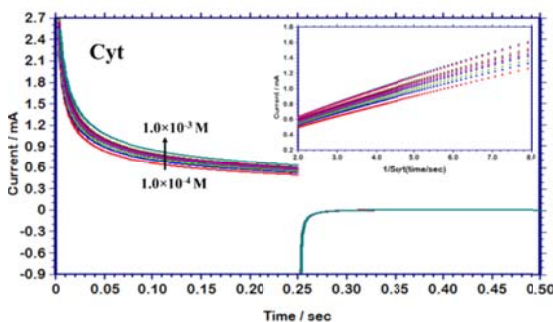


Figure 4.15: Overlay of chronoamperograms obtained for various concentrations of Cyt in 0.1 M NaOH on *p*(GA)/GCE. Inset shows the corresponding I vs $t^{-1/2}$ plots

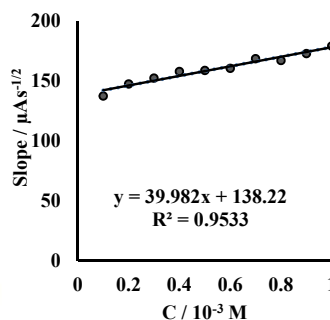


Figure 4.16: Plot of slope (I vs $t^{-1/2}$) against concentration of Cyt

The diffusion coefficient of Cyt by chronoamperometric determination using $p(\text{GA})/\text{GCE}$ was calculated to be $2.3 \times 10^{-5} \text{ cm}^2 \text{ s}^{-1}$. Compared to the diffusion coefficient obtained using bare GCE ($6.6 \times 10^{-5} \text{ cm}^2 \text{ s}^{-1}$), there is a decrease in diffusion coefficient.

The obtained results are consolidated in Table 4.4. The highest value of **D**, was obtained for Ad and the lowest for Cyt.

Table 4.4: Diffusion coefficient of DNA bases

Analyte	Slope [Slope of (I vs $t^{-1/2}$) vs C]		D $\text{cm}^2 \text{ s}^{-1}$	
	GCE	$p(\text{GA})/\text{GCE}$	GCE	$p(\text{GA})/\text{GCE}$
Thy	7.7	36.1	4.5×10^{-6}	7.8×10^{-5}
Gu	18.9	68.8	6.9×10^{-6}	7.1×10^{-5}
Ad	9.8	68.0	1.8×10^{-6}	2.7×10^{-4}
Cyt	29.3	39.9	6.6×10^{-5}	2.3×10^{-5}

When compared to the values obtained on bare GCE, all the DNA bases except Cyt showed an increase in **D** on the $p(\text{GA})/\text{GCE}$. The highest increase was observed for Ad with an increase of two orders of magnitude. If the increase in surface area of the electrode upon modification alone was the reason for increase in the value of **D**, the increase in diffusion coefficient for all the bases would have been the comparable. Structure specific interaction between the $p(\text{GA})/\text{GCE}$ and the bases may be another reason for this.

The diffusion coefficient obtained from the chronoamperometric studies was used for the calculation of Nicholson-Shain heterogeneous rate constant for electro-oxidation of the corresponding DNA base.

4.2.9.2 Heterogeneous rate constant

Scan rate studies in LSV mode is a useful method for extracting information about the kinetics of electrode process.

The variation of peak potential for the electro-oxidation of each of the DNA bases on *p*(GA)/GCE, with scan rate obtained in the range from 0.1 Vs⁻¹ to 1.0 Vs⁻¹ is shown in Table 4.5.

Table 4.5: Kinetic studies

	Regression equation		$(1 - \alpha)n_\alpha$	αn_α	α	n_α^*
	E vs $\ln v$	E vs v				
Thy	$E = 0.018 \ln v + 0.915$	$E = 0.431 v + 0.834$	0.688	0.619	0.472	1(1.3)
Gu	$E = 0.015 \ln v + 0.445$	$E = 0.345 v + 0.381$	0.877	1.014	0.536	2 (1.9)
Ad	$E = 0.012 \ln v + 0.649$	$E = 0.168 v + 0.607$	1.066	0.355	0.250	1(1.4)
Cyt	$E = 0.017 \ln v + 0.910$	$E = 0.246 v + 0.841$	0.749	1.192	0.613	2 (1.9)

**calculated value is given in brackets*

By making use of the Nicholson- Shain equation,

$$E = E^0 + \frac{RT}{(1 - \alpha)nF} \left[0.78 - \ln \frac{k_h}{D^{1/2}} + \frac{1}{2} \ln \frac{(1 - \alpha)nFv}{RT} \right]$$

and the Laviron equation,

$$E = E^0 + \frac{RT}{(1 - \alpha)nF} \left[\ln \frac{(1 - \alpha)nF}{RTk_s} + \ln v \right]$$

and employing the method described in Chapter 3, Section 3.2.9.2, the standard heterogeneous rate constant k_h and the surface reaction rate constant k_s for the electro-oxidation of DNA bases has been calculated. The values are presented in table 4.6.

Table 4.6: Rate constants for electro-oxidation

	Nicholson-Shain (k_h) cm s^{-1}		Laviron (k_s) s^{-1}	
	GCE	$p(\text{GA})/\text{GCE}$	GCE	$p(\text{GA})/\text{GCE}$
Thy	1.65×10^{-3}	1.25×10^{-2}	0.45	0.69
Gu	1.18×10^{-3}	1.35×10^{-2}	2.07	0.93
Ad	4.55×10^{-4}	4.06×10^{-2}	2.43	2.56
Cyt	6.31×10^{-3}	7.51×10^{-3}	0.37	1.02

On the $p(\text{GA})/\text{GCE}$, Nicholson-Shain rate constant was highest for Ad and the lowest for Cyt. The values of Nicholson-Shain k_h followed the trend Ad > Gu > Thy > Cyt. The highest value of diffusion coefficient was also observed for Ad on the $p(\text{GA})/\text{GCE}$. The diffusion coefficients as well as Nicholson-Shain rate constant obtained for Gu and Thy on the $p(\text{GA})/\text{GCE}$ were comparable. Ad showed the highest value of Laviron, surface rate constant and the lowest value was obtained for Thy.

On comparing the values of rate constants obtained on GCE and $p(\text{GA})/\text{GCE}$, all the DNA bases showed an increase in Nicholson-Shain rate constant on the modified electrode. The increase was tremendous for Ad for which the rate constant was increased by almost two orders of magnitude. Electro-oxidation kinetics of Gu and Thy also showed an increase by an order of magnitude. But for Cyt the increase in Nicholson-Shain rate constant on $p(\text{GA})/\text{GCE}$ was not as significant. Even though the diffusion coefficient of Cyt was found to be decreased when measured using $p(\text{GA})/\text{GCE}$, the value of Nicholson-Shain rate constant was higher on the $p(\text{GA})/\text{GCE}$ than the GCE.

Regarding the Laviron kinetics, Gu showed a decrease in the value of rate constant on the modified electrode. All others showed an increase in Laviron rate constant on $p(\text{GA})/\text{GCE}$ although the increase was not as

significant as that for Nicholson-Shain rate constant. Highest increase in Laviron rate constant was observed for Cyt. But Nicholson-Shain rate constant was lowest for Cyt. This points to the predominance of diffusion kinetics over electron transfer kinetics on the *p*(GA)/GCE for Ad, Thy and Gu, whereas for Cyt electron transfer kinetics was more significant than diffusion kinetics.

4.3 Conclusions

The SW voltammetric response of DNA bases on *p*(GA)/GCE was studied and the maximum lowering of oxidation potential was observed for Thy, the gradation being Thy > Ad > Gu > Cyt. Under optimised conditions (0.1 M NaOH as supporting electrolyte and *p*(GA)/GCE fabricated with 20 cycles of polymerisation) the oxidation current of Thy on *p*(GA)/GCE was found to be linear in the range 1.0×10^{-3} M to 3.0×10^{-5} M. The LOD was found to be 9.2×10^{-6} M. The oxidation of Thy on the *p*(GA)/GCE was found to be diffusion controlled and irreversible. Even though interference produced by Ad and Cyt presented a limitation for the application of the sensor for Thy determination in DNA, the sensor proved efficient for determination of Thy in synthetic blood serum and urine samples.

Chronoamperometry was used to determine the diffusion coefficients of the DNA bases under the sensor conditions. The highest value of diffusion coefficient was obtained for Ad. The kinetics of electro-oxidation of DNA bases was explored using LSV. From the data obtained by scan rate studies in LSV mode, the values of standard heterogeneous rate constants were extracted. Ad gave the best figures for the rate constants as well as diffusion coefficient. Thy gave the lowest value for Laviron rate constant and Cyt with the lowest value of diffusion coefficient showed the lowest Nicholson-Shan rate constant.

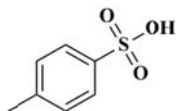
..... 

**Poly(para Toluene Sulfonic Acid)
modified Glassy Carbon Electrode as
Sensor for Simultaneous Determination of
Guanine, Adenine and Uric acid as well as
Guanine, Thymine and Uric Acid**

The chapter elucidates the development of an electrochemical sensor for determination of the bases, guanine, adenine, thymine and uric acid, fabricated using a glassy carbon electrode modified with poly(para toluene sulfonic acid). In square wave voltammetric mode, the modified glassy carbon electrode was able to produce well defined and well separated oxidation peaks for guanine, adenine and uric acid with 0.1 M sodium hydroxide as the supporting electrolyte. The oxidation peaks of guanine, thymine and uric acid were also well separated to enable simultaneous determination. Oxidation peak currents for guanine and adenine, showed a dynamic range from $1.0 \times 10^{-4}M - 1.0 \times 10^{-5}M$ and $8.0 \times 10^{-5}M - 2.0 \times 10^{-5}M$ with a limit of detection of $3.5 \times 10^{-7}M$ and $7.8 \times 10^{-5}M$ respectively when determined simultaneously along with uric acid. In simultaneous determination, uric acid also showed a linear increase of oxidation peak current in the concentration range of $1.0 \times 10^{-4}M - 1.0 \times 10^{-5}M$, with a limit of detection of $5.8 \times 10^{-6}M$. Simultaneous determination of guanine, thymine and uric acid showed linear range of $1.0 \times 10^{-3}M - 2.0 \times 10^{-5}M$ for guanine and uric acid, and $1.0 \times 10^{-4}M - 4.0 \times 10^{-3}M$ for thymine. The limits of detection were obtained to be $2.5 \times 10^{-6}M$, $1.7 \times 10^{-6}M$ and $5.7 \times 10^{-6}M$ respectively for guanine, thymine and uric acid. The variation of peak parameters with scan rate was studied to determine the nature of electro-oxidation and the number of electrons involved in the electrode process. The simultaneous determination of guanine, adenine and uric acid in acid denatured Herring sperm using the fabricated sensor is described. Chronoamperometric determination of diffusion coefficient of the DNA bases and uric acid using the developed sensor is explained. Nicholson-Shain model and Laviron model kinetics of the electro-oxidation process on the modified electrode has been determined.

5.1 Introduction

Para Toluene Sulfonic Acid (TSA) $C_7H_8O_3S$, is a white crystalline solid which is soluble both in water and organic solvents.



para toluene sulfonic acid

Its IUPAC name is 4-methyl benzene 1-sulfonic acid. TSA is a strong organic acid with pKa value of -1.34 [152].

Electropolymerisation of TSA on carbon electrodes for sensing applications has been reported in literature.

Nabais and co-workers have polymerised TSA onto the surface of a carbon vitreous electrode from an aqueous solution of the monomer in 0.5 M H_2SO_4 by cyclic potential scanning between 0 V to 1.69 V at the scan rate of 0.05 Vs^{-1} . They have conducted a theoretical study of the electronic structure of the polymer formed on the electrode surface [153].

GCE modified with electropolymerised films of TSA was fabricated for the voltammetric sensing of Ua and ascorbic acid by Wang and colleagues [97]. They achieved the electropolymerisation from a $1.0 \times 10^{-3} \text{ M}$ TSA solution in 0.1 M NaCl by cyclic potential sweeping from -2.0 to 2.5 V at 0.1 V s^{-1} .

The procedure reported by Wang and colleagues was used by Huang et al., for fabricating a sensor for the simultaneous determination of dopamine and ascorbic acid [115]. Our group has reported the use of

p(TSA)/GCE fabricated by the method adopted by Wang et al., for the voltammetric study of pyridine-2-aldoxime methochloride [104].

p(TSA)/GCE having, electron rich sulfonic acid groups, is not much explored as chemical modification for electrode surface for sensing applications. In anticipation of an affinity between the electron rich sulfonic acid group and the electron deficient nucleobases, the *p*(TSA)/GCE fabricated by the electropolymerisation scheme adopted by Wang et al. [97] was used to study the electrochemical behaviour of DNA bases.

5.2 Results and discussion

The fabrication of *p*(TSA)/GCE was carried out as described in Section 2.3 of Chapter 2 and the fabricated electrode characterised by SEM imaging and EIS measurements (Chapter 2, Section 2.4). Optimisation of the electrode performance for the electro-oxidation of DNA bases was conducted.

5.2.1 Optimisation of experimental parameters

Choice of supporting electrolyte is an experimental parameter that can influence the electro-oxidation potential. Electrochemical oxidation of Gu, Ad, Thy and Ua was studied in 0.1 M concentration of various supporting electrolytes such as sulfuric acid, hydrochloric acid, ABS, CBS, sodium chloride, potassium chloride, PBS, NaOH and potassium hydroxide. For all the bases under study, the lowest oxidation potential was recorded when 0.1 M NaOH was used as the supporting electrolyte. Hence 0.1 M NaOH was fixed as the supporting electrolyte for further experiments.

The electrochemical response of Gu on the GCE modified with *p*(TSA) film deposited at various cycles of polymerisation was studied

(Fig. 5.1). The best response was obtained on the *p*(TSA) film deposited by 20 cycles of polymerisation. Therefore, *p*(TSA) film formed by 20 cycles of polymerisation was used for electrochemical experiments.

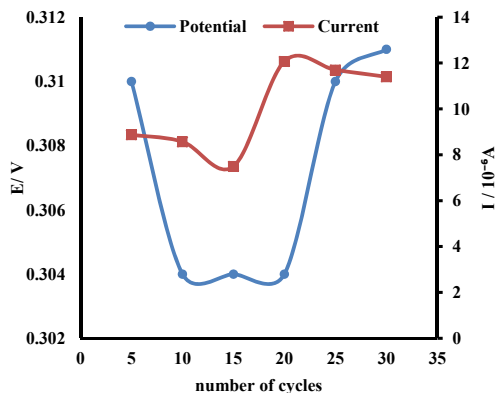


Figure 5.1: Variation of peak parameters of 1.0×10^{-4} M Gu with number of cycles of polymerisation

5.2.2 Electrochemical behaviour of DNA bases on the *p*(TSA)/GCE

The electro-oxidation of 3.0×10^{-4} M concentrations of Gu, Ad, Thy and Cyt on the bare GCE took place at 0.348 V, 0.632 V, 0.780 V and 1.004 V. On the *p*(TSA)/GCE, the corresponding peaks appeared at 0.304 V, 0.608 V, 0.760 V and 0.896 V when determined individually in SWV mode, with 0.1 N NaOH as supporting electrolyte., indicating that *p*(TSA) showed electro-catalytic activity towards the oxidation of these bases. Ua, the primary product of purine metabolism was electrocatalytically oxidised on the *p*(TSA)/GCE, at -0.108 V in contrast with -0.080 V on the bare GCE. Well separated peaks were obtained for Ua, Gu and Ad as well as Ua, Gu and Thy, indicating the possibility of simultaneous determination. The peaks due to Ad and Thy as well as Thy and Cy with less than 0.160 V separation between them would overlap making simultaneous determination difficult.

SW voltammograms obtained for a solution containing 3.0×10^{-4} M each of Ua, Gu and Ad on the bare GCE and *p*(TSA)/GCE is shown in Fig. 5.2 and that for a solution of 3.0×10^{-4} M Ua, Gu and Thy each is shown in Fig. 5.3. In both cases the supporting electrolyte used is 0.1 M NaOH. From the figures, it is clear that there is a decrease in oxidation peak and an enhancement in peak current on the *p*(TSA)/GCE as compared to the bare GCE indicating that the *p*(TSA) layer deposited on the GCE indeed has an electrocatalytic effect on the oxidation of these DNA bases.

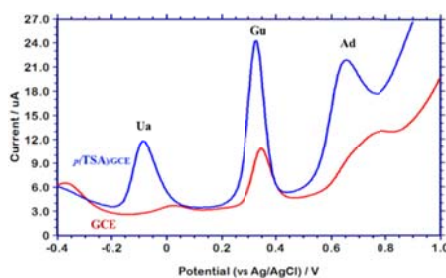


Figure 5.2: SW voltammograms of 3.0×10^{-4} M Ua, Gu and Ad on *p*(TSA)/GCE and GCE

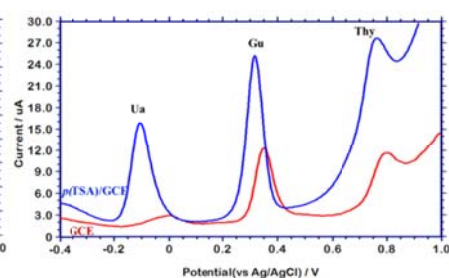


Figure 5.3: SW voltammograms of 3.0×10^{-4} M Ua, Gu and Thy on *p*(TSA)/GCE and GCE

The EIS Nyquist plots of the bare and *p*(TSA)/GCE in 5.0×10^{-4} M solutions of Gu, Ad, Thy and Ua in 0.1 M NaOH in the frequency range 1.0 – 1.0×10^5 Hz at the corresponding oxidation potential is shown in Fig 5.4.

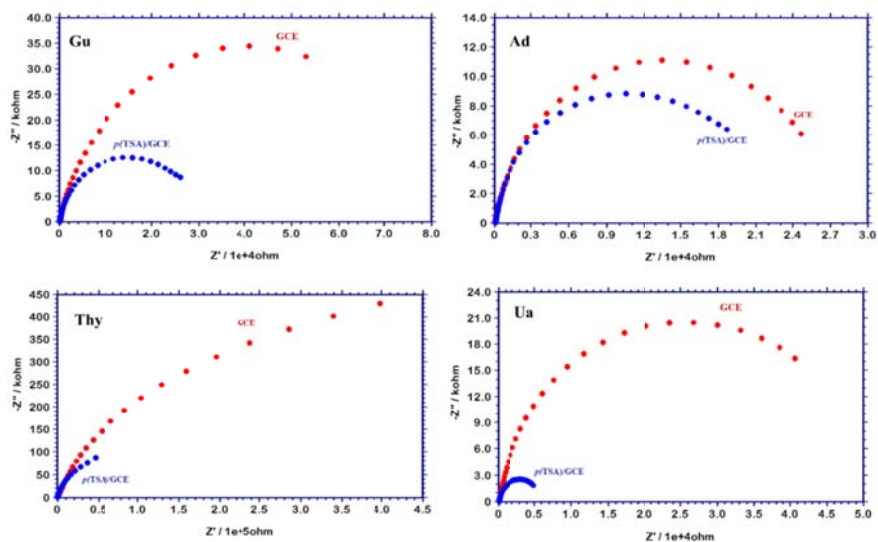


Figure 5.4: EIS Nyquist plots obtained on bare GCE and $p(\text{TSA})/\text{GCE}$ for 5.0×10^{-4} M concentrations of Gu, Ad, Thy and Ua in 0.1 M NaOH in the frequency range $1.0 - 1.0 \times 10^5$ Hz at the corresponding oxidation potential

For all the analytes, a semi-circular portion is obtained at high frequencies. Diameter of the semi-circular portion, which indicates the charge transfer resistance R_{ct} , is smaller on the $p(\text{TSA})/\text{GCE}$ than the bare GCE for all the analytes indicating that R_{ct} has decreased upon modification. The charge transfer resistance R_{ct} obtained on the bare GCE and $p(\text{TSA})/\text{GCE}$ for each of the analytes (fitted to the circuit $[R_s[C_{dl}(R_{ct}W)]$ using the ZSimpWin software] are given in Table 5.1.

Table 5.1: R_{ct} values fitted from Nyquist plots

	GCE ($10^5 \Omega$)	$p(\text{TSA})/\text{GCE}$ ($10^5 \Omega$)
Gu	7.580	0.236
Ad	0.262	0.197
Thy	6.692	0.189
Ua	1.780	0.417

The lowering of R_{ct} is further evidence for the electrocatalytic effect of p (TSA).

5.2.3 Electro active surface area

Cyclic voltammograms of 2.0×10^{-3} M $K_3[Fe(CN)_6]$ were recorded at different scan rates (0.02 Vs^{-1} to 0.20 Vs^{-1}) on the bare and modified GCE (Fig. 5.5) and the variation of oxidation peak current with square root of scan rate was determined (Fig. 5.6).

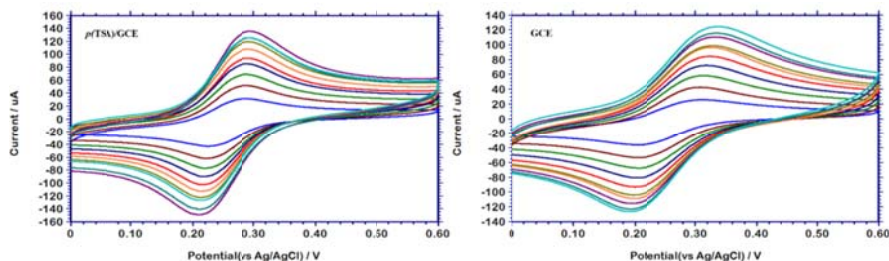


Figure 5.5: Cyclic voltammograms at different scan rates (0.02 Vs^{-1} to 0.20 Vs^{-1}) for the oxidation of 2.0×10^{-3} M $K_3[Fe(CN)_6]$ on p (TSA)/GCE and bare GCE

For p (TSA)/GCE,

$$I(A) = 2.92 \times 10^{-4} \nu^{1/2}(\text{Vs}^{-1}) + 6.35 \times 10^{-6}$$

And for GCE

$$I(A) = 2.11 \times 10^{-4} \nu^{1/2}(\text{Vs}^{-1}) + 1.99 \times 10^{-6}$$

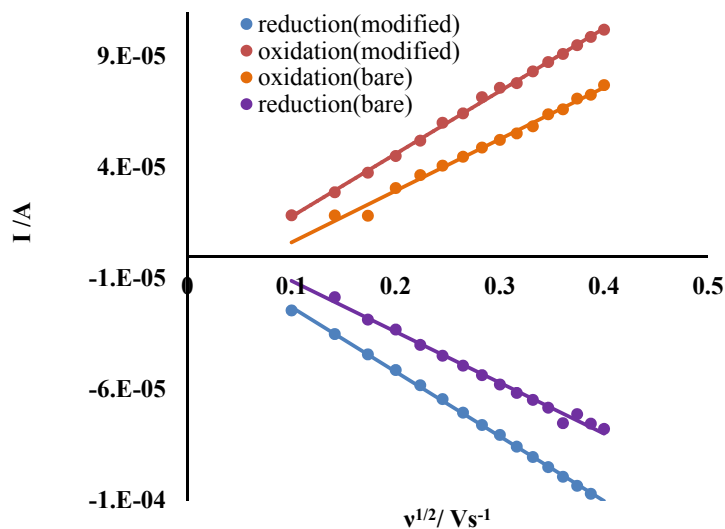


Figure 5.6: Plot of I vs $v^{1/2}$ for 2.0×10^{-3} M $K_3[Fe(CN)_6]$ at different scan rates

Using the approach described in chapter 3 (Section 3.2.4), the electro-active surface area of the $p(TSA)/GCE$ was found to be 0.197 cm^2 whereas that on the bare GCE it was calculated to be 0.140 cm^2 , indicating a 40% increase in surface area upon formation of the $p(TSA)$ layer.

5.2.4 Calibration

The variation of oxidation peak current with concentration under the optimised conditions was studied for Gu, Ad, Thy and Ua in the SWV mode. The analytical parameters such as linear range and LOD were also determined.

5.2.4.1 Guanine

On the $p(TSA)/GCE$, the oxidation of Gu took place at 0.304 V and its peak current increased with increase in concentration of Gu (Fig. 5.7). The variation of oxidation current with concentration (Fig. 5.8) was linear in

the concentration range, 3.0×10^{-4} M to 1.0×10^{-5} M and 1.0×10^{-5} M to 3.0×10^{-6} M (Fig. 5.9) with the lower LOD of 7.9×10^{-9} M.

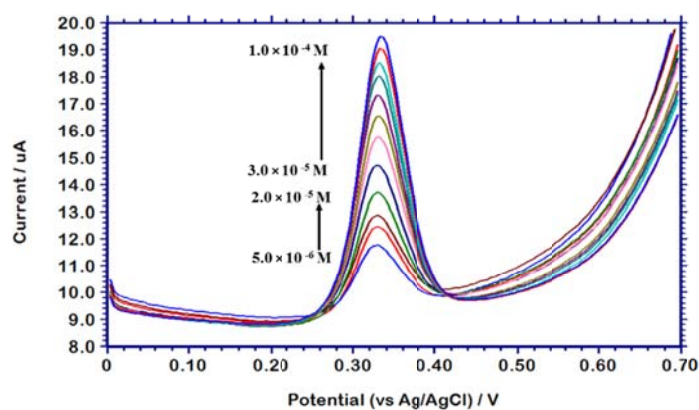


Figure 5.7: SW voltammograms for the oxidation of various concentrations of Gu in 0.1 M NaOH on *p*(TSA)/GCE

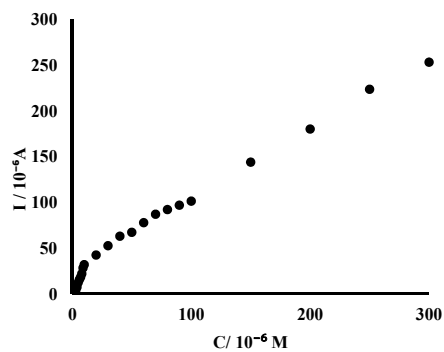


Figure 5.8: Variation of anodic peak current with concentration of Gu

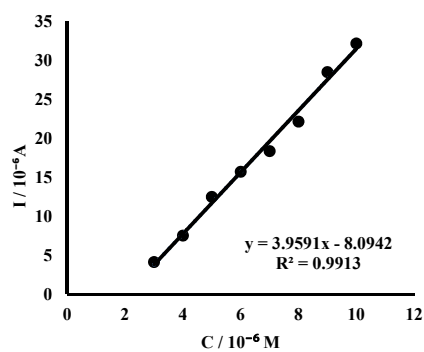


Figure 5.9: Calibration curve for Gu in the lower linear range

5.2.4.2 Adenine

For Ad, the oxidation peak appeared at 0.608 V on the *p*(TSA)/GCE and its peak current increased with increase in concentration (Fig.5.10 and Fig.5.11). A linear relationship was observed in the range from 1.5×10^{-3} M to 5.0×10^{-5} M (Fig. 5.12) and from 4.5×10^{-5} M to 5.0×10^{-6} M. The lowest LOD was calculated to be 9.4×10^{-7} M.

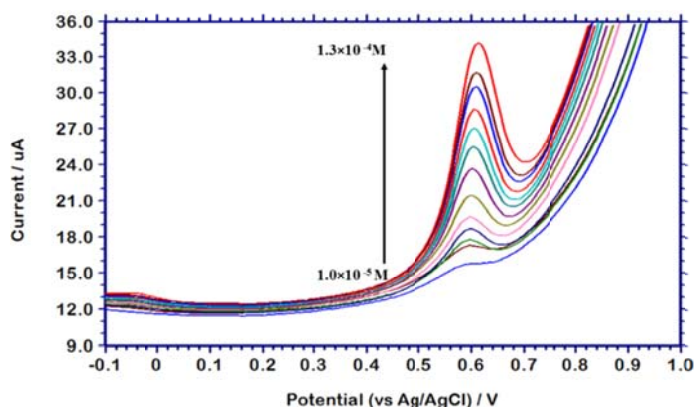


Figure 5.10: SW voltammograms for the oxidation of various concentrations of Ad in 0.1 M NaOH on *p*(TSA)/GCE

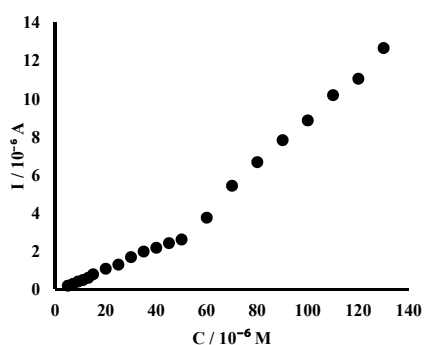


Figure 5.11. Variation of anodic peak current with concentration of Ad

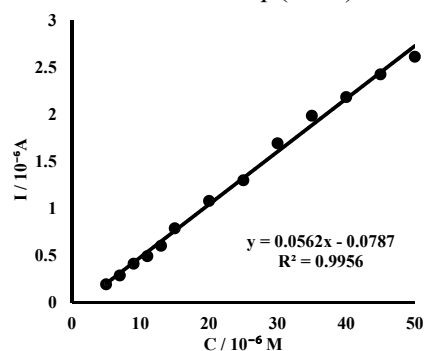


Figure 5.12. Calibration curve for Ad

5.3.4.3 Thymine

The peak corresponding to the electro-oxidation of Thy appeared at 0.760 V and its current showed an increase with increase in concentration (Fig. 5.13). The variation was linear in the range from 1.0×10^{-3} M to 2.0×10^{-5} M (Fig. 5.14) with a detection limit of 1.4×10^{-6} M.

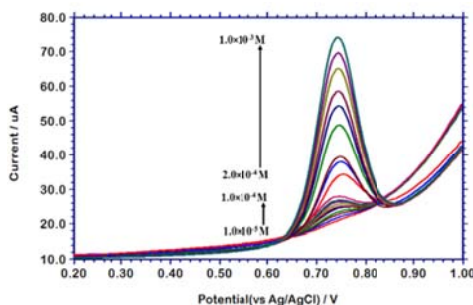


Figure 5.13: SW voltammograms of various concentrations of Thy in 0.1 M NaOH on p(TSA)/GCE

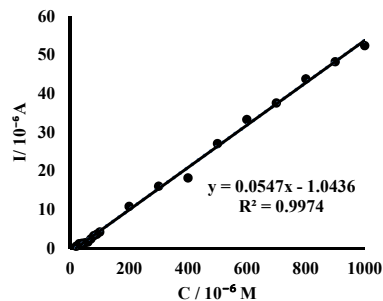


Figure 5.14: Calibration curve for Thy

5.2.4.4 Uric acid

In the square wave mode, an anodic peak appeared at -0.108 V corresponding to the electro-oxidation of Ua. The increase in peak current with increase in concentration of Ua is represented in Fig. 5.15. The variation was linear in the range 1.5×10^{-3} M to 9.0×10^{-5} M and from 1.0×10^{-4} M to 2.0×10^{-5} M. The lowest limit of detection, as calculated by the equation $3S/m$, where **S** is the standard deviation of the lowest measurement from six replicate measurements and **m** is the slope of the calibration curve (Fig.5.17) was obtained to be 3.3×10^{-6} M.

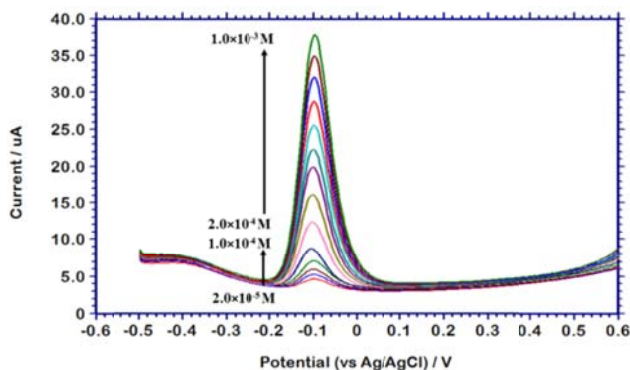


Figure 5.15: Overlay of SW voltammograms for the oxidation of various concentrations of Ua on *p*(TSA)/GCE in 0.1 M NaOH

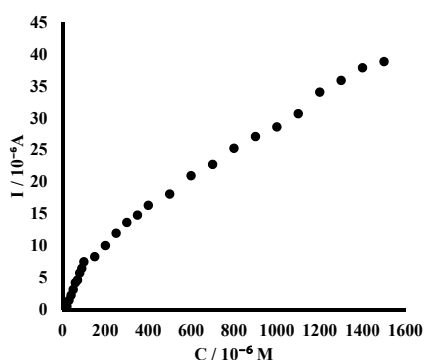


Figure 5.16: Variation of anodic peak current with concentration of Ua

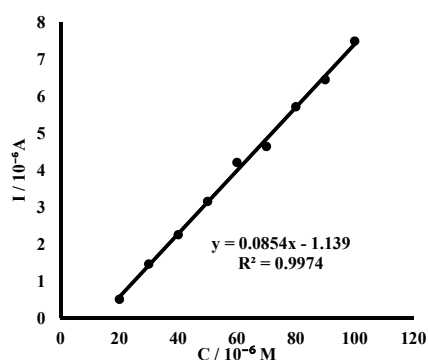


Figure 5.17: Calibration curve for Ua

5.2.5 Simultaneous determination

5.2.5.1 Uric acid, Guanine and Adenine

The oxidation peaks of Ua, Gu and Ad when recorded in the SWV mode from a solution containing equimolar concentrations of these compounds showed an increase in peak current with concentration of the corresponding analyte (Fig. 5.18). For Gu and Ua, the variation of peak current was linear in the range from 1.0×10^{-4} M to 1.0×10^{-5} M (Fig 5.19) giving the values of LOD as 3.5×10^{-7} M and 5.8×10^{-6} M respectively. The

variation of peak current for Ad was linear in the range 1.0×10^{-4} M to 2.0×10^{-5} M with LOD 5.8×10^{-6} M.

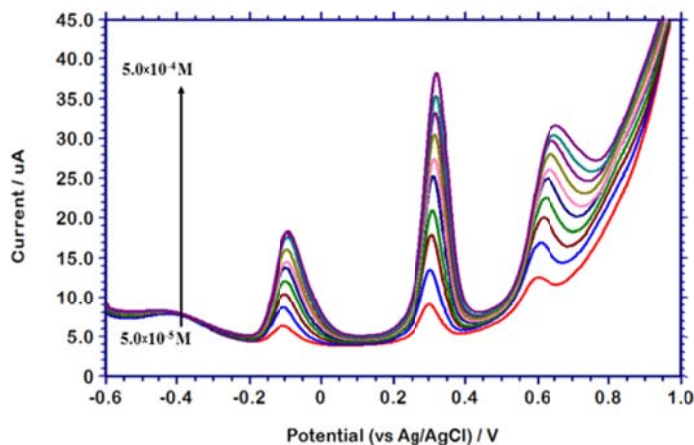


Figure 5.18: Overlay of SW voltammograms of various equimolar solutions of Ua, Gu and Ad on *p*(TSA)/GCE in 0.1 M NaOH

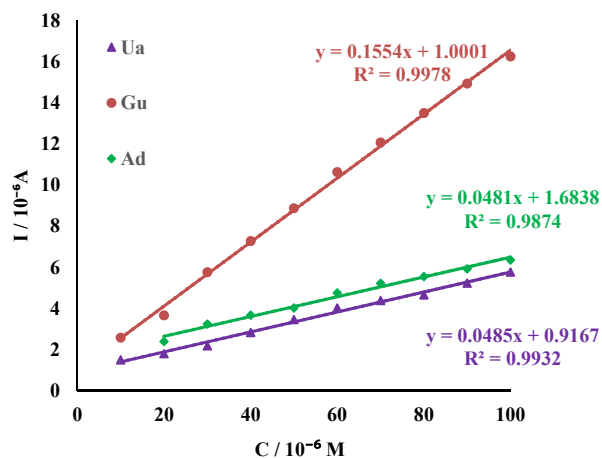


Figure 5.19: Calibration plot for simultaneous determination of Ua, Gu and Ad on *p*(TSA)/GCE

5.2.5.2 Uric acid, Guanine and Thymine

The voltammetric peaks corresponding to the oxidation of equimolar concentrations of Ua, Gu and Thy on *p*(TSA)/GCE, are shown in Fig 5.20. The

peak current due to each analyte showed an increase with increase in concentration of the corresponding analyte. The current response for Gu and Ua was linear over a wide range from 1.0×10^{-3} M to 2.0×10^{-5} M and for Thy, the concentration range over which current response showed linearity was from 1.0×10^{-3} M to 4.0×10^{-5} M. The LODs were obtained to be 2.5×10^{-6} M, 1.7×10^{-6} M and 5.7×10^{-6} M for Ua, Gu and Thy respectively.

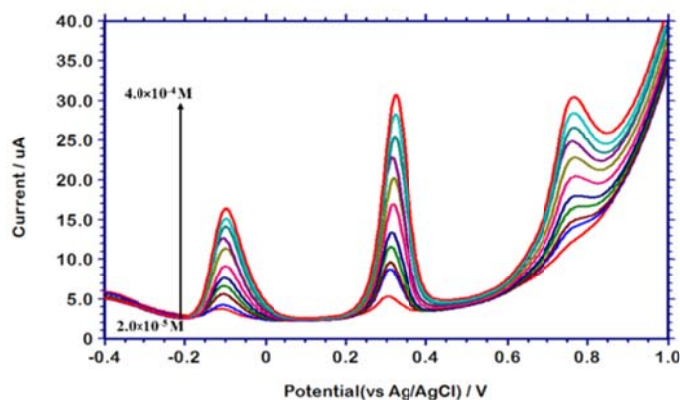


Figure 5.20: SW voltammograms recorded in various equimolar solutions of Ua, Gu and Thy on *p*(TSA)/GCE in 0.1 M NaOH

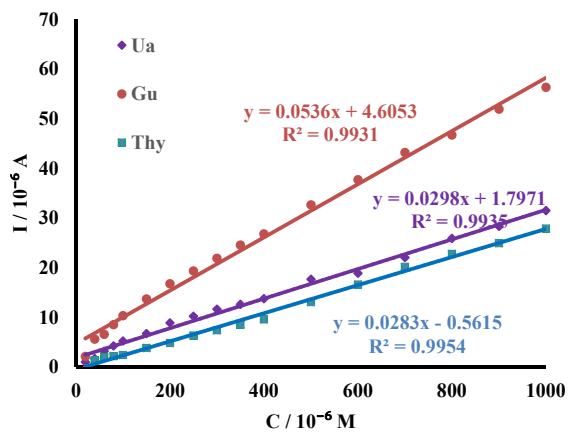


Figure 5.21: Calibration plot for simultaneous determination of Ua, Gu and Thy on *p*(TSA)/GCE

5.2.6 Mechanistic Studies

For Ua, Gu, Ad and Thy, the effect of scan rate on peak parameters such as potential and current was studied using LSV technique (Fig. 5.22). The relation between peak parameters and scan rate for each analyte are represented in Table 5.2.

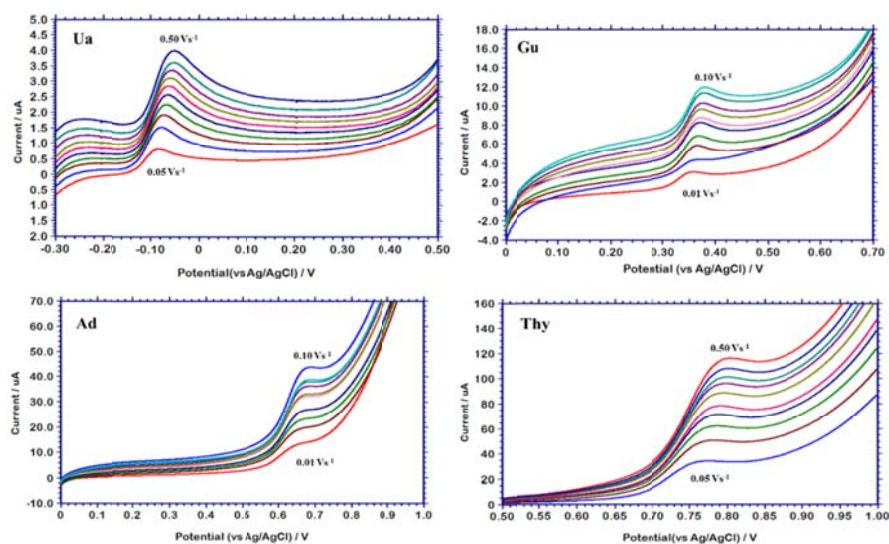


Figure 5.22: Linear sweep voltammograms for the oxidation of 1.0×10^{-3} M Ua, Gu, Ad and Thy in 0.1 M NaOH on the *p*(TSA)/GCE at different scan rates

Table 5.2: Variation of peak parameters with scan rate

	$E(V) \text{ vs } \ln v \text{ (Vs}^{-1}\text{)}$	$\log I \text{ (A) vs } \log v \text{ (Vs}^{-1}\text{)}$
Ua	$E = 0.024 \ln v - 0.051$ [$R^2 = 0.994$]	$\log I = 0.279 \log v - 5.349$ [$R^2 = 0.997$]
Gu	$E = 0.013 \ln v + 0.410$ [$R^2 = 0.990$]	$\log I = 0.356 \log v - 4.982$ [$R^2 = 0.995$]
Ad	$E = 0.030 \ln v + 0.760$ [$R^2 = 0.985$]	$\log I = 0.521 \log v - 3.965$ [$R^2 = 0.987$]
Thy	$E = 0.012 \ln v + 0.808$ [$R^2 = 0.982$]	$\log I = 0.577 \log v - 3.396$ [$R^2 = 0.991$]

The slope of $\log I$ vs $\log v$ for Ua, Gu, Ad and Thy are closer to the theoretical value of 0.5 expected for a diffusion controlled process [131]. Hence it can be concluded that the electro-oxidation of Ua, Gu, Ad and Thy on the *p*(TSA)/GCE is controlled by the diffusion of electroactive species

from the bulk of the solution rather than adsorption of electro-active species on to the electrode surface.

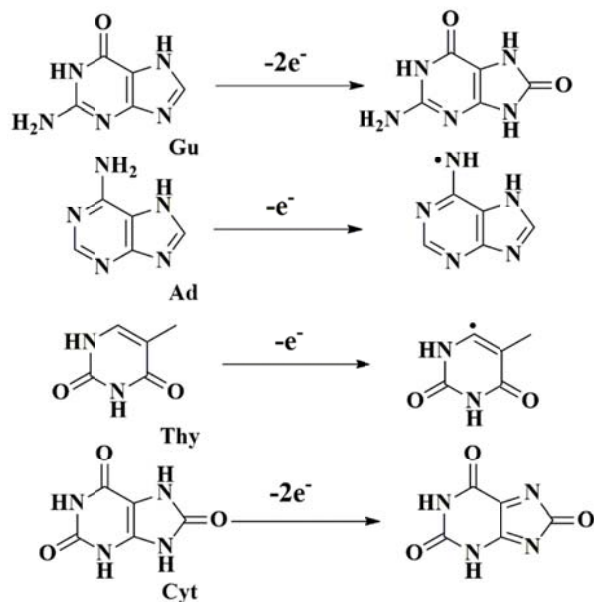
For Ua, Gu, Ad and Thy, the value of Tafel slope, $\frac{RT}{2(1-\alpha)n_{\alpha}F}$ obtained from the E vs $\ln v$ plot was used to calculate the value of $(1 - \alpha)n_{\alpha}$ and the value of $\alpha n_{\alpha} = \frac{0.047}{E - E_{1/2}}$ was calculated from the values of peak potential E and half peak potential $E_{1/2}$ from LS voltammogram at scan rate 0.1 Vs^{-1} . These values for the analytes and the corresponding values α and αn_{α} are listed in Table 5.3.

Table 5.3: Kinetic parameters for electro-oxidation

	$(1 - \alpha)n_{\alpha}$	αn_{α}	α	n_{α}
Ua	0.537	1.163	0.58	2(1.78)
Gu	1.404	1.305	0.50	2 (2.08)
Ad	0.462	0.626	0.57	1(1.09)
Thy	1.026	0.392	0.28	1(1.41)

*calculated value is shown in brackets

In accordance with these observations, the mechanism of the electrochemical reactions can be represented as scheme 5.1. Gu undergoes a two-electron oxidation [150]. Ad forms a free radical by removal of an electron [67] which undergoes further reaction in solution. Thy also forms a free radical by one electron oxidation [150] which then undergoes chemical reaction in solution. Two electron electrochemical oxidation of Ua is observed which has been widely reported [135].



Scheme 5.1: Electro-oxidation of Gu, Ad, Thy and Ua on *p*(TSA)/GCE

5.2.7 Selectivity and Interferences

In order to examine the selectivity of the sensor towards the simultaneous determination of each of the studied analytes, the individual determination was carried out in the presence of the others.

For Gu, the determination was carried out in the presence of 1.0×10^{-4} M concentrations of Ad and Ua (Fig. 5.23) as well as 1.0×10^{-4} M concentrations of Thy and Ua (Fig. 5.24). In presence of 1.0×10^{-4} M concentrations of Ad and Ua, the variation in peak current for Gu was linear in the range from 2.0×10^{-4} M to 2.0×10^{-5} M and from 1.0×10^{-3} M to 2.5×10^{-4} M with the lowest LOD 3.1×10^{-6} M. In presence of 1.0×10^{-4} M concentrations of Thy and Ua, the linear range for the determination of Gu was found to be from 1.5×10^{-4} M to 2.0×10^{-5} M and from 1.0×10^{-3} M to 1.0×10^{-4} M with the lower detection limit of 4.2×10^{-6} M.

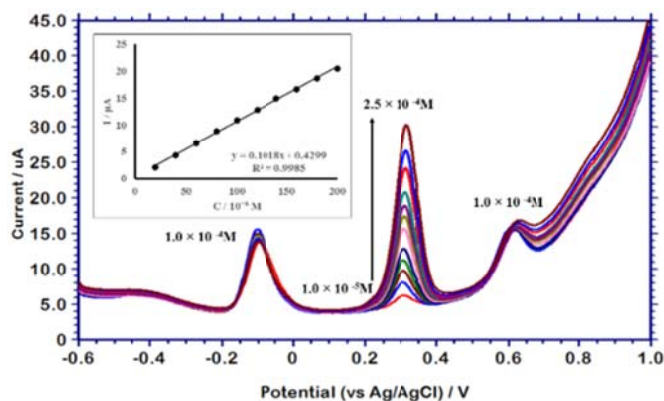


Figure 5.23: Variation of oxidation current with concentration for Gu in presence of 1.0×10^{-4} M Ua and Ad. Inset shows the corresponding calibration curve

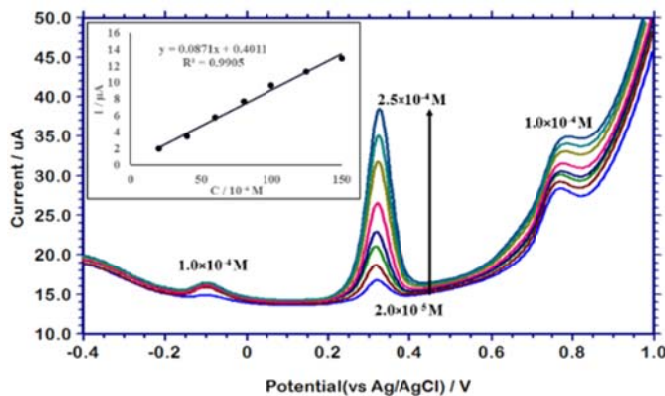


Figure 5.24: Variation of oxidation current with concentration for Gu in presence of 1.0×10^{-4} M Ua and Thy. Inset shows the corresponding calibration curve

The determination of Ua when carried out in presence of 1.0×10^{-4} M Gu and Ad (Fig. 5.25), a linear relation with peak current was obtained in the concentration range 1.1×10^{-4} M to 2.0×10^{-5} M and from 1.0×10^{-3} M to 1.0×10^{-4} M with LOD 7.5×10^{-6} M. In presence of 1.0×10^{-4} M Gu and Thy (Fig. 5.26), the variation in peak current for Ua was linear in the range from 1.0×10^{-3} M to 2.0×10^{-5} M with a lower LOD 1.1×10^{-6} M.

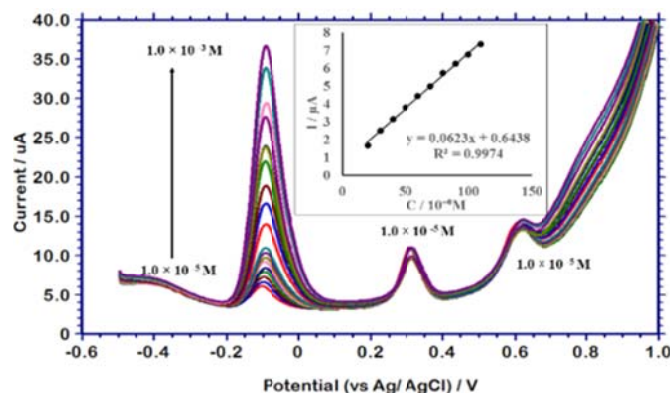


Figure 5.25: Variation of oxidation current with concentration for Ua in presence of 1.0×10^{-5} M Gu and Ad. Inset shows the corresponding calibration curve

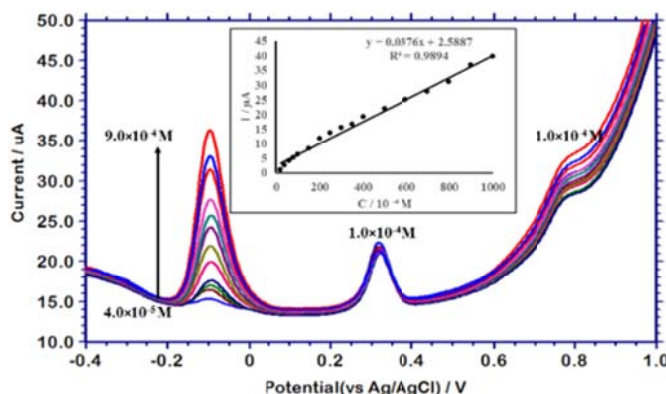


Figure 5.26: Variation of oxidation current with concentration for Ua in presence of 1.0×10^{-5} M Gu and Thy. Inset shows the corresponding calibration curve

Ad, when determined in the presence of 5.0×10^{-5} M Ua and Gu (Fig. 5.27), gave a linear relation between peak current and concentration in the range 1.2×10^{-4} M to 1.0×10^{-5} M with a lower LOD of 3.1×10^{-6} M. For Thy, the variation of peak current was linear in the range from 1.0×10^{-3} M to 4.0×10^{-5} M in the presence of 1.0×10^{-4} M concentrations of Ua and Gu (Fig. 5.28). The lower LOD was obtained to be 1.0×10^{-5} M.

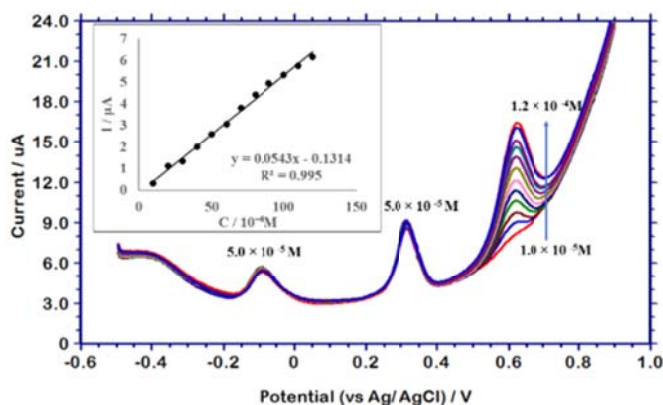


Figure 5.27: Variation of oxidation current with concentration for Ad in presence of $5.0 \times 10^{-5} \text{ M}$ Gu and Ua. Inset shows the corresponding calibration curve

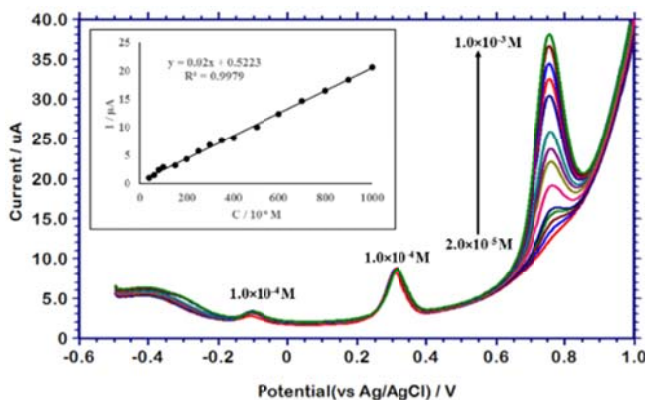


Figure 5.28: Variation of oxidation current with concentration for Thy in presence of $1.0 \times 10^{-4} \text{ M}$ Gu and Ua. Inset shows the corresponding calibration curve

Effect of other chemical species on the analytical signal, at a particular, analyte to added species molar ratio is presented in Table 5.4. Other nucleic acid bases like Cyt and Uracil did not interfere with the determination of Ua, Gu and Ad when present in 1:1 molar ratio. Ad and Thy interfered with the determination of each other when present in fivefold

lower concentrations. The simultaneous determination of Ua, Gu and Ad and Ua, Gu and Thy, was found to be free from interferences due to ionic species like K^+ , Cl^- , PO_4^{2-} etc., at 1:1 concentration ratio. Homovanillic acid interfered with the determination of Ad at equimolar concentrations whereas dopamine interfered with the determination of Gu when present in equimolar concentrations. When present in 1:1 concentration ratio, the hormones melatonin and serotonin showed interference in the determination of all the four analytes. Ascorbic acid interfered with the analytical signal of Ua at fivefold lower concentrations.

Table 5.4: Influence of chemical species on the analytical signal

Species	Molar Ratio	Signal change (%)			
		Gu	Ad	Thy	Ua
Cytosine	1:1	-1.1	-4.3	Peak distortion	-2.5
Uracil	1:1	-0.1	-3.4	-2.2	-4.5
Homovanillic Acid	5:1	-1.3	-10.0	+4.2	-4.7
Dopamine	1:1	-6.8	-3.7	-1.4	-2.9
Serotonin	1:1	> +20.0	-5.4	-4.9	>+20
Melatonin	1:1	> +20.0	Peak disappears	Peak distortion	Peak disappears
Glutathione	1:1	-0.8	-4.0	-3.8	-4.3
Ascorbic Acid	5:1	-3.4	-8.3	+3.9	Peak disappears
K^+ , Cl^- , PO_4^{2-}	1:1	<+2.0	<+2.0	<+2.0	<-2.0
Ca^{2+}	1:1	+8.4	-1.3	-1.8	-6.4

5.2.8 Application Studies

5.2.8.1 HS DNA

DNA sample was subjected to acid denaturation as described in section 2.7.4 of chapter 2. In acid denatured HS DNA (0.608 g mL^{-1}), peaks appear at 0.308 V and 0.608 V corresponding to the oxidation of Gu and Ad respectively in SWV mode using the $p(\text{TSA})/\text{GCE}$. With increase in

concentration of DNA solution, the peak current also increases linearly (Fig. 5.29). Using standard addition method, the percentages of Gu and Ad was found to be 24.7% and 32.7% respectively which gave the value $[(\text{Gu}+\text{Cyt})/(\text{Ad}+\text{Thy})]$ as equal to 0.754. This is comparable with the theoretical value of 0.770 expected for acid denatured HS DNA [35].

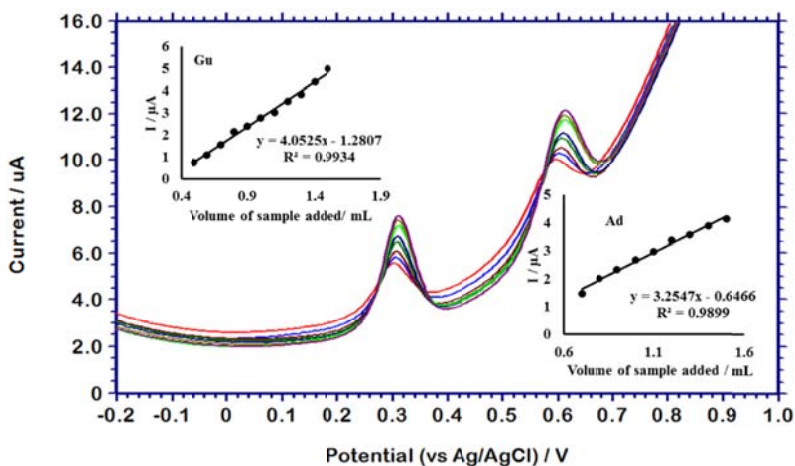


Figure 5.29: SW voltammograms for various concentrations of DNA sample recorded on *p*(TSA)/GCE using 0.1 M NaOH as supporting electrolyte. Inset shows the variation of peak current with concentration of DNA solution.

The peaks corresponding to oxidation of Ua and Thy were not observed in the SWV. Ua maybe absent in the solution and Thy could be detected only if its concentration was 10 times higher than the purines [151]. The DNA sample was spiked with Ua and determination was carried out using standard addition method. The recovery value obtained (Table 5.5) indicate that the sensor is suitable for the determination of Ua in real samples.

Table 5.5: Determination of Ua in spiked DNA

Sample	Ua		Recovery %	RSD %*
	Added (M)	Found (M)		
Herring Sperm DNA (acid denatured)	1.20×10^{-4} $- 1.00 \times 10^{-5}$	1.23×10^{-4} $- 1.05 \times 10^{-5}$	98	3.63

*for 6 measurements

5.2.8.2 Synthetic Urine and Serum

Synthetic urine and synthetic serum were prepared as explained in section 2.7.7 and 2.7.8 of chapter 2 and was spiked with Ua, Gu and Ad. The simultaneous determination was carried out using the *p*(TSA)/GCE. Similarly, the determination of Thy in these fluids spiked with Ua, Gu and Thy was carried out. The results are presented in Table 5.6. Good recovery values are obtained, pointing to the utility of the sensor for real sample analysis.

Table 5.6: Determination of Ua, Gu and Ad using *p*(TSA)/GCE in spiked samples

Sample	Analyte	Added (M)	Found (M)	Recovery	RSD* (%)
Urine	Gu	$1.00 \times 10^{-4} - 2.00 \times 10^{-5}$	$9.92 \times 10^{-5} - 2.03 \times 10^{-5}$	101	1.2
	Ad	$1.00 \times 10^{-5} - 2.50 \times 10^{-5}$	$9.97 \times 10^{-6} - 2.49 \times 10^{-5}$	98	1.4
	Thy	$5.00 \times 10^{-4} - 5.00 \times 10^{-5}$	$4.89 \times 10^{-4} - 4.94 \times 10^{-5}$	97	3.3
	Ua	$1.00 \times 10^{-5} - 2.50 \times 10^{-5}$	$1.02 \times 10^{-5} - 2.54 \times 10^{-5}$	99	2.6
Serum	Gu	$1.00 \times 10^{-4} - 1.50 \times 10^{-5}$	$1.02 \times 10^{-4} - 1.53 \times 10^{-5}$	103	1.9
	Ad	$1.00 \times 10^{-5} - 2.50 \times 10^{-5}$	$9.87 \times 10^{-6} - 2.40 \times 10^{-5}$	98	1.7
	Thy	$5.00 \times 10^{-4} - 5.00 \times 10^{-5}$	$4.77 \times 10^{-4} - 4.81 \times 10^{-5}$	96	3.8
	Ua	$1.00 \times 10^{-5} - 2.50 \times 10^{-5}$	$9.79 \times 10^{-6} - 2.63 \times 10^{-5}$	101	2.9

*for 6 measurements

5.2.9 Repeatability and reproducibility

In order to explore the reproducibility and repeatability of the measurements on the developed sensor, relative standard deviation (RSD) of the intra and inter-assay was calculated. To conduct the intra assay five different $p(\text{TSA})/\text{GCE}$ were prepared and the peak currents for a solution containing 1.0×10^{-5} M each of Gu, Ad and Ua, were measured. The RSD for the measurement for Gu, Ad and Ua was found to be 0.25%, 0.30% and 0.84% respectively. For the inter assay, the peak current measured on a $p(\text{TSA})/\text{GCE}$ was noted five times in a solution containing 1.0×10^{-5} M each of Gu, Ad and Ua. The RSD ($n = 5$) for the inter assay for Gu, Ad and Ua was found to be 0.32%, 2.08% and 3.36% respectively. The RSD values for intra and inter-assays indicate that the $p(\text{TSA})/\text{GCE}$ show good reproducibility and repeatability.

5.2.10 Kinetics of electro-oxidation on $p(\text{TSA})/\text{GCE}$

5.2.10.1 Chronoamperometry

Under the optimised sensor conditions, the Cottrellian decay of current I with time t was studied with chronoamperometry for various concentrations of the analytes. The obtained chronoamperograms for Gu, Ad, Thy and Cyt are shown in Fig. 5.30. The decaying current I was plotted against $t^{-1/2}$ for each concentration. The slope obtained for each concentration was plotted against the corresponding concentration (Fig. 5.31) and the slope of the resulting curve was used in the Cottrell equation as explained in Section 3.2.9.1. The diffusion coefficients of Gu, Ad, Thy and Cyt under the optimised sensor conditions are obtained to be 2.66×10^{-6} cm^2s^{-1} , 4.86×10^{-6} cm^2s^{-1} , 7.13×10^{-7} cm^2s^{-1} and 4.08×10^{-3} cm^2s^{-1} respectively.

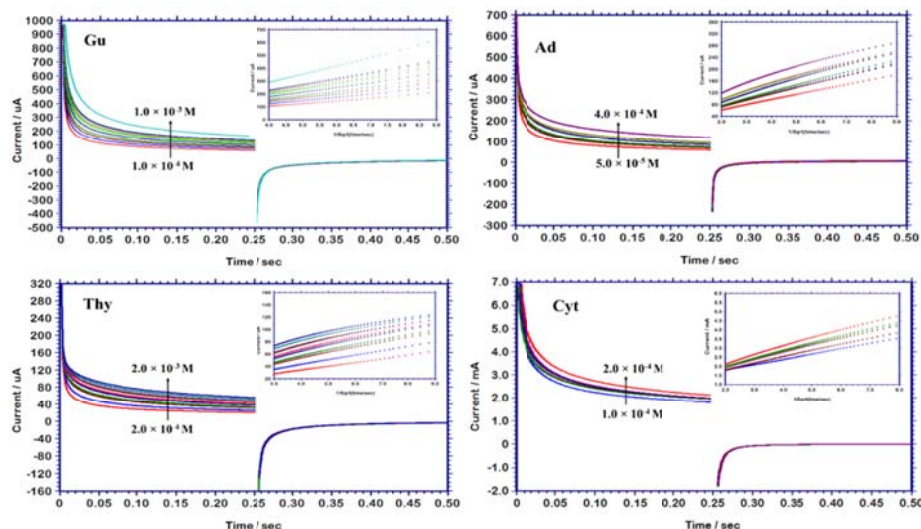


Figure 5.30: Overlay of Chronoamperograms obtained on the p(TSA)/GCE for various concentrations of Gu, Ad, Thy and Cyt. The inset of each chronoamperogram shows the corresponding plot of **I** against $t^{-1/2}$

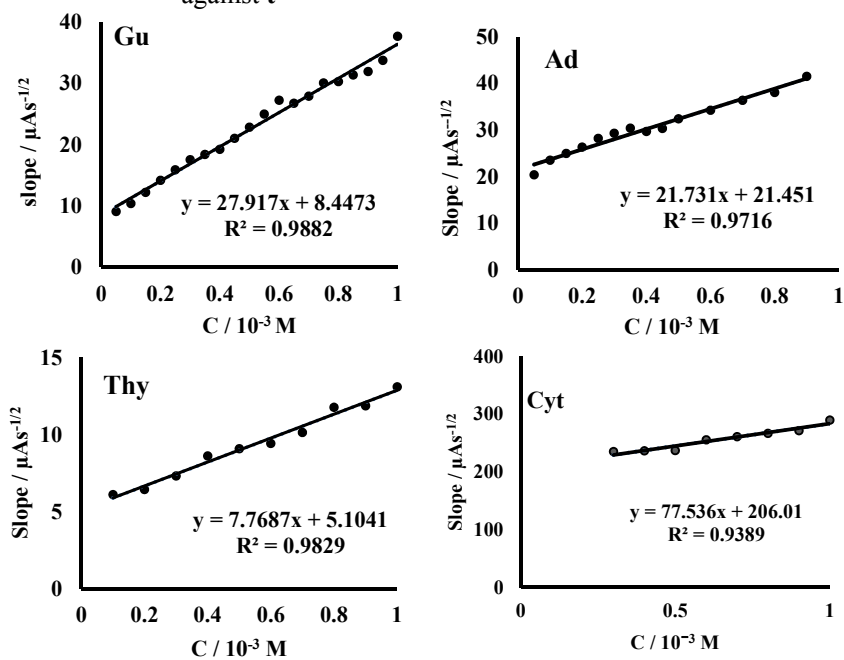


Figure 5.31: Plot of slope (**I** vs $t^{-1/2}$) against concentration for Gu, Ad, Thy and Cyt

The chronoamperograms and the corresponding I vs $t^{-1/2}$ plots at different concentrations of Ua are shown in Fig. 5.32. From the slope of the plot $\frac{dI}{dt^{-1/2}}$ vs C (Fig. 5.33), the diffusion coefficient of Ua was obtained to be $3.20 \times 10^{-6} \text{ cm}^2 \text{ s}^{-1}$ using $p(\text{TSA})/\text{GCE}$.

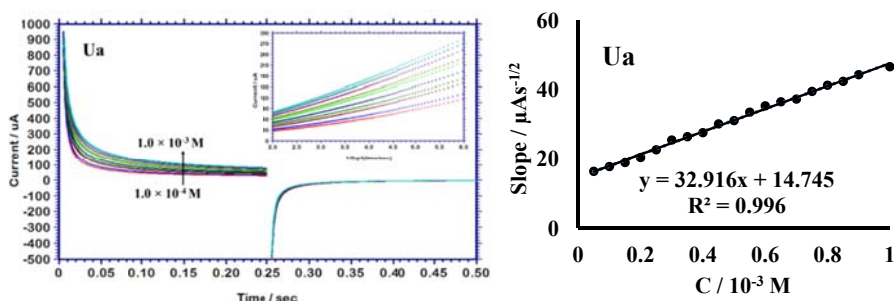


Figure 5.32: Overlay of chronoamperograms obtained for various concentrations of Ua in 0.1 M NaOH on $p(\text{GA})/\text{GCE}$. Inset shows the corresponding I vs $t^{-1/2}$ plots

Figure 5.33: Plot of slope (I vs $t^{-1/2}$) against concentration of Ua

A comparison of the diffusion coefficients of Ua, Gu, Ad, Thy and Cyt on the bare GCE and $p(\text{TSA})/\text{GCE}$ is given in table 5.7. There is an increase in the value of D obtained on the $p(\text{TSA})/\text{GCE}$ for Cyt and Ua as well as Gu, although the increase is not as significant for Gu as for Cyt and Ua. For Cyt there is a sixty-fold increase in D , for Ua tenfold increase and for Gu sesquifold (1.5) increase when compared to the GCE. For Ad, the diffusion coefficient determined using $p(\text{TSA})/\text{GCE}$ was 1.4 times lower than that obtained using bare GCE. In case of Thy the diffusion coefficient obtained on the $p(\text{TSA})/\text{GCE}$ was sixfold lower than that on bare GCE. If the increase in electro-active surface area alone was the reason for increase

in diffusion coefficient, all the analytes under study should have given comparable changes in D for the $p(\text{TSA})/\text{GCE}$. Hence the prevalence of electro-static interaction between the modified electrode and the analyte might be the reason for the change in diffusion coefficient.

Table 5.7: Calculated values of diffusion coefficients

Analyte	$D \text{ (cm}^2 \text{ s}^{-1}\text{)}$	
	GCE	$p(\text{TSA})/\text{GCE}$
Gu	1.8×10^{-6}	2.7×10^{-6}
Ad	6.9×10^{-6}	4.9×10^{-6}
Thy	4.5×10^{-6}	7.1×10^{-7}
Cyt	6.6×10^{-5}	4.1×10^{-3}
Ua	2.9×10^{-7}	3.2×10^{-6}

5.2.10.2 Heterogeneous rate constant

In accordance with the Nicholson-Shain equation, the slope of E versus $\ln v$ is equal to $\frac{RT}{2(1-\alpha)nF}$ and its intercept equals to $E^0 + \frac{RT}{(1-\alpha)nF} \left[0.78 - \ln \frac{k_h}{D^{1/2}} + \frac{1}{2} \ln \frac{(1-\alpha)nF}{RT} \right]$, where E^0 is the intercept of the plot of E vs v .

By the Laviron approach for the determination of k_s , slope of E versus $\ln v$ is equal to $\frac{RT}{(1-\alpha)nF}$ and its intercept equals to $E^0 + \frac{RT}{(1-\alpha)nF} \left[\ln \frac{(1-\alpha)nF}{RTk_s} \right]$, where E^0 is the intercept of the plot of E vs v .

Table 5.8: Kinetic studies

	Regression equation		$(1 - \alpha)n_\alpha$	αn_α	α	n_α^*
	E vs $\ln v$	E vs v				
Gu	$E = 0.013 \ln v + 0.411$	$E = 0.611 v + 0.346$	1.044	1.305	0.56	2 (2.34)
Ad	$E = 0.030 \ln v + 0.760$	$E = 0.049 v + 0.643$	0.462	0.626	0.57	1 (1.09)
Thy	$E = 0.012 \ln v + 0.808$	$E = 0.068 v + 0.773$	1.026	0.392	0.28	1 (1.41)
Cyt	$E = 0.019 \ln v + 0.908$	$E = 0.335 v + 0.831$	0.675	0.681	0.50	1 (1.35)
Ua	$E = 0.024 \ln v - 0.051$	$E = 0.371 v - 0.091$	0.537	1.163	0.58	2 (1.78)

*calculated value is shown in brackets

The results obtained for scan rate studies on the electro-oxidation of Gu, Ad, Thy, Cyt and Ua are presented in Table 5.8. The value of rate constant calculated according to Nicholson-Shain and Laviron models are presented in table 5.9.

Table 5.9: Rate constants for electro-oxidation

	k_h (cm s ⁻¹)		k_s (s ⁻¹)	
	GCE	$p(\text{TSA})/\text{GCE}$	GCE	$p(\text{TSA})/\text{GCE}$
Gu	1.18×10^{-3}	1.53×10^{-3}	2.07	0.65
Ad	4.55×10^{-4}	1.71×10^{-3}	2.43	0.69
Thy	1.65×10^{-3}	2.76×10^{-3}	0.45	4.50
Cyt	6.31×10^{-3}	4.33×10^{-2}	0.37	1.25
Ua	3.33×10^{-4}	3.43×10^{-4}	0.40	11.42

The highest value of Nicholson - Shain rate constant was obtained for Cyt which gave the highest value for **D**. Among the analytes studied, Nicholson -Shain rate constant varied in the order Cyt > Ad > Gu > Ua > Thy which follows a similar pattern as variation of **D**. The Laviron rate constant followed the trend Ua > Thy > Cyt > Ad > Gu.

Compared to the bare GCE, a significant change in Nicholson-Shain kinetics was observed only for Cyt and Ad. In case of Laviron kinetics Ua, Thy and Cyt showed increase on the $p(\text{TSA})/\text{GCE}$ in comparison to the bare

GCE whereas Gu and Ad showed decrease in kinetics. From these observations, it is concluded that diffusion and electron transfer kinetics have improved on the *p*(TSA)/GCE for Cyt. Although the diffusion effects improved for Ad, the electron transfer kinetics on the *p*(TSA)/GCE was lowered. In case of Gu, *p*(TSA)/GCE caused increase in diffusion kinetics whereas for Thy, *p*(TSA)/GCE produced increase in electron transfer kinetics than diffusion kinetics. Thus, *p*(TSA)/GCE produced analyte specific effects. For the purine DNA bases, diffusion kinetics were predominant whereas for the pyrimidine DNA bases both diffusion and electron transfer effects contributed to the kinetics of electro-oxidation.

5.3 Conclusions

Simultaneous electrochemical oxidation of Gu and Ad in the presence of Ua, is studied in the SWV mode on a *p*(TSA)/GCE, with NaOH as the supporting electrolyte. In highly alkaline medium, well defined and well separated irreversible peaks were obtained for the electro oxidation of Gu, Ad and Ua, which facilitate their simultaneous determination. The simultaneous determination of Gu, Thy and Ua was also possible. The *p*(TSA)/GCE sensor gave good working linear ranges and low detection limits for the determination of these analytes in alkaline medium. The electro-oxidation processes were found to be diffusion controlled and irreversible. The method was successfully applied to the determination of purine bases in HS DNA. The determination of Ua in spiked HS DNA with the developed sensor gave reasonably good recoveries with acceptable RSD values. The utility of the sensor for the determination of Gu, Ad, Thy and Ua in synthetic urine and synthetic blood serum has also been demonstrated.

Although there has been reports of polymer modified electrodes being used for the simultaneous determination of Gu and Ad in the presence of Ua and also with other targets, the determination occurs at higher overpotentials. It is under such a status quo that, a *p*(TSA)/GCE, which is easily fabricated via electropolymerisation of the very prevalent and available TSA, becomes significant. It not only decreases the overpotential for the electro-oxidation process, but also gives LODs comparable to that of analogues sensors.

Kinetics of electro-oxidation of all the DNA bases on the *p*(TSA)/GCE was studied. The highest value of diffusion coefficient was obtained for Cyt. The electro-oxidation of Cyt proceeded with the highest rate constant with regard to Nicholson-Shain kinetic model which considers both mass transport and charge transfer. In terms of the Laviron model, which considers only the charge transfer at the electrode, rate of oxidation of Thy was the highest among all the DNA bases.

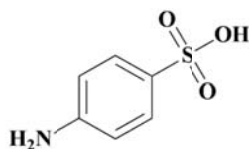
..... ✨.....

— Poly(para Amino Benzene Sulfonic Acid) modified Glassy Carbon Electrode as Sensor for Simultaneous Determination of Guanine, Adenine and Uric acid

The present chapter details the development of a poly(para amino benzene sulfonic acid) modified glassy carbon electrode as a sensor for the simultaneous determination of guanine, adenine and uric acid. Optimisation of experimental parameters to obtain the best sensor performance has been explained. The sensor response has been calibrated for both simultaneous and individual determination. The selectivity of the sensor for simultaneous determination has been checked among the purine bases as well as in the presence of other possibly co-existing species. The sensor has been demonstrated to be efficient for the determination of guanine and adenine in acid denatured herring sperm DNA. The mechanistic and kinetic parameters for the electro-oxidation of all the DNA bases and uric acid on the poly(para amino benzene sulfonic acid) modified glassy carbon electrode has also been determined.

6.1 Introduction

Para amino benzene sulfonic acid (ABSA) commonly known as sulfanilic acid ($C_6H_7NO_3S$) finds a number of applications in electroanalysis.



para amino benzene sulfonic acid

There are several reports of electropolymerisation of ABSA on GCE and its use for the determination of various analytes.

Xu and co-workers reported the polymerisation of ABSA from 1.0×10^{-3} M solution in 0.01 M HCl by cyclic potential sweeping from -0.6 V to 1.1 V at the scan rate of 0.1 Vs^{-1} for 6 cycles. The electrode was then subjected to cyclic scanning from 0.0 to 1.0 V in PBS pH 5.0. The fabricated electrode was used for the determination of dopamine [154].

Influence of pH on the electrochemical behaviour of conducting polymer films electrosynthesised from aminobenzoic acids and amino benzene sulphonic acids has been studied by Brett and Thiemann [155]

The electropolymerisation of ABSA from a 2.0×10^{-3} M solution in 0.1 M NaCl by repetitive potential cycling between -1.5 V to 2.5 V for 10 scans was reported by Jin, Zang and Chen [156]. The electro-activation was carried out by CV from -1.0 V to 1.0 V in pH 7 ABS. The simultaneous determination of dopamine and ascorbic acid was carried out using the *p*(ABSA)/GCE.

Electropolymerisation of *p*(ABSA) on to GCE from 2.0×10^{-3} M monomer solution in 0.1 M HNO₃ by cyclic potential sweeping from -0.5 V to 2.0 V was proposed by Kumar and Chen [116]. They studied the electrocatalytic reduction of oxygen and hydrogen peroxide on the devised electrode.

The *p*(ABSA)/GCE, formed by subjecting GCE to cyclic potential sweeping from 0.6 V to 1.2 V in a 1.0×10^{-3} M solution of ABSA in 0.1 M KCl at the scan rate of 0.05 Vs^{-1} was modified with poly(aniline) nano networks and used for the simultaneous determination of ascorbic acid and uric acid (Ua) by Zhang, Zhang and Lian [157].

Chen and co-workers reported the determination of Rutin on *p*(ABSA)/GCE, prepared by cycling the potential on the GCE from -1.5 V to 2.5 V (scan rate 0.1 Vs⁻¹) in a solution of 2.0 × 10⁻³ M ABSA in 0.1 M PBS pH 6.8 [158].

The use of *p*(ABSA)/GCE fabricated by the same method adopted by Chen and co-workers was used for the determination of Ua [159] and the study of electrocatalytic oxidation of hydrazine [160] by Sadikoglu and co-workers.

A layer-by-layer assembly of *p*(ABSA)/quaternary amine functionalized carbon nanotube/ *p*(ABSA)/GCE, composite film on GCE for the determination of ascorbic acid has been reported by Xi et al. [161]. The first layer of *p*(ABSA) was formed by cyclic potential sweeping from 0.6 to 1.2 V for 10 cycles (scan rate of 0.05 V s⁻¹) in 2.0 × 10⁻³ M ABSA solution in 0.1 M KCl. After incorporating functionalised carbon nano-tubes the second layer of *p*(ABSA) was electropolymerised on to the electrode from 0.5 M sulfuric acid solution containing 5.0 × 10⁻² M ABSA by cyclic potential sweep from -0.2 to 1.5 V for 5 cycles.

p(ABSA)/GCE prepared by the method reported by Kumar and Chen was modified with gold nanoparticles and used for the determination of the synthetic antioxidant propyl gallate by Cyriac et al. [107] from our group.

Simultaneous voltammetric determination of Ua, guanine (Gu) and adenine (Ad) on the *p*(ABSA)/GCE, fabricated by subjecting the GCE to cyclic potential sweeping from -0.5 V to 2.0 V in 2.0 × 10⁻³ M monomer solution in 0.1 M HNO₃ [107] is described in this chapter.

6.2 Results and discussion

Modification of GCE with *p*(ABSA) was carried out as described in chapter 2 (Section 2.4.1) and the prepared *p*(ABSA)/GCE was characterised as described in section 2.4.2. The experimental parameters to derive best performance of the prepared electrode towards electro-oxidation of analytes under study, Ua, Gu and Ad was determined.

6.2.1 Optimisation of experimental parameters

For all analytes under study, the lowest potential for electro-oxidation was recorded when 0.1 M NaOH was used as supporting electrolyte. Hence 0.1 M NaOH was chosen as the supporting electrolyte for further studies.

The effect of number of cycles of electropolymerisation on electrochemical response of Ua, Gu and Ad was studied. A significant change in anodic potential was not observed with change in number of cycles. The current response was almost the same for *p*(ABSA)/GCE devised with 5 and 15 cycles of polymerisation (Fig. 6.1). Considering the lower time required for polymerisation, *p*(ABSA)/GCE devised with 5 polymerisation cycles was decided as the optimum sensor and used for further studies.

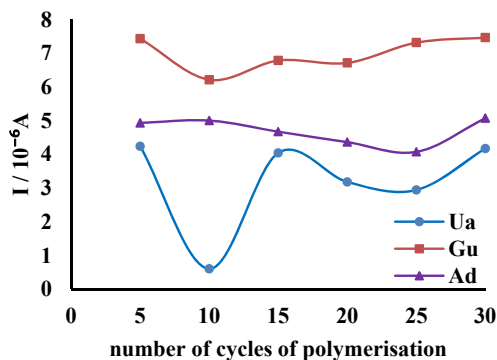


Figure 6.1: Effect of number of cycles of polymerisation on the anodic peak current of 5.0×10^{-5} M Ua, Gu and Ad in 0.1 M NaOH

6.2.2 Electrochemical behaviour of DNA bases on *p*(ABSA)/GCE

The electrochemical oxidation of the DNA bases on *p*(ABSA)/GCE has been studied in 0.1 M NaOH using SWV. On the bare GCE, the peaks due to the electro-oxidation of 5.0×10^{-5} M Gu and Ad appeared at 0.348 V and 0.632 V respectively whereas for 5.0×10^{-5} M Thy and Cyt, the electro-oxidation peaks were not observed. Electro-oxidation peaks for 5.0×10^{-5} M Gu, Ad and Thy appeared at 0.284 V, 0.588 V and 0.758 V on *p*(ABSA)/GCE whereas 5.0×10^{-5} M Cyt did not show any peak on *p*(ABSA)/GCE. For the purine base, uric acid the electro-oxidation peak for 5.0×10^{-5} M concentration appeared at -0.132 V on *p*(ABSA)/GCE as opposed to -0.080 V on the bare GCE. Overlay of SW voltammograms for the simultaneous oxidation of Ua, Gu and Ad on the bare GCE and *p*(ABSA)/GCE is shown in Fig. 6.2. The oxidation peaks of Ua and Gu were separated by 0.416 V and that of Gu and Ad by 0.304 V. The well separated peaks hints that the sensor maybe suitable for simultaneous determination of Ua, Gu and Ad. Although it appears that the peak separation for Ad and Thy is 0.170 V, when determined simultaneously, the

peaks were wide and close together that their resolution was not possible. Hence in the present study, the simultaneous determination of Ua, Gu and Ad was attempted. Individual determination of Thy was not attempted because at concentrations lower than 5.0×10^{-5} M, the oxidation peak for Thy was not detected and at concentrations higher than 1.0×10^{-4} M, the peak was distorted thereby giving a very narrow working linear range.

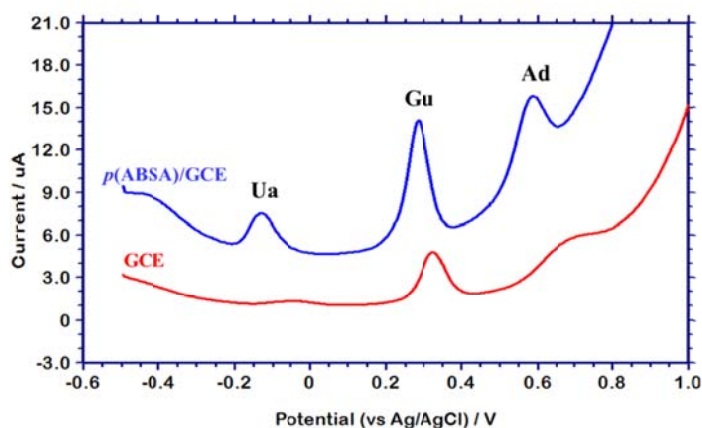


Figure 6.2: SW voltammograms for simultaneous oxidation of 5.0×10^{-5} M Ua, Gu and Ad in 0.1 M NaOH on *p*(ABSA)/GCE and GCE

Electrochemical impedance response of 5.0×10^{-4} M Ua, Gu and Ad on the bare GCE and *p*(ABSA)/GCE (0.1 M NaOH as supporting electrolyte) in the frequency range $1.0 - 1.0 \times 10^5$ Hz at the corresponding oxidation potentials is represented by the Nyquist plots shown in Fig. 6.3. It is apparent from the figure that the charge transfer resistance has decreased on the *p*(ABSA)/GCE compared to bare GCE for all the three analytes. On the bare GCE, the charge transfer resistance R_{ct} , for the electro-oxidation of Gu, Ad and Ua were found to be $7.58 \times 10^5 \Omega$, $2.62 \times 10^4 \Omega$ and $1.78 \times 10^5 \Omega$ respectively. On the *p*(ABSA)/GCE the R_{ct} has been decreased

to $1.12 \times 10^4 \Omega$, $8.75 \times 10^3 \Omega$ and $1.67 \times 10^4 \Omega$ respectively. This indicates that the electro-oxidation of Gu, Ad, Thy and Ua is facilitated by the presence of the conducting polymer film.

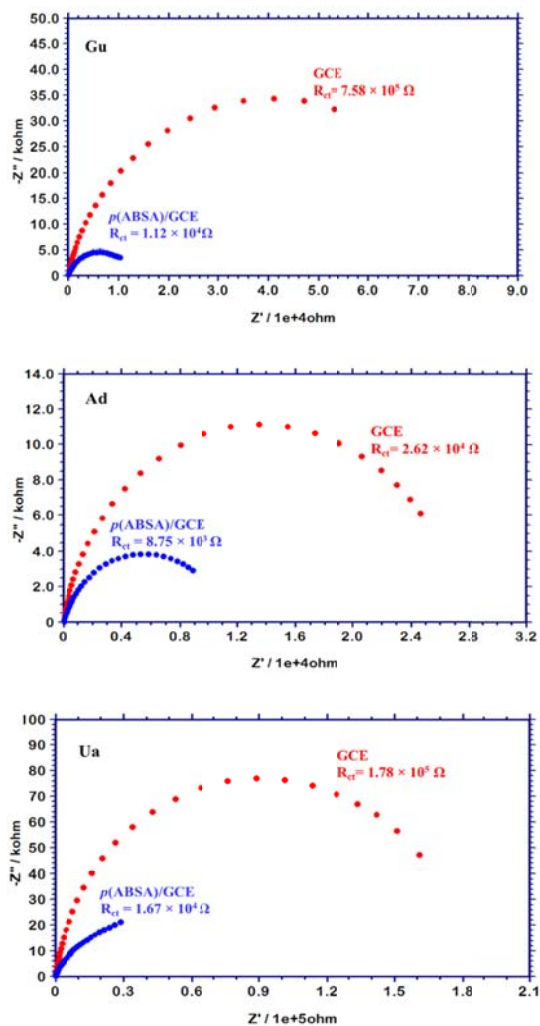


Figure 6.3: EIS Nyquist plots obtained on GCE and *p*(ABSA)/GCE for 5.0×10^{-4} M concentrations of Gu, Ad and Ua in 0.1 M NaOH in the frequency range 1.0 - 1.0×10^5 Hz at the corresponding oxidation potential

A comparison of the R_{ct} values of bare and modified GCE is shown in Table 6.1

Table 6.1: R_{ct} values fitted from Nyquist plots

	GCE ($10^5 \Omega$)	<i>p</i> (TSA)/GCE ($10^5 \Omega$)
Gu	7.580	0.112
Ad	0.262	0.087
Ua	1.780	0.167

Both SW voltammograms and Nyquist plots suggest that the *p*(ABSA) film deposited on GCE catalyses the electrochemical oxidation of Ua, Gu and Ad. There is a decrease in oxidation potential and increase in oxidation current on *p*(ABSA)/GCE as well as a significant lowering of charge transfer resistance, R_{ct} for all the electro-oxidation reactions on *p*(ABSA)/GCE.

6.2.3 Electro active surface area

Electro-active surface area of *p*(ABSA)/GCE was calculated by application of Randles-Sevcik equation as described in Chapter 3 (Section 3.2.4). The cyclic voltammograms of 2.0×10^{-3} M $K_3[Fe(CN)_6]$ were recorded at different scan rates (0.02 Vs^{-1} to 0.20 Vs^{-1}) on bare GCE as well as *p*(ABSA)/GCE (Fig 6.4) and the variation of oxidation peak current with square root of scan rate was studied.

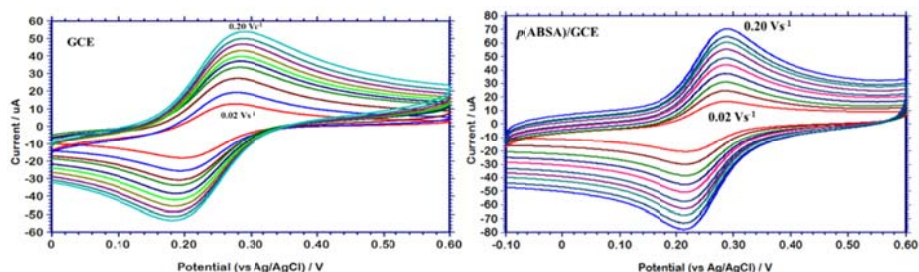


Figure 6.4: Cyclic voltammograms obtained for the oxidation of 2.0×10^{-3} M $K_3[Fe(CN)_6]$ on bare GCE and $p(ABSA)/GCE$ at different scan rates (0.02 Vs^{-1} to 0.20 Vs^{-1})

For bare GCE, $I(A) = 9.72 \times 10^{-5} \nu^{1/2}(Vs^{-1}) - 3.89 \times 10^{-7}$

For $p(ABSA)/GCE$, $I(A) = 1.22 \times 10^{-4} \nu^{1/2}(Vs^{-1}) - 1.96 \times 10^{-6}$

The electroactive surface area of the bare GCE and $p(ABSA)/GCE$ was obtained to be 0.066 cm^2 and 0.082 cm^2 respectively. A 24% enhancement in electroactive surface area was observed upon modification.

6.2.4 Calibration

The variation of anodic peak current for each of the analytes on the $p(ABSA)/GCE$ with concentration was studied using SWV. The concentration range over which peak current was linear is termed as working linear range. The lowest LOD was calculated using the formula $3S/m$ where S is the standard deviation of the lowest oxidation current detected and m is the slope of the calibration curve.

6.2.4.1 Guanine

The oxidation of Gu on the $p(ABSA)/GCE$ took place at 0.284 V and the anodic current increased with increase in concentration (Fig. 6.5). The variation was linear over the concentration range 2.0×10^{-4} M to 1.0×10^{-5} M (Fig. 6.6) and from 1.0×10^{-3} M to 2.0×10^{-5} M with lower LOD 3.0×10^{-6} M.

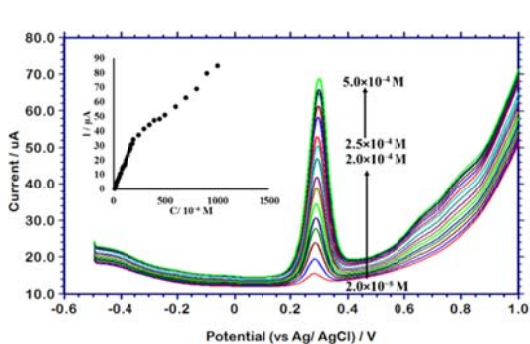


Figure 6.5: SW voltammograms for the oxidation of different concentrations of Gu in 0.1 M NaOH on *p*(ABSA)/GCE. Inset shows variation of anodic peak current with concentration

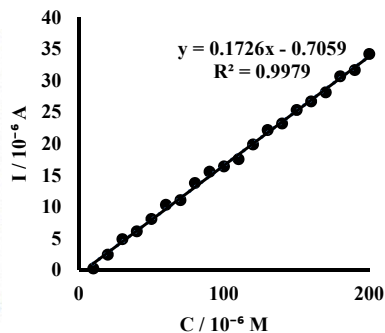


Figure 6.6: Calibration curve for Gu

6.2.4.2 Adenine

The electro-oxidation of Ad took place at 0.588 V on the *p*(ABSA)/GCE and the variation in oxidation peak current was linear in the range 2.0×10^{-4} M to 1.0×10^{-5} M (Fig. 6.7 and 6.8). At concentrations higher than 2.0×10^{-4} M, the peak gets distorted. The LOD for Ad was obtained as 8.6×10^{-6} M.

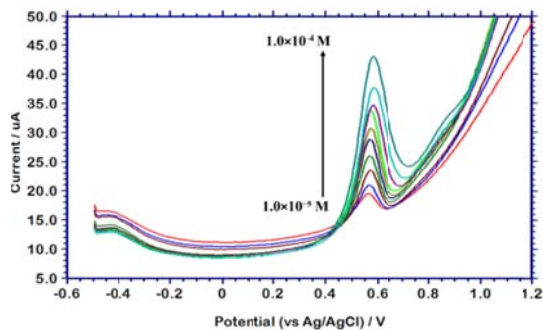


Figure 6.7: Overlay of SW voltammograms for the oxidation of Ad on *p*(ABSA)/GCE

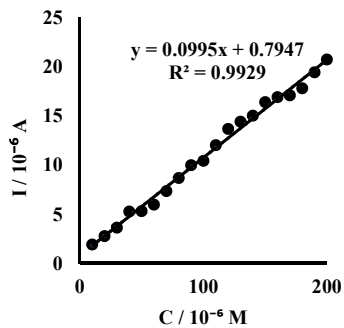


Figure 6.8: Calibration curve for Ad

6.2.4.3 Uric Acid

The peak corresponding to the oxidation of Ua on the *p*(ABSA)/GCE appeared at -0.132 V. The overlay of SW voltammogram for the oxidation of 5.0×10^{-3} M to 2.0×10^{-5} M Ua is presented in Fig. 6.9. The variation of peak current was found to be linear from 1.5×10^{-4} M to 2.0×10^{-5} M and from 1.0×10^{-3} M to 1.5×10^{-4} M (Fig. 6.10). The LOD was found to be 1.0×10^{-6} M.

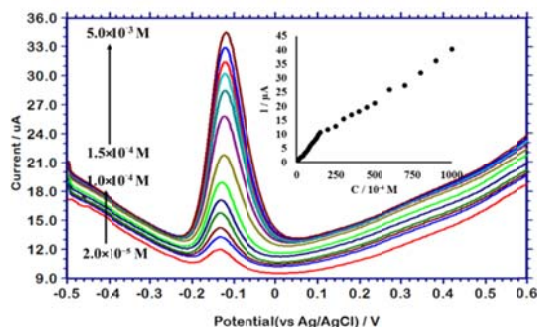


Figure 6.9: Overlay of SW voltammograms for the oxidation of Ua on *p*(ABSA)/GCE. Inset shows variation of anodic peak current with concentration

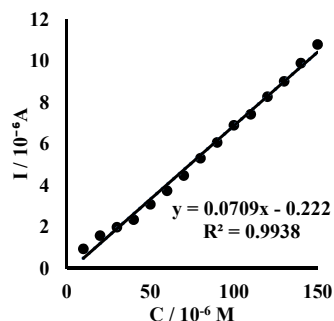


Figure 6.10: Calibration curve for Ua

6.2.4.4 Simultaneous determination

On *p*(ABSA)/GCE, an equimolar mixture of Ua, Gu and Ad showed well defined and well separated peaks whose peak currents increased with increase in concentration of the corresponding analytes (Fig.6.11). When determined simultaneously, the variation of peak current with concentration of Gu was linear in the range from 2.0×10^{-4} M to 1.0×10^{-5} M with a calculated LOD of 4.3×10^{-6} M with regression equation, $I (\mu\text{A}) = 0.120 C (\mu\text{M}) + 1.598$ [$R^2 = 0.993$]. For Ad, the linear relation, $I (\mu\text{A}) =$

$0.054 C (\mu\text{M}) + 1.067 [R^2 = 0.956]$ was observed in the range from $1.5 \times 10^{-4} \text{ M}$ to $2.0 \times 10^{-5} \text{ M}$ and gave a LOD of $1.1 \times 10^{-5} \text{ M}$. The peak current varied linearly with concentration for Ua in the range from $2.0 \times 10^{-4} \text{ M}$ to $2.0 \times 10^{-5} \text{ M}$ as per the equation, $I (\mu\text{A}) = 0.052 C (\mu\text{M}) - 0.453 [R^2 = 0.970]$, with a LOD $5.9 \times 10^{-6} \text{ M}$.

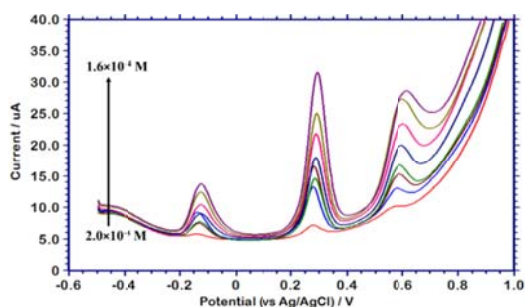


Figure 6.11: Overlay of SW voltammograms recorded in equimolar solutions of Ua, Gu and Ad on *p*(ABSA)/GCE in 0.1 M NaOH

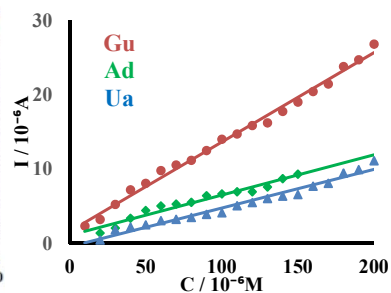


Figure 6.12: Variation of peak current with concentration of Ua, Gu and Ad on *p*(ABSA)/GCE

6.2.5 Mechanistic Studies

An insight into the mechanism of the electrochemical process can be obtained from LSV at different scan rates. Overlay of linear sweep voltammograms for $1.0 \times 10^{-4} \text{ M}$ concentrations of Gu, Ad and Ua in 0.1 M NaOH at various scan rates are represented in Fig. 6.13.

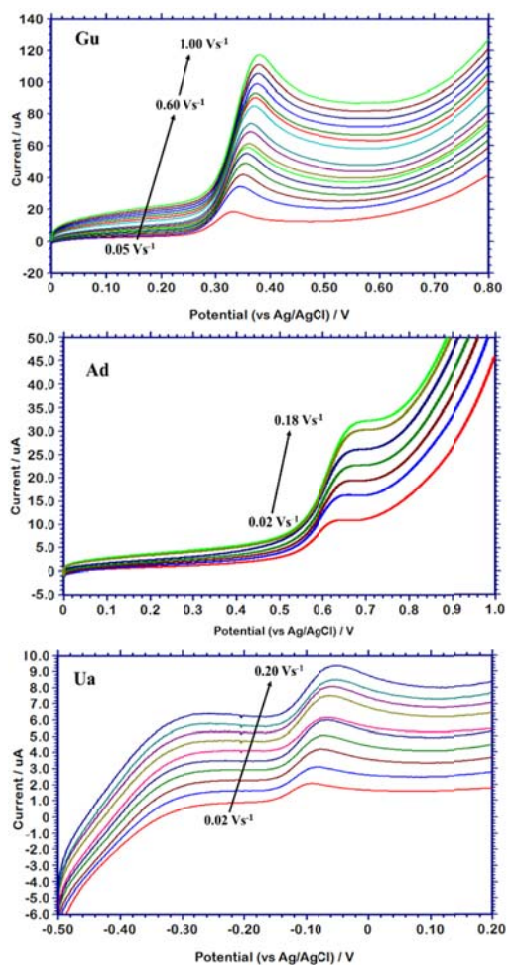


Figure 6.13: Linear sweep voltammograms for the oxidation of 1.0×10^{-3} M Gu, Ad and Ua in 0.1 M NaOH on the *p*(ABSA)/GCE at different scan rates

In table 6.2, the relation between the peak parameters and scan rate for each analyte is presented. It can be seen that for all the analytes the slope of the plot of $\log I$ vs $\log v$ is closer to the theoretical value of 0.5 expected for a diffusion controlled process. Hence it maybe concluded that the electro-oxidation of Ua, Gu and Ad on the *p*(ABSA)/GCE is controlled by diffusion of the species from the bulk to the electrode surface.

Table 6.2: Variation of peak parameters with scan rate

	E(V) vs ln v (Vs⁻¹)	log I (A) vs log v (Vs⁻¹)
Ua	E = 0.024 ln v – 0.009 [R² = 0.984]	log I = 0.417 log v – 5.210 [R² = 0.990]
Gu	E = 0.014 ln v + 0.389 [R² = 0.997]	log I = 0.393 log v – 3.957 [R² = 0.988]
Ad	E = 0.012 ln v + 0.657 [R² = 0.988]	log I = 0.508 log v – 4.166 [R² = 0.983]

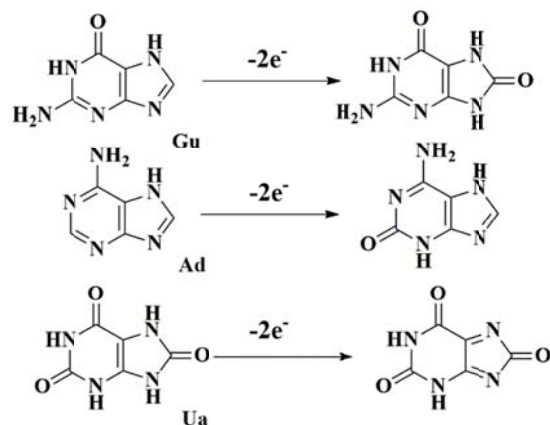
Slope of **E vs ln v** plot gives the value of $\frac{RT}{2(1-\alpha)n_{\alpha}F}$ and from the LSV at scan rate 0.1 Vs⁻¹, the value of peak potential **E** and half peak potential **E**_{1/2} being known, $\alpha n_{\alpha} = \frac{0.047}{E-E_{1/2}}$. Using these two equations, the values of the charge transfer coefficient **α** and **n_α**, the number of electrons involved in the rate determining step has been calculated (Table 6.3). The electro-oxidation of Gu, Ad and Ua on the *p*(ABSA)/GCE was found to proceed via a rate determining step involving two electrons each with **α** values 0.56, 0.52 and 0.66 respectively.

Table 6.3: Kinetic parameters for electro-oxidation

	(1 – α)n_α	αn_α	α	n_α[*]
Ua	0.521	1.06	0.66	2 (1.6)
Gu	0.930	1.19	0.56	2 (2.1)
Ad	1.052	1.13	0.52	2 (2.2)

**calculated value is shown in brackets*

The possible mechanism of the electro-oxidation reactions on the *p*(ABSA)/GCE consistent with these observations is represented in Scheme 6.1.



Scheme 6.1: Electro-oxidation of Gu, Ad and Ua [150,135]

6.2.6 Selectivity and Interferences

Selectivity is an important criterion for a sensor which denotes the efficiency with which it can determine a particular analyte from a mixture of analytes. To ascertain that *p*(ABSA)/GCE is selective, the determination of each of the analyte under study was carried out in the presence of a fixed concentration of the other (Fig. 6.14).

In presence of 7.0×10^{-5} M Gu and Ad, the relation $I (\mu A) = 0.215 C (\mu M) + 1.468$ [$R^2 = 0.987$] hold in the concentration range 1.0×10^{-5} M to 1.2×10^{-3} M for Ua. The lower LOD for Ua on the *p*(ABSA)/GCE in the presence of Gu and Ad was calculated to be 3.4×10^{-7} M. In the case of Gu, the peak current showed the relation, $I (\mu A) = 0.209 C (\mu M) + 2.176$ [$R^2 = 0.990$] with concentration in the range 2.0×10^{-5} M to 1.0×10^{-4} M and $I (\mu A) = 0.052 C (\mu M) + 14.88$ [$R^2 = 0.990$] in the range 1.5×10^{-4} M to 9.0×10^{-4} M with detection limit 2.4×10^{-6} M. For Ad, the relation, $I (\mu A) = 0.098 C (\mu M) + 1.182$ [$R^2 = 0.992$] in the range 1.0×10^{-5} M to 2.0×10^{-4} M with LOD

8.7×10^{-6} M. The sensitivities and detection limits are comparable with those obtained in individual determinations in the absence of other analytes indicating that the sensor is highly selective.

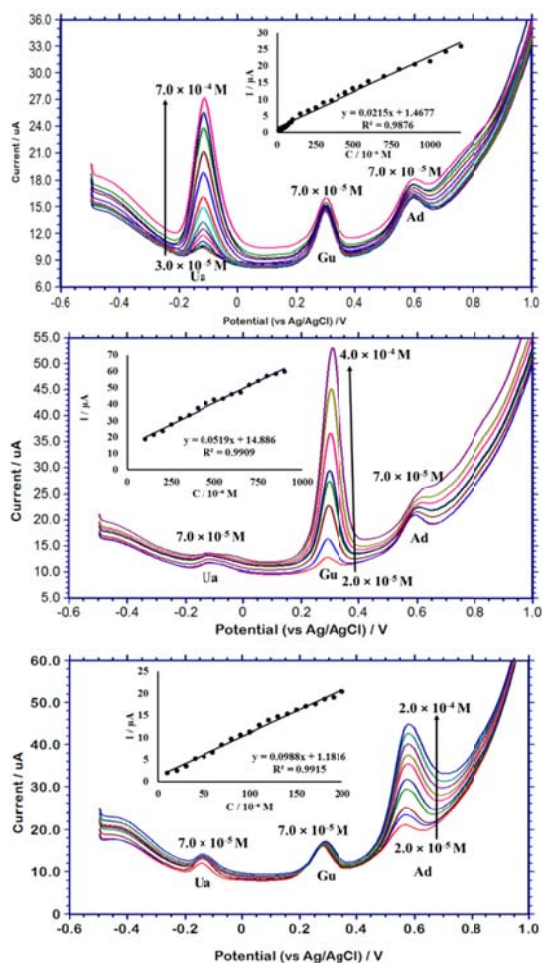


Figure 6.14: Variation of oxidation current with concentration for an analyte in presence of a specific concentration of the other two

The signal change produced by commonly co-existing species on the simultaneous signal of 2.0×10^{-5} M Ua, Gu and Ad on *p*(ABSA)/GCE is presented in Table 6.4. As can be observed from the data presented in the

table, the nucleic acid bases Cyt and Uracil did not interfere with the simultaneous determination in equimolar concentrations, where as a fivefold lower concentration of Thy produced a signal change above the tolerance limit (5%) for Ad. But Thy did not interfere with the determination of Ua and Gu even at tenfold excess concentration. Ascorbic acid interfered with the determination of Ad at fivefold lower concentrations and Ua at equimolar concentrations. Homovanillic acid produced a new peak at 0.152 V which interfered with the determination of Ad at fivefold lower concentration and with Gu only at tenfold excess concentration. Phosphate ion and dextrose sugar as well as ions like K^+ and Ca^{2+} did not interfere with the simultaneous determination even at tenfold higher concentrations.

Table 6.4: Interference Study

Species	Molar Ratio (analyte:species)	Signal change (%)		
		Gu	Ad	Ua
Cyt	1:1	Nil	-3.3	-0.8
Thy	5:1	-0.9	-5.4	-2.5
Uracil	1:1	-0.6	-4.8	-1.4
Homovanillic Acid	5:1	-2.2	-5.4	-4.6
Sucrose	1:1	Nil	-0.5	-0.7
Ascorbic Acid	5:1	+2.4	+2.3	+4.9
PO_4^{2-}	1:10	-0.7	-2.1	-2.9
K^+	1:10	-1.3	+0.9	-3.5
Ca^{2+}	1:1	+8.4	-1.3	-6.4

6.2.7 Application Studies

6.2.7.1 HS DNA

SW voltammogram of acid denatured DNA (prepared as described in section 2.7.4 of chapter 2) on *p*(ABSA)/GCE using 0.1 M NaOH as supporting electrolyte gave peaks at 0.288 V and 0.588 V corresponding to the oxidation of free Gu and Ad.

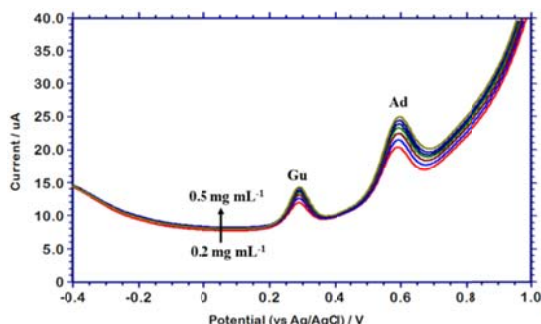


Figure 6.15: Overlay of SW voltammograms for various concentrations of DNA sample recorded on *p*(ABSA)/GCE using 0.1 M NaOH as supporting electrolyte

Using standard addition method, the percentages of Gu and Ad in HS DNA was found to be 24.7% and 31.4% respectively. The value of [(Gu+Cyt)/(Ad+Thy)] in acid denatured HS DNA determined by the developed sensor was found to be 0.786, which is comparable to the standard value of 0.770 for HS DNA [35] indicating that the sensor can be successfully applied to the determination of Gu and Ad in real samples.

A peak corresponding to the electro-oxidation of Ua was absent in the SW voltammogram indicating its absence in the sample. The acid denatured HS DNA was spiked with Ua and the determination was carried out and the results are presented in Table 6.5. Good recovery values were obtained pointing to the utility of the sensor for determination of Ua in real samples.

Table 6.5: Determination of Ua in spiked HS DNA

Sample	Ua		Recovery %	RSD %*
	Added (M)	Found (M)		
HS DNA (acid denatured)	1.0×10^{-4} - 1.0×10^{-5}	9.9×10^{-4} - 1.0×10^{-5}	100	4.2

*for 6 measurements

6.2.8 Kinetics of electro-oxidation of on *p*(ABSA)/GCE

6.2.8.1 Chronoamperometry

On stepping the working electrode to the oxidation potential, the decay of the faradaic current produced for each analyte is studied using chronoamperometry. Chronoamperograms were recorded at different concentrations, **C** and the corresponding **I vs t^{-1/2}** graphs were plotted for Ua, Gu (Fig. 6.16) and Cyt. As described in Chapter 3 (Section 3.2.9.1), making use of the Cottrell equation, the diffusion coefficient **D** was calculated for each analyte from the slope $\frac{d(I \text{ vs } t^{-1/2})}{dC}$. The highest value of **D** was obtained for Gu and the lowest value for Ua.

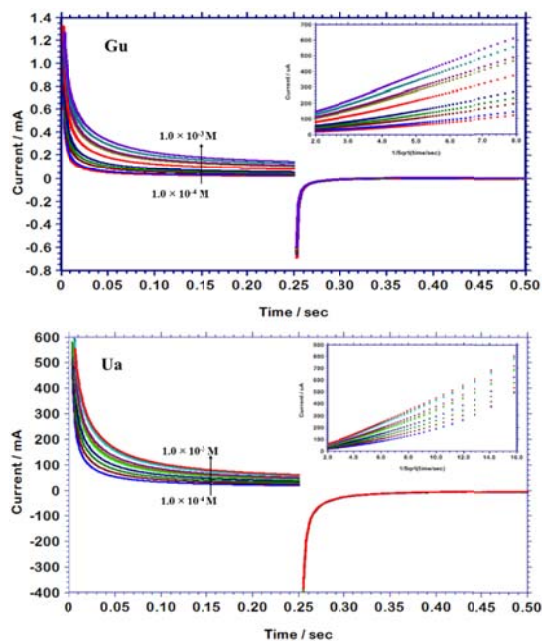


Figure 6.16: Chronoamperograms obtained for the oxidation of various concentrations of Gu and Ua on *p*(ABSA)/GCE with 0.1 M NaOH as supporting electrolyte. Inset of each chronoamperogram shows the corresponding plot of **I vs t^{-1/2}**

For Ad and Thy, the plot of $\frac{dI}{d(t^{-1/2})}$ against C , was not linear over a reasonable concentration range. Hence the slope of I vs $t^{-1/2}$ at 1.0×10^{-4} M concentration was directly used in the Cottrell equation and the diffusion coefficient was calculated.

The values obtained are presented in Table 6.6.

Table 6.6: Diffusion Coefficient

Analyte	D (cm ² s ⁻¹)	
	GCE	<i>p</i> (ABSA)/GCE
Gu	1.8×10^{-6}	7.6×10^{-5}
Ad	6.9×10^{-6}	1.9×10^{-5}
Thy	4.5×10^{-6}	2.4×10^{-5}
Cyt	6.6×10^{-5}	7.5×10^{-5}
Ua	2.9×10^{-7}	1.2×10^{-5}

The highest value of **D** is obtained for Gu and the lowest value for Ua. The order of magnitude of **D** was the same for all the analytes. Compared to the bare GCE, the diffusion coefficient for all the analytes is found to be increased when determined using *p*(ABSA)/GCE. For Gu, Ad and Thy, the diffusion coefficient is increased by an order of magnitude, whereas for Ua, there is an increase by two orders of magnitude. For Cyt, a prominent increase in diffusion coefficient is not observed. These observations indicate that the increase in surface area of the modified electrode alone is not the reason for increase in **D**. The electrostatic interaction between the functionalised electrode surface and the analyte should be contributing towards the change in **D** observed.

6.2.8.2 Heterogeneous rate constant

The standard heterogeneous rate constant for the irreversible oxidation of DNA bases on *p*(ABSA)/GCE was calculated by making use of the data extracted from scan rate studies in the LSV mode (Table 6.7).

Table 6.7: Kinetic studies

	Regression equation		$(1 - \alpha)n_\alpha$	αn_α	α	n_α^*
	E vs $\ln v$	E vs v				
Gu	$E = 0.014 \ln v + 0.389$	$E = 0.285 v + 0.330$	0.930	1.19	0.56	2 (2.1)
Ad	$E = 0.012 \ln v + 0.657$	$E = 0.131 v + 0.614$	1.052	1.13	0.52	2 (2.2)
Thy	$E = 0.016 \ln v + 0.791$	$E = 0.195 v + 0.736$	0.802	1.06	0.57	2 (1.8)
Cyt	$E = 0.018 \ln v + 0.898$	$E = 0.230 v + 0.834$	0.719	1.01	0.58	2 (1.7)
Ua	$E = 0.024 \ln v - 0.009$	$E = 0.228 v - 0.091$	0.521	1.06	0.66	2 (1.6)

*calculated value is shown in brackets

As described in previous chapters, Nicholson-Shain and Laviron models were used to determine the rate constants. The results obtained are consolidated in Table 6.8.

Table 6.8: Rate constants for electro-oxidation

	k_h (cm s^{-1})		k_s (s^{-1})	
	GCE	<i>p</i> (ABSA)/GCE	GCE	<i>p</i> (ABSA)/GCE
Gu	1.18×10^{-3}	1.35×10^{-2}	2.07	1.01
Ad	4.55×10^{-4}	1.01×10^{-2}	2.43	2.32
Thy	1.65×10^{-3}	9.60×10^{-3}	0.45	1.59
Cyt	6.31×10^{-3}	1.65×10^{-2}	0.37	1.30
Ua	3.33×10^{-4}	6.35×10^{-3}	0.40	1.37

The lowest value of standard heterogeneous rate constant for the Nicholson-Shain model was obtained for Ua and the highest value for Cyt. Considering only the DNA bases, the Nicholson-Shain rate constant values for all the DNA bases obtained on the *p*(ABSA)/GCE were comparable. The

trend in Nicholson-Shain rate constant was Thy > Ad > Gu > Cyt, even though the trend in diffusion coefficient was Gu > Cyt > Thy > Ad. The Laviron model too, gave comparable values for the rate constants measured on *p*(ABSA)/GCE. The maximum value was obtained for Ad and minimum for Gu following the trend Ad > Thy > Cyt > Gu.

On the *p*(ABSA)/GCE, the Nicholson-Shain rate constant for the electro-oxidation of Gu, Ad, Thy and Cyt has been found to be increased as compared to the bare GCE. The purine bases Gu and Ad showed a tenfold and twenty-fold increase in Nicholson-Shain rate constant whereas the pyrimidine bases Thy and Cyt showed a sixfold and threefold increase, respectively. For Gu, the Laviron surface reaction rate constant k_s was lowered to onehalf on the modified electrode whereas for Ad, the value of k_s on the bare and *p*(ABSA)/GCE were comparatively similar. In the case of Thy and Cyt, k_s obtained on *p*(ABSA)/GCE was 3.5 times higher than that observed on bare GCE.

These observation points to the predominance of diffusion kinetics in the case of Gu and Ad and electron transfer kinetics in the case of Thy and Cyt indicating a structure specific electrocatalysis by *p*(ABSA).

6.3 Conclusions

A voltammetric sensor for the simultaneous as well as individual determination of Gu, Ad and Ua was devised using a GCE modified with *p*(ABSA). These purine bases underwent electro-oxidation with lower overpotential and higher currents on the *p*(ABSA)/GCE in comparison with bare GCE. The optimum experimental parameters of the sensor were determined. On the developed sensor, good working linear ranges were

observed for simultaneous determination with calculated LODs 4.3×10^{-6} M, 1.1×10^{-5} M and 5.9×10^{-6} M respectively for Gu, Ad and Ua. The sensor has been proved useful for the simultaneous determination of Gu, Ad and Ua in acid denatured HS DNA. The mechanistic aspects of the electro-oxidation of DNA bases and Ua on *p*(ABSA)/GCE has been probed using LSV. Making use of the information obtained from LSV and chronoamperometric studies on the analytes the standard heterogeneous rate constants and surface reaction rate constants for the electro-oxidation of DNA bases and Ua on *p*(ABSA)/GCE were determined.

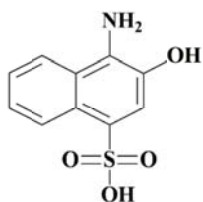
..... *SC*.....

Poly(4-amino-3-hydroxy naphthalene-1-sulfonic acid) modified Glassy Carbon Electrode as Sensor for Simultaneous determination of Guanine, Adenine, Cytosine and Uric acid as well as individual determination of Thymine

The development of a simple, easy to fabricate, selective and sensitive sensor for simultaneous determination of nucleic acid bases guanine, adenine and cytosine along with uric acid is described in this chapter. Glassy carbon electrode with an electropolymerised layer of 4-amino-3-hydroxy naphthalene-1-sulfonic acid could resolve the oxidation peaks of uric acid, guanine, adenine and cytosine using 0.1 M NaOH as supporting electrolyte. The electrocatalytic oxidation current was found to be linear in the range from $2.5 \times 10^{-4} M - 1.0 \times 10^{-5} M$ for uric acid, guanine and adenine and $2.5 \times 10^{-4} M - 8.0 \times 10^{-5} M$ for cytosine with detection limit $9.3 \times 10^{-6} M$, $9.3 \times 10^{-7} M$, $6.2 \times 10^{-6} M$ and $9.2 \times 10^{-6} M$ respectively for simultaneous determination by square wave voltammetry. For Thy, the variation of peak current was linear in the range from $1.5 \times 10^{-3} M - 1.0 \times 10^{-4}$ with limit of detection $1.7 \times 10^{-5} M$. The electrode processes were found to be diffusion controlled, which eliminate the fouling effect produced by adsorption of these organic compounds on the electrode surface. Application of developed sensor for the determination of these compounds in acid denatured herring sperm DNA as well as in body fluids such as urine and serum has been explained. The kinetics of electro-oxidation of DNA bases on the modified glassy carbon electrode has also been elucidated.

7.1 Introduction

4-amino-3-hydroxy-naphthalene 1-sulfonic acid (AHNSA), easily undergoes electropolymerisation, resulting in a polymer having special properties suitable for various applications.



4-amino-3-hydroxy-naphthalene 1-sulfonic acid

While the sulfonic acid groups increase the solubility of the polymer in polar solvents, the naphthalene nucleus confers hydrophobic nature to the polymer film [162].

Electropolymerisation of AHNSA and the sensing application of the resulting electropolymer modified electrode has been reported in literature.

Fabrication of *p*(AHNSA)/GCE for electrochemical detection of ephedrine in human urine has been reported by Amare, Lakew and Admassie. The *p*(AHNSA) was grown on GCE potentiodynamically by scanning the potential between -0.8 and 2.0 V at a scan rate of 0.1 Vs⁻¹ from a 2.0×10⁻³ M AHNSA solution in 0.1 M HNO₃ [163]. Amare and Admassie have also reported the application of the *p*(AHNSA)/GCE for the determination of caffeine in coffee [164] and theophylline [165]. Geto, Amare, Tessema and Admassie used *p*(AHNSA)/GCE fabricated by the same procedure for the determination of nicotine [111] and quinine in human urine and pharmaceutical formulations [166]. Multiwalled carbon nano-tubes were coated on *p*(AHNSA)/GCE and the resulting composite electrode was used for the determination of histamine in fish muscle by Geto, Tessema and Admassie [167].

Using the procedure reported by Geto, Amare, Tessema and Admassie [111], *p*(AHNSA)/GCE was fabricated and the voltammetric behaviour of DNA bases as well as Ua on the electrode was studied, in an effort to develop a sensor.

7.2 Results and discussion

GCE modified with *p*(AHNSA) was prepared and characterised as described in Chapter 2, section 2.5. The experimental conditions to obtain efficient electro-oxidation of DNA bases on the *p*(AHNSA)/GCE was determined at the onset.

7.2.1 Optimisation of experimental parameters

The electro-oxidation of the analytes under study was seen to be influenced by the supporting electrolyte used. The performance of the sensor was tested in 0.1 M concentration of various supporting electrolytes such as H₂SO₄, HNO₃, NaCl, KCl, ABS, CBS, PBS, NaOH and KOH. The electro-oxidations were observed at lowest potentials in NaOH and hence NaOH was chosen as the supporting electrolyte.

The current response on the *p*(AHNSA)/GCE fabricated by different cycles of polymerisation was noted (Fig.7.1).

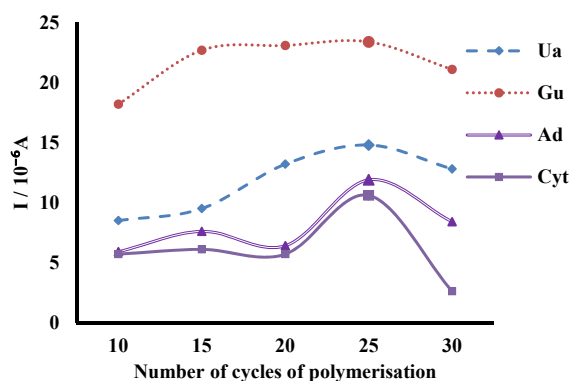


Figure 7.1: Variation of peak currents of 5.0×10^{-4} M Ua, Gu, Ad and Cyt in 0.1 M NaOH with number of cycles of polymerisation

For 5.0×10^{-4} M concentrations of Ua, Gu, Ad and Cyt, the best current response was observed with *p*(AHNSA)/GCE fabricated by 25

cycles of polymerisation. Hence 25 cycles of polymerisation were decided as optimum for the sensor.

7.2.2 Electrochemical behaviour of DNA bases on the *p*(AHNSA)/GCE

The electrocatalytic activity of *p*(AHNSA)/GCE towards oxidation of Ua, Gu, Ad and Cyt in 0.1 M NaOH was studied using SWV. For 5.0×10^{-5} M concentrations, electro-oxidation of Ua, Gu and Ad on bare GCE was observed at -0.080V, 0.348 V and 0.632 V respectively whereas for Thy and Cyt, the electro-oxidation/reduction peaks were not observed. On *p*(AHNSA)/GCE, oxidation peaks were observed at -0.130 V, 0.292 V, 0.596 V and 0.876 V corresponding to the oxidation of 5.0×10^{-5} M Ua, Gu, Ad and Cyt. Under the same conditions, for 1.0×10^{-4} M Thy oxidation peak appeared at 0.756 V. The overlay of SWV for simultaneous oxidation of Ua, Gu, Ad and Cyt on the bare and *p*(AHNSA)/GCE is shown in Fig. 7.2. It is evident from the figure that *p*(AHNSA) has an electrocatalytic effect on the electro-oxidation processes. There is a significant enhancement in peak current for all the analytes on the *p*(AHNSA)/GCE.

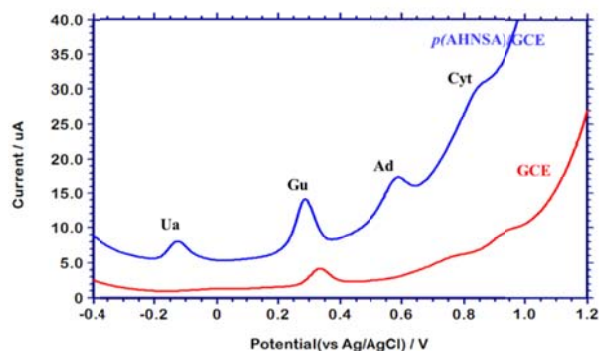


Figure 7.2: SW voltammogram for simultaneous oxidation of 5.0×10^{-5} M Ua, Gu, Ad and Cyt on *p*(AHNSA)/GCE and GCE

For 5.0×10^{-4} M concentration of Ua, Gu, Ad and Cyt, the EIS response is represented in Fig.7.3. The charge transfer resistance for the electro-oxidation of all the analytes has been found to decrease on the *p*(AHNSA)/GCE in comparison to the bare GCE (Table 7.1) i.e., on the *p*(AHNSA)/GCE, the electro-oxidation has become much easier. This points to electrocatalytic nature of the *p*(AHNSA) film present on the GCE surface.

Table 7.1: R_{ct} values fitted from Nyquist plots

	GCE ($10^5 \Omega$)	<i>p</i> (AHNSA)/GCE ($10^5 \Omega$)
Ua	1.780	0.190
Gu	7.580	5.590
Ad	0.262	0.096
Cyt	0.031	0.017

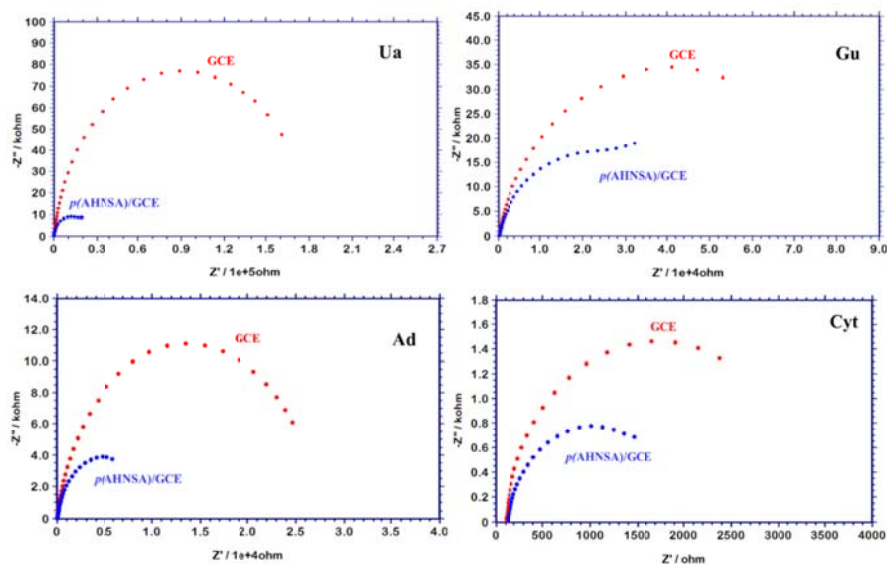


Figure 7.3: EIS Nyquist plots obtained for bare GCE and *p*(AHNSA)/GCE in 5.0×10^{-4} M Ua, Gu, Ad and Cyt in 0.1 M NaOH

7.2.3 Electro active surface area

Applying the approach described in chapter 3 (Section 3.2.4) the electro-active surface area of the bare and modified GCE was calculated. The variation of the redox peak currents of 2.0×10^{-3} M $\text{K}_3[\text{Fe}(\text{CN})_6]$ with scan rate was studied in the range 0.02 Vs^{-1} to 0.20 Vs^{-1} on GCE and $p(\text{AHNSA})/\text{GCE}$ (Fig. 7.4).

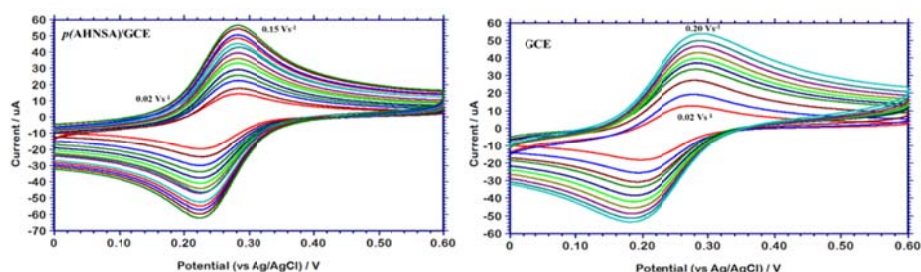


Figure 7.4: Overlay of cyclic voltammograms obtained for the oxidation of 2.0×10^{-3} M $\text{K}_3[\text{Fe}(\text{CN})_6]$ on $p(\text{AHNSA})/\text{GCE}$ and bare GCE at different scan rates

For GCE, $I(\text{A}) = 9.71 \times 10^{-5} \nu^{1/2} (\text{Vs}^{-1}) - 3.89 \times 10^{-6}$

For $p(\text{AHNSA})/\text{GCE}$, $I(\text{A}) = 1.58 \times 10^{-4} \nu^{1/2} (\text{Vs}^{-1}) + 5.20 \times 10^{-6}$

Making use of the Randles-Sevcik equation, the electroactive surface area of the bare GCE and $p(\text{AHNSA})/\text{GCE}$ are obtained as 0.066 cm^2 and 0.108 cm^2 respectively. Upon modification, there is a 64% increase in the electroactive surface area, indicating that the modified electrode has more active sites than the bare electrode which may be responsible for the electrocatalytic behaviour.

7.2.4 Calibration

The current response on the *p*(AHNSA)/GCE with concentration for the analytes was studied individually as well simultaneously. The concentration range over which the response is linear is determined in each case and the calibration graph plotted. The lower limit of detection was calculated statistically ($3S/m$ where *S* is the standard deviation of the lowest current response and *m* is the slope of the calibration graph).

7.2.4.1 Guanine

Overlay of SWV at different concentrations of Gu is shown in Fig. 7.5. The oxidation of Gu at the *p*(AHNSA)/GCE takes place at 0.292 V and as the concentration increases the peak current increases. The variation of peak current was linear in the range from 1.0×10^{-3} M to 2.5×10^{-4} M and from 1.0×10^{-4} M to 5.0×10^{-5} M with a lower LOD of 1.0×10^{-6} M (Fig.7.6).

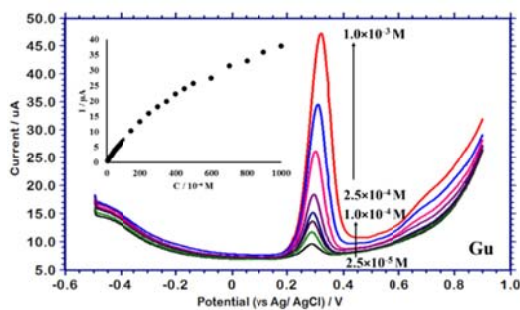


Figure 7.5: Overlay of SWV voltammograms of different concentrations of Gu on *p*(AHNSA)/GCE. Inset shows the variation of peak current with concentration

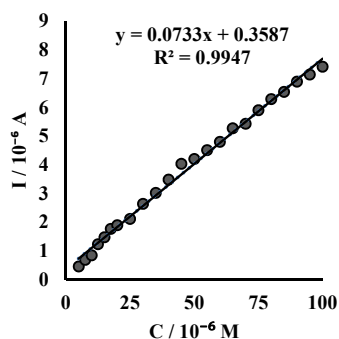


Figure 7.6: Calibration plot for Gu on *p*(AHNSA)/GCE

7.2.4.2 Adenine

Electro-oxidation of Ad on *p*(AHNSA)/GCE took place at 0.596 V, the peak current of which increased with increase in concentration of Ad (Fig. 7.7). Variation of oxidation current was linear in the range from 4.0×10^{-5} M to 8.0×10^{-6} M (Fig. 7.8). An upper linear range was also observed in the concentration range from 4.0×10^{-4} M to 7.5×10^{-5} M. The lower detection limit was calculated to be 2.3×10^{-6} M.

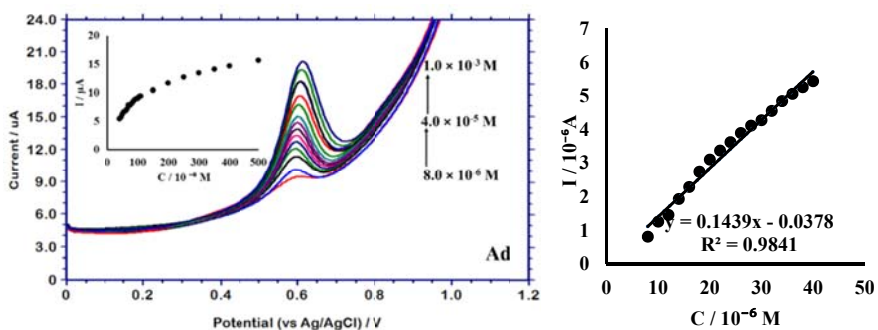


Figure 7.7: Overlay of SW voltammograms of different concentrations of Ad on *p*(AHNSA)/GCE. Inset shows the variation of peak current with concentration

Figure 7.8: Calibration plot for Ad on *p*(AHNSA)/GCE

7.2.4.3 Thymine

Thymine underwent electro-oxidation on the *p*(AHNSA)/GCE at 0.756 V and the peak current increased with concentration of Thy (Fig. 7.9). The variation was linear from 1.5×10^{-3} M to 2.0×10^{-4} M and from 2.0×10^{-4} M to 6.0×10^{-5} M (Fig. 7.10) with limit of detection 1.7×10^{-5} M.

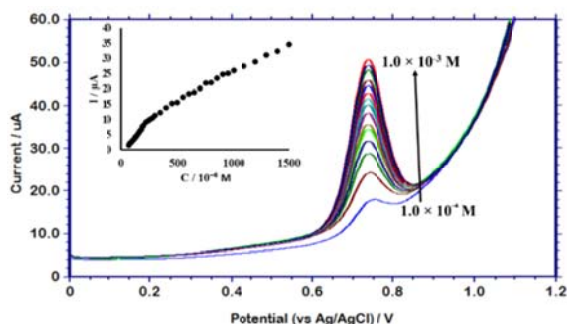


Figure 7.9: Overlay of SW voltammograms of different concentrations of Thy on *p*(AHNSA)/GCE. Inset shows the variation of peak current with concentration

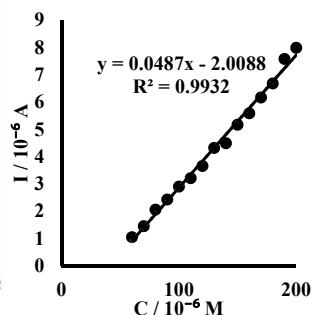


Figure 7.10: Calibration plot for Thy on *p*(AHNSA)/GCE

7.2.4.4 Cytosine

The pyrimidine base Cyt, underwent electro-oxidation at 0.896 V at the *p*(AHNSA)/GCE. The overlay of SWV for various concentrations of Cyt is shown in Fig. 7.11. As the concentration of Cyt increases, the peak current also increases linearly over a wide range from 5.0×10^{-3} M to 5.0×10^{-4} M and from 1.0×10^{-3} M to 6.0×10^{-5} M (Fig.7.12) with the lowest limit of detection being 1.5×10^{-6} M.

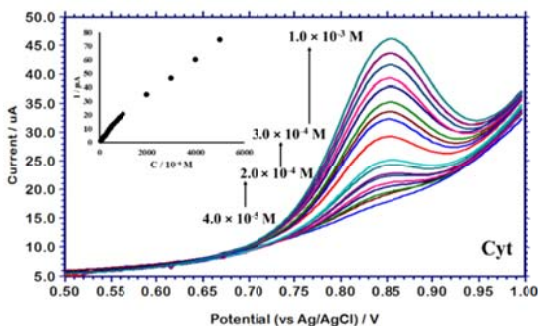


Figure 7.11: Overlay of SW voltammograms for the oxidation of Cyt on *p*(AHNSA)/GCE. Inset shows the variation of peak current with concentration

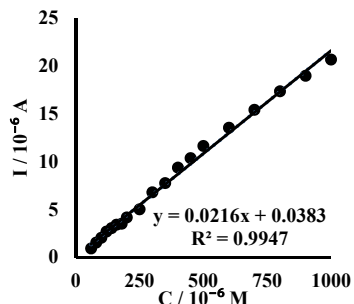


Figure 7.12: Calibration plot for Cyt on *p*(AHNSA)/GCE

7.2.4.5 Uric Acid

Fig. 7.13 shows the overlay of SW voltammograms at different concentrations of Ua. The electro-oxidation peak of Ua appears at -0.130 V and its peak current varies with concentration of Ua. The variation of peak current with concentration of Ua was found to be linear in the range from 5.0×10^{-3} M to 5.0×10^{-4} M and from 2.0×10^{-4} M to 1.0×10^{-5} M (Fig. 7.14) with the calculated value of LOD being 8.1×10^{-6} M.

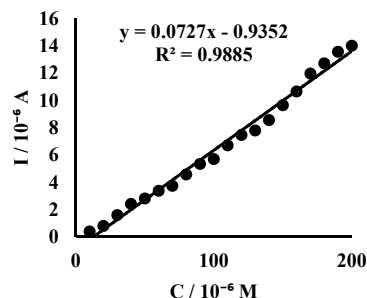
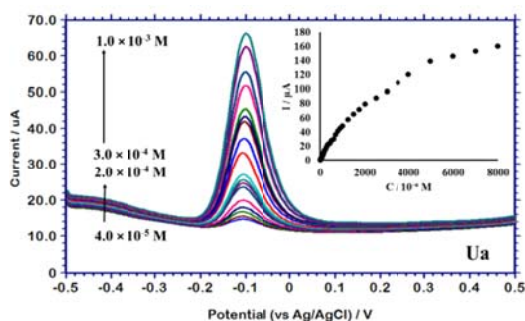


Figure 7.13: Overlay of SW voltammograms of different concentrations of Ua on *p*(AHNSA)/GCE. Inset shows the variation of peak current with concentration

Figure 7.14: Calibration plot for Ua on *p*(AHNSA)/GCE

7.2.4.6 Simultaneous determination

The simultaneous determination of Ua, Gu, Ad and Cyt on the optimised *p*(AHNSA)/GCE gave well resolved peaks corresponding to the oxidation of the analytes. The overlay of SW voltammograms for the simultaneous electro-oxidation of various concentrations of analytes are shown in Fig. 7.15 and the variation of peak current with concentration of analyte in Fig. 7.16.

For Ua, a linear relation, $I (\mu\text{A}) = 0.046 C (\mu\text{M}) + 1.385$ [$R^2 = 0.992$] was observed in the concentration range 2.5×10^{-3} M to 1.0×10^{-5} M

with the LOD being 9.3×10^{-6} M when determined simultaneously. For simultaneous determination, Gu and Ad, similar to Ua showed the linear range 2.5×10^{-3} M to 1.0×10^{-5} M. The variation of oxidation current with concentration of Gu showed the relation, $I (\mu\text{A}) = 0.109 C (\mu\text{M}) + 2.667$ [$R^2 = 0.996$] with LOD 9.3×10^{-7} M. Whereas, for Ad, the regression equation was $I (\mu\text{A}) = 0.053 C (\mu\text{M}) + 1.889$ [$R^2 = 0.994$] and LOD 6.2×10^{-6} M. For Cyt, the current response was linear over the concentration range 2.5×10^{-4} M to 8.0×10^{-5} M, $I (\mu\text{A}) = 0.035 C (\mu\text{M}) + 1.862$ [$R^2 = 0.986$], giving a detection limit of 9.2×10^{-6} M.

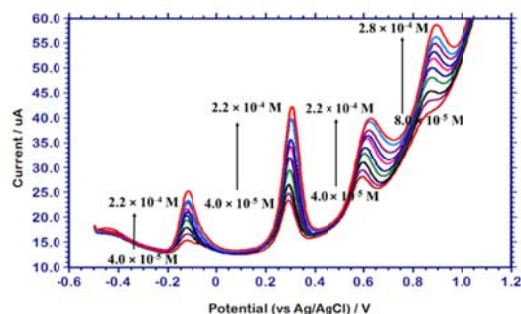


Figure 7.15: Overlay of SW voltammograms recorded in equimolar solutions of Ua, Gu, Ad and Cyt using *p*(AHNSA)/GCE

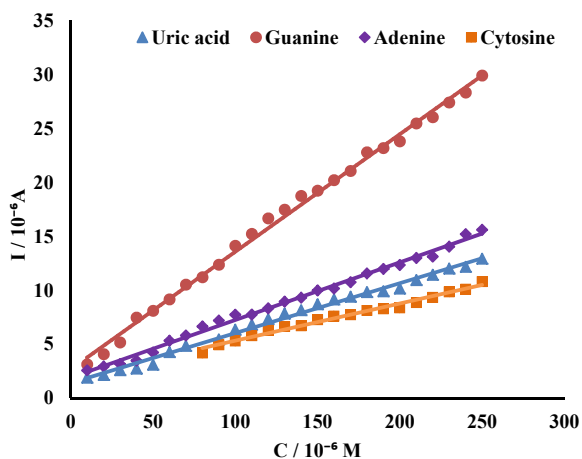


Figure 7.16: Calibration plot for the simultaneous determination of Ua, Gu, Ad and Cyt on *p*(AHNSA)/GCE

Table 7.2: Analytical Parameters

	Sensitivity (AM^{-1})		Lowest Linear range (M)				LOD (M)					
	Ind	Ind *	Sim	Ind	Ind *	Sim	Ind	Ind *				
Ua	0.0512	0.0472	0.0463	1.0×10^{-3}	-1.0×10^{-5}	1.3×10^{-4}	-1.0×10^{-5}	2.5×10^{-4}	-1.0×10^{-5}	8.08	8.93	9.31
Gu	0.0733	0.1648	0.1090	1.0×10^{-4}	-5.0×10^{-5}	1.0×10^{-4}	-1.0×10^{-5}	2.5×10^{-4}	-1.0×10^{-5}	1.40	0.62	0.93
Ad	0.1469	0.0773	0.0535	4.0×10^{-5}	-8.0×10^{-6}	1.4×10^{-4}	-2.0×10^{-5}	2.5×10^{-4}	-1.0×10^{-5}	2.27	4.31	6.24
Cyt	0.0216	0.0232	0.0345	1.0×10^{-3}	-6.0×10^{-5}	2.0×10^{-3}	-5.0×10^{-5}	2.5×10^{-4}	-8.0×10^{-5}	14.70	14.69	9.20

Ind – Individual, Ind* - Individual in presence of other three, Sim - simultaneous

The effect of possibly co-existing or chemically similar species on the peak currents of Ua, Gu, Ad and Cyt was studied at various analyte : species ratios (Table 7.3). Thy and Uracil, other pyrimidine bases produced peaks at 0.756 V and 0.984 V on *p*(AHNSA)/GCE, causing distortion of the peak due to Cyt at tenfold excess concentrations. But did not produce interference in the determination of Ua, Gu and Ad. At tenfold lower concentration of Thy and Uracil did not interfere in the determination of any of the analytes. Barbituric acid which oxidised at 0.712 V on the *p*(AHNSA)/GCE did not interfere with the determinations at fifty-fold excess but produced signal change for Ad and Cyt at hundred-fold excess concentration. Other species like ascorbic acid, sucrose, PO₄²⁻, Cl⁻, K⁺, Ca²⁺ did not cause any signal change for Ua, Gu, Ad or Cyt at equimolar concentrations. Homovanillic acid interfered with the determination of Gu, causing a peak distortion at equimolar concentrations, even though it did not interfere with the determination of Ua, Ad or Cyt at tenfold excess.

Table 7.3: Interference study

Species	Molar Ratio	Signal change (%)			
		Gu	Ad	Cyt	Ua
Thymine	1:10	-0.9	-1.4	Peak distortion	-1.1
Uracil	1:10	-0.6	-4.8	Peak distortion	-1.4
Barbituric Acid	1:100	-0.9	-2.2	Peak distortion	-0.9
Homovanillic Acid	1:10	Peak distortion	-1.0	-1.1	-2.2
Sucrose	1:10	-0.6	-1.1	-0.1	-1.3
Ascorbic Acid	1:1	+2.4	+2.3	-1.1	+4.9
PO ₄ ²⁻	1:10	-0.7	-2.1	-2.1	-2.9
K ⁺	1:1	-1.3	+0.9	-0.5	-3.5
Ca ²⁺	1:1	+4.4	-1.3	-2.2	-3.4

7.2.6 Application Studies

7.2.6.1 HS DNA

p(AHNSA)/GCE was used for the determination of nucleobases in acid denatured HS DNA (Chapter 2, section 2.7.4). In acid-denatured HS DNA only two peaks corresponding to those of standard Gu and Ad was observed. The peaks corresponding to Ua and Cyt were not obtained in the prepared DNA sample. Applying standard addition method, the percentage of Gu and Ad in HS DNA was found to be 23.1% and 28.6% respectively. The Chargaff ratio $[(\text{Gu}+\text{Cyt})/(\text{Ad}+\text{Thy})]$ was found to be 0.80 which is very close to the theoretical value of 0.77 expected for HS DNA [35].

The peaks corresponding to oxidation of Ua and Cyt were not observed in HS DNA. Hence the DNA solution was spiked with Ua and Cyt and Ua, Gu, Ad and Cyt was determined simultaneously. The results are compiled in Table 7.4. Good recoveries were obtained for Ua. But for Cyt, the recoveries were higher. A possible reason maybe that even though Cyt was not initially detected in DNA, it was originally present in the sample. Brett et al., [9] had reported that the determination of pyrimidine bases in DNA was difficult when the ratio of purines to pyrimidines is greater than 10. The determination of Gu and Ad in the DNA spiked with Ua and Cyt also gave the value of 0.80 for $[(\text{Gu}+\text{Cyt})/(\text{Ad}+\text{Thy})]$.

7.2.6.2 Synthetic Urine and Serum

Simultaneous determination of Ua, Gu, Ad and Cyt was also conducted in spiked synthetic urine and serum (Section 2.7.7 and section 2.7.8 of chapter 2). Good recoveries were obtained in the case of both synthetic urine and serum pointing to the potential application of the sensor in physiological fluids. R. S. D values of the measurements for six replicate measurements of each was also well within the acceptable limits.

Table 7.4: Application studies

Sample	Analyte	Added (M)	Found (M)	Recovery (%)	RSD (%)
H S DNA	Gu	-	1.01×10^{-5}	-	0.5
	Ad	-	1.25×10^{-5}	-	1.8
	Cyt	$2.25 \times 10^{-4} - 1.00 \times 10^{-4}$	$3.66 \times 10^{-4} - 1.58 \times 10^{-4}$	160	3.0
	Ua	$1.25 \times 10^{-4} - 1.50 \times 10^{-5}$	$1.25 \times 10^{-4} - 1.47 \times 10^{-5}$	99	1.4
Urine	Gu	$1.25 \times 10^{-4} - 1.50 \times 10^{-5}$	$1.25 \times 10^{-4} - 1.49 \times 10^{-5}$	100	0.5
	Ad	$1.25 \times 10^{-4} - 1.50 \times 10^{-5}$	$1.23 \times 10^{-4} - 1.50 \times 10^{-5}$	98	2.3
	Cyt	$2.25 \times 10^{-4} - 1.00 \times 10^{-5}$	$2.24 \times 10^{-4} - 1.02 \times 10^{-5}$	100	3.2
	Ua	$1.25 \times 10^{-4} - 1.50 \times 10^{-5}$	$1.24 \times 10^{-4} - 1.51 \times 10^{-5}$	99	2.1
Serum	Gu	$1.25 \times 10^{-4} - 1.50 \times 10^{-5}$	$1.25 \times 10^{-4} - 1.52 \times 10^{-5}$	100	0.7
	Ad	$1.25 \times 10^{-4} - 1.50 \times 10^{-5}$	$1.26 \times 10^{-4} - 1.54 \times 10^{-5}$	101	2.7
	Cyt	$2.25 \times 10^{-4} - 1.00 \times 10^{-5}$	$2.25 \times 10^{-4} - 9.95 \times 10^{-6}$	100	1.4
	Ua	$1.25 \times 10^{-4} - 1.50 \times 10^{-5}$	$1.26 \times 10^{-4} - 1.52 \times 10^{-5}$	100	2.0

7.2.7 Repeatability, reproducibility and stability

Determination of oxidation currents of 1.0×10^{-4} M concentrations of Ua, Gu, Ad and Cyt was carried out five times consecutively using the same *p*(AHNSA)/GCE. RSD for the measurements were found to be 1.3%, 0.5%, 2.0% and 2.8% for Ua, Gu, Ad and Cyt respectively, indicating that measurements made on *p*(AHNSA)/GCE are repeatable. The measurement of peak currents of Ua, Gu, Ad and Cyt in a solution containing 1.0×10^{-4} M concentration of each were carried out on five different *p*(AHNSA)/GCE prepared by the same procedure. For Ua, Gu, Ad and Cyt, the RSD values for measurements were obtained as 1.7%, 0.5%, 1.9% and 3.1% respectively pointing to the reproducibility of the sensor. Further, after 10 days of its preparation, the measurement of oxidation current of 1.0×10^{-4} M concentrations of Ua, Gu, Ad and Cyt using the *p*(AHNSA)/GCE gave result with RSD values of 1.4%, 0.7%, 2.1% and 3.4% respectively. Thus, it can be safely assumed that the developed sensor is stable.

7.2.8 Mechanistic Studies

The effect of scan rate on the peak parameters for the electro-oxidation of 1.0×10^{-4} M concentrations of Ua, Gu, Ad, Thy and Cyt was studied using LSV. Overlay of the linear sweep voltammograms of Gu, Ad, Thy and Cyt are shown in Fig. 7.18 and that of Ua in Fig. 7.19.

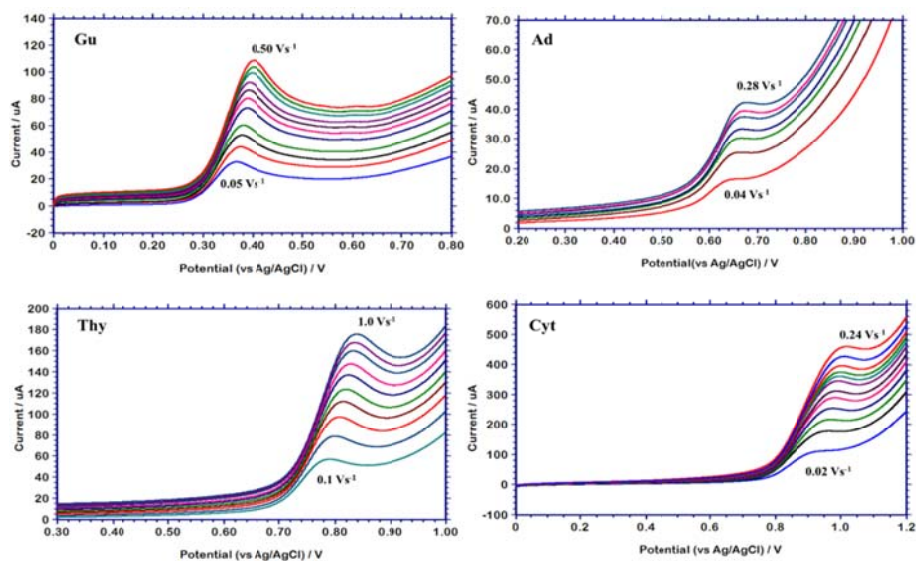


Figure 7.18: Linear sweep voltammograms of 1.0×10^{-3} M concentrations of Gu, Ad, Thy and Cyt on *p*(AHNSA)/GCE at different scan rates

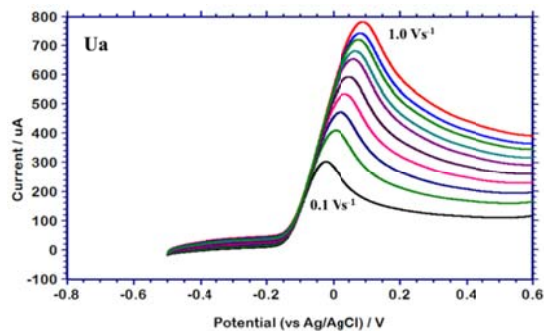


Figure 7.19: Overlay of linear sweep voltammograms of 1.0×10^{-3} M Ua on *p*(AHNSA)/GCE at different scan rates

Table 7.5: Variation of peak parameters with scan rate

	E(V) vs ln v (Vs⁻¹)	log I (A) vs log v (Vs⁻¹)
Ua	E = 0.046 ln v + 0.081 [R ² = 0.991]	log I = 0.406 log v - 3.138 [R ² = 0.993]
Gu	E = 0.012 ln v + 0.403 [R ² = 0.973]	log I = 0.442 log v - 3.912 [R ² = 0.996]
Ad	E = 0.019 ln v + 0.766 [R ² = 0.996]	log I = 0.443 log v - 4.331 [R ² = 0.998]
Thy	E = 0.012 ln v + 0.819 [R ² = 0.995]	log I = 0.461 log v - 3.873 [R ² = 0.997]
Cyt	E = 0.021 ln v + 1.031 [R ² = 0.969]	log I = 0.404 log v - 3.399 [R ² = 0.992]

The obtained variation of peak parameters with scan rate for each of the analytes are presented in Table 7.5

The plot of **log I vs log v** gave slopes of 0.41, 0.44, 0.44, 0.46 and 0.40 respectively for Ua, Gu, Ad, Thy and Cyt, which are closer to the theoretical value of 0.50 expected of a diffusion controlled electrochemical process [131]. This confirms that all the electrode processes are diffusion controlled. The peak potential shifted to more positive values with scan rate pointing to the irreversibility of all the five electrode processes [13].

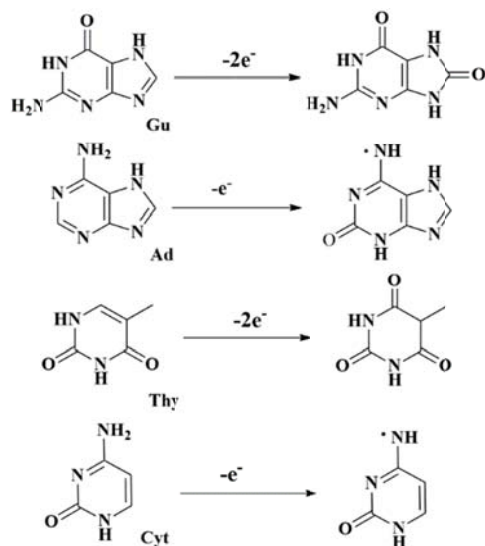
The slope of the plot **E vs ln v** for an irreversible diffusion controlled reaction is given by $\frac{RT}{2(1-\alpha)n_{\alpha}F}$ where α is the charge transfer coefficient. The relation between, the peak potential and **E_{1/2}**, the half peak potential as given by Bard and Faulkner is $E - E_{1/2} = \frac{0.047}{\alpha n_{\alpha}}$. Combining these two relations, the value of α and n_{α} has been calculated for Ua, Gu, Ad, Thy and Cyt and the values are presented in Table 7.6.

Table 7.6: Kinetic parameters for electro-oxidation

	$(1 - \alpha)n_{\alpha}$	αn_{α}	α	n_{α}^*
Ua	0.283	0.645	0.65	1(0.98)
Gu	0.985	0.917	0.48	2(1.90)
Ad	0.652	0.367	0.36	1(1.01)
Thy	1.087	0.837	0.44	2(1.92)
Cyt	0.597	0.391	0.40	1(0.98)

*calculated value is shown in brackets

The results obtained indicate that on the *p*(AHNSA)/GCE, Ua, Ad and Cyt undergoes one electron oxidation, whereas the oxidation of Gu and Thy involves transfer of 2 electrons each. Such electro-oxidation of Ad [135] Gu, Thy and Cyt [150] has been reported in literature. The one electron oxidation of Ua though rare has been reported [169]. The possible electro-oxidation of Gu, Ad and Cyt on *p*(AHNSA)/GCE is shown in Scheme 7.1.

**Scheme 7.1.** Electro-oxidation of Gu, Ad, Thy and Cyt on *p*(AHNSA)/GCE

7.2.9 Kinetics of electro-oxidation on p(AHNSA)/GCE

7.2.9.1 Chronoamperometry

Decay of the faradaic current produced by the electrochemical event, with time was recorded by chronoamperometry and used to determine the diffusion coefficient. In accordance with Cottrell equation, the current **I** varied linearly with $t^{-1/2}$ for Gu, Ad, Thy, Cyt (Fig. 7.20) and Ua (Fig. 7.21). The variation of current **I** with $t^{-1/2}$ was studied in the concentration range 1.0×10^{-3} M to 1.0×10^{-4} M for Ua, Gu, Ad and Thy, and in the range 2.0×10^{-3} M to 2.0×10^{-4} M for Cyt.

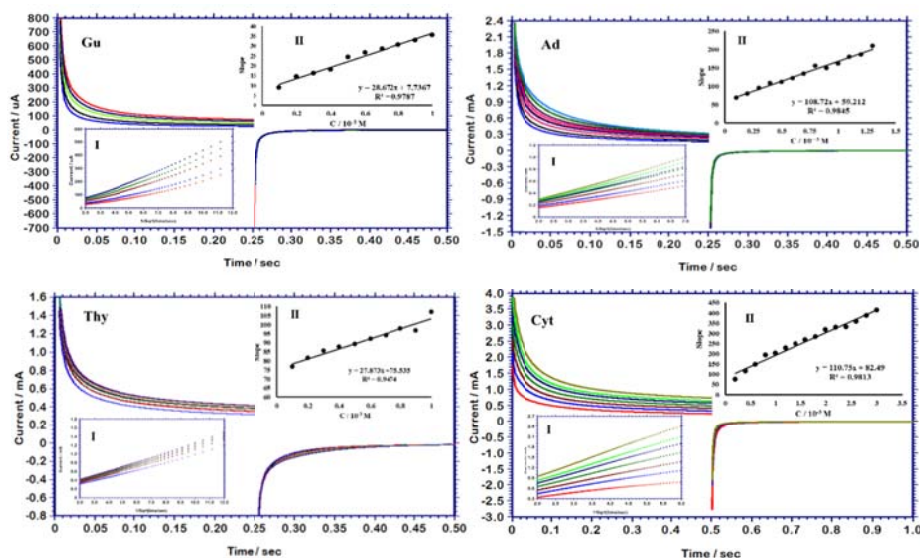


Figure 7.20: Overlay of chronoamperograms obtained for various concentrations of Gu, Ad, Thy and Cyt. Inset I) of each overlay shows the corresponding I vs $t^{-1/2}$ plots and Inset II) shows the plot of $\frac{dI}{dt^{-1/2}}$ vs C

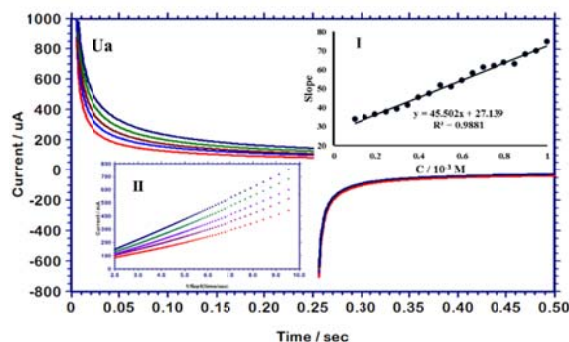


Figure 7.21: Overlay of chronoamperograms obtained for various concentrations of Ua. Inset I) shows the corresponding **I** vs $t^{-1/2}$ plot and Inset II) shows the plot of $\frac{dI}{dt^{-1/2}}$ vs **C**

By the use of Cottrell equation, as explained in chapter 3 (Section 3.2.9.1), the diffusion coefficients were calculated, and the values obtained are presented in Table 7.7.

Table 7.7: Calculated values of diffusion coefficients

Analyte	D (cm² s⁻¹)	
	GCE	p(AHNSA)/GCE
Gu	1.8×10^{-6}	6.15×10^{-6}
Ad	6.9×10^{-6}	3.51×10^{-4}
Thy	4.5×10^{-6}	5.77×10^{-6}
Cyt	6.6×10^{-5}	3.47×10^{-4}
Ua	2.9×10^{-7}	6.11×10^{-5}

On p(AHNSA)/GCE, the highest value of diffusion coefficient was obtained for Ad and the lowest value for Thy, following the order Ad > Cyt > Ua > Gu > Thy, with Ad and Cyt as well as Gu and Thy giving comparable values of **D**. Compared to the bare GCE, there is an increase in **D** for all the analytes under study. For Gu, the value of **D** obtained on the p(AHNSA)/GCE is 3.5 times the value obtained on bare GCE whereas for Ad, a fifty-fold increase is observed on the p(AHNSA)/GCE. The value of

D for Thy on the bare and *p*(AHNSA)/GCE were comparable and that for Cyt was 5 times higher on the modified electrode than the bare GCE. The highest increase in **D** was observed for Ua which showed a 200 times enhancement in **D**. Such changes in the value of **D** points to the presence of structure specific electrostatic interaction between the modified electrode and the analytes.

7.2.9.2 Heterogeneous rate constant

The standard heterogeneous rate constant for the electro-oxidation on *p*(AHNSA)/GCE was calculated from the data obtained from LSV at different scan rates. By the use of Nicholson-Shain equation,

$$E = E^0 + \frac{RT}{(1-\alpha)nF} \left[0.78 - \ln \frac{k_h}{D^{1/2}} + \frac{1}{2} \ln \frac{(1-\alpha)nFv}{RT} \right]$$

and the Laviron equation,

$$E = E^0 + \frac{RT}{(1-\alpha)nF} \left[\ln \frac{(1-\alpha)nF}{RTk_s} + \ln v \right]$$

as described in previous chapters, the values of k_h and k_s for the electro-oxidation processes taking place at the electrode were calculated and the values are presented in Table 7.8.

Table 7.8: Rate constants for electro-oxidation

	k_h (cm s^{-1})		k_s (s^{-1})	
	GCE	<i>p</i> (AHNSA)/GCE	GCE	<i>p</i> (AHNSA)/GCE
Gu	1.18×10^{-3}	4.25×10^{-3}	2.43	1.25
Ad	4.55×10^{-4}	7.09×10^{-2}	2.07	6.03
Thy	1.65×10^{-3}	4.38×10^{-3}	0.45	1.41
Cyt	6.31×10^{-3}	5.38×10^{-2}	0.37	0.29
Ua	3.33×10^{-4}	1.59×10^{-2}	0.40	1.76

The Nicholson-Shain rate constants for the electro-oxidation on *p*(AHNSA)/GCE follow the trend, Ad > Cyt > Ua > Thy > Gu, whereas Laviron rate constant show the trend, Ad > Ua > Thy > Gu > Cyt. Ad gave the highest value of both Nicholson-Shain and Laviron rate constants. For Ad, both diffusion kinetics and electron transfer kinetics has improved on the *p*(AHNSA)/GCE. Thy, whose diffusion coefficient was not significantly changed on the *p*(AHNSA)/GCE, showed an increase in both k_h and k_s pointing to the predominance of electron transfer kinetics over diffusion kinetics. Gu and Cyt showed a decrease in k_s and increase in k_h on the modified electrode indicating that diffusion kinetics predominated electron transfer kinetics. These facts point to the possibility of a species specific electrocatalysis by the *p*(AHNSA).

7.3 Conclusions

The simultaneous resolution of voltammetric signals of Ua, Gu, Ad and Cyt is achieved on AHNSA modified GCE. Well defined and well resolved peaks were obtained for the electro-oxidation of these compounds on the *p*(AHNSA)/GCE under optimised experimental conditions. The electrocatalytic oxidation on the proposed sensor was found to be diffusion controlled, thereby eliminating the fouling of electrode response due to adsorption of these bases on the electrode surface. The developed sensor was found to give stable, reproducible and reliable results even in the presence of other chemical species. The sensor gave comparable sensitivities for simultaneous as well as individual determination of these compounds. Further, the applicability of the sensor for simultaneous determination of the nucleic acid bases in HS DNA, synthetic urine and synthetic serum has been established.

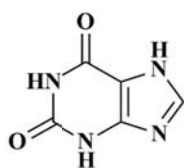
Chronoamperometry and LSV were used to extract information regarding the kinetics of the electro-oxidation processes. The highest value of diffusion coefficient was obtained for Ad. Among the DNA bases, the maximum value of Nicholson-Shain rate constant as well as Laviron rate constant was obtained for Ad.

..... ❧.....

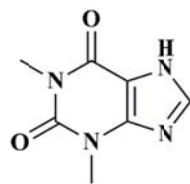
— Poly(para Amino Benzene Sulfonic Acid) modified Glassy Carbon Electrode as Sensor for Simultaneous Determination of Xanthine, Theophylline and Caffeine along with uric acid

Xanthine and its methyl derivatives, theophylline and caffeine are purines which have important roles in biological systems. The simultaneous voltammetric behaviour of these purines has been studied on a glassy carbon electrode modified with an electropolymerised film of para amino benzene sulfonic acid. Well defined and well separated peaks were obtained for the oxidation of xanthine, theophylline and caffeine on the polymer modified electrode in the square wave mode. The experimental requirements to obtain the best results for individual as well as simultaneous determination were optimised. The signal for the electro-oxidation was found to be free of interferences from each other in the range $1.0 \times 10^{-4} M - 9.0 \times 10^{-7} M$, in the case of xanthine; from $1.0 \times 10^{-4} M - 1.0 \times 10^{-5} M$, in the case of theophylline and from $1.0 \times 10^{-4} M - 6.0 \times 10^{-5} M$ for caffeine with detection limits $3.5 \times 10^{-7} M$, $7.0 \times 10^{-6} M$ and $1.1 \times 10^{-6} M$ respectively. The simultaneous determination of uric acid, the final metabolic product of xanthine oxidation in biological systems could also be accomplished along with xanthine, theophylline and caffeine at physiological pH. The mechanistic aspects of the electro-oxidation on the polymer modified electrode was studied using linear sweep voltammetry. Chronoamperometry was employed to determine the diffusion coefficient of these xanthines. The standard heterogeneous rate constants for electro-oxidation of xanthine, theophylline and caffeine on the developed sensor has been determined. The developed sensor has been demonstrated to be suitable for the determination of these compounds in real samples without much pre-treatment.

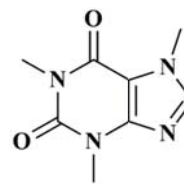
8.1 Introduction



Xanthine



Theophylline



Caffeine

Xanthine (XT) or 3,7-dihydropurine-2,6-dione is a vital compound in biological systems, as it is an intermediate in the metabolism of the purines, Ad and Gu to Ua [170]. Typically, the concentration of XT in blood is 100 times lower than that of Ua, while in urine; it is 10000 times lower than that of Ua [171]. Presence of abnormal levels of XT in serum and urine has been identified as a risk marker for conditions such as xanthinuria, perinatal asphyxia, acute hypoxia stress, cerebral ischemia, Lesch-Nyhan syndrome, gout etc. [171, 172]. XT levels in fish and meat products also serve as an indicator for freshness of these products [173]. XT along with its methyl derivatives, theophylline (TP), theobromine, theacrine and caffeine (CF) has been reported to be present in many food products namely tea, coffee, cocoa beans and chocolate [174].

Theophylline (TP) is the dimethyl derivative of XT whereas caffeine (CF) is the trimethyl derivative. TP is 3,7-dihydro-1,3-dimethyl-1H-purine-2,6-dione and CF is 3,7-dihydro-1,3,7-trimethyl-1H-purine-2,6-dione. These two methyl xanthines are identified with marked physiological effects [170]. Both TP and CF are reported to have diuretic, cardiac stimulant and smooth muscle relaxant effects [175, 176]. CF is also known to promote secretion of gastric juice and ease the effects of migraine [176] and is frequently added to energy drinks and other similar beverages. TP in the range 2–10 mg mL⁻¹ in blood plasma is known to have therapeutic action in the treatment of

asthma and chronic pulmonary diseases [177], whereas higher levels lead to toxicity ranging from tachycardia to even death [178]. The therapeutic action of CF is predominant when its level is below 15 mg L^{-1} . However daily intake of CF above 2.5 mg per kg of body weight can result in hyperactivity, cardiovascular diseases, depression as well as complications in pregnant women [179]. Hence the determination of these purines is of importance from pharmaceutical, clinical diagnostic and food analysis point of view.

Several methods have been reported for the determination of these xanthines, such as chromatography [174, 180, 181], fluorimetry [182] and spectrophotometry [183] as well as electrochemical (EC) methods. Electrochemical methods for XT determination are mostly based on biosensors which immobilize xanthine oxidase on its surface which converts XT to Ua and hydrogen peroxide which results in the analytical signal [171]. Such enzymatic electrochemical sensors are not very effective in making specific determination, due to its low specificity among various xanthine derivatives [184]. They are also expensive, requires complicated fabrication steps and offer low stability and sensitivity. Non-enzymatic EC sensors, on the other hand are comparatively less expensive, simple, stable and offer sensitive, selective and simultaneous determination [172]. There have been several reports of the simultaneous non -enzymatic determination of different xanthines on various chemically modified electrodes.

Literature reports of non-enzymatic electrochemical XT sensors largely report detection of hypoxanthine or uric acid simultaneously with XT. A. S. Kumar and R. Shanmugham made use of a GCE modified with multiwalled carbon nanotubes for the simultaneous determination of Ua, XT

and hypoxanthine in fish samples [185]. Simultaneous determination of Ua, XT and hypoxanthine in poly(bromocresol purple) modified GCE was proposed by Wang and Tong [186]. Large mesoporous carbon modified GCE has been demonstrated to be useful for the simultaneous determination of Ua, XT and hypoxanthine by Liu et al [172]. Highly sensitive electrochemical sensor for the simultaneous determination of Ua, XT and hypoxanthine has been proposed by Ojani et al., based on poly(L-methionine) modified GCE [187]. Ua, XT, hypoxanthine and CF were simultaneously determined in human blood serum and urine was reported by Amal Raj and Abrahan John using electrochemically reduced graphene oxide modified electrode [188]. Luo and co-workers [189] have reported sulfonic groups functionalized nitrogen-doped graphene modified GCE for the simultaneous determination of Ua, XT and hypoxanthine. The developed sensor showed wide linear ranges of 2 orders of magnitude and low detection limits. An ultrasensitive electrochemical sensor for simultaneous determination of XT, hypoxanthine and Ua based on Co doped CeO₂ nanoparticles has been reported by Lavanya et al. [190].

Individual determination of TP has been reported on multi walled carbon nanotube modified GCE [191]; *p*(AHNSA)/GCE [165]; CdSe microparticle modified GCE [192]; gold nanoparticle/L-cysteine/graphene/Nafion modified GCE [175]; manganese oxide nanoparticle/ionic liquid/chitosan composite modified GCE [193], multiwalled carbon nano tube paste electrode [194]. Electrochemical sensors for the determination of CF has been extensively reviewed by Švorc [195]. Individual determination of CF has been reported on Nafion modified electrodes [196-198]; Nafion–ruthenium oxide pyrochlore chemically modified electrode [199]; *p*(AHNSA)/GCE [164]; poly(safraninT)/Nafion

modified GCE [200]; Graphene modified GCE [201,202]; poly(ortho amino phenol) molecularly imprinted GCE [203]; DNA-functionalized single-walled carbon nanotube modified GCE [204] etc.

Even though reports for the determination of TP and CF along with other compounds are plenty, reports for simultaneous determination of TP along with CP is few. Gao and co-workers have reported the simultaneous determination of TP and CF on large mesoporous carbon and Nafion modified GCE [205]. Simultaneous determination of TP and CF on anisotropic gold nanoparticle–chitosan–ionic liquid/graphene modified GCE has been reported by Yang et al. [206]. The only report of simultaneous voltammetric determination of XT, TP and CF is on unmodified boron doped diamond electrode [170].

To the best of our knowledge simultaneous voltammetric determination of XT, TP and CF on GCE modified with benzene sulfonic acid has not been reported before.

8.2 Results and discussion

The modification of GCE with *p*(ABSA) was performed as described in Section 2.4.1 of chapter 2 and characterised by SEM imaging and EIS measurements (Section 2.4.2). The performance of the prepared electrode towards electro-oxidation of XT, TP and CF was optimised.

8.2.1 Optimisation of experimental parameters

8.2.1.1 Supporting electrolyte

The electro-oxidation of XT, TP and CF on *p*(ABSA)/GCE was studied in 0.1 M solutions of various supporting electrolytes such as perchloric acid, CBS, ABS, BR buffer, sodium chloride, PBS and sodium

hydroxide. The lowest oxidation potential and highest peak current for electro oxidation was obtained with BR buffer for individual determination of TP and CF, but the oxidation of TP and CF took place at very close potentials thus making simultaneous determination difficult in BR buffer. Well defined and well separated peaks for simultaneous determination was obtained in PBS. Hence 0.1 M PBS was selected as the supporting electrolyte.

8.2.1.2 pH of the supporting electrolyte

The variation of electro-oxidation peak parameters with pH of PBS was studied in the range from 3-9. The peak potential (**E**) varied according to the following equations.

$$\text{For XT; } \mathbf{E(V) = 1.093 - 0.064 \text{ pH}}$$

$$\text{For TP; } \mathbf{E(V) = 1.365 - 0.056 \text{ pH}}$$

$$\text{For CF, } \mathbf{E(V) = 1.315 + 0.038 \text{ pH}}$$

In the case of XT and TP, the peak potential shifted negatively with pH and the peak current showed a decrease with increase in pH. In the case of CF, the potential did not show a significant change with pH of the medium and **E** showed a positive shift [189] unlike in the case of XT and TP, the best peak separation for the simultaneous determination of XT, TP and CF was obtained with pH 7 and hence pH 7 was chosen as the optimum pH for the simultaneous determination.

8.2.1.3 Number of cycles of polymerisation

The thickness of the polymer film on the surface of the electrode is governed by the number of cycles of electropolymerisation. The optimum

number of cycles of polymerisation which formed the polymer film giving the best response for the simultaneous electro-oxidation of 1.0×10^{-5} M XT, TP and CF in 0.1 M PBS of pH 7 was determined to be 20 cycles. All further studies were carried out in 0.1 M PBS using the *p*(ABSA)/GCE fabricated by 20 cycles of electro-polymerisation.

8.2.2 Electrochemical response for XT, TP and CF on *p*(ABSA)/GCE

The SW voltammetric oxidation of 5.0×10^{-5} M XT, TP and CF in 0.1 M PBS pH 7, on the bare GCE took place at 0.656 V, 0.964 V and 1.328 V respectively. In 0.1 M PBS pH 7, the *p*(ABSA)/GCE shows a small background current in the SWV mode. On addition of 5.0×10^{-5} M each of XT, TP and CF peaks appear at 0.640 V, 0.952 V and 1.332 V with peak currents 7.8×10^{-6} A, 1.8×10^{-6} A and 1.1×10^{-6} A corresponding to the oxidation of XT, TP and CF respectively. The overlay of SW voltammograms obtained on the bare GCE and *p*(ABSA)/GCE is shown in Fig.8.1. From the figure, it is clear that there is a pronounced enhancement in peak current on the *p*(ABSA)/GCE for all the three electrooxidation process pointing to the electrocatalytic effect of the *p*(ABSA) film.

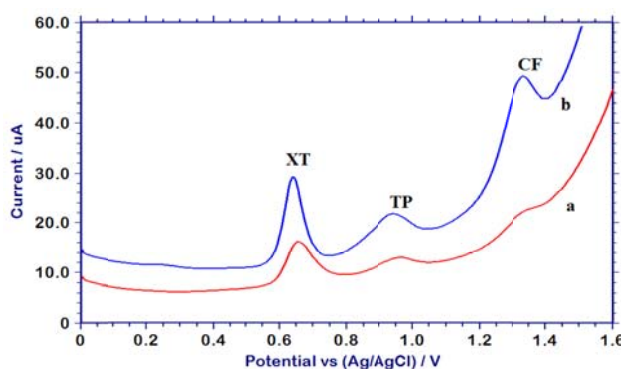


Figure 8.1: SW voltammograms for the oxidation of 5.0×10^{-5} M XT, TP and CF on (a) bare GCE and (b) *p*(ABSA)/GCE (0.1 M PBS pH 7)

The cyclic voltammogram of each analyte did not show any peak in the reverse scan indicating that the electro-oxidation of XT, TP and CF are irreversible.

The Nyquist plots for the bare GCE and *p*(ABSA)/GCE in 5.0×10^{-5} M solution of each analyte in 0.1 M PBS pH 7 is shown in Fig.8.2. The Nyquist plots were recorded in the frequency range 1.0×10^{-1} to 1.0×10^4 Hz at a potential of 0.75 V for XT; 1.0×10^{-1} to 1.0×10^4 Hz at a potential of 1.05 V for TP and 1.0 to 1.0×10^5 Hz at a potential of 1.5 V for CF.

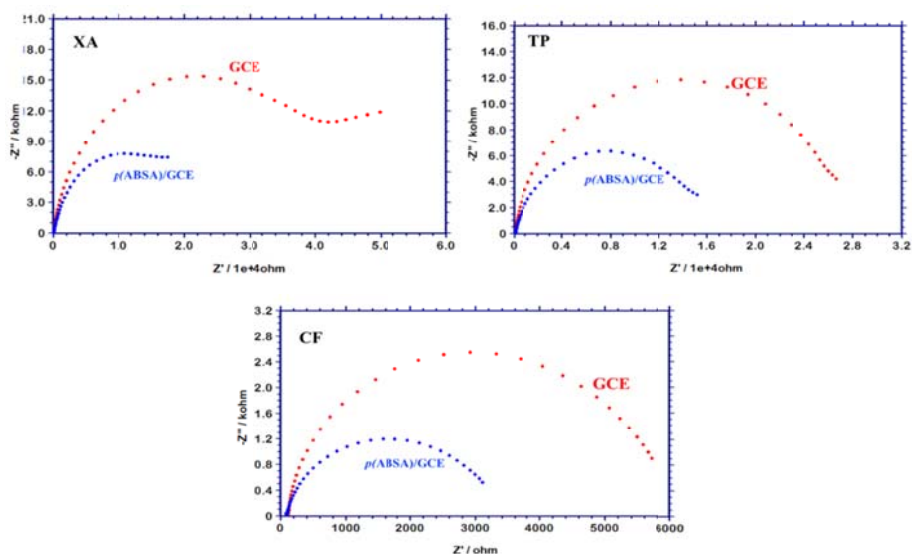


Figure 8.2: Nyquist plots obtained on bare and modified GCE for 5.0×10^{-4} M concentrations of XT, TP and CF (0.1 M PBS pH 7)

The charge transfer resistance, R_{ct} values fitted from the equivalent Randles-Ershler circuit using the ZSimpWin software is given in Table 8.1. For all the three analytes, the R_{ct} values have decreased on the *p*(ABSA)/GCE compared to the bare GCE. The electrostatic interaction between the conducting polymer film and the purine bases may result in an

electrocatalytic effect [207] on electro-oxidation which in turn may be the reason for decrease in charge transfer resistance.

Table 8.1: R_{ct} values fitted from Nyquist plots

	GCE (Ω)	<i>p</i> (ABSA)/GCE (Ω)	Change in R_{ct} (Ω)
XT	3.60×10^{-4}	1.78×10^{-4}	1.82×10^{-4}
TP	2.55×10^{-4}	1.50×10^{-4}	1.05×10^{-4}
CF	5.60×10^{-3}	3.00×10^{-3}	2.60×10^{-3}

8.2.3 Electro active surface area

Variation of cyclic voltammetric peak currents of 2.0×10^{-3} M $K_3[Fe(CN)_6]$ in 0.1 M KNO_3 with cyclic scan rate was used to determine the electro-active surface area of *p*(ABSA)/GCE, as described in Section 3.2.4 of chapter 3.

For bare GCE, $I(A) = 9.72 \times 10^{-5} v^{1/2}(Vs^{-1}) - 3.89 \times 10^{-7}$

For *p*(ABSA)/GCE (20 cycles), $I(A) = 1.38 \times 10^{-4} v^{1/2}(Vs^{-1}) - 1.28 \times 10^{-5}$

By making use of the Randles-Sevcik equation, the electro-active surface area of the bare GCE and *p*(ABSA)/GCE fabricated by 20 cycles of polymerisation was found to be 0.066 cm^2 and 0.095 cm^2 respectively. The 44% enhancement in the effective surface area of the GCE on modification combined with the electrostatic affinity of the purine bases for the sulfonic acid group of the modifier on the electrode surface maybe the result for the enhancement in peak current observed for the electro-oxidation.

8.2.4 Calibration

The SW voltammetric response of XT, TP and CF at various concentrations was recorded using the *p*(ABSA)/GCE. The concentration

range over which the peak current was linear was determined. The slope (**m**) of the calibration graph in the linear concentration range was used to determine the detection limit ($3S/m$, **S** being the standard deviation of the lowest measurement). The calibration was carried out for both individual as well as simultaneous determination.

8.2.4.1 Xanthine

The voltammetric peak at 0.640 V corresponding to the electro-oxidation of XT showed an increase in peak current with increase in concentration of XT (Fig. 8.3). The current response was found to be linear in the range from 5.0×10^{-4} M to 1.0×10^{-3} M with a regression equation, $I (\mu\text{A}) = 0.094C (\mu\text{M}) + 30.281$ [$R^2 = 0.981$] and from 1.0×10^{-4} M to 9.0×10^{-7} M with linear regression equation, $I (\mu\text{A}) = 0.371C (\mu\text{M}) + 1.358$ [$R^2 = 0.986$] (Fig. 8.4). The LOD for the determination of XT was found to be 2.8×10^{-7} M.

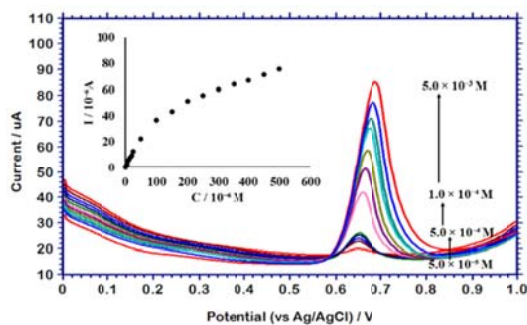


Figure 8.3: SW voltammograms for the oxidation of different concentrations of XT on *p*(ABSA)/GCE (0.1 M PBS pH 7). Inset shows variation of anodic peak current with concentration

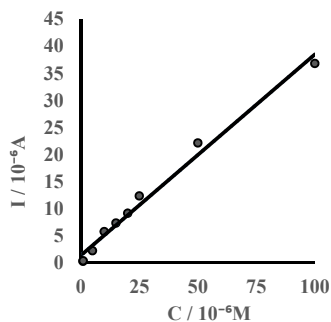


Figure 8.4: Calibration plot for XT in the lower linear range

8.2.4.2 Theophylline

For TP, the oxidation peak appeared at 0.952 V whose peak current increased with increase in concentration of TP. (Fig. 8.5). The variation of peak current was linear in the range from 3.0×10^{-4} M to 2.5×10^{-6} M (Fig. 8.6) with a regression equation, $I (\mu\text{A}) = 0.290 C (\mu\text{M}) - 1.323$ [$R^2 = 0.991$] and LOD was calculated to be 2.3×10^{-6} M.

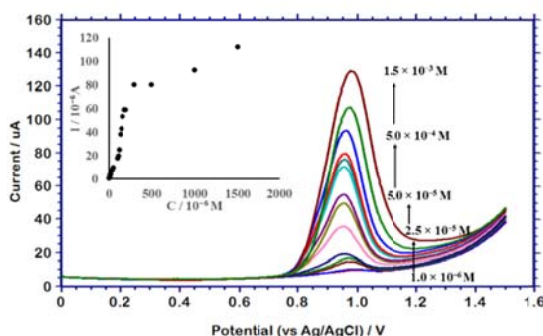


Figure 8.5: SW voltammograms for the oxidation of different concentrations of TP on *p*(ABSA)/GCE (0.1 M PBS pH 7). Inset shows variation of anodic peak current with concentration

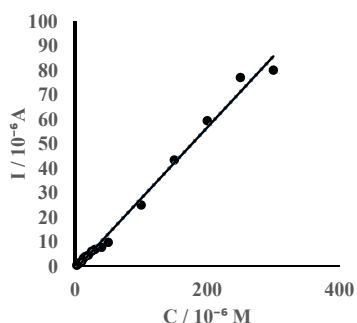


Figure 8.6: Calibration plot for TP

8.2.4.3 Caffeine

In the case of CF, electro-oxidation took place at 1.332 V on *p*(ABSA)/GCE. Overlay of SW voltammograms obtained for the oxidation of various concentrations of CF under the optimised experimental conditions is shown in Fig. 8.7. The linear regression equation, $I (\mu\text{A}) = 0.115 C (\mu\text{M}) - 1.386$ [$R^2 = 0.992$] was obtained in the range from 2.0×10^{-4} M to 2.0×10^{-5} M (Fig. 8.8) and the LOD for CF determination was obtained to be 5.6×10^{-6} M.

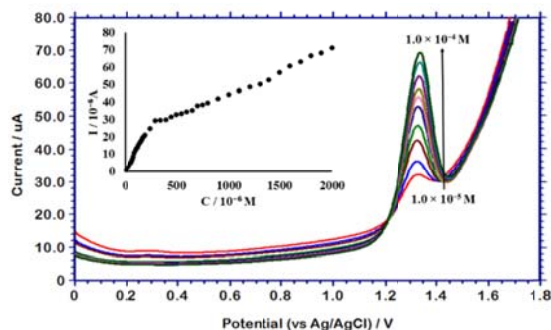


Figure 8.7: SW voltammograms for the oxidation of different concentrations of CF on *p*(ABSA)/GCE (0.1 M PBS pH 7). Inset shows variation of anodic peak current with concentration

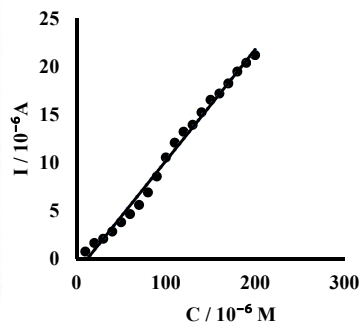


Figure 8.8: Calibration plot for CF

8.2.4.4 Simultaneous determination of XT, TP and CF

The simultaneous oxidation of XT, TP and CF on the *p*(ABSA)/GCE was studied in the range from 1.0×10^{-4} M to 1.0×10^{-6} M. The overlay of SW voltammograms obtained for the simultaneous oxidation of 2.0×10^{-5} M to 2.0×10^{-6} M concentrations of XT and 2.0×10^{-4} M to 2.0×10^{-5} M concentrations of TP and CF is shown in Fig. 8.9.

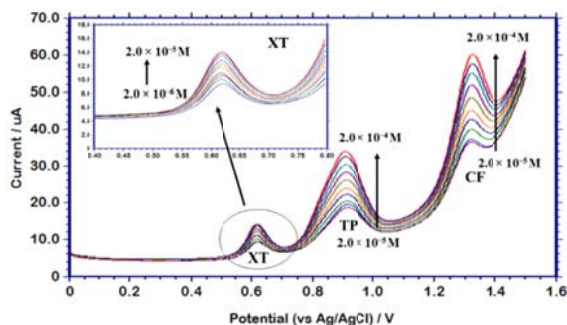


Figure 8.9: Overlay of SW voltammograms for the simultaneous electro-oxidation of XT, TP and CF in 0.1 M PBS pH 7 on the *p*(ABSA)/GCE at various concentrations. Inset shows the magnification of the overlay of SWV for the electro-oxidation of XT

The variation in peak current for the simultaneous determination was found to be linear from 1.5×10^{-5} M to 3.0×10^{-6} M for XT (Fig. 8.10) and from 1.5×10^{-4} M to 1.0×10^{-5} M for TP and 1.5×10^{-4} M to 6.0×10^{-5} M for CF (Fig. 8.11) on *p*(ABSA)/GCE. The LOD obtained for simultaneous determination was 3.5×10^{-7} M for XT, 7.0×10^{-6} M for TP and 1.1×10^{-5} M for CF.

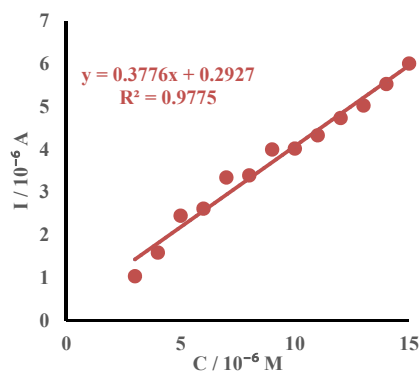


Figure 8.10: Calibration plot for XT when determined simultaneously with TP and CF

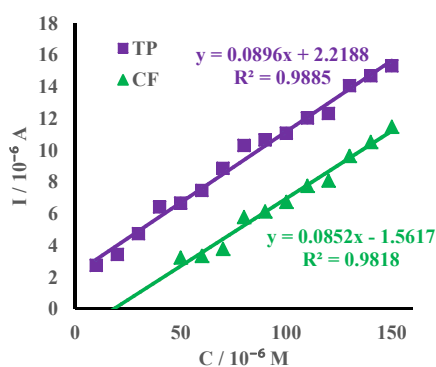


Figure 8.11: Calibration plot for TP and CF when determined simultaneously with XT

8.2.5 Selectivity and interferences

To check the selectivity of the sensor for the determination of the compounds under investigation, individual determination of XT, TP and CF was conducted in the presence of a definite concentration of the other two. The overlay of SW voltammograms obtained for the electro-oxidation of different concentrations of XT, TP and CF in presence of 5.0×10^{-5} M concentrations of the other two is shown in Figure 8.12.

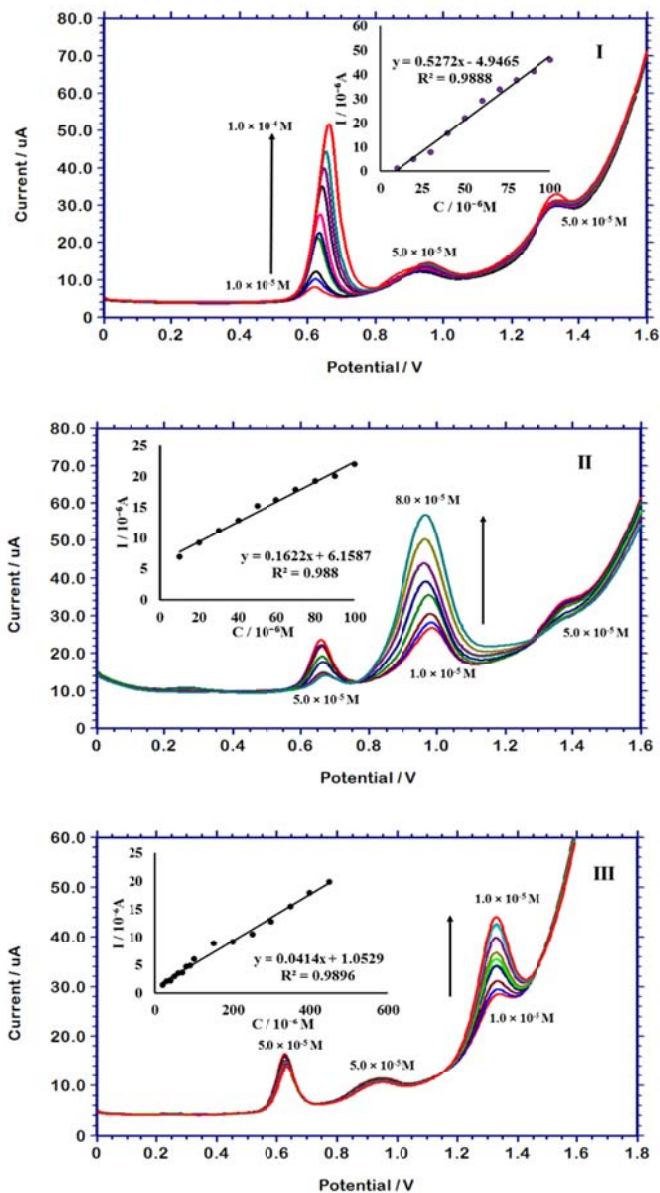


Figure 8.12: Overlay of SW voltammograms for the oxidation of various concentrations of XT(I), TP (II) and CF (III) in presence of $5.0 \times 10^{-5}\text{M}$ concentrations of the other two. Inset of each graph shows the corresponding calibration plot

In the presence of 5.0×10^{-5} M concentrations of the other two, the SW voltammetric current response for XT, TP and CF was studied in the range from 1.0×10^{-3} M to 1.0×10^{-5} M. For XT and TP, the response was found to be linear in the range from 1.0×10^{-4} M to 1.0×10^{-5} M with a LOD of 6.4×10^{-7} M and 4.1×10^{-6} M respectively, whereas for CF, the current response was linear from 4.5×10^{-4} M to 2.0×10^{-5} M with LOD of 6.4×10^{-6} M.

Ua is the final degradation product of purine metabolism and may be present together with these purines in biological samples. Under the optimum performance conditions, on the *p*(ABSA)/GCE, the oxidation of Ua gave a peak at 0.240 V with a peak current of 1.5×10^{-6} A. A peak separation of 0.380 V with XT, 0.740 V with TP and 1.08 V with CF indicates that the simultaneous determination of Ua, XT, TP and CF was possible. The determination of Ua could be accomplished together with XT, TP and CF (Fig. 8.13) on the *p*(ABSA)/GCE with a linear range of 8.0×10^{-5} M to 1.0×10^{-5} M (Fig. 8.14) with detection limit of 1.0×10^{-7} M. In presence of Ua, the current response for XT, TP and CF was linear over the range 1.0×10^{-5} M to 1.0×10^{-4} M with detection limits, 1.9×10^{-7} M, 1.4×10^{-6} M and 6.4×10^{-6} M respectively.

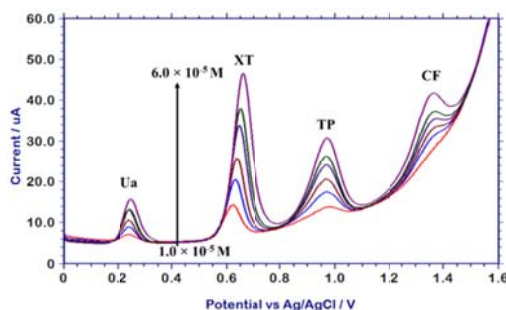


Figure 8.13: Overlay of SW voltammograms obtained on the *p*(ABSA)/GCE, for the oxidation of various equimolar solutions of Ua, XT, TP and CF in 0.1 M PBS pH 7

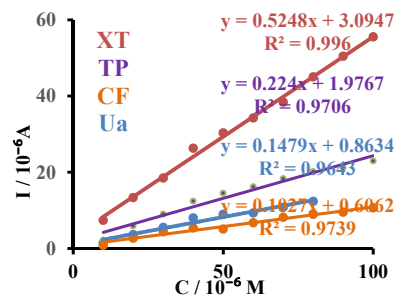


Figure 8.14: Calibration plot for the simultaneous determination of Ua, XT, TP and CF

The individual determination of Ua was also conducted on the *p*(ABSA)/GCE (Fig. 8.15) which gave a linear range of 1.0×10^{-4} M to 1.0×10^{-5} M and LOD of 2.9×10^{-8} M (Fig. 8.16)

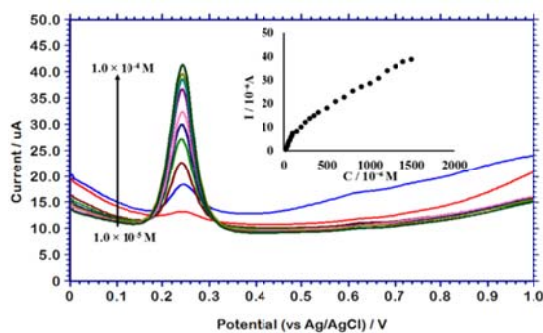


Figure 8.15: SW voltammograms for the oxidation of different concentrations of Ua in 0.1 M PBS pH 7, on *p*(ABSA)/GCE. Inset shows variation of anodic peak current with concentration

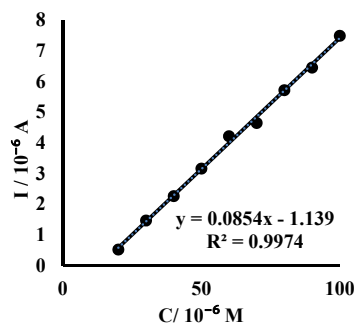


Figure 8.16: Calibration plot for Ua

Effect of other purines like Ad, Gu and hypoxanthine on the SW voltammetric signal of 1.0×10^{-4} M concentration of XT, TP and CF was studied. Ad did not interfere with the signal for XT and CF even when present in fifty-fold excess concentration. But for TP the presence of Ad caused an increase in signal by 70% when present in the same concentration, thereby making selective determination not possible. Interference produced by fifty-fold excess concentration of Gu on the SW voltammetric signal of TP and CF was well within the tolerance limit but for XT, the presence of 1:1 concentration of Gu caused an increase in peak current by 86%. Electro-oxidation of hypoxanthine on the *p*(ABSA)/GCE was observed at 0.979 V, very close to the potential at which electro-oxidation of TP takes place. Hypoxanthine did not interfere with the SW voltammetric response of XT or CF on the *p*(ABSA)/GCE when present in hundred-fold excess concentration. But the signal due to TP was enhanced by the presence of equimolar concentration of hypoxanthine, producing a signal change above the tolerance limit.

Ascorbic acid is an important antioxidant which is found to co-exist with the purine bases in body fluids as well as other biological matrices. On *p*(ABSA)/GCE the oxidation peak of 5.0×10^{-4} M ascorbic acid appears at 0.06 V with a peak current of 2.5×10^{-6} A. The signal change produced by the presence of fifty-fold higher concentration of ascorbic acid, on the peak parameters of 1.0×10^{-5} M XT, TP and CF was well within the acceptable tolerance limit.

In pharmaceutical formulations, TP and CF are usually found in combination with paracetamol. The oxidation of 1.0×10^{-4} M paracetamol took place at 0.34 V with a peak current of 6.4×10^{-5} A on the

$p(\text{ABSA})/\text{GCE}$, which was well below the potential at which electro-oxidation of TP and CF took place. The presence of hundred-fold excess of paracetamol produced a signal change well within the tolerance limit for both TP and CF indicating that TP and CF determination could be carried out effectively in presence of paracetamol. Other compounds such as urea, creatine, creatinine, glucose, fructose etc. and ions like K^+ , Ca^{2+} etc. which are commonly found in biological fluids did not produce signal change beyond the tolerance limit (5%) when present in tenfold excess concentrations.

Table 8.2: Interference Study

Species	E (V)	Concentration ratio	Signal change (%)		
			XT 1.0×10^{-5} M	TP 1.0×10^{-5} M	CF 1.0×10^{-5} M
Adenine	0.980	1:1	nil	>+20	-1.1
Guanine	0.640	1:1	>+20	-2.3	-0.4
Hypoxanthine	0.979	1:1	-1.2	>+20	-1.1
Ascorbic Acid	0.060	1:1	+2.4	+2.3	+3.9
Paracetamol	0.340	1:10	-1.7	-3.1	-0.9
Urea	nil	1:10	-0.2	-0.4	-1.4
Creatine	nil	1:10	-3.5	-3.3	-1.9
Creatinine	nil	1:10	nil	Nil	nil
Glucose	nil	1:10	-0.6	-1.1	-1.3
Fructose	nil	1:10	-0.7	-1.6	-2.1
K^+	nil	1:10	-1.3	-3.3	-2.9
Ca^{2+}	nil	1:10	+2.1	-1.6	-2.2

8.2.6 Determination of the purines in real samples

The $p(\text{ABSA})/\text{GCE}$ was applied for the direct determination of the purines with very simple pre-treatment in commercially available tea and coffee as well as TP and CF in pharmaceutical preparations. Sample solutions of tea and coffee were prepared as described in section 2.7.5 and

those of pharmaceutical preparations as described in Section 2.7.6, of chapter 2. Standard addition method was employed for the determination of the amount of the xanthines. In the tea sample, peaks appeared at the same potentials as that observed in the case of standard XT and CF whereas for the coffee sample, oxidation peak occurred at potential corresponding to standard CF. Results obtained by the standard addition method are shown in Table 8.3. The relative standard deviation (RSD) produced are significantly low indicating the reliability of the measurements.

Table 8.3: Determination of XT, TP and CF in commercially available samples

Sample	Found (mg L ⁻¹)				RSD (%)*			
	XT	TP	CF	Ua	XT	TP	CF	Ua
Tea bag (<i>Twinning's</i>)	0.33	-	5.50	-	0.04	-	0.08	-
Blended Coffee powder (<i>Nescafe Sunrise</i>)	-	-	12.00	-	-	-	2.02	-

*for six replicate measurements

In pharmaceutical formulations, the oxidation peaks appeared at potentials corresponding to that of the standard compound. There is good agreement between the declared and found amounts of these xanthines (Table 8.4).

Table 8.4: Determination of TP and CF in pharmaceutical formulations

Sample	Declared (mg)	Found (mg)	RSD (%)*
Theophylline Tablet (<i>Unicontin-E</i>)	400.0	402.3	1.3
Caffeine Tablet (<i>Dolopar</i>)	25.0	25.1	3.6

*for six replicate measurements

Determination of Ua, XT, TP and CF were also carried out in spiked body fluids. Recoveries obtained in the measurement of these compounds in the synthetic urine and blood serum (Table 8.5) are indicative of prospective applications in clinical diagnostics.

Table 8.5: Determination of XT, TP, CF and Ua in spiked synthetic urine and serum

		Added (M)	Found (M)	Recovery (%)	RSD* (%)
Urine	XT	9.0×10^{-5} - 1.5×10^{-5}	8.96×10^{-5} - 1.51×10^{-5}	100	0.6
	TP	3.5×10^{-4} - 2.5×10^{-5}	3.25×10^{-4} - 2.56×10^{-5}	101	1.4
	CF	2.4×10^{-4} - 6.0×10^{-5}	2.39×10^{-4} - 5.98×10^{-5}	100	1.0
	Ua	1.0×10^{-5} - 8.0×10^{-5}	8.01×10^{-5} - 1.02×10^{-5}	101	0.7
Serum	XT	9.0×10^{-5} - 1.5×10^{-5}	9.04×10^{-5} - 1.50×10^{-5}	100	0.2
	TP	3.5×10^{-4} - 2.5×10^{-5}	3.26×10^{-4} - 2.57×10^{-5}	101	1.2
	CF	2.4×10^{-4} - 6.0×10^{-5}	2.39×10^{-4} - 6.12×10^{-5}	101	1.3
	Ua	8.0×10^{-5} - 1.0×10^{-5}	7.96×10^{-5} - 1.02×10^{-5}	100	0.5

*for six replicate measurements

8.2.7 Mechanistic Studies

Linear Sweep Voltammetry (LSV) at different scan rates was used to study the mechanism of the electrochemical process. The variation of peak parameters with scan rate ν in Vs^{-1} for each analyte is presented in Table 8.6. The peak potential shifted to more positive values with increase in scan rate for all the three xanthenes indicating that all the electro-oxidations are irreversible in nature [13]. The peak current varied linearly with square root of scan rate for XT, TP, CF and Ua. Moreover, the slope of the plot of I versus $\log \nu$ was obtained as 0.471, 0.535, 0.395 and 0.599 respectively for XT, TP, CF and Ua closer to the theoretical value of 0.50 [131], indicating the diffusion controlled nature of the electrode processes.

Table 8.6: Variation of peak parameters with scan rate

	I(A)	E(V)
XT	$I = 1.84 \times 10^{-4} \nu^{1/2} + 4.49 \times 10^{-6}$	$E = 0.031 \ln \nu + 0.827$
TP	$I = 1.01 \times 10^{-4} \nu^{1/2} + 4.86 \times 10^{-6}$	$E = 0.015 \ln \nu + 1.045$
CF	$I = 3.09 \times 10^{-4} \nu^{1/2} + 2.76 \times 10^{-5}$	$E = 0.021 \ln \nu + 1.481$
Ua	$I = 1.14 \times 10^{-4} \nu^{1/2} - 6.86 \times 10^{-6}$	$E = 0.015 \ln \nu + 0.319$

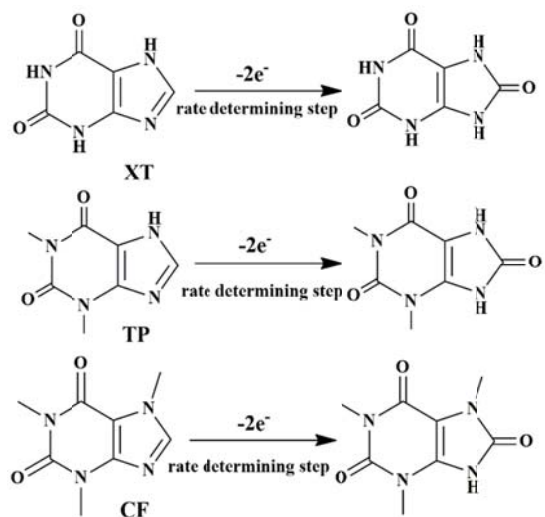
The mechanistic parameters such as number of electrons involved in the rate determining step and the charge transfer coefficient were calculated from the data obtained from the linear sweep voltammograms recorded at various scan rates. By the method proposed by Galvez [134] as described in chapter 3, the mechanistic parameters for the electro-oxidation processes has been determined and the results are presented in Table 8.7.

Table 8.7: Mechanistic parameters

	n_{α}^*	α
XT	2 (1.7)	0.418
TP	2 (1.5)	0.764
CF	2 (1.8)	0.614
Ua	2 (2.2)	0.681

*calculated value is shown in brackets

The possible mechanism of the electrochemical processes in accordance with these observations is represented in Scheme 8.1. [172, 165, 206]



Scheme 8.1: Electro-oxidation of XT, TP and CF on *p*(ABSA)/GCE

8.2.8 Kinetic Studies

8.2.8.1 Chronoamperometry

The Cottrellian decay of the transient current **I** for electro-oxidation of XT, TP and CF with time **t**, was studied by chronoamperometry at different concentrations using the *p*(ABSA)/GCE. The slopes of the experimental plots of **I** versus $t^{-1/2}$ were plotted against the corresponding concentrations of the analytes and its slope was used to calculate the diffusion coefficient **D**. In Figure 8.17, the chronoamperograms and the corresponding **I** versus $t^{-1/2}$ plots are shown. The value of **D** for XT, TP and CF in 0.1M PBS pH 7 was obtained as $2.87 \times 10^{-5} \text{ cm}^2 \text{ s}^{-1}$, $2.92 \times 10^{-5} \text{ cm}^2 \text{ s}^{-1}$ and $2.17 \times 10^{-5} \text{ cm}^2 \text{ s}^{-1}$ respectively. The values obtained indicate that on the *p*(ABSA)/GCE XT and its methyl derivatives have comparable diffusion coefficients within the margin of error.

The value of diffusion coefficients for XT, TP and CF under the experimental conditions were obtained to be $2.87 \times 10^{-5} \text{ cm}^2 \text{ s}^{-1}$, $2.92 \times 10^{-5} \text{ cm}^2 \text{ s}^{-1}$ and $2.17 \times 10^{-5} \text{ cm}^2 \text{ s}^{-1}$ respectively. The diffusion coefficients of all the xanthenes were found to be comparable indicating that diffusion effects due to depletion of the electrical double layer at the electrode-electrolyte interface is similar for XT, TP and CF.

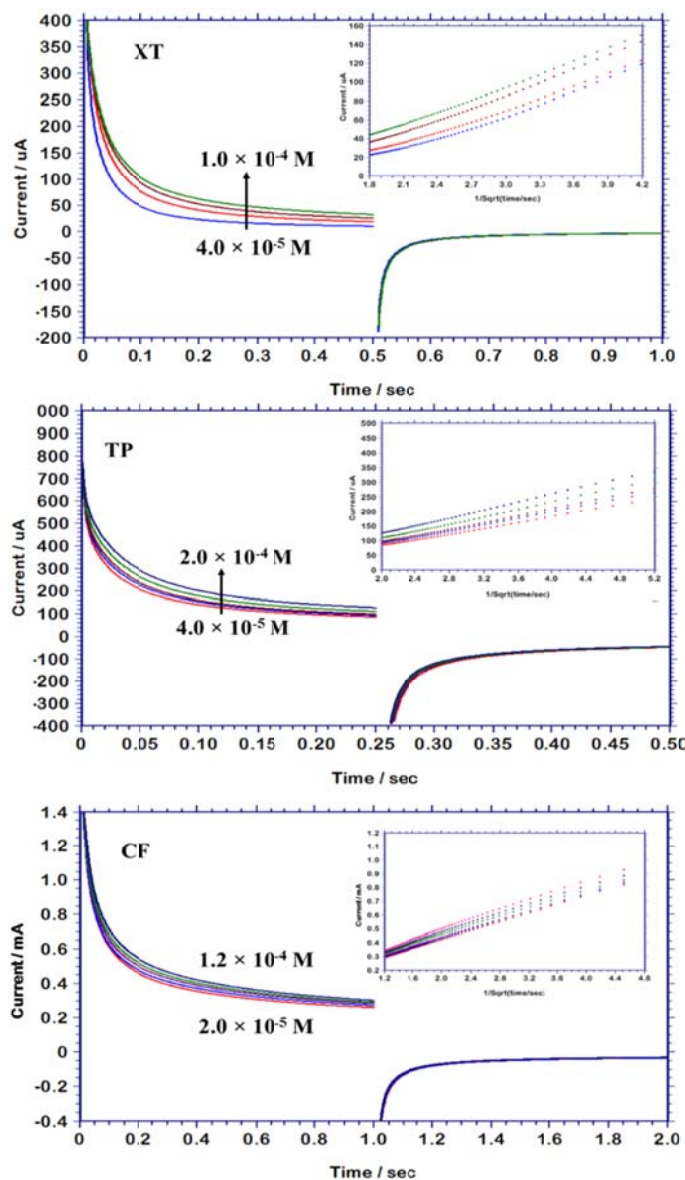


Figure 8.17: Chronoamperograms obtained for the oxidation of various concentrations of XT, TP and CF on *p*(ABSA)/GCE with 0.1 M PBS pH 7 as supporting electrolyte. Inset of each chronoamperogram shows the corresponding plot of I vs $t^{-1/2}$

8.2.8.2 Heterogeneous rate constant

The rate constant for the electro-oxidation of XT, TP and CF on the p(ABSA)/GCE was calculated using the Nicholson-Shain and Laviron models. In Nicholson-Shain model, information obtained from LSV at different scan rates as well as the diffusion coefficient obtained from chronoamperometric studies at different concentrations were utilised. Information from LSV at different scan rates was used in Laviron model. The value of standard heterogeneous rate constant determined by these models are presented in Table 8.8.

Table 8.8: Kinetics of electro-oxidation

	E vs ln v		E ⁰	D cm ² s ⁻¹	rate constant	
	slope	intercept			k _h cm s ⁻¹	k _s s ⁻¹
XT	0.031	0.839	0.714	2.87 × 10 ⁻⁵	1.42 × 10 ⁻¹	0.572
TP	0.015	1.045	0.986	2.92 × 10 ⁻⁵	5.91 × 10 ⁻²	1.305
CF	0.021	1.481	1.383	2.17 × 10 ⁻⁵	2.33 × 10 ⁻²	0.447

Standard heterogeneous rate constant, **k_h** calculated using Nicholson-Shain model followed the trend, XT > TP > CF. The rate constants are in the ratio 6:3:1. The diffusion coefficients of XT and TP are the same within the margin of error. But the value of **k_h** of XT oxidation is twice that of TP oxidation. Hence it could be deduced that diffusion effects do not contribute much towards the kinetics of electro-oxidation.

The numerical values obtained for Laviron **k_s** in the case of XT and CF are comparable but the value of **k_s** for TP oxidation is twice that of XT and thrice that of CF. The charge transfer resistance for oxidation on p(ABSA)/GCE was highest for CF (Table 8.1) which points to the sluggish electron transfer across the electrode surface and hence the low value of

Nicholson-Shain and Laviron k_s for CF. But the higher value of k_h for XT oxidation and k_s for TP oxidation cannot be accounted for.

8.3 Conclusions

Study of electro chemical oxidation of XT and its methyl derivatives TP and CF as well as its oxidation product, Ua on a *p*(ABSA)/GCE has been described in this chapter. In square wave mode, well defined and well separated peaks were obtained for the electro-oxidation of XT, TP and CF, which facilitated their simultaneous determination. The conditions to obtain the ideal SW response has been optimized. Although other purines interfered for example Gu interfered with the determination of XT; Ad and hypoxanthine interfered with the determination of TP, selective determination of XT, TP and CF together with Ua was possible even in presence of other possibly co-existing chemical species. Thus, a simple, selective and sensitive sensor has been proposed for the simultaneous determination of XT, TP and CF whose utility in real sample analysis has been demonstrated. The developed method is suitable for direct determination of these compounds in real samples and requires very simple pre-treatment steps. The electrochemical kinetic parameters for the oxidation of the xanthines on the *p*(ABSA)/GCE has also been determined.

..... 

Summary and Conclusions

This chapter summarises the main results of the work presented in this thesis and tries to derive conclusions out of them. Various parameters like oxidation potential, limit of detection and rate constants for the electro-oxidation of DNA bases on the developed polymer modified electrodes are compared. The performance of each of the developed sensors is also compared with other polymer modified electrodes.

Keeping in accordance with the objectives of the research work undertaken, glassy carbon electrode (GCE) modified with five different electropolymers, poly(aspartic acid) [*p*(AspA)], poly(glutamic acid) [*p*(GA)], poly(para toluene sulfonic acid) [*p*(TSA)], poly(para amino benzene sulfonic acid) [*p*(ABSA)] and poly(4-amino-3-hydroxy naphthalene-1-sulfonic acid) [*p*(AHNSA)], have been developed as sensors for DNA bases. The electrochemical behaviour of DNA bases, guanine (Gu), adenine (Ad), thymine (Thy) and cytosine (Cyt) on the developed sensors have been studied. The suitability of the developed sensors for real sample analysis has been demonstrated.

Further, the kinetics of electro-oxidation of DNA bases on the developed electrodes have been explored. In addition, the simultaneous and individual determination of uric acid (Ua) along with DNA bases on the developed sensors have been carried out.

The success encountered with the determination of purines on the developed sensors prompted us to extend the efforts to the development of a sensor for other purines. The sixth sensor developed is one for the simultaneous

as well as individual determination of other purines – xanthine (XT) and its derivatives theophylline (TP) and caffeine (CF) together with Ua.

The various sensors developed during the course of this research are listed in the table 9.1.

Table 9.1: Various sensors developed by the present work

	Individual	Simultaneous
<i>p</i> (AspA)/GCE	Ad	-
<i>p</i> (GA)/GCE	Thy	-
<i>p</i> (TSA)/GCE	Gu, Ad, Thy, Ua	Gu, Ad, Ua and Gu, Thy, Ua
<i>p</i> (ABSA)/GCE	Gu, Ad, Ua, XT, TP, CF	Gu, Ad, Ua and XT, TP, CF and Ua
<i>p</i> (AHNSA)/GCE	Gu, Ad, Cyt, Thy and Ua	Gu, Ad, Cyt and Ua

On all the sensors, the electro-oxidation of DNA bases were observed at the lowest potential when 0.1 M NaOH was used as the supporting electrolyte. The electro-oxidation of DNA bases on the various polymer modified electrodes developed in the present work has been found to be irreversible and diffusion controlled. Electro-oxidation of DNA bases on different modified electrodes has been reported to be adsorption controlled processes thereby causing fouling of the electrode surface. The sensors described in this work, produce diffusion controlled electro-oxidation and thereby reduce the electrode fouling and hence can be reused.

For each analyte three parameters were mainly addressed. The oxidation potential (Table 9.2), the limit of detection (Table 9.3) and the heterogeneous rate constant (Table 9.4).

Table 9.2: Oxidation potential of DNA bases on the developed electrodes

	E (V)			
	Gu 5.0×10^{-5} M	Ad 5.0×10^{-5} M	Thy 1.0×10^{-4} M	Cyt 5.0×10^{-4} M
GCE (SWV)	0.348	0.632	0.780	-
<i>p</i> (AspA)/GCE (DPV)	0.332	0.568	0.765	0.964
<i>p</i> (GA)/GCE (SWV)	0.330	0.610	0.752	-
<i>p</i> (TSA)/GCE (SWV)	0.304	0.608	0.760	0.896
<i>p</i> (ABSA)/GCE (SWV)	0.284	0.588	0.758	-
<i>p</i> (AHNSA)/GCE (SWV)	0.292	0.596	0.756	0.876

For Gu, the lowest oxidation potential was obtained in *p*(ABSA)/GCE in SW voltammetric mode while for Ad, the lowest potential was observed in *p*(AspA)/GCE in DP voltammetric mode. The oxidation of Thy took place at the lowest potential on *p*(GA)/GCE, whereas for Cyt, the electro-oxidation took place with lowest potential on *p*(AHNSA)/GCE. It could be concluded that each of the polymer modified electrode offered structure specific electrocatalysis for the electro-oxidation of each of the DNA bases.

Regarding the detection limit (Table 9.3), *p*(TSA)/GCE gave the lowest value of LOD for Gu, Ad and Thy. A good working linear range for Cyt was observed only with *p*(AHNSA)/GCE.

Comparing all the factors like lower oxidation potential, wide linear range and low detection limit, among the developed sensors *p*(AHNSA)/GCE can be considered as the best sensor for DNA bases.

Table 9.3: Limit of detection for individual analytes obtained on various electrodes

	Gu	Ad	Thy	Cyt
<i>p</i> (AspA)/GCE	-	6.7×10^{-6} M	-	-
<i>p</i> (GA)/GCE	-	-	9.2×10^{-6} M	-
<i>p</i> (TSA)/GCE	7.9×10^{-9} M	9.4×10^{-7} M	1.4×10^{-6} M	-
<i>p</i> (ABSA)/GCE	3.0×10^{-6} M	8.6×10^{-6} M	-	-
<i>p</i> (AHNSA)/GCE	1.0×10^{-6} M	2.3×10^{-6} M	1.7×10^{-5} M	1.5×10^{-6} M

The calculated value of Nicholson-Shain rate constant k_h and Laviron rate constant k_s for the DNA bases on the fabricated electrodes and bare GCE are consolidated in Table 9.4. The standard heterogeneous rate constant k_h for all the DNA bases are in the range $10^{-2} - 10^{-3} \text{ cm s}^{-1}$ and its value has increased on all the modified electrodes in comparison with bare GCE. The maximum value of k_h for Gu was observed on $p(\text{AspA})/\text{GCE}$ with an increase of an order of magnitude. For Ad, the value of k_h observed on $p(\text{AHNSA})/\text{GCE}$ was two orders of magnitude higher than that on bare GCE. Thy and Cyt showed maximum value of k_h with an increase of an order of magnitude on $p(\text{GA})/\text{GCE}$ and $p(\text{AHNSA})/\text{GCE}$ respectively. It seems that there is an analyte specific influence on kinetics by the polymer modified electrodes.

Table 9.4: Rate constant for electro-oxidation on various electrodes

	$k_h \text{ (cm s}^{-1}\text{)}$				$k_s \text{ (s}^{-1}\text{)}$			
	Gu	Ad	Thy	Cyt	Gu	Ad	Thy	Cyt
GCE	1.18×10^{-3}	4.55×10^{-4}	1.65×10^{-3}	6.31×10^{-3}	2.07	2.43	0.45	0.37
$p(\text{AspA})/\text{GCE}$	1.86×10^{-2}	1.94×10^{-2}	2.46×10^{-3}	4.60×10^{-2}	2.06	2.90	0.29	0.45
$p(\text{GA})/\text{GCE}$	1.35×10^{-2}	4.06×10^{-2}	1.25×10^{-2}	7.51×10^{-3}	0.93	2.56	0.69	1.02
$p(\text{TSA})/\text{GCE}$	1.53×10^{-3}	1.71×10^{-3}	2.76×10^{-3}	4.33×10^{-2}	0.65	0.69	4.50	1.25
$p(\text{ABSA})/\text{GCE}$	1.35×10^{-2}	1.01×10^{-2}	9.60×10^{-3}	1.65×10^{-2}	1.01	2.32	1.59	1.30
$p(\text{AHNSA})/\text{GCE}$	4.25×10^{-3}	7.09×10^{-2}	4.38×10^{-3}	5.38×10^{-2}	1.25	6.03	1.41	0.29

In terms of the Laviron or surface rate constant k_s , a trend is not observed. For Gu oxidation, k_s obtained on all the developed electrodes were less than that obtained on bare GCE, except for $p(\text{AspA})/\text{GCE}$ which gave a similar value as that obtained on bare GCE. For Ad, the value of k_s was found to be comparable with that obtained on bare GCE on all electrode except $p(\text{TSA})/\text{GCE}$ and $p(\text{AHNSA})/\text{GCE}$. $p(\text{TSA})/\text{GCE}$ gave a

lower value than bare GCE and $p(\text{AHNSA})/\text{GCE}$ a higher value. Compared to the bare GCE, the value of k_s for electro-oxidation of Thy was found to be increased on all the developed electrodes except $p(\text{AspA})/\text{GCE}$ and the highest value was observed on $p(\text{TSA})/\text{GCE}$. In the case of Cyt, a lowering of k_s was observed on $p(\text{AHNSA})/\text{GCE}$ in comparison to the bare GCE. On all the other electrodes, its value was found to be higher than that on bare GCE, with the highest value observed on $p(\text{ABSA})/\text{GCE}$.

The Laviron rate constant k_s , has been derived on the assumption that diffusion effects are absent and there is an adsorption of the species on the electrode surface before electron transfer. In such a case, these observations indicate that for the electro-oxidation of DNA bases, diffusion effects are prevalent, and adsorption is negligible. This may be the reason that although the value of k_h for electro-oxidations on all the electrodes was found to be increased compared to the bare GCE, the value of k_s was found to be decreased in most cases.

A comparison of the performance characteristics of the developed electropolymer based sensors with some other polymer modified electrodes for simultaneous determination of DNA bases along with Ua is given in table 9.5.

From the table it is clear that, the sensors developed in the present work report the lowest oxidation potentials for the electro-oxidation of DNA bases. Although the detection limits are not as low as some of the other sensors, the electropolymer based sensors can be easily fabricated and can give comparable results.

Table 9.5: Comparison of performance characteristics of the developed sensors with previously reported sensors for simultaneous determination

Electrode	Technique	Analyte	E (V)	Linear range (M)	LOD (M)	Reference
Ag-<i>p</i>(Mel)/GCE	SWV	Gu	0.850	$5.0 \times 10^{-5} - 1.0 \times 10^{-7}$	8.0×10^{-9}	[74]
		Ad	1.100	$6.0 \times 10^{-5} - 1.0 \times 10^{-7}$	8.0×10^{-9}	
		Ua	0.450	$5.0 \times 10^{-5} - 1.0 \times 10^{-7}$	1.0×10^{-7}	
nano-Au/DNA/nano-Au/ <i>p</i>(SFR)/GCE	DPV	Gu	0.520	$5.0 \times 10^{-6} - 9.0 \times 10^{-9}$	5.0×10^{-10}	[75]
		Ad	0.900	$8.0 \times 10^{-7} - 6.0 \times 10^{-8}$	8.0×10^{-9}	
		Ua	0.320	$1.2 \times 10^{-5} - 9.0 \times 10^{-8}$	8.0×10^{-9}	
<i>p</i>(Imox)-GO/GCE	DPV	Gu	0.880	$1.0 \times 10^{-4} - 3.3 \times 10^{-6}$	4.8×10^{-7}	[77]
		Ad	1.200	$2.2 \times 10^{-4} - 9.6 \times 10^{-6}$	1.2×10^{-6}	
		Ua	0.530	$2.5 \times 10^{-4} - 3.6 \times 10^{-6}$	5.9×10^{-7}	
MWCNTs-<i>p</i>NF/GCE	CV	Gu	0.707	$3.5 \times 10^{-3} - 1.0 \times 10^{-4}$	9.6×10^{-5}	[87]
		Ad	1.027	$7.9 \times 10^{-3} - 1.0 \times 10^{-5}$	7.9×10^{-6}	
		Thy	1.153	$1.5 \times 10^{-2} - 2.0 \times 10^{-5}$	1.6×10^{-5}	
<i>p</i>(ANI)/MnO₂/GCE	DPV	Gu	0.610	$1.0 \times 10^{-4} - 1.0 \times 10^{-5}$	4.8×10^{-6}	[91]
		Ad	0.880	$1.0 \times 10^{-4} - 1.0 \times 10^{-5}$	2.9×10^{-6}	
		Thy	1.090	$1.0 \times 10^{-4} - 1.0 \times 10^{-5}$	1.3×10^{-6}	
		Cyt	1.260	$1.0 \times 10^{-4} - 1.0 \times 10^{-5}$	1.3×10^{-6}	
<i>p</i>(TSA)/GCE	SWV	Gu	0.304	$1.0 \times 10^{-4} - 1.0 \times 10^{-5}$	3.5×10^{-7}	this work
		Ad	0.608	$1.0 \times 10^{-4} - 2.0 \times 10^{-5}$	7.8×10^{-6}	
		Ua	-0.108	$1.0 \times 10^{-4} - 1.0 \times 10^{-5}$	5.8×10^{-6}	
<i>p</i>(ABSA)/GCE	SWV	Gu	0.284	$2.0 \times 10^{-4} - 1.0 \times 10^{-5}$	4.3×10^{-6}	this work
		Ad	0.588	$1.5 \times 10^{-4} - 2.0 \times 10^{-5}$	1.0×10^{-5}	
		Ua	-0.132	$1.5 \times 10^{-4} - 2.0 \times 10^{-5}$	5.9×10^{-6}	
<i>p</i>(AHNSA)/GCE	SWV	Gu	0.292	$2.5 \times 10^{-4} - 1.0 \times 10^{-5}$	9.3×10^{-7}	this work
		Ad	0.596	$2.5 \times 10^{-4} - 1.0 \times 10^{-5}$	6.2×10^{-6}	
		Cyt	0.867	$2.5 \times 10^{-4} - 8.0 \times 10^{-5}$	9.2×10^{-6}	
		Ua	-0.120	$2.5 \times 10^{-4} - 1.0 \times 10^{-5}$	9.3×10^{-6}	

Ag-*p*(Mel): poly-melamine and nano Ag hybridized film-modified electrode

nano-Au/DNA/nano-Au/*p*(SFR): 3D gold nanoparticles on poly safranine

p(Imox)-GO: Overoxidized polyimidazole/graphene oxide copolymer

p(ANI)/MnO₂: polyaniline/MnO₂

MWCNTs-*p*(NF): multi-walled carbon nanotubes incorporated with poly (new fuchsin) composite film

Future perspectives

Sensors are the need of the hour in the present world as it finds applications in every field of life, be it quality control, medical diagnostics, environmental monitoring etc. Maybe that is the reason why it is one of the most active areas of research.

The present work is part of an attempt to develop simple and viable sensors for clinical analysis. Electropolymer based sensors have been developed which gave reasonably good working ranges and detection limits. In future, electropolymers with different free functionalities can be studied for possible sensor applications. The performance of these sensors can be enhanced by using electropolymer composites as the modification rather than the electropolymer alone. Composites of electropolymers with nanoparticles, quantum dots, metal complexes, macrocycles etc. could give better performance as sensors. Further, commercialisation of the developed sensors can be made possible by attempting device fabrication incorporating the developed sensor in miniature form.

Study of the kinetics of electro-oxidation processes can be of use in understanding the nuances of analyte-sensor interactions which can further help in developing better sensors. Combining the kinetic study with computational analysis, better understanding of the electrode processes can be achieved. Combining the principles of analytical chemistry, physical chemistry and computational chemistry there are chances of developing high performing sensors suitable for high throughput applications.

Supplementary Information

In the thesis, the electrochemical impedance measurements have been carried out using two different probe solutions.

For the characterisation of the modified electrode, the EIS measurements of the modified electrode were carried using the redox probe $[\text{Fe}(\text{CN})_6]^{-3/4}$ and compared with the EIS measurement on bare electrode. The change in the charge transfer resistance gives an idea about how effective the modification is for the electron transfer for the oxidation reaction, $\text{Fe}^{2+} \rightarrow \text{Fe}^{3+} + \text{e}^-$.

EIS measurements were also carried out on the bare and modified electrodes using the target analyte solution under the optimum experimental conditions. This gives information regarding how effective the modification is for the charge transfer for the respective electrode reaction taking place under the optimised experimental conditions.

..... 

References

- [1] J. Wang, *Analytical Electrochemistry 3rd Edition*, John Wiley and Sons, New Jersey (2006)
- [2] A. C. Power, A. Morrin, *Electroanalytical Sensor Technology, Electrochemistry. Dr. Mohammed Khalid (Ed.), InTech*, Available from: <https://www.intechopen.com/books/electrochemistry/electroanalytical-sensor-technology> [Accessed on: 24th August 2017]
- [3] C. M. A. Brett, A. M. O. Brett, *Electroanalysis*, Oxford University Press, Oxford (1998)
- [4] D. T. Sawyer, A. Sobkowiak, J. L. Roberts, *Electrochemistry for Chemists 2nd Edition*, Wiley, New York (1995)
- [5] F. Rouessac, A. Rouessac, *Chemical Analysis Modern Instrumentation Methods and Techniques 2nd Edition*, John Wiley and Sons, Chichester (2000)
- [6] F. G. Thomas, G. Henze, *Introduction to Voltammetric Analysis: Theory and Practice*, CSIRO Publishing, Australia (2001)
- [7] S. Alegret, A. Merkoçi (eds.), *Electrochemical sensor analysis. Vol. 49*, Elsevier, Netherlands (2007)
- [8] M. Noel, K. I. Vasu, *Cyclic Voltammetry and the Frontiers of Electrochemistry*, Oxford and IBH Publishing Co. Pvt. Ltd, New Delhi, (1999)
- [9] R. C. Alkire, D. M. Kolb, J. Lipkowski, P. N Ross, *Chemically modified electrodes Vol. 22*, John Wiley & Sons. (2009)

References

- [10] R. A. Durst, A. J. Baumner, R. W. Murray, R. P. Buck, C. P. Andrieux, *Pure & App. Chem.*, **69**, 1317 (1997)
- [11] F. Scholz (ed.), *Electroanalytical methods*. Springer-Verlag, Berlin Heidelberg (2010)
- [12] A. J. Bard, *J. Chem. Ed.* **60**, 302 (1983)
- [13] D. A. C. Brownson, C. E. Banks, *The handbook of graphene electrochemistry*, Springer London. (2014)
- [14] D. A. Skoog, F. J. Holler, S. R. Crouch, *Principles of Instrumental Analysis 6th Edition*, Thomson Brooks/Cole (2007).
- [15] C. M. A. Brett, A. M. O. Brett, *Electrochemistry Principles, Methods, and Applications*, Oxford University Press, New York (1993)
- [16] A. J. Bard, L. R. Faulkner, *Electrochemical Methods Fundamentals and Applications 2nd Edition*, John Wiley and Sons Inc., New York (2001)
- [17] K. Aoiki, J. Osteryoung, R. A. Osteryoung, *J. Electroanal. Chem. Interfacial Electrochem.*, **110**, 1 (1980)
- [18] F. A. Settle (ed), *Handbook of Instrumental Techniques for Analytical Chemistry*, Prentice Hall PTR, New Jersey (1999)
- [19] F. G. Cottrell, *Z. Phys. Chem.*, **42**, 385 (1902)
- [20] A. N. Frumkin, *J. Electroanal. Chem.*, **9**, 173 (1979)
- [21] A. E. Vikraman, D. Thomas, S. T. Cyriac, K. Girish Kumar, *J. Electrochem. Soc.*, **161**, B305 (2014)
- [22] R. S. Nicholson, I. Shain, *Anal. Chem.*, **36**, 706 (1964)
- [23] E. Laviron, *J. Electroanal. Chem.*, **101**, 19 (1965)
- [24] A. Hulanicki, S. Geab, F. Ingman, *Pure & App. Chem.*, **63**, 1247 (1991)

- [25] U. Yogeswaran, S-M. Chen, *Sensors*, **8**, 290 (2008)
- [26] R. W. Cattrall, *Chemical Sensors*, Oxford University Press Inc. New York (1997)
- [27] N. R. Stradiotto, H. Yamanaka, M. V. B. Zanon, *J. Braz. Chem. Soc.*, **14**, 159 (2003)
- [28] D. Grieshaber, R. MacKenzie, J. Vörös, E. Reimhult, *Sensors*, **8**, 1400 (2008)
- [29] S. Cosnier, M. Holzinger, *Chem. Soc. Rev.*, **40**, 2146 (2011)
- [30] G. S. Shapova, A. V. Gorodyskii, *Russ. Chem. Reviews*, **42**, 370 (1973)
- [31] C. M. A. Brett, *Electroanalysis*, **11**, 1013 (1999)
- [32] V. S. Bagotsky, *Fundamentals of Electrochemistry*, John Wiley & Sons, Inc., New Jersey (2009)
- [33] M. Lyons, *Electroactive Polymer Electrochemistry: Part 1: Fundamentals*, Springer Science + Business Media, New York (1994)
- [34] R. F. Weaver, *Molecular biology*, McGraw-Hill, New York (2012)
- [35] P. Wang, H. Wu, Z. Dai, X. Zou, *Biosens. Bioelectron.*, **26**, 3339 (2011)
- [36] T. Husband, *The chemistry of human nature*, The Royal Society of Chemistry, Cambridge (2017)
- [37] P. Silwal, K. Shin, S. Choi, S. W. Kang, J. B. Park, H-J. Lee, S-J. Koo, K.-H. Chung, U. Namgung, K. Lim, J-Y. Heo, J. Il Park, S-K Park, *Molecular Immunology*, **65**, 242 (2015)
- [38] R. N. Goyal, S. Chatterjee, S. Bishnoi, *Electroanalysis*, **21**, 1369 (2009)

References

- [39] A. Weimann, D. Belling, H. E. Poulsen, *Nucleic Acids Res.* **30**, e7 (2002)
- [40] J. A. J. M. Bakkeren, R.A. De Abreu, R.C. Sengers, F.J. Gabreëls, J.M. Maas, W.O. Renier, *Clin. Chim. Acta*, **140**, 247 (1984)
- [41] J. Parker, *Cytosine*, In *Encyclopedia of Genetics*, edited by Sydney Brenner and Jefferey H. Miller, Academic Press, New York (2001)
- [42] Wikipedia contributors, *Cytarabine*, *Wikipedia, The Free Encyclopedia*, <https://en.wikipedia.org/w/index.php?title=Cytarabine&oldid=791258317> [Accessed September 1, 2017]
- [43] G. P. Gupta, *Molecular Biology*, Discovery Publishing House, India (2004)
- [44] D. Anandhi, *Introduction to Biochemistry and Metabolism*, Pearson, India (2014)
- [45] L. M. Niu, K. Q. Lian, H. M. Shi, Y. B. Wu, W. J. Kang, S. Y. Bi, *Sensors Actuators B Chem.*, **178**, 10 (2013)
- [46] L. Z. Zheng, S. G. Wu, X. Q. Lin, L. Nie, L. Rui, *Electroanalysis*, **13**, 1351 (2001)
- [47] S. R. J. Maxwell, H. Thomason, D. Sandler, C. Leguen, M. A. Baxter, G. H. Thorpe, A. F. Jones, A. H. Barnett, *Eur. J. Clin. Invest.*, **27**, 484 (1997)
- [48] C. Deng, Y. Xia, C. Xiao, Z. Nie, M. Yang, S. Si, *Biosens. Bioelectron.*, **31**, 469 (2012)
- [49] H. Li, X. Wang, Z. Yu, *J. Solid State Electrochem.*, **18**, 105 (2014)

- [50] J. Wang, S. Bollo, J. L. L Paz, E. Sahlin, B. Mukherjee, *Anal. Chem.*, **71**, 1910 (1999)
- [51] A. M. O. Brett, L. A. Silva, C. M. A Brett, *Langmuir*, **18**, 2326 (2002)
- [52] D. W. Pang, Y-P. Qi, Z-L. Wang, J-K. Cheng, J-W. Wang, *Electroanalysis*, **7**, 774 (1995)
- [53] O. Niwa, J. Jia, Y. Sato, D. Kato, R. Kurita, K. Maruyama, K. Suzuki, S. Hirono, *J. Am. Chem. Soc.*, **128**, 7144 (2006)
- [54] R. N. Goyal, A. Kumar, A. Mittal, *J. Chem. Soc.-Perkin Trans. 2*, 1369 (1991)
- [55] A. M. O. Brett, V. Diculescu, J. A. P. Piedade, *Bioelectrochemistry*, **55**, 61 (2002)
- [56] L. Svorc, K. Kalcher, *Sensors Actuators B Chem.*, **194**, 332 (2014)
- [57] A. M. O. Brett, F-M. Matysik, *J. Electroanal. Chem.*, **429**, 95 (1997)
- [58] P. Singhal, W. G. Kuhr, *Anal. Chem.*, **69**, 3552 (1997)
- [59] M. Zhou, Y. M. Zhai, S. J. Dong, *Anal. Chem.*, **81**, 5603 (2009)
- [60] R. Zhang, G. D. Jin, X. Y. Hu, *J. Solid State Electrochem.*, **13**, 1545 (2009)
- [61] Q. Xu, M. Sun, Q. Du, X. Bian, D. Chen, *Curr. Pharm. Anal.*, **5**, 190 (2009)
- [62] Y. Song, J.-Z. Li, *Instrum. Sci. Technol.*, **39**, 261 (2011)
- [63] M. Arvand, A. Niazi, R. Motaghd Mazhabi, P. Biparva, *J. Mol. Liq.*, **173**, 1 (2012)
- [64] A. Abbaspour, M. A. Mehrgardi, R. Kia, *J. Electroanal. Chem.*, **568**, 261 (2004)

References

- [65] M. Mazloun Ardakani, Z. Taleat, H. Beitollahi, M. Salavati-Niasari, B. B. F. Mirjalili, N. Taghavinia, *J. Electroanal. Chem.*, **624**, 73 (2008)
- [66] P. Kanyong, S. Rawlinson, J. Davis, *Sensors Actuators B Chem.*, **233**, 528 (2016)
- [67] A. Abbaspour, A Noori, *Analyst*, **133**, 1664 (2008)
- [68] H. Yin, Y. Zhou, Q. Ma, S. Ai, P. Ju, L. Zhu, L. Lu, *Process Biochemistry*, **45**, 1707 (2010)
- [69] A. Ferancová, S. Rengaraj, Y. Kim, J. Labuda, M. Sillanpää, *Biosens. Bioelectron.*, **26**, 314 (2010)
- [70] T. Liu, X. Zhu, L. Cui, P. Ju, X. Qu, S. Ai, *J. Electroanal. Chem.*, **651**, 216 (2011)
- [71] Y. Fan, K-J. Huang, D-J. Niu, C-P. Yang, Q-S. Jing, *Electrochim. Acta*, **56**, 4685 (2011)
- [72] K. Q. Deng, H. X. Li, Y. L. Ling, G. R. Xu, X. F. Li, *Chin. Chem. Lett.*, **22**, 981 (2011)
- [73] X. Niu, W. Yang, J. Ren, H. Guo, S. Long, J. Chen, J. Gao, *Electrochim. Acta*, **80**, 346 (2012)
- [74] X. Liu, L. Luo, Y. Ding, Q. Wu, Y. Wei, D. Ye, *J. Electroanal. Chem.*, **675**, 47 (2012)
- [75] L. M. Niu, K. Q. Lian, H. M. Shi, Y. B. Wu, W. J. Kang, S. Y. Bi, *Sensors Actuators B Chem.*, **178**, 10 (2013)
- [76] A. A. Ensafi, M. Jafari-Asl, B. Rezaei, A.R. Allafchian, *Sensors Actuators B Chem.*, **177**, 634 (2013)
- [77] X. Liu, L. Zhang, S. Wei, S. Chen, X. Ou, Q. Lu, *Biosens. Bioelectron.*, **57**, 232 (2014)

- [78] G. Wang, G. Shi, X. Chen, R. Yao, F. Chen, *Microchim. Acta*, **182**, 315 (2015)
- [79] T. Yang, R. Yang, H. Chen, F. Nan, T. Ge, *ACS Appl. Mater. Interfaces*, **7**, 2867 (2015)
- [80] H. Ibrahim, Y. Temerk, N. Farhan, *RSC Adv.*, **6**, 90220 (2016)
- [81] H. Song, S. Huo, J. Dong, J. Xu, *Electroanalysis*, **29**, 1618 (2017)
- [82] S. Wu, L. Zheng, L. Rui, X. Lin, *Electroanalysis*, **13**, 967 (2001)
- [83] Z. Wang, Y. Wang, G. Luo, *Electroanalysis*, **15**, 1129 (2003)
- [84] W. Sun, M. Xi, L. Zhang, T. Zhan, H. Gao, K. Jiao, *Electrochim. Acta*, **56**, 222 (2010)
- [85] H. Han, J-Z. Li, Y. Li, X-Z. Pang, *Ionics*, **19**, 989 (2013)
- [86] Q. Shen, X. Wang, *J. Electroanal. Chem.*, **632**, 149 (2009)
- [87] C. Tang, U. Yogeswaran, S-M. Chen, *Anal. Chim. Acta*, **636**, 19 (2009)
- [88] L-J. Feng, X-H. Zhang, P. Liu, H-Y. Xiong, S-F. Wang, *Anal. Biochem.*, **419**, 71 (2011)
- [89] A. Ambrosia, M. Pumera, *Phys. Chem. Chem. Phys.*, **12**, 8943 (2010)
- [90] R. Ghavamia, A. Salimia, A. Navaee, *Biosens. Bioelectron.*, **26**, 3864 (2011)
- [91] M. U. Anu Prathap, R. Srivastavaa, B. Satpati, *Electrochim. Acta*, **114**, 285 (2013)
- [92] J-Y. Chen, S-M. Chen, W-H. Weng, Y. Li, S-D. Yeh, *Int. J. Electrochem. Sci.*, **8**, 3963 (2013)
- [93] B. Kaur, R. Srivastava, *Electrochim. Acta*, **133**, 428 (2014)
- [94] S. Ren, H. Wang, H. Zhang, L. Yu, M. Li, M. Li, *J. Electroanal. Chem.*, **750**, 65 (2015)

References

- [95] R. K. Shervedani, S. B. Dehaghi, M. S. Foroushani, *Electroanalysis*, **28**, 874 (2016)
- [96] L. Zhang, X. Lin, *Analyst*, **126**, 367 (2001)
- [97] L. Wang, P. Huang, J. Bai, H. Wang, X. Wu, *Int. J. Electrochem. Sci.*, **1**, 334 (2006)
- [98] X. Lin, G. Kang, L. Lu, *Bioelectrochemistry*, **70**, 235 (2007)
- [99] H. Tang, G. Hu, S. Jiang, X. Liu, *J. Appl. Electrochem.*, **39**, 2323 (2009)
- [100] R. Zhang, G-D. Jin, D. Chen, X-Y. Hu, *Sensors Actuators B Chem.*, **138**, 174 (2009)
- [101] A. A. Ensafi, M. Taei, T. Khayamian, A. Arabzadeh, *Sensors Actuators B Chem.*, **147**, 213 (2010)
- [102] U. Sivasankaran, A. Thomas, A. R. Jose, K. Girish Kumar, *J. Electrochem. Soc.*, **164**, B292 (2017)
- [103] H. Li, X. Wang, Z. Wang, W. Zhao, *J. Solid State Electrochem.*, **20**, 2223 (2016)
- [104] S. Issac, K. Girish Kumar, *Anal. Methods*, **2**, 1484 (2010)
- [105] T. Jos, A. R. Jose, U. Sivasankaran, K. Girish Kumar, *J. Electrochem. Soc.*, **162**, B94 (2015)
- [106] D. Thomas, Z. Rasheed, J. S. Jagan, K. Girish Kumar, *J. Food Sci. Technol.*, **52**, 6719 (2015)
- [107] S. T. Cyriac, D. Thomas, A. E. Vikraman, K. Girish Kumar, *J. Electrochem. Soc.*, **163**, B683 (2016)
- [108] G. D. Christian, *Analytical Chemistry 6th edition*, John Wiley and Sons, Singapore (2007)
- [109] Z-Y. Yu, X. C. Li, X. L. Wang, J. J. Li, K. W. Cao, *Int. J. Electrochem. Sci.*, **6**, 3890 (2011)

- [110] A-M. Yu, H-Y. Chen, *Anal. Chim. Acta*, **344**, 181 (1997)
- [111] A. Geto, M. Amare, M. Tessema, S. Admassie, *Electroanalysis*, **24**, 659 (2012)
- [112] J. Liu, L. Yang, K. Zhang, K. Li, X. Wu, B. Ye, *Anal. Methods*, **5**, 2712 (2013)
- [113] L. Zang, X. Lin, *Analyst*, **126**, 367 (2001)
- [114] Y. Tao, J. Dai, Y. Kong, Y. Sha, *Anal. Chem.*, **86**, 2633 (2014)
- [115] P. F. Huang, L. Wang, J. Y. Bai, H. J. Wang, Y. Q. Zhao, S. D. Fan, *Microchim. Acta*, **157**, 41 (2007)
- [116] S. A. Kumar, S. M. Chen, *J. Mol. Catal. A: Chem.*, **278**, 244 (2007)
- [117] A. M. O. Brett, S. H. P. Serrano, *J. Braz. Chem. Soc.*, **1**, 97 (1995)
- [118] J. B. Henry, *Clinical Diagnosis and Management*, W. B. Saunders Co, Philadelphia (1989)
- [119] Ringer's solution (pH 7.3–7.4), Cold Spring Harb Protoc (2008), <http://dx.doi.org/10.1101/pdb.rec11273>
- [120] J. R. Partington, *A History of Chemistry Volume 4*, Martino Publishing, USA (1996)
- [121] L. Zhang, X. Lin, *Anal. Bioanal. Chem.*, **382**, 1669 (2005)
- [122] L. Wang, P-F. Huang, H. J. Wang, J. Y. Bai, L. Y. Zhang, Y. Q. Zhao, *Ann. Chim.*, **97**, 395 (2007)
- [123] X-G. Wang, J. Li, Y-J. Fan, *Microchim. Acta*, **169**, 173 (2010)
- [124] Z-Y. Yu, X. C. Li, X. L. Wang, J. J. Li, K. W. Cao *Int. J. Electrochem. Sci.*, **6**, 3890 (2011)
- [125] Y. Yu, X. Li, X. Wang, X. Ma, X. Li, K. Cao, *J. Chem. Sci.*, **124**, 537 (2012)
- [126] J. Li, X. Xang, *Am. J. Analyt. Chem.*, **3**, 195 (2012)

References

- [127] J. Liu, L. Yang, K. Zhang, K. Li, X. Wu, B. Ye, *Anal. Methods*, **5**, 2712 (2013)
- [128] J. Liu, Y. Li, G. Song, K. Zhang, B. Ye, *Intern. J. Environ. Anal. Chem.*, **94**, 884 (2014)
- [129] A. Babaei, M. Sohrabi, *Anal. Methods*, **8**, 1135 (2016)
- [130] D. Thomas, A. E. Vikraman, T. Jos, K. Girish Kumar, *LWT Food Sci. Technol.*, **63**, 1294 (2015)
- [131] A. J. Bard, *Electrochemical Methods: Fundamentals and Applications Vol. 2*, Wiley, New York (1980)
- [132] Z. Rasheed, A.E. Vikraman, D. Thomas, J. S. Jagan, K. Girish Kumar, *Food Anal. Methods*, **8**, 213 (2015)
- [133] A. Thomas, A.E. Vikraman, D. Thomas, K. Girish Kumar, *Food Anal. Methods*, **8**, 2028 (2015)
- [134] Y. Gu, W. Liu, R. Chen, L. Zhang, Z. Zhang, *Electroanalysis*, **25**, 1209 (2013)
- [135] A. M. Oliveira-Brett, J. A. P. Piedade, L.A. Silva, V. C. Diculescu, *Anal. Biochem.*, **332**, 321 (2004)
- [136] R. Khan, *A Textbook of Biotechnology Volume-I Genetics and Molecular Biology 2nd Edition*, University Science Press, New Delhi (2010)
- [137] National Center for Biotechnology Information. PubChem Compound Database; CID=33032, <https://pubchem.ncbi.nlm.nih.gov/compound/33032> [Accessed Sept. 8, 2017]
- [138] A-M. Yu, H-Y. Chen, *Anal. Lett.*, **30**, 599 (1997)
- [139] D. P. Santos, M. F. Bergamini, A. G. Fogg, M. V. B. Zanoni, *Microchim. Acta*, **151**, 127 (2005)

- [140] L. Wang, P. Huang, J. Bai, H. Wang, L. Zhang, *Int. J. Electrochem. Sci.*, **2**, 123 (2007)
- [141] Y. Zang, L. Luo, Y. Ding, X. Liu, Z. Qian, *Microchim. Acta*, **171**, 133 (2010)
- [142] X. Liu, L. Luo, Y. Ding, D. Ye, *Bioelectrochemistry*, **82**, (2011)
- [143] M-P. N. Bui, C. A. Li, G. H. Seong, *Biochip J.*, **6**, 149 (2012)
- [144] M-P. N. Bui, C. A. Li, K. N. Han, X. H. Pham, *Sensors. Actuators B Chem.*, **174**, 318 (2012)
- [145] X. Zhou, X. Zheng, R. Lv, D. Kong, Q. L. Li, *Electrochim. Acta*, **107**, 164 (2013)
- [146] X. Zhou, B. Tan, X. Zheng, D. Kong, Q. Li, *Anal. Biochem.*, **489**, 9 (2015)
- [147] P.S. Ganesh, B.E.K. Swamy, *J. Electroanal. Chem.*, **752**, 17 (2015)
- [148] S. Donmez, F. Arslan, H. Arslan, *Appl. Biochem. Biotechnol.*, **176**, 1431 (2015)
- [149] M. Raj, R. N. Goyal, *Sensors Actuators B Chem.*, **250**, 552 (2017)
- [150] A. Brotons, F. J. Vidal-Iglesias, J. Solla-Gullón, J. Iniesta, *Anal. Methods*, **8**, 702 (2016)
- [151] A. M. Oliveira-Brett, J. A. P. Piedade, L.A. Silva, V. C. Diculescu, *Anal. Biochem.*, **332**, 321 (2004)
- [152] National Centre for Biotechnology Information. PubChem Compound Database; CID=6101, <https://pubchem.ncbi.nlm.nih.gov/compound/6101> [Accessed Sept. 11, 2017]
- [153] C. Nabais, R. P. S. Fartaria, F. M. S. Silva Fernandes, L. M. Abrantes, *Int. J. Quantum Chem.*, **99**, 11 (2004)

References

- [154] F. Xu, M. Gao, L. Wang, G. Shi, W. Zhang, L. Jin, J. Jin, *Talanta*, **55**, 329 (2001)
- [155] C. M. A. Brett, C. Theimann, *J. Electroanal. Chem.*, **215**, 538 (2002)
- [156] G. Jin, Y. Zhang, W. Chen, *Sensors Actuators B Chem.*, **107**, 528 (2005)
- [157] L. Zhang, C. Zhang, J. Lian, *Biosens. Bioelectron.*, **24**, 690 (2008)
- [158] X. Chen, Z. Wang, F. Zhang, L. Zhu, Y. Li, *Che. Pharm. Bull.*, **58**, 475 (2010)
- [159] M. Sadikoglu, G. Taskin, F. Demirtas, B. Selvi, M. Barut, *Int. J. Electrochem. Sci.*, **7**, 11550 (2012)
- [160] M. Sadikoglu, S. Yilmaz, I. Kurt, B. Selvi, H. Sari, N. Erduran, E. Usta, G. Saglikoglu, *Russ. J. Electrochem.*, **52**, 539 (2016)
- [161] L. Xi, D. Zhang, F. Wang, Z. Huang, T. Ni, *J. Electroanal. Chem.*, **767**, 91 (2016)
- [162] A. Geto, C. M. A. Brett, *J. Solid State Electrochem.*, **20**, 2969 (2016)
- [163] M. Amare, W. Lakew, S. Admassie, *Anal. Bioanal. Electrochem.*, **3**, 365 (2011)
- [164] M. Amare, S. Admassie, *Talanta*, **93**, 122 (2012)
- [165] M. Amare, S. Admassie, *Bull. Chem. Soc. Ethiop.*, **26**, 73 (2012)
- [166] A. Geto, M. Amare, M. Tessema, S. Admassie, *Anal. Bioanal. Chem.*, **404**, 525 (2012)
- [167] A. Geto, M. Tessema, S. Admassie, *Synthetic Metals*, **191**, 135 (2014)
- [168] A. Brotons, F.J. Vidal-Iglesias, J. Solla-Gullon, J. Iniesta, *Anal. Methods*, **8**, 702 (2016)

- [169] M. Mazloum Ardakani, Z. Akrami, H. Kazemian, H.R. Zare, *J. Electroanal. Chem.*, **31**, 586 (2006)
- [170] N. Spaftrua, B. V. Sarada, D. A. Tryk, A. Fujishima, *Electroanalysis*, **14**, 721 (2002)
- [171] C. S. Pundir, R. Devi, *Enzyme Microb. Tech.*, **57**, 55 (2014)
- [172] L. Liu, H. Wang, X. Bo, L. Yang, L. Guo, *Electroanalysis*, **24**, 1401 (2012)
- [173] S. Çevik, *Biotechnol. Bioprocess Eng.*, **21**, 314 (2016)
- [174] X. R. Yang, C. X. Ye, J. K. Xu, Y. M. Jiang, *Food Chemistry*, **100**, 1132 (2007)
- [175] L. Zi, J. Li, Y. Mao, R. Yang, L. Qu, *Electrochim. Acta*, **78**, 434 (2012)
- [176] X. Kan, T. Liu, C. Li, H. Zhou, Z. Xing, A. Zhu et.al., *J. Solid State Electrochem.*, **16**, 3207 (2012)
- [177] Y. Zhu, Z. Zhang, D. Pang, *J. Electroanal. Chem.*, **581**, 303 (2005)
- [178] Y. Gao, H. Wang, L. Guo, *J. Electroanal. Chem.*, **706**, 7 (2013)
- [179] C. W. Huck, W. Guggenbichler, G. K. Bonn, *Anal. Chim. Acta*, **538**, 195 (2005)
- [180] R. Kock, B. Delvoux, H. Greiling. *Clin. Chem. Lab. Med.*, **31**, 303 (1993)
- [181] W. D. Pu, H. W. Zhao, L. P. Wu, X. Y. Zhao, *Microchim. Acta.*, **182**, 395 (2015)
- [182] S. Menon, K. Girish Kumar, *LWT Food Sci. Technol.*, **86**, 8 (2017)
- [183] D. K. Singh, A. Sahu, *Anal. Biochem.*, **349**, 176 (2006)
- [184] M. G. Bonini, S. Miyamoto, P. Di Mascio, O. Augusto, *J. Biol. Chem.*, **279**, 51836 (2004)

References

- [185] Y. Wang, L-L. Tong, *Sensors Actuators B Chem.*, **150**, 43 (2010)
- [186] A.S. Kumar, R. Shanmugham, *Anal. Methods*, **3**, 2088 (2011)
- [187] R. Ojani, A. Alinezhad, Z. Abedi, *Sensors Actuators B Chem.*, **188**, 621 (2013)
- [188] M. Amal Raj, S. Abraham John, *Anal. Chim. Acta*, **771**, 14 (2013)
- [189] A. Luo, Q. Lian, Z. An, Z. Li, Y. Guo, D. Zhang, Z. Xue, X. Zhou, X. Lu, *J. Electroanal. Chem.*, **756**, 22 (2015)
- [190] N. Lavanya, C. Sekar, R. Murugan, G. Ravi, *Mater. Sci. Eng. C*, **65**, 278 (2016)
- [191] Y-H. Zhu, Z-L. Zhang, D-W. Pan, *J. Electroanal. Chem.*, **581**, 303 (2005)
- [192] H. Yin, X. Meng, H. Su, M. Xu, S. Ai, *Food Chemistry*, **134**, 1225 (2012)
- [193] S. M. Majd, H. Teymourian, A. Salimia, R. Hallaj, *Electrochim. Acta*, **108**, 707 (2013)
- [194] S. J. Malode, N. P. Shetti, S. T. Nandibewoor, *Colloids Surf. B: Biointerfaces*, **97**, 1 (2012)
- [195] I. Švorc, *Int. J. Electrochem. Sci.*, **8**, 5755 (2013)
- [196] B. Brunetti, E. Desimoni, P. Casati, *Electroanalysis*, **19**, 385 (2007)
- [197] C. A. Martínez-Huitle, N. S. Fernandes, S. Ferro, A. De Battisti, M.A. Quiroz, *Diamond Relat. Mater.*, **19**, 1188 (2010)
- [198] A. Carolina Torres, M.M. Barsan, C. M.A. Brett, *Food Chemistry*, **149**, 215 (2014)
- [199] J. M. Zen, Y. S. Ting, Y. Shih, *Analyst*, **123**, 1145 (1998)
- [200] S. Guo, Q. Zhu, B. Yang, J. Wang, B. Ye, *Food Chemistry*, **129**, 1311 (2011)

- [201] J-Y. Sun, K-J. Huang, S-Y. Wei, Z-W. Wu, F-P. Ren, *Colloids Surf. B: Biointerfaces*, **84**, 421 (2011)
- [202] W. Y. H. Khoo, M. Pumera, A. Bonanni, *Anal. Chim. Acta*, **804**, 92 (2013)
- [203] X. Kan, T. Liu, C. Li, H. Zhou, Z. Xing, A. Zhu, *J. Solid State Electrochem.*, **16**, 3207 (2012)
- [204] Y. Wang, X. Wei, F. Wang, M. Li, *Anal. Methods*, **6**, 7525 (2014)
- [205] Y. Gao, H. Wang, L. Guo, *J. Electroanal. Chem.*, **706**, 7 (2013)
- [206] G. Yang, F. Zhao, B. Zeng, *Talanta*, **127**, 116 (2014)
- [207] S. Can, S. Yilmaz, G. Saglikoglu, M. Sadikoglu, *Electroanalysis*, **27**, 2431 (2015)

ADDITIONAL REFERENCES

- [49a] E. Paleček, *Naturwiss.*, **45**, 186 (1958)
- [49b] E. Paleček, *Coll. Czech. Chem. Commun.*, **25**, 2283 (1960)
- [49c] E. Paleček, *Nature*, **188**, 656 (1960)
- [49d] E. Paleček, *Anal. Biochem.*, **108**, 129 (1980)
- [49e] E. Paleček, *Bioelectrochem. Bioenerg.*, **20**, 179 (1988)
- [49f] E. Paleček, F. Jelen, *Critical Reviews in Analytical Chemistry*, **32**, 261 (2002)
- [49g] E. Paleček, *Talanta*, **56**, 807 (2002)
- [49h] E. Paleček., *In Electrochemistry of Nucleic Acids and Proteins. Towards Electrochemical Sensors for Genomics and Proteomics*, edited by E. Palecek, F.Scheller, J. Wang, Elsevier: Amsterdam (2005)
- [49i] E. Paleček, M. Bartosík, *Chem. Rev.*, **112**, 342 (2012)

..... 

—Publications based on the present work

Journals

1. **S. Jesny**, K. Girish Kumar, Electrocatalytic resolution of guanine, adenine and cytosine along with uric acid on poly(4-amino-3-hydroxy naphthalene-1-sulfonic acid) modified glassy carbon electrode, *Journal of Electroanalytical Chemistry*, **801**, 153 (2017)
2. **S. Jesny**, K. Girish Kumar, Non-enzymatic electrochemical sensor for the simultaneous determination of xanthine, its methyl derivatives theophylline and caffeine as well as its metabolite uric acid, *Electroanalysis*, **29**, 1828 (2017)
3. **S. Jesny**, Z. Rasheed, K. Girish Kumar, A biopolymer-based voltammetric sensor for thymine: Elucidation of electrochemical kinetics, *Ionics*, **23**, 1533 (2017)
4. **S. Jesny**, S. Menon, K. Girish Kumar, Simultaneous determination of Guanine and Adenine in the presence of Uric Acid by poly(para toluene sulfonic acid) mediated electrochemical sensor in alkaline medium, *RSC Advances*, **6**, 75741 (2016)

Conference Proceedings

1. Polymer modified electrode as multianalyte sensor for theophylline and caffeine (**Jesny S.** and K. Girish Kumar, Prof. K.V. Thomas Endowment International Symposium on New Trends in Applied Chemistry (NTAC-2017); Sacred Heart College, Thevara, February 2017) ISBN: 978-81-930558-2-3
2. Polymer modified electrode for the simultaneous sensing of adenine and guanine in DNA samples (**Jesny S.** and K. Girish Kumar A National Seminar on Current Trends in Chemistry CTriC 2017; Cochin University of Science and Technology, Kochi, January 2017)

Publications based on the present work

3. Voltammetric determination of guanine and its primary metabolite uric acid, simultaneously in body fluids (**Jesny S.** and K. Girish Kumar, 26th Swadeshi Science Congress, A National Seminar, Central Marine Fisheries Research Institute, Kochi, November 2016)
4. Evaluation of Kinetic Parameters of Electro Oxidation of Thymine on a poly(l-Glutamic Acid) modified Glassy Carbon Electrode. (**Jesny S.** and K. Girish Kumar, National Symposium Electrochemical Science and Technology NSEST, IISc Bangalore, July 2016)
5. Electrochemical determination of Uric Acid in alkaline media on a Glassy Carbon electrode modified with poly(p-toluene sulfonic acid). (**Jesny S.** and K. Girish Kumar, National Symposium Electrochemical Science and Technology NSEST, IISc Bangalore, July 2016)
6. Glassy Carbon Electrode modified with poly(Glutamic Acid) as a probe for the voltammetric determination of Thymine. (**Jesny S.** and K. Girish Kumar, Frontier Areas in Chemical Technologies FACTs 2016, Alagappa University, Karaikudi, March 2016). ISBN: 978-81-928690-7-0
7. Poly(Aspartic Acid) Modified Glassy Carbon Electrode for the Determination of Adenine (**Jesny S.** and K. Girish Kumar, MatCon2016, CUSAT, Kochi, January 2016) ISBN: 978-93-80095-738

..... *✍*.....

Other publications

Journals

1. U. Sivasankaran, **S. Jesny**, A. R. Jose, K. Girish Kumar, Fluorescence determination of glutathione using paper-derived carbon dots as fluorophores, *Analytical Sciences*, **33**, 281 (2017)
2. M. Sheela Gopal, I. Anitha, **S. Jesny**, Shalini Menon, Development of a 2-methoxy phenyl -4,5-dicarbomethoxy cycl[3.2.2]azine fluorescent sensor for Co^{2+} , *Journal of Luminescence*, **179**, 361 (2016)
3. Shalini Menon, **S. Jesny**, Unni Sivasankaran, Krishnapillai Girish Kumar, Fluorimetric Determination of Epinephrine: A Green Approach, *Analytical Sciences*, **32**, 999 (2016)
4. Shalini Menon, Ammu Rosin Jose, **S. Jesny**, Krishnapillai Girish Kumar, A colorimetric and fluorometric sensor for the determination of norepinephrine, *Analytical Methods*, **8**, 5801 (2016)
5. Shalini Menon, Anuja. Elavathoor. Vikraman, **S. Jesny**, Krishnapillai Girish Kumar, "Turn On" Fluorescence Determination of Nitrite Using Green Synthesized Carbon Nanoparticles, *Journal of Fluorescence*, **26**, 129 (2015)
6. Divya Thomas, Zafna Rasheed, **Jesny S.**, Krishnapillai Girish Kumar, Study of kinetic parameters and development of a voltammetric sensor for the determination of butylated hydroxyanisole (BHA) in oil samples, *Journal of Food Science and Technology*, **52**, 6719 (2015)
7. Zafna Rasheed, Anuja. Elavathoor. Vikraman, Divya Thomas, **Jesny S.**, Krishnapillai Girish Kumar, Carbon-nanotube-based sensor for the determination of butylated hydroxyl anisole in food samples. *Food Analytical Methods*, **8**, 213 (2015)

Conference Proceedings

1. Electrochemical behaviour of Metanil Yellow on a bare gold electrode (**Jesny S.** and K. Girish Kumar, Swadeshi Science Congress, Kalady, December 2015)
2. Study of electrochemical oxidation of sulphite on a gold electrode modified with multi-walled carbon nano-tubes (**Jesny S.** and K. Girish Kumar, Swadeshi Science Congress, M.G. University, Kottayam, November 2013)
3. Surface modification of gold electrode with multiwalled carbon nanotubes for sulphite sensing. (**Jesny S.** and K. Girish Kumar, RASS – 2013, Gandhigram Rural Institute- Deemed University, Tamil Nadu, February 2013) ISBN: 978-93-82338-36-9
4. Voltammetric behavior of sulfite on a gold electrode modified with multiwalled carbon nanotubes. (**Jesny S.** and K. Girish Kumar, CTric, Cochin University of Science and Technology, Kochi, March 2011)

..... *END*.....

RESUME OF THE AUTHOR

Jesny S.

Assistant Professor
Department of Chemistry
S. N. College,
Cherthala
Mobile: 9447740268

No 7, ECHCS Presidency
Indira Nagar, Kadavantra,
Kochi-682020
E-mail: jesny@mail@gmail.com

PERSONAL PROFILE

Age and Date of Birth	-	37 years, 11 th July 1980
Nationality	-	Indian
Religion	-	Hindu
Caste	-	Ezhava
Marital status	-	Married
Languages Known	-	English, Hindi and Malayalam
Hobbies	-	Reading, Cooking

ACADEMIC PROFILE

Course	Institution	Year of passing	% of marks and class	University / Board
SSLC	St. Antony's High School, Ernakulam	1996	92.3 % Distinction	Board of Public Examinations, Kerala
Pre-Degree	St. Teresa's College, Ernakulam	1998	88.6 % Distinction	M.G.University
B.Sc.	St. Teresa's College, Ernakulam	2001	93.7 % First Class	M.G.University
M.Sc.	Sacred Heart College, Ernakulam	2003	83.4 % First Class with Distinction (4 th position)	M.G.University
M.Phil.	Dept. of Applied Chemistry, CUSAT	2010	75.6 % First Class with first rank	CUSAT
Ph.D	Dept of Applied Chemistry, CUSAT	2010-till date		CUSAT

Achievements

- ◆ Qualified NET in Chemical Sciences (December 2002).
- ◆ Qualified GATE with a percentile score of 89.14 (February 2003).

Teaching Experience

Institution	Designation	Period
St. Paul's College, Ernakulam	Guest Lecturer	June 2004– November 2004
S. N. College, Cherthala	Assistant Professor	December 2004 – till date

Membership in Professional Organisations

- Life member: Swadeshi Science Movement (SSM)
- Life member: Indian Society for Electroanalytical Chemists (ISEAC)
- Life member: Centre for Environment Education and Technology (CEET)
- Life member: Academy of Chemistry Teachers (ACT)

DECLARATION

I hereby declare that the above-mentioned details are true to the best of my knowledge and belief.

Jesny S.

Ernakulam
16-11-2017